

Heavy-light mesons in lattice HQET and QCD

DISSERTATION

zur Erlangung des akademischen Grades
doctor rerum naturalium
(Dr. rer. nat.)
im Fach Physik

eingereicht an der
Mathematisch-Naturwissenschaftlichen Fakultät I
Humboldt-Universität zu Berlin

von
Herrn Dipl.-Phys. Damiano Guazzini
geboren am 15.11.1980 in Grosseto, Italien

Präsident der Humboldt-Universität zu Berlin:

Prof. Dr. Christoph Marksches

Dekan der Mathematisch-Naturwissenschaftlichen Fakultät I:

Prof. Dr. Christian Limberg

Gutachter:

1. Dr. Rainer Sommer
2. Prof. Dr. Ulrich Wolff
3. Dr. Mike Peardon

eingereicht am: 29. März 2007
Tag der mündlichen Prüfung: 28. Juni 2007

DESY-THESIS-2007-034

Abstract

We present a study of a combination of HQET and relativistic QCD to extract the b-quark mass and the B_s -meson decay constant from lattice quenched simulations. We start from a small volume, where one can directly simulate the b-quark, and compute the connection to a large volume, where finite size effects are negligible, through a finite size technique. The latter consists of steps extrapolated to the continuum limit, where the b-region is reached through interpolations guided by the effective theory.

With the lattice spacing given in terms of the Sommer's scale r_0 and the experimental B_s and K masses, we get the final results for the renormalization group invariant mass $M_b = 6.88(10)$ GeV, translating into $\bar{m}_b(\bar{m}_b) = 4.42(6)$ GeV in the $\overline{\text{MS}}$ scheme, and $f_{B_s} = 191(6)$ MeV for the decay constant.

A renormalization condition for the chromo-magnetic operator, responsible, at leading order in the heavy quark mass expansion of HQET, for the mass splitting between the pseudoscalar and the vector channel in mesonic heavy-light bound states, is provided in terms of lattice correlations functions which well suits a non-perturbative computation involving a large range of renormalization scales and no valence quarks.

The two-loop expression of the corresponding anomalous dimension in the Schrödinger functional (SF) scheme is computed starting from results in the literature; it requires a one-loop calculation in the SF scheme with a non-vanishing background field. The cutoff effects affecting the scale evolution of the renormalization factors are studied at one-loop order, and confirmed by non-perturbative quenched computations to be negligible for the numerical precision achievable at present.

Keywords:

Lattice QCD, HQET, Hadron spectrum, Chromo-magnetic interaction

Zusammenfassung

Wir stellen eine Untersuchung einer Kombination zwischen HQET und relativistischer QCD vor, die das Ziel hat, die b-Quark Masse und die Zerfallskonstante des B_s -Mesons aus Gitter-Simulationen, unter Nichtbeachtung virtueller Fermionenschleifen, zu gewinnen. Wir beginnen mit einem kleinen Volumen, in dem man das b-Quark direkt simulieren kann, und stellen die numerische Verbindung mit einem großen Volumen, wo “finite-size” Effekte vernachlässigbar sind, mit Hilfe einer “finite-size” Methode her. Diese besteht aus zum Kontinuum extrapolierten Schritten, wobei der Massenpunkt, der der physikalischen b-Quark Masse entspricht, durch eine Interpolation erreicht wird. In diese Interpolation fließen die in der HQET erzielten Resultate ein.

Mit dem durch die Sommersche Skale r_0 bestimmten Gitterabstand und den experimentalen Werten für die B_s - und K-Massen erhalten wir die Endergebnisse für die renormierungsgruppeninvariante Masse $M_b = 6.88(10)$ GeV, äquivalent zu $\bar{m}_b(\bar{m}_b) = 4.42(6)$ GeV in dem \overline{MS} -Schema und $f_{B_s} = 191(6)$ MeV für die Zerfallskonstante.

Eine Renormierungsbedingung für den Chromo-magnetischen Operator, der in führender Ordnung der Entwicklung in der schweren Quarkmasse in HQET für die Massenaufspaltung zwischen dem pseudoskalaren und dem vektoriellen Kanal mesonischer schwer-leicht gebundener Zustände verantwortlich ist, wird auf der Basis von Gitter-Korrelationsfunktionen bereitgestellt. Dies eignet sich gut für eine nicht-störungstheoretische Rechnung, welche einen großen Bereich der Renormierungsskala umfasst und keine Valenz-Quarks beinhaltet.

Die Zwei-Schleifen Ordnung der entsprechenden anomalen Dimension im Schrödinger-Funktional-Schema wird mit Hilfe von veröffentlichten Ergebnissen berechnet; dies erforderte eine neue Ein-Schleifen Rechnung im SF-Schema mit einem nicht verschwindenden Hintergrundfeld. Die Gitterartefakte bezüglich der Skalenentwicklung des Renormierungsfaktors werden zur Ein-Schleifen Ordnung untersucht, und es wird von nicht-störungstheoretischen Simulationen, unter Nichtbeachtung virtueller Fermionenschleifen, bestätigt, dass sie für die gegenwärtige verfügbare numerische Präzision vernachlässigbar sind.

Schlagwörter:

Gitter-QCD, HQET, Hadronspektrum, Chromo-magnetische Wechselwirkung

Contents

| | | |
|----------|--|-----------|
| 1 | Introduction | 1 |
| 2 | Phenomenology of the heavy quarks | 8 |
| 2.1 | Strong interactions | 8 |
| 2.2 | Spin-flavor symmetry | 10 |
| 2.3 | The effective Lagrangian | 11 |
| 2.4 | Symmetries of the effective Lagrangian | 14 |
| 2.5 | Renormalization of the effective theory | 15 |
| 2.6 | Matching of the effective theory with QCD | 18 |
| 3 | The Schrödinger functional | 21 |
| 3.1 | Definition | 21 |
| 3.2 | Lattice formulation | 25 |
| 3.3 | Expectation values and Monte Carlo integration | 29 |
| 3.4 | Improvement | 33 |
| 3.5 | Correlation functions | 39 |
| 3.5.1 | Definition | 39 |
| 3.5.2 | Improvement | 44 |
| 3.5.3 | Renormalization | 45 |
| 4 | Combining HQET and relativistic QCD | 49 |
| 4.1 | The Step Scaling Method | 49 |
| 4.2 | Simulation parameters | 51 |
| 4.2.1 | Action | 51 |
| 4.2.2 | Scale setting | 52 |
| 4.2.3 | Quark masses | 53 |
| 4.2.4 | Improvement coefficients and renormalization factors | 58 |
| 4.2.5 | Quark mass scheme conversion | 59 |

| | | |
|----------|--|------------|
| 4.3 | Computation of the b-quark mass | 59 |
| 4.3.1 | General strategy | 59 |
| 4.3.2 | The results | 62 |
| 4.4 | Computation of the meson decay constant | 68 |
| 4.4.1 | General strategy | 68 |
| 4.4.2 | The results | 70 |
| 4.5 | Summary | 75 |
| 5 | Renormalization of the chromo-magnetic operator in HQET | 78 |
| 5.1 | Spin splitting | 78 |
| 5.2 | Definition of the renormalization scheme | 80 |
| 5.3 | Connection between different schemes | 83 |
| 5.4 | Perturbation theory in the SF scheme | 86 |
| 5.4.1 | The gauge fixed action | 86 |
| 5.4.2 | The total action | 89 |
| 5.5 | Expectation values of Wilson loops at one-loop order | 91 |
| 5.5.1 | Parametrization of the observable | 91 |
| 5.5.2 | Single gluon radiative corrections | 93 |
| 5.5.3 | Tadpole contributions | 94 |
| 5.5.4 | Improvement | 95 |
| 5.5.5 | Summary | 96 |
| 5.6 | Two-loop anomalous dimension and cutoff effects | 97 |
| 5.7 | Non-perturbative step scaling functions | 103 |
| 5.8 | Summary | 106 |
| 6 | The Matlab code <code>WLINE</code> | 108 |
| 6.1 | The automated code | 109 |
| 6.2 | The propagators | 114 |
| 6.2.1 | The ghost propagator | 114 |
| 6.2.2 | The gluon propagator | 117 |
| 6.2.3 | The quark propagator | 127 |
| 6.3 | Tadpoles and improvement | 134 |
| 6.3.1 | Ghost tadpole | 134 |
| 6.3.2 | Gluon tadpole | 136 |
| 6.3.3 | Quark tadpole | 138 |
| 6.3.4 | Improvement | 140 |
| 6.4 | Tests of the code | 140 |
| 6.4.1 | The average plaquette | 140 |

| | | |
|----------|---|------------|
| 6.4.2 | Comparison with Monte Carlo results | 142 |
| 6.5 | Summary | 142 |
| 7 | Conclusions | 145 |
| A | Notations and conventions | 156 |
| A.1 | The Dirac matrices | 156 |
| A.2 | The basis of the Lie algebra | 157 |
| A.3 | The non-vanishing background field | 158 |
| B | Statistical uncertainties in Monte Carlo simulations | 161 |
| B.1 | Thermalization | 161 |
| B.2 | Autocorrelation and errors estimate | 161 |
| B.2.1 | The Gamma method | 162 |
| B.2.2 | Jackknife | 164 |
| C | Simulation results | 166 |
| C.1 | Static data | 166 |
| C.2 | Relativistic QCD data | 173 |
| D | Correlated errors in both coordinates | 176 |
| E | Fit of the correlated relativistic QCD data | 178 |
| E.1 | Performing the continuum limits | 178 |
| E.2 | Fitting the mass dependence | 179 |
| F | Estimate of the uncertainty related to the scale setting | 183 |
| F.1 | Static decay constant | 184 |
| F.2 | Static meson step scaling function | 185 |
| G | Perturbation theory results | 187 |
| G.1 | Tree-level | 187 |
| G.2 | One-loop | 189 |

List of Figures

| | | |
|-----|---|-----|
| 4.1 | Linear interpolation for κ_{crit} . The data refer to a lattice with $\beta = 6.0914$, $L/a = 10$, $T = 2L$ and $\theta = 0.0$. All points are statistically independent. | 58 |
| 4.2 | Plot of the step scaling function $\sigma_m(x, L_2)$ vs. $x = x(m_h, L_2)$ | 66 |
| 4.3 | Plot of the step scaling function $\sigma_m(x, L_1)$ vs. $x = x(m_h, L_1)$ | 67 |
| 4.4 | Plot of $\rho(x, L_0)$ vs. $x = x(m_h, L_0)$ | 67 |
| 4.5 | Plot of the step scaling function $\sigma_f(x, L_2)$ vs. $x = x(m_h, L_2)$ | 73 |
| 4.6 | Plot of the step scaling function $\sigma_f(x, L_1)$ vs. $x = x(m_h, L_1)$ | 73 |
| 4.7 | Plot of the renormalized pseudoscalar decay constant on the small volume $Y_{\text{PS}}(x, L_0)$ vs. $x = x(m_h, L_0)$ | 74 |
| 5.1 | One-loop contribution $\Sigma_{\text{mag}}^{(1)}(a/L)$ to the quenched step scaling function of the chromo-magnetic operator. | 98 |
| 5.2 | One-loop order of Z_{mag} after removing the logarithmic divergent part. The plotted points refer to $L/a \geq 6$ | 100 |
| 5.3 | One-loop contribution $\Sigma_{\text{mag}}^{(1)}(a/L)$ to the step scaling function of the chromo-magnetic operator in the $N_f = 2$ case. | 101 |
| 5.4 | One-loop order of Z_{mag} , with $N_f = 2$, after removing the logarithmic divergent part. The plotted points refer to $L/a \geq 6$ | 102 |
| 5.5 | Continuum limit extrapolations for the step scaling function $\Sigma_{\text{mag}}^{\text{SF}}$ | 105 |
| 6.1 | Computational cost for the gluon propagator for a fixed momentum. Test performed on a PC with a processor Intel Pentium 4 with 2.6 GHz. | 122 |
| 6.2 | Comparison of the perturbative results with the non-perturbative ($N_f = 0$) ones. | 143 |
| C.1 | On the left: β -dependence of $a\Gamma_{\text{stat}}(L_1)$. The red curve shows the quadratic fit of the data with c_A^{stat} at 1-loop (blue points), while the green one fits the data with c_A^{stat} at tree-level (magenta points). The two curves almost overlap. On the right: continuum extrapolation to get $\sigma_m^{\text{stat}}(L_2)$ | 171 |
| C.2 | Various HQET continuum limit extrapolations for the Step Scaling Method. | 172 |

| | | |
|-----|---|-----|
| C.3 | Continuum limit extrapolations for the relativistic QCD data used in the Step Scaling Method. | 175 |
| E.1 | Importance of data correlation for the step scaling function $\sigma_f(L_2)$ | 182 |
| F.1 | Estimate on the propagation of the uncertainty on r_0/a for the static meson step scaling function. | 185 |

List of Tables

| | | |
|-----|---|-----|
| 4.1 | Uncertainties on the regularization dependent part of the total renormalization factor Z_M | 56 |
| 4.2 | 4-loop β -function and anomalous dimension of the mass in the \overline{MS} scheme. The references are only for the highest order computations; there one finds also the references for the lower orders too. | 60 |
| 4.3 | Results of the interpolation of $\sigma_m(x_2, L_2)$ and $\sigma_m(x_1, L_1)$. For the computation of the masses (4.56) and (4.57) the quadratic fit results have been used. | 75 |
| 4.4 | Results of the computation of $\sigma_f(x_2, L_2)$, $\sigma_f(x_1, L_1)$ and $Y_{PS}(x_0, L_0)$. For the computation of (4.83) and (4.84) the linearly interpolated step scaling functions have been used. | 76 |
| 5.1 | Lattice spacing effects of Σ_{mag} at one-loop order. | 103 |
| 5.2 | Results for the (quenched) non-perturbative step scaling function $\Sigma_{\text{mag}}^{\text{SF}}$. The simulations have been performed with c_t set to its two-loop value (3.101). | 105 |
| A.1 | C_a, R_a and ϕ_a for the gauge group SU(3). The other coefficients are $C_2 = C_1, C_5 = C_4, C_7 = C_6, R_2 = R_1, R_5 = R_4, R_7 = R_6, \phi_2 = -\phi_1, \phi_5 = -\phi_4$ and $\phi_7 = -\phi_6$ | 159 |
| C.1 | Collection of all simulation parameters for the HQET part of the Step Scaling Method. | 167 |
| C.2 | Collection of all continuum limit extrapolations for the HQET part of the Step Scaling Method. The result $Y_{\text{SF}}(L_2, \mu)$ is taken from [1], and is intended to be multiplied by $I^{\text{stat}}(\mu = (1.436r_0)^{-1}) = 0.9191(83)$ computed in [2] to get eq. (4.75). | 167 |
| C.3 | Collection of results at finite lattice spacing, for the computation of the static step scaling functions of the meson mass. | 168 |
| C.4 | Collection of results at finite lattice spacing for the static pseudoscalar decay constant. All numbers are obtained with the 1-loop expression of b_A^{stat} | 169 |
| C.4 | (continued) | 170 |
| C.5 | Continuum limit results for the relativistic QCD data used in the Step Scaling Method. | 174 |

| | | |
|-----|--|-----|
| F.1 | Results of the test for aK_{stat} | 186 |
| G.1 | Raw data for $Z^{(0)}$ defined in eq. (G.3). | 188 |
| G.2 | Expectation values for the one-loop diagrams of \mathcal{P}_3 . The tadpole contributions in the fourth column are restricted to the ghost and gluon cases. | 190 |
| G.3 | Expectation values for the one-loop diagrams of $\mathcal{P}_{3,\text{ins}}$. The tadpole contributions in the fourth column are restricted to the ghost and gluon cases. | 191 |
| G.4 | Expectation values for the one-loop quark tadpole contributions. | 192 |
| G.5 | $O(a)$ -improvement counterterms for $\mathcal{P}_{3,\text{ins}}$ at one-loop order. The simple Polyakov loop \mathcal{P}_3 does not require any counterterm. | 193 |

Chapter 1

Introduction

In the seventeenth century the scientific method was born. Its father, Galileo Galilei, proposed it as the correct way to understand nature, focusing the attention on the concepts of reproducibility of a physical phenomenon and predictivity of its theoretical description. Along this method, present-day particle physics research represents the most ambitious and most organized effort to understand world's underlying structure.

Besides the gravitational one, modern physicists have counted three fundamental interactions: strong, weak and electromagnetic. To date, almost all experimental tests of the three forces have well agreed with the predictions of the Standard Model. This is not really surprising, since the latter has been built from the experimental observations. Its mathematical framework is represented by quantum field theory, where each type of particle is described in terms of a field, obeying to a local gauge principle, with the gauge group

$$SU(3)_c \times SU(2)_L \times U(1)_Y.$$

Quantum chromodynamics (QCD) is associated with the first of these groups, and is the theory of the strong interactions. The matter constituents are fermions; six quarks, organized in three generations

$$\begin{pmatrix} u \\ d \end{pmatrix}, \quad \begin{pmatrix} s \\ c \end{pmatrix}, \quad \begin{pmatrix} b \\ t \end{pmatrix},$$

whose color interaction is mediated by vector bosons, the gluons. The latter have a color charge too, and, like all other non-Abelian gauge theories (and unlike quantum electrodynamics), they interact with one another by the same force that affects the quarks.

QCD enjoys two peculiar properties: asymptotic freedom and confinement. The former is relevant at high energies, or short distances, where quarks and gluons are

found to be weakly coupled. As the energy scales become arbitrarily large, one is left with a non-interacting theory. This pattern has been verified in several experimental observations, especially in deep inelastic lepton-hadron scatterings. The theoretical explanation of the phenomenon came in 1973 thanks to D. Gross, D. Politzer and F. Wilczek [3, 4], in the framework of the renormalization group. For sufficiently short distances or large momentum transfer, an asymptotically free theory, amenable to perturbation theory calculations using Feynman diagrams, emerges. Such situations are therefore more theoretically tractable, under the analytical point of view, than the long-distance, strong-coupling behavior, where confinement dominates. Although an analytical proof is still missing, confinement is widely accepted, and explains the consistent failure of free quark searches, as well as many other accurate experimental data, like hadron masses. In the low-energy regime, the coupling constant assumes values, which are too large to have a reliable perturbative expansion. It follows that the theoretical predictions need other techniques. The answer came in 1974, when K. Wilson proposed [5] a way to quantize a gauge field theory on a discrete lattice in Euclidean space-time, preserving exact gauge invariance. The lattice gauge theory he developed has a computable strong-coupling limit, where it is possible to show the color confinement, and thus the absence of free quarks. Lattice QCD shares with the continuum QCD formulation the property of relying on very few parameters, and allows first-principle predictions without any additional assumption. The lattice provides a regularization of the theory, which becomes ultraviolet finite thanks to the presence of a cutoff proportional to the inverse of the lattice spacing a , while infrared divergences can be avoided by choosing either non-vanishing quark masses or particular boundary conditions. Such a theory suits well the implementation on a computer, or even on a cluster of them, and is not restricted to the low-energy regime. Perturbative lattice computations are possible and useful; however, they are generally more complicated than in the continuum.

Once a lattice setup has been chosen, the desired observable can be computed by evaluating the corresponding Feynman path integrals via Monte Carlo techniques. Apart from statistical errors, such an evaluation is, however, only an approximation of the wished result, because of the finiteness of the lattice cutoff. As for any other regularization method, the regulator has to be removed. This amounts to take the continuum limit. The lattice discretization is made finer and finer, and, at the same time, one is asked to tune the bare parameters of the theory according to the renormalization group equations, in order to keep fixed the corresponding physical quantities. The fineness of the lattice is strongly limited by the available computer facilities as well as by the details of the Monte Carlo samplings. As a set of lattices have been simulated, one in general expects to find discretization errors vanishing linearly with the lattice

spacing. This can be trusted if a is small enough compared to the other involved scales. Furthermore, it often constrains one to vary a over a large range before having a controlled estimate of the size of the lattice artifacts. The latter can also be quite large. The issue can be solved by “decorating” the action and the correlation functions with irrelevant terms, i.e. vanishing in the continuum limit, which, properly tuned, cancels the $O(a)$ -artifacts.

The Feynman path integrals involve the fermion determinant that is non-local and very expensive to evaluate numerically. In order to bring the computational effort to an acceptable level, lattice physicists have introduced the quenched approximation. The latter amounts to disregard the fermionic contributions in the generation of the gauge configurations. In the language of Feynman diagrams, it can be interpreted as the removal of all virtual quark lines. The drawback is that one is confronted with an uncontrolled approximation. Deviations from full, or unquenched, QCD results are almost unpredictable, as long as the latter are unknown. Still, quenched simulations have led to results in many cases in very good agreement with experiments, and represent a powerful tool to test techniques intended for later use in full QCD.

In spite of the richness of physical phenomena associated with the strong interactions, there are many phenomenologically interesting subjects which are not directly related with QCD alone. Among others, it is the case of the weak interactions. Lattice QCD allows to study observables, encoding important informations upon matrix elements of the effective weak Hamiltonian between QCD bound states. Outstanding examples are form factors and decay constants.

However, a scan through a review of particle properties gives a rough idea of the abundance of open questions. As one intends to face all of them armed with lattice QCD, one discovers that a brute force computational approach is clearly doomed.

A way to solve the problem is to find alternative discretizations of the theory, as well as more efficient computational algorithms. This is helpful, but in many cases not sufficient to obtain predictions precise enough to be competitive with most recent experimental determinations.

A powerful tool is represented by the approximated symmetries of the theory. The light quarks u and d have masses which are much smaller than the typical QCD scale Λ_{QCD} , which is of the order of a few hundreds of MeV. Consequently, for many QCD processes it is a good approximation to take the limit $m_{u,d} \rightarrow 0$. In this limit the theory shows a symmetry, associated with the group $SU(2)_L \times SU(2)_R$, called chiral symmetry, and many low-energy properties of QCD are related to a few matrix elements. One may also approximate the strange quark to be massless, thus having an enlarged symmetry $SU(3)_L \times SU(3)_R$, but also expect finite quark mass corrections to be not small.

Analogously, one observes that the remaining three quarks, namely the charm, the bottom and the top quarks, have masses much bigger than the QCD scale. Lattice gauge theory is then found to face a multi-scale problem. Let us consider the case of a heavy-light meson, i.e. a hadron composed¹ of a heavy quark (e.g. the bottom), and a light antiquark (e.g. the antistrange). Due to the small Compton wavelength associated with the former, one would require a cutoff a^{-1} much bigger than the quark mass in order to have a good control over the aforementioned discretization errors. At the same time, the light antiquark wave function introduces a widely spread object, demanding a large volume in physical units in order to have negligible finite volume effects. It is not possible to fulfill both requirements at the same time, because one would need a lattice resolution which is not affordable even by the most recent supercomputers.

Several ways of dealing with this problem have been proposed and investigated. Instead of mentioning all of them, we focus our attention on the conceptually simplest but all the while very powerful approach, the Heavy Quark Effective Theory (HQET). When the Compton wavelength $1/m$ of the heavy quark is much smaller than the size of the meson, the low energy properties of the latter are scantily sensitive to the heavy quark mass. The non-perturbative dynamics of the meson can thus be approximated [6] by considering the heavy quark to be static, i.e. propagating only in time in the rest frame of the hadron. While this approximation describes the correct asymptotic behavior of the bound state in the limit $m \rightarrow \infty$, and is interesting by itself, finite quark mass corrections can be studied in a systematic way through an expansion in powers of $1/m$, and allow to make closer contact with phenomenology. In the static approximation the heavy quark is seen just as a static source of color by the light degrees of freedom surrounding it. They are blind to the flavor and the spin of the static quark. It means that one has at one's disposal further symmetries in addition to the ones QCD already comprises, and thus promising tools to extract interesting properties of heavy-light bound states by using a lattice formulation of HQET. How big the finite quark mass corrections are, it cannot be said a priori. They depend on the involved masses as well as on the observable itself.

Another interesting approach has roots in HQET, but exploits the QCD Lagrangian. Proposed by the Tor Vergata group [7], it is based on a finite size technique, called Step Scaling Method, where the heavy-light system is simulated, by using the QCD Lagrangian, on a volume small enough, in physical units, to allow an accurate treatment of the heavy quark dynamics, and to extrapolate to the continuum limit with confidence. The light degrees of freedom are clearly squeezed in such a box. Through several steps, one then performs the connection to an ideally infinite volume. In prac-

¹Of course these considerations hold also for a meson made of a heavy antiquark and a light quark, and even more generally for heavy-light hadronic bound states.

tice, the latter is a box large enough to let consider the finite size effects negligible in comparison with the numerical precision on the computed observables. The steps consist in doubling the volume and halving the heavy quark mass in physical units, in order to keep the discretization errors under control. Each step is performed for several heavy quark masses and extrapolated to the continuum limit. The main assumption of the method is that the step scaling functions have a mild dependence on the heavy quark mass. One can thus join the heavy quark region of interest through an extrapolation, while the light quark mass is held fixed to its phenomenological value during the whole evolution.

The Step Scaling Method represents a very attractive approach to study the properties of heavy-light bound states; still, it entails extrapolations which cannot be considered reliable a priori, especially if the simulated heavy quark masses are much lighter than the extrapolated ones, and if a very high precision is desired.

By combining the static limit of HQET and the Step Scaling Method one can turn the extrapolations of the latter into interpolations in all volumes. The upshot is a method which promises to allow to study heavy-light meson properties with astonishing confidence and precision also in the b-quark energy scale.

The interplay of HQET and the QCD Step Scaling Method can be exploited also to extract important informations concerning the magnitude of the finite heavy quark mass corrections to the static limit. These can be directly studied in HQET too. At order $1/m$ the terms in the Lagrangian breaking the spin-flavor symmetry of the static theory are two [8, 9]. One is the kinetic term, responsible for the spatial motion of the heavy quark in the rest frame of the hadron, and the second is the chromo-magnetic term, describing the interaction of the heavy quark spin with the gluon field. Restricting our attention to the heavy-light mesons, we stress that the chromo-magnetic interaction is responsible, among other effects, for the mass splitting between the ground state pseudoscalar and vector mesons. Since the splitting is known from experiments with very high accuracy, it represents an excellent testing ground for the effective theory, both in the bottom channel and in the charm one.

In this context the renormalization of the chromo-magnetic operator plays a crucial role. The renormalization procedure is simplified by the absence of operator mixing [9]. Furthermore, one would like to relate the mass splitting to a scale and scheme independent matrix element. This is possible by exploiting the general strategy of the ALPHA collaboration [10, 11, 12], which addresses the question how the perturbative regime is related to the observed hadronic properties. The key idea is the introduction of a renormalization scheme, the Schrödinger functional, in which the scale evolution of the renormalization factor of the chromo-magnetic operator can be computed non-perturbatively from low to very high energies. In the high-energy regime one

can continue the scale evolution using perturbation theory, which allows to determine the renormalization group invariant operator. Working in a mass independent renormalization scheme, the scale evolution of the renormalization factor is ruled by the renormalization group equations, where the renormalized coupling, the corresponding β -function, and the anomalous dimension of the operator appear. A precise perturbative knowledge of the latter is an important brick to bridge the high-energy regime with an ideally infinite energy scale, where the RGI renormalization factor can be determined.

The rest of the thesis is organized as follows. In chapter 2 an introduction to HQET with special care to the phenomenological aspects is given. The static approximation and its symmetries are discussed, and the importance of a non-perturbative renormalization is stressed. The final section concerns the matching of the effective theory with QCD. The basic ideas are explained in order to make easier the reading of the following chapters.

Chapter 3 is dedicated to the Schrödinger functional scheme. After its definition in the continuum, the lattice discretization is introduced and followed by a short description of the Monte Carlo methods, employed for the non-perturbative computations of this work. The basic concepts of the $O(a)$ -improvement of both relativistic QCD and HQET are explained, and are of central importance throughout the following. The last section is strongly connected with chapter 4. In the former, explicit expressions for correlation functions and observables, stemming from relativistic quark and static-light bilinears, are derived. In addition, their connection to physical quantities like decay constants and hadron masses is set up. The improvement of the correlation function is discussed, and the last subsection deals with their renormalization.

With chapter 4 one enters the main part of the thesis. The first section explains how the interplay between HQET and the QCD Step Scaling Method works. Before presenting the results, the choice of the simulation parameters is motivated, and all details necessary to compute them are provided. The definition of renormalization group invariant quark mass is expounded too. The rest of the chapter is split into two parts, containing the main results of this work on the combination of the effective theory and relativistic QCD. The first part discusses the non-perturbative computation of the b -quark mass, by starting simply from the B_s -meson and Kaon masses. The second part exploits the same experimental inputs, and achieves a non-perturbative computation of the B_s -meson decay constant. All simulations are performed in the quenched approximation.

Chapter 5 provides an expression of the mass splitting between the pseudoscalar and the vector heavy-light mesons in terms of HQET. At order $1/m$, it can be expressed as a matrix element of the chromo-magnetic operator, for which a proposal for the non-

perturbative renormalization is furnished. The main point is that it involves the computation of only pure gauge observables. In order to get the total renormalization factor relating the bare operator to the renormalization group invariant one, perturbation theory plays a fundamental role. After explaining the basics of the perturbative expansion in the Schrödinger functional scheme, and of the connection between the latter and the $\overline{\text{MS}}$ scheme, a formalism for the computation and the improvement of Wilson loops at one-loop order is provided, with special care dedicated to its implementation on a computer. The remaining part of the chapter presents the main results on the subject: the two-loop expression of the anomalous dimension of the chromo-magnetic operator in the Schrödinger functional scheme, and a study of the cutoff effects affecting the corresponding renormalization factor. The latter are also compared with non-perturbative simulations at weak coupling and in the quenched approximation.

In chapter 6 the code used for the perturbative computations of chapter 5 is presented. It enables the user to compute up to and including the one-loop order of any Wilson loop in the Schrödinger functional scheme, as well as the improvement counterterms, with or without non-vanishing background field. The first section is thought as a basic documentation, which lets the reader understand the structure of the code and how to use it without entering in the details of the underlying subroutines. The following sections are devoted to an explanation of the modules constituting the pillars of the program. Each of them is an important part of the program, but can also be used separately from the rest. Finally, two of the tests performed to check the correctness of the program are discussed.

Part of the appendices are simply a report of the details of the numerical results, while the remaining appendices present the details of the analysis procedure, and are thought as tools not restricted to this work only.

Finally, the last chapter summarizes all results and discusses an outlook.

Chapter 2

Phenomenology of the heavy quarks

2.1 Strong interactions

A deep insight in the hadronic structure was given in the late 1960s by the SLAC-MIT deep inelastic scattering experiments. These experiments were a decisive test for models, in which hadrons behave like a complex cloud of softly bounded constituents. In scatterings between an electron beam and a hydrogen target, these models predicted very low scattering rates. Instead, the SLAC-MIT experiments showed a substantial rate for hard scatterings of electrons from protons, where only in rare cases did a single proton emerge from the process.

The explanation of these phenomena was given by the simple model advanced by Bjorken and Feynman: the parton model. The latter predicts that a hadron is a loosely bound assemblage of a small number of pointlike constituents (quarks and antiquarks), obeying to the Fermi statistics, and carrying electric charge, and possibly other kinds of interaction, responsible for their binding.

Historically Quantum Chromodynamics was born as a development of this model, and it exploits the power of quantum field theory to explain the strong interactions, which bind quarks and antiquarks together in the observed hadrons.

Quarks are identified by a flavor quantum number and are triplets of the SU(3) gauge symmetry, the color. Under a gauge transformation $g(x)$, which is a matrix in the gauge group representation, the quark field ψ transforms according to

$$\psi(x) \rightarrow \psi^g(x) = g(x)\psi(x). \quad (2.1)$$

Quarks interact through the corresponding gauge quanta, the gluons, described by the gauge potential $A_\mu(x)$. The latter is a vector field belonging to the $su(3)$ Lie algebra,

and transforming as

$$A_\mu(x) \rightarrow A_\mu^g(x) = g(x)A_\mu(x)g^{-1}(x) + g(x)\partial_\mu g^{-1}(x). \quad (2.2)$$

The covariant derivative D_μ ,

$$D_\mu = \partial_\mu + A_\mu, \quad (2.3)$$

transforms as follows

$$\begin{aligned} D_\mu(x) &\rightarrow D_\mu^g(x) = g(x)D_\mu(x)g^{-1}(x) \\ &= \partial_\mu + g(x)A_\mu(x)g^{-1}(x) + g(x)\partial_\mu g^{-1}(x). \end{aligned} \quad (2.4)$$

The curvature tensor

$$F_{\mu\nu} = [D_\mu, D_\nu] = \partial_\mu A_\nu - \partial_\nu A_\mu + [A_\mu, A_\nu]. \quad (2.5)$$

is an element of the $su(3)$ Lie algebra as well, and transforms as

$$F_{\mu\nu}(x) \rightarrow F_{\mu\nu}^g(x) = g(x)F_{\mu\nu}(x)g^{-1}(x). \quad (2.6)$$

With all these ingredients we can write down the QCD Lagrangian

$$\mathcal{L}_{\text{QCD}} = -\frac{1}{2g_0^2} \text{tr} \{F_{\mu\nu}F_{\mu\nu}\} + \sum_{f=1}^{N_f} \bar{\psi}_f(\not{D} + m_f)\psi_f, \quad (2.7)$$

where g_0 is the bare gauge coupling and the color indices are omitted. The last term in the r.h.s. of eq. (2.7) is the Dirac Lagrangian for N_f flavors, with the covariant derivative $\not{D} = D_\mu \gamma_\mu$, and m_f is the bare quark mass of the flavor f . We have chosen the Euclidean metric, and the definition of the Euclidean γ -matrices is given in App. A.

Given an operator \mathcal{O} , a gauge invariant product of fields, one computes its expectation value in QCD by evaluating

$$\langle \mathcal{O} \rangle_{\text{QCD}} = \frac{1}{\mathcal{Z}_{\text{QCD}}} \int_{\text{all fields}} \mathcal{O} e^{-\int d^4x \mathcal{L}_{\text{QCD}}}, \quad (2.8)$$

where \mathcal{Z}_{QCD} is the QCD partition function

$$\mathcal{Z}_{\text{QCD}} = \int_{\text{all fields}} e^{-\int d^4x \mathcal{L}_{\text{QCD}}}, \quad (2.9)$$

normalized in such a way that $\langle 1 \rangle_{\text{QCD}} = 1$. A more rigorous definition of the partition function and of the evaluation of the integral in eq. (2.8) is provided in the next chapter within the lattice regularization.

As shown in eq. (2.2), the gauge field A_μ non trivially transforms under the gauge group. As a consequence, the curvature tensor $F_{\mu\nu}$ is not gauge invariant, and thus not directly a physical observable.

At high energies, as in the SLAC-MIT deep inelastic scattering experiments, quarks behave almost like free particles, as indicated by the parton model. This property has been theoretically clarified in the early 1970s by Politzer, Gross and Wilczek [3, 4], and is known under the name of asymptotic freedom. Quarks are still bound inside the hadrons, and their binding force asymptotically vanishes as they get closer and closer. Corrections to the free quark theory can be computed by performing a perturbative expansion in powers of the coupling. As the coupling itself, these corrections vanish only in the infinite energy limit.

Increasing the distance between the quarks, the perturbative computations become less and less accurate. The coupling becomes stronger and stronger, compromising the accuracy of the perturbative expansion. As a consequence, no free quarks have ever been observed at large distance.

A complete study of the hadron properties requires one to be able to deal with both energy regimes, and this can be achieved only through non-perturbative methods, like lattice QCD.

2.2 Spin-flavor symmetry

Considering a meson composed by a heavy quark (e.g. the bottom quark) and a light antiquark, one is found to face a non-perturbative two-scale problem, which is difficult to be solved, with the Lagrangian in eq. (2.7), by brute force computations.

By taking the limit of infinite quark mass, important symmetries appear, which can be exploited to compute interesting meson properties. In this limit the heavy quark is static, i.e. it propagates only in time in the rest frame of the meson. The quark is surrounded by a complicated cloud of gluons and quark-antiquark pairs, and the light valence antiquark. They form the light degrees of freedom. They can see neither the flavor nor the spin of the static quark, because the latter is infinitely heavy; they just see it as a static source of color.

Since the flavor and the spin of the static quark are irrelevant, the symmetry group is $SU(2)$. In general one can consider the case of N_h heavy flavors, thus getting an $SU(2N_h)$ spin-flavor symmetry.

A simple physical picture of the system can be got by remembering that the heavy quark and the light antiquark are particles with spin $1/2$. The total spin operator and

its component along the \hat{z} axis are given respectively by

$$\vec{S} = \vec{S}_h + \vec{S}_l, \quad (2.10)$$

$$\vec{S}^z = \vec{S}_h^z + \vec{S}_l^z, \quad (2.11)$$

with eigenvalues $s(s+1)$ for $S^2 = \vec{S} \cdot \vec{S}$ and s_z for \vec{S}^z . It is then simple to construct a singlet with spin and parity $s^\pi = 0^-$, and a triplet with $s^\pi = 1^-$:

$$s^\pi = 1^- \Leftrightarrow \begin{cases} |1, +1\rangle = |\uparrow\uparrow\rangle, \\ |1, 0\rangle = \frac{1}{\sqrt{2}}(|\uparrow\downarrow\rangle + |\downarrow\uparrow\rangle), \\ |1, -1\rangle = |\downarrow\downarrow\rangle, \end{cases} \quad (2.12)$$

$$s^\pi = 0^- \Leftrightarrow |0, 0\rangle = \frac{1}{\sqrt{2}}(|\uparrow\downarrow\rangle - |\downarrow\uparrow\rangle), \quad (2.13)$$

where in the kets the numeric labels are the values of s and s_z , and the first arrow refers to the spin of the heavy quark along the \hat{z} axis, while the second arrow refers to that of the light antiquark.

In the infinite quark mass limit the spin \vec{S}_h of the heavy quark and the spin of the light antiquark \vec{S}_l are separately conserved by the strong interactions, and the four states in eqs. (2.12, 2.13) are degenerate in mass.

Nevertheless the system is still not trivial, because the interaction between the static quark and the light degrees of freedom is strong, and must be solved in a non-perturbative way.

The physical picture that we have just discussed corresponds to the leading order of the Heavy Quark Effective Theory (HQET) [13].

In nature the heavy quark has a finite mass, and the finite quark mass corrections can be systematically computed in HQET. The starting point for such computations is the Lagrangian derived in the next section.

2.3 The effective Lagrangian

In this section we derive the continuum effective Lagrangian of HQET at the classical level, following the idea of [14, 15].

The goal is to describe the dynamics of a hadron containing one heavy quark (e.g. the b-quark) and a light antiquark, in the frame where the hadron is at rest. As in

Sect. 2.1 we keep the Euclidean metric. We start from the QCD Lagrangian appearing in eq. (2.7), and focus our attention on the heavy flavor with mass m , dropping the corresponding flavor index to simplify the notation. The fermion part of the Lagrangian reads

$$\mathcal{L} = \bar{\psi}(\not{D} + m)\psi = \tilde{\psi}\mathcal{D}\psi, \quad (2.14)$$

$$\bar{\psi} = \tilde{\psi}\gamma_0, \quad \mathcal{D} = m\gamma_0 + D_0 + \gamma_0 D_k \gamma_k, \quad (2.15)$$

and, in analogy to the derivation of the corrections to the nonrelativistic approximation of QCD, we perform a Foldy-Wouthuysen transformation to derive the Lagrangian of a static quark, with the symmetry properties described in Sect. 2.2, and take into account the finite quark mass corrections through an expansion in powers of $1/m$. The transformation

$$\psi \rightarrow \eta = e^{iS}\psi, \quad \tilde{\psi} \rightarrow \tilde{\eta} = \tilde{\psi}e^{-iS}, \quad \mathcal{D} \rightarrow \mathcal{D}' = e^{iS}\mathcal{D}e^{-iS}, \quad (2.16)$$

with $S = -\frac{i}{2m}D_k\gamma_k$, leaves the Lagrangian invariant

$$\mathcal{L} \rightarrow \tilde{\eta}\mathcal{D}'\eta = \mathcal{L}, \quad (2.17)$$

and has the property

$$S = S^\dagger. \quad (2.18)$$

The hermicity in eq. (2.18) simply follows from the fact that in the Euclidean metric $D_k^\dagger = (\partial_k^\dagger + A_k^\dagger) = -D_k$ and $\gamma_k^\dagger = \gamma_k$ as shown in App. A. Further, the assumptions

$$D_0\psi = \mathcal{O}(m)\psi, \quad S\psi = \mathcal{O}(1/m)\psi, \quad (2.19)$$

are justified at the end of this section.

The new operator \mathcal{D}' can be computed by making use of the general identity

$$e^A B e^{-A} = \sum_{n=0}^{\infty} \frac{1}{n!} \underbrace{[A, [A, [\dots [A, B] \dots]]}_{n \text{ times}}, \quad (2.20)$$

obtained by a formal Taylor expansion of $e^{\varepsilon A} B e^{-\varepsilon A}$ at $\varepsilon = 1$, giving

$$\begin{aligned} \mathcal{D}' &= \mathcal{D} + [iS, \mathcal{D}] + \frac{1}{2}[iS, [iS, \mathcal{D}]] + \dots \\ &= \mathcal{D} + \frac{1}{2m}[D_k\gamma_k, \mathcal{D}] + \frac{1}{8m^2}[D_l\gamma_l, [D_k\gamma_k, \mathcal{D}]] + \mathcal{O}\left(\frac{1}{m^2}\right). \end{aligned} \quad (2.21)$$

In particular

$$\begin{aligned} [D_k\gamma_k, \mathcal{D}] &= mD_k[\gamma_k, \gamma_0] + [D_k, D_0]\gamma_k + [D_k\gamma_k, \gamma_0 D_n \gamma_n] \\ &= -2m\gamma_0 D_k \gamma_k + F_{k0}\gamma_k + [D_k\gamma_k, \gamma_0 D_n \gamma_n], \end{aligned} \quad (2.22)$$

where $F_{\mu\nu}$ is defined in eq. (2.5), and

$$[D_k \gamma_k, \gamma_0 D_n \gamma_n] = \gamma_0 [D_k, D_n] \gamma_n \gamma_k - 2\gamma_0 D_k D_k. \quad (2.23)$$

Inserting eq. (2.22) into the r.h.s. of eq. (2.21), and using eq. (2.23) in the second step, gives

$$\begin{aligned} \mathcal{D}' &= \mathcal{D} + \frac{1}{2m} [D_k \gamma_k, \mathcal{D}] - \frac{1}{4m} [D_l \gamma_l, \gamma_0 D_k \gamma_k] + \mathcal{O}\left(\frac{1}{m^2}\right) \\ &= \mathcal{D} + \frac{1}{2m} \left(-2m\gamma_0 D_k \gamma_k + F_{k0} \gamma_k + D_{\text{spin}} - \gamma_0 D^2 \right) + \mathcal{O}\left(\frac{1}{m^2}\right), \end{aligned} \quad (2.24)$$

with

$$D_{\text{spin}} = -\frac{1}{2} \gamma_0 [D_k, D_l] \gamma_k \gamma_l = -\frac{1}{2i} \gamma_0 [D_k, D_l] \sigma_{kl}, \quad (2.25)$$

$$\sigma_{kl} = \frac{i}{2} [\gamma_k, \gamma_l], \quad D^2 = D_k D_k. \quad (2.26)$$

We are now ready to write eq. (2.24) in the form

$$\mathcal{D}' = \gamma_0 \left\{ \gamma_0 D_0 + m + \frac{1}{2m} \left(-D^2 - \frac{1}{2i} F_{kl} \sigma_{kl} + F_{k0} \gamma_0 \gamma_k \right) \right\} + \mathcal{O}\left(\frac{1}{m^2}\right). \quad (2.27)$$

Through the projectors $P_{\pm} = (1 \pm \gamma_0)/2$ we split the fields ψ and $\bar{\psi}$ in their upper and lower components

$$\psi_h = P_+ \psi \bar{\psi}_h = \bar{\psi} P_+, \quad (2.28)$$

$$\psi_{\bar{h}} = P_- \psi \bar{\psi}_{\bar{h}} = \bar{\psi} P_-, \quad (2.29)$$

letting us write the Lagrangian as

$$\mathcal{L} = \mathcal{L}_h^{\text{stat}} + \mathcal{L}_{\bar{h}}^{\text{stat}} + \left(\mathcal{L}_h^{(1)} + \mathcal{L}_{\bar{h}}^{(1)} + \mathcal{L}_{h\bar{h}}^{(1)} \right) + \mathcal{O}\left(\frac{1}{m^2}\right), \quad (2.30)$$

$$\mathcal{L}_h^{\text{stat}} = \bar{\psi}_h (D_0 + m) \psi_h, \quad (2.31)$$

$$\mathcal{L}_{\bar{h}}^{\text{stat}} = \bar{\psi}_{\bar{h}} (-D_0 + m) \psi_{\bar{h}}, \quad (2.32)$$

$$\mathcal{L}_h^{(1)} = \frac{1}{2m} \bar{\psi}_h \left(-D^2 - \frac{1}{2i} F_{kl} \sigma_{kl} \right) \psi_h, \quad (2.33)$$

$$\mathcal{L}_{\bar{h}}^{(1)} = \frac{1}{2m} \bar{\psi}_{\bar{h}} \left(-D^2 - \frac{1}{2i} F_{kl} \sigma_{kl} \right) \psi_{\bar{h}}, \quad (2.34)$$

$$\mathcal{L}_{h\bar{h}}^{(1)} = \frac{1}{2m} \left\{ \bar{\psi}_h F_{k0} \gamma_k \psi_{\bar{h}} + \bar{\psi}_{\bar{h}} F_{k0} \gamma_k \psi_h \right\}. \quad (2.35)$$

For our purposes we can drop the term $\mathcal{L}_{h\bar{h}}^{(1)}$, because it does not contribute in the computation of correlation functions involving only a heavy quark (or antiquark). Only double insertions of this term would contribute, and they are of order $1/m^2$.

The fields ψ_h , $\bar{\psi}_h$, $\psi_{\bar{h}}$ and $\bar{\psi}_{\bar{h}}$ actually have only two Dirac components. Nevertheless we keep the four components notation, with two vanishing components for each field.

Inspection of the Dirac equation, obtained from the static Lagrangians $\mathcal{L}_h^{\text{stat}}$ and $\mathcal{L}_{\bar{h}}^{\text{stat}}$, justifies the kinematics $D_0\psi = O(m)\psi$ given in (2.19). To prove the second equation in (2.19), we start from the observation that a very heavy quark inside a hadron moves with essentially the hadron's velocity and is almost on-shell. We can write its momentum as $P = m + k$, with k “measuring” its off-shellness and $k \ll m$. This quantity is often referred to as residual momentum. Interactions of the heavy quark with the light degrees of freedom change it by an amount of order $\Delta k \sim \Lambda_{\text{QCD}}$, and the lowest order, in the $1/m$ expansion of the Lagrangian, where it is taken into account is in $\mathcal{L}_h^{(1)}$, through the operator D_k . It is thus correct to state that $S\psi = O(\Lambda_{\text{QCD}}/m)\psi$, but in this section we are discussing the classical theory, where Λ_{QCD} makes no sense, and it would then be more appropriate to write $S\psi = O(\varepsilon)\psi$. In a somewhat sloppy notation, we write $O(1/m)$ instead of $O(\varepsilon)$.

Finally we would like to get rid of the mass term appearing in $\mathcal{L}_h^{\text{stat}}$ and $\mathcal{L}_{\bar{h}}^{\text{stat}}$. This can be easily achieved by observing that the operators appearing in the $O(1/m)$ correction terms, namely D^2 and $F_{kl}\sigma_{kl}$ in eq. (2.33) and eq. (2.34) respectively, commute with γ_0 , and we redefine the fields according to

$$\psi_h \rightarrow e^{-m\gamma_0 x_0} \psi_h, \quad \bar{\psi}_h \rightarrow \bar{\psi}_h e^{m\gamma_0 x_0}, \quad (2.36)$$

$$\psi_{\bar{h}} \rightarrow e^{m\gamma_0 x_0} \psi_{\bar{h}}, \quad \bar{\psi}_{\bar{h}} \rightarrow \bar{\psi}_{\bar{h}} e^{-m\gamma_0 x_0}, \quad (2.37)$$

where x_0 is the usual time coordinate. This has exactly the effect of cancelling the mass term in $\mathcal{L}_h^{\text{stat}}$ and $\mathcal{L}_{\bar{h}}^{\text{stat}}$, which now read

$$\mathcal{L}_h^{\text{stat}} = \bar{\psi}_h (D_0 + \varepsilon^+) \psi_h, \quad (2.38)$$

$$\mathcal{L}_{\bar{h}}^{\text{stat}} = \bar{\psi}_{\bar{h}} (-D_0 + \varepsilon^+) \psi_{\bar{h}}, \quad (2.39)$$

where the infinitesimal, positive ε^+ prescription plays the role of selecting the appropriate time propagation.

Notice that dropping the mass term in $\mathcal{L}_h^{\text{stat}}$ and $\mathcal{L}_{\bar{h}}^{\text{stat}}$, corresponds exactly to an energy shift by an amount of m in all single heavy quark (or antiquark) states.

2.4 Symmetries of the effective Lagrangian

We focus our attention on the heavy quark static Lagrangian of eq. (2.38) (the antiquark case is analogous), and we now show that it is invariant under the symmetries described in Sect. 2.2, which are absent in finite mass QCD.

The spin symmetry can be seen as invariance under the rotations [13, 16, 17]

$$\psi_h \rightarrow V \psi_h, \quad \bar{\psi}_h \rightarrow \bar{\psi}_h V^{-1}, \quad V = \exp \left\{ -i \phi_i \varepsilon_{ijk} \sigma_{jk} \right\}, \quad (2.40)$$

with ϕ_i an arbitrary parameter. This simply follows from the fact that σ_{jk} commutes with γ_0 , as noticed in Sect. 2.3.

Another symmetry, corresponding to the local conservation of the quark number, is the invariance under phase transformations [18]

$$\psi_h \rightarrow e^{i\eta(\mathbf{x})} \psi_h, \quad \bar{\psi}_h \rightarrow \bar{\psi}_h e^{-i\eta(\mathbf{x})}, \quad (2.41)$$

where it is important to underline that the parameter $\eta(\mathbf{x})$ is time independent; it depends only on the spatial coordinates. The proof is trivial, because in the static Lagrangian only the time derivative appears.

The symmetry under rotations in flavor space mentioned in Sect. 2.2 is irrelevant in our case, because we have only one heavy flavor.

These symmetries are broken by the $O(1/m)$ correction terms. We adopt a more compact notation for the operators in eq. (2.33)

$$\mathcal{L}_h^{(1)} = -\frac{1}{2m} (\mathcal{O}_{\text{kin}} + \mathcal{O}_{\text{spin}}), \quad (2.42)$$

$$\mathcal{O}_{\text{kin}} = \bar{\psi}_h D_k D_k \psi_h = \bar{\psi}_h D^2 \psi_h, \quad (2.43)$$

$$\mathcal{O}_{\text{spin}} = \bar{\psi}_h \frac{1}{2i} F_{kl} \sigma_{kl} \psi_h = \bar{\psi}_h \boldsymbol{\sigma} \cdot \mathbf{B} \psi_h. \quad (2.44)$$

The kinetic operator \mathcal{O}_{kin} does not break the spin symmetry (eq. (2.40)). It describes, at leading order in the $1/m$ expansion, the spatial motion of the heavy quark.

The spin symmetry is broken by the ‘‘hyperfine’’ chromo-magnetic term $\mathcal{O}_{\text{spin}}$, which is obviously invariant under the phase transformations described in (2.41).

2.5 Renormalization of the effective theory

The leading order Lagrangian, eq. (2.38), contains local fields of mass dimension $d \leq 4$, and it is thus power counting renormalizable. At this order only a finite number of counterterms are needed. The latter must be compatible with the symmetries described in the previous section, and the only possible counterterm with dimension $d \leq 4$, involving the fields $\bar{\psi}_h$ and ψ_h , and invariant under the symmetries of the static action, is $\bar{\psi}_h \psi_h$.

Indicating with δm its coefficient, one is thus left with the formal static Lagrangian

$$\mathcal{L}_h^{\text{stat}} = \bar{\psi}_h (D_0 + \delta m) \psi_h. \quad (2.45)$$

As noticed in Sect. 2.3, such a term amounts only to an energy shift of exactly δm for all single heavy quark states.

If we now allow finite quark mass corrections, we can use the HQET Lagrangian

$$\mathcal{L}_h^{\text{HQET}} = \mathcal{L}_h^{\text{stat}} + \mathcal{L}_h^{(1)} + \mathcal{O}\left(\frac{1}{m^2}\right). \quad (2.46)$$

The renormalization of the operators appearing in $\mathcal{L}_h^{(1)}$ may introduce new terms compatible with the symmetries of the theory and dimension $d \leq 5$. Under these constraints no new terms are needed, and the coefficients of the operators \mathcal{O}_{kin} and $\mathcal{O}_{\text{spin}}$ are only parameters depending on the bare coupling and on the mass m . The $\mathcal{O}(1/m)$ Lagrangian has thus the form

$$\mathcal{L}_h^{(1)} = -(\omega_{\text{kin}} \mathcal{O}_{\text{kin}} + \omega_{\text{spin}} \mathcal{O}_{\text{spin}}), \quad (2.47)$$

$$\omega_{\text{kin}} = \mathcal{O}\left(\frac{1}{m}\right), \quad \omega_{\text{spin}} = \mathcal{O}\left(\frac{1}{m}\right). \quad (2.48)$$

Since $\mathcal{L}_h^{(1)}$ contains dimension five operators, one may conclude that, for dimensional reasons the theory is not renormalizable. This happens to be true for NRQCD, but not for HQET [19].

We consider an operator $\mathcal{O}(x)$ containing light and heavy degrees of freedom, and we expand it at tree-level in a power series in $1/m$,

$$\mathcal{O}(x) = \sum_{\nu=0}^n \mathcal{O}^{(\nu)}(x), \quad \mathcal{O}^{(\nu)}(x) = \sum_i \alpha_i^{(\nu)} \mathcal{O}_i^{(\nu)}(x), \quad (2.49)$$

with $\mathcal{O}_i^{(\nu)}$ of dimension $3 + \nu$ and $\alpha_i^{(\nu)} = \mathcal{O}(1/m^\nu)$. The terms of the expansion can be obtained by applying a Foldy-Wouthuysen transformation as in Sect. 2.3. A typical example is the $\mu = 0$ component of heavy-light axial vector current $A_\mu(x)$,

$$A_\mu(x) = \bar{\psi}_1(x) \gamma_\mu \gamma_5 \psi(x), \quad (2.50)$$

giving

$$A^{(0)}(x) = \alpha_0^{(0)} A_0^{\text{stat}}(x), \quad A_0^{\text{stat}}(x) = \bar{\psi}_1(x) \gamma_0 \gamma_5 \psi_h(x), \quad (2.51)$$

$$A^{(1)}(x) = \alpha_1^{(1)} A_1^{(1)}(x), \quad A_1^{(1)}(x) = \bar{\psi}_1(x) \gamma_j \gamma_5 \overleftarrow{D}_j \psi_h(x), \quad (2.52)$$

with $\alpha_0^{(0)} = 1$ and $\alpha_1^{(1)} = 1/m$.

To evaluate the expectation value (e.g. between two heavy-light meson states) of the operator in HQET, we introduce the partition function

$$\begin{aligned}\mathcal{Z}_{\text{HQET}} &= \int_{\bar{\psi}_h, \psi_h, U_1} e^{-\int_x (\mathcal{L}_h^{\text{HQET}}[\bar{\psi}_h(x), \psi_h(x), U_1(x)] + \mathcal{L}_{\text{light}}[U_1(x)])} \\ &= \int_{\bar{\psi}_h, \psi_h, U_1} e^{-\int_x (\mathcal{L}_h^{\text{stat}}[\bar{\psi}_h(x), \psi_h(x), U_1(x)] + \mathcal{L}_{\text{light}}[U_1(x)])} \\ &\quad \times \left\{ 1 - \int_x \mathcal{L}_h^{(1)}[\bar{\psi}_h(x), \psi_h(x), U_1(x)] + \mathcal{O}\left(\frac{1}{m^2}\right) \right\},\end{aligned}\quad (2.53)$$

where U_1 is a shorthand for the light degrees of freedom, and $\mathcal{L}_{\text{light}}$ the corresponding Lagrangian. A more rigorous definition of the partition function is given in the next chapter. From eq. (2.49) it follows that the expectation value of $\mathcal{O}(x)$ is defined as

$$\begin{aligned}\langle \mathcal{O}(x) \rangle_{\text{HQET}} &\equiv \langle \mathcal{O}^{(0)}(x) \rangle_{\text{stat}} + \langle \mathcal{O}^{(1)}(x) \rangle_{\text{stat}} \\ &\quad + \omega_{\text{kin}} \langle \mathcal{O}^{(0)}(x) \int_y \mathcal{O}_{\text{kin}}(y) \rangle_{\text{stat}} \\ &\quad + \omega_{\text{spin}} \langle \mathcal{O}^{(0)}(x) \int_y \mathcal{O}_{\text{spin}}(y) \rangle_{\text{stat}} + \mathcal{O}\left(\frac{1}{m^2}\right),\end{aligned}\quad (2.54)$$

where

$$\langle \mathcal{O} \rangle_{\text{stat}} = \frac{1}{\mathcal{Z}_{\text{stat}}} \int_{\bar{\psi}_h, \psi_h, U_1} \mathcal{O} e^{-\int_x (\mathcal{L}_h^{\text{stat}}[\bar{\psi}_h(x), \psi_h(x), U_1(x)] + \mathcal{L}_{\text{light}}[U_1(x)])}, \quad (2.55)$$

and the path integral is normalized by $\mathcal{Z}_{\text{stat}}$ such that $\langle 1 \rangle_{\text{stat}} = 1$. It is clear from eq. (2.54) and eq. (2.55) that the expectation values are evaluated with respect to the leading order of the HQET action, which is power counting renormalizable.

The operator \mathcal{O} has still to be renormalized, and eq. (2.54) tells us that this is just a problem of renormalizing correlation functions of local composite operators in the static effective theory. One has to include all local operators with dimension not exceeding n , the one of the highest-dimensional operator, and compatible with the symmetries of the theory. Being interested in the continuum theory up to $\mathcal{O}(1/m^2)$, we have $n = 5$. The coefficients are then computed by requiring the cancellation of the divergences and the respect of the imposed renormalization conditions of all expectation values [20].

The sums over all space-time coordinates in eq. (2.54) may lead to additional singularities due to contact terms. However the terms needed to remove these singularities must respect the dimensional and symmetry properties described above, and they are already included in the expansion in eq. (2.54).

As a regularization of the theory breaks scale invariance, there exist power divergences in the $O(1/m)$ corrections to the HQET matrix elements [21]. These divergences must be subtracted non-perturbatively. This fact is simply due to the mixing of operators of different dimensions in HQET Lagrangian. To explain it in a simple way, let us consider the Lagrangian in eq. (2.46) with the $O(1/m)$ term given in eq. (2.47). To regularize the theory we can take a lattice discretization with lattice spacing a . Because of the mixing between the operator D^2 appearing in \mathcal{O}_{kin} and $D_0\gamma_0$ from the static Lagrangian, a perturbative estimate of ω_{kin} at order g_0^{2l} would leave a perturbative remainder

$$\Delta\omega_{\text{kin}} \sim g_0^{2(l+1)} a^{-1} \sim a^{-1} [\ln(a\Lambda_{\text{QCD}})]^{-(l+1)} \xrightarrow{a \rightarrow 0} \infty. \quad (2.56)$$

This means that the theory is still affected by ultraviolet divergences and is not renormalizable in perturbation theory. If one considers higher orders in the $1/m$ expansion, further UV-divergences can appear because of operator mixings, but they are not discussed here.

2.6 Matching of the effective theory with QCD

The effective Lagrangian and the effective matrix elements derived in the previous sections correctly reproduce the long-distance physics of the full theory. However the light degrees of freedom interact with the heavy quark exchanging momenta, which can be soft or hard. Soft momenta correspond to long wavelengths, and they are well identified by using the partition function in eq. (2.53). Hard momenta can resolve the short-distance properties of the heavy quark, which are truncated in the expansion of eq. (2.54). It means that short-distance corrections are needed in order to produce a predictive description of the heavy-light mesons. They introduce a logarithmic dependence on the heavy quark mass m through the strong coupling constant $\bar{g}(m)$. Given the smallness of the latter, they can be safely computed in perturbation theory, by performing the matching to QCD of the matrix elements computed in the effective theory.

Here the quark mass m is renormalized and defined at the scale $\mu = m$ itself. The exact definition of the renormalization procedure is irrelevant for the present discussion. The dependence on the space-time coordinates is omitted throughout the following in order to lighten the notation.

We consider a matrix element $\langle \mathcal{O}(\mu, m)_{\text{R}} \rangle_{\text{QCD}}$ computed in QCD, and renormalized at the scale μ . The matching means that we require it to be equal to the matrix element of the same operator computed in the effective theory up to $O(1/m)$. The

equivalence is achieved through the Wilson coefficient $C_{\mathcal{O},\text{match}}(\mu, m)$

$$\langle \mathcal{O}_{\text{R}}(\mu, m) \rangle_{\text{QCD}} = C_{\mathcal{O},\text{match}}(\mu, m) \langle \mathcal{O}_{\text{R}}(\mu) \rangle_{\text{stat}} + \mathcal{O}\left(\frac{1}{m}\right). \quad (2.57)$$

For our purposes it is convenient to renormalize the operator in the effective theory in the $\overline{\text{MS}}$ scheme [22, 23], thus having an expansion

$$C_{\mathcal{O},\text{match}}(\mu, m) = 1 + c_1^{\mathcal{O}}(\mu, m) \bar{g}_{\overline{\text{MS}}}^2(\mu) + \mathcal{O}(\bar{g}_{\overline{\text{MS}}}^4(\mu)), \quad (2.58)$$

with $\bar{g}_{\overline{\text{MS}}}$ being the renormalized coupling in the $\overline{\text{MS}}$ scheme. The relation between the renormalized operator appearing on the r.h.s. of eq. (2.57) and the bare one can be written in the form

$$\mathcal{O}_{\overline{\text{MS}}}(\mu) = Z^{\mathcal{O},\overline{\text{MS}}}(\mu) \mathcal{O}. \quad (2.59)$$

The scale dependence of the renormalization factor is governed by the renormalization group equation

$$\gamma^{\mathcal{O},\overline{\text{MS}}}(\bar{g}_{\overline{\text{MS}}}(\mu)) = \mu \frac{\partial \ln Z^{\mathcal{O},\overline{\text{MS}}}(\mu)}{\partial \mu}, \quad (2.60)$$

and the renormalization group function γ , the anomalous dimension, has a perturbative expansion ($\bar{g} = \bar{g}_{\overline{\text{MS}}}(\mu)$),

$$\gamma^{\mathcal{O},\overline{\text{MS}}}(\bar{g}) \stackrel{\bar{g} \rightarrow 0}{\sim} -\bar{g}^2 \left\{ \gamma_0^{\mathcal{O},\overline{\text{MS}}} + \gamma_1^{\mathcal{O},\overline{\text{MS}}} \bar{g}^2 + \gamma_2^{\mathcal{O},\overline{\text{MS}}} \bar{g}^4 + \dots \right\}. \quad (2.61)$$

The same holds for the renormalized coupling

$$\mu \frac{\partial \bar{g}}{\partial \mu} = \beta_{\overline{\text{MS}}}(\bar{g}) \stackrel{\bar{g} \rightarrow 0}{\sim} -\bar{g}^3 \left\{ b_0 + b_1 \bar{g}^2 + b_2^{\overline{\text{MS}}} \bar{g}^4 + \dots \right\}. \quad (2.62)$$

The coefficients b_0 and b_1 are universal, whereas the higher order coefficients, here $b_2^{\overline{\text{MS}}}, b_3^{\overline{\text{MS}}}, \dots$, depend on the chosen renormalization scheme.

The scale dependence of $\langle \mathcal{O}_{\text{R}}(\mu) \rangle_{\text{stat}} = \langle \mathcal{O}_{\overline{\text{MS}}}(\mu) \rangle_{\text{stat}}$ is removed by introducing the renormalization group invariant (RGI) matrix element $\langle \mathcal{O}_{\text{RGI}} \rangle_{\text{stat}}$, defined as

$$\begin{aligned} \langle \mathcal{O}_{\text{RGI}} \rangle_{\text{stat}} &= \langle \mathcal{O}_{\overline{\text{MS}}}(\mu) \rangle_{\text{stat}} [2b_0 \bar{g}^2(\mu)]^{-\gamma_0^{\mathcal{O},\overline{\text{MS}}}/(2b_0)} \\ &\times \exp \left\{ - \int_0^{\bar{g}(\mu)} dg \left[\frac{\gamma^{\mathcal{O},\overline{\text{MS}}}(g)}{\beta_{\overline{\text{MS}}}(g)} - \frac{\gamma_0^{\mathcal{O},\overline{\text{MS}}}}{b_0 g} \right] \right\}. \end{aligned} \quad (2.63)$$

With the same technique one is able to compute the RGI matrix element in QCD, and by setting the renormalization scale to the heavy quark mass, the matching condition now reads

$$\langle \mathcal{O}_{\text{RGI}}(m) \rangle_{\text{QCD}} = C_{\mathcal{O}}(m) \langle \mathcal{O}_{\text{RGI}} \rangle_{\text{stat}} + \mathcal{O}\left(\frac{1}{m}\right), \quad (2.64)$$

where the matching coefficient $C_{\mathcal{O}}(m)$ is defined through eqs. (2.57, 2.64)

$$C_{\mathcal{O}}(m) = C_{\mathcal{O},\text{match}}(m, m) \frac{\langle \mathcal{O}_{\overline{\text{MS}}}(m) \rangle_{\text{stat}}}{\langle \mathcal{O}_{\text{RGI}} \rangle_{\text{stat}}} \frac{\langle \mathcal{O}_{\text{RGI}}(m) \rangle_{\text{QCD}}}{\langle \mathcal{O}_{\text{R}}(m, m) \rangle_{\text{QCD}}}. \quad (2.65)$$

This equation allows to define the anomalous dimension γ_{match} in the matching scheme through

$$C_{\mathcal{O}}(m) = [2b_0 \bar{g}^2(m)]^{\gamma_0^{\mathcal{O}}/(2b_0)} \times \exp \left\{ \int_0^{\bar{g}(m)} dg \left[\frac{\gamma_{\text{match}}^{\mathcal{O}}(g)}{\beta_{\overline{\text{MS}}}(g)} - \frac{\gamma_0^{\mathcal{O}}}{b_0 g} \right] \right\}, \quad (2.66)$$

$$\gamma_{\text{match}}^{\mathcal{O}}(\bar{g}) \stackrel{\bar{g} \rightarrow 0}{\sim} -\bar{g}^2 \left\{ \gamma_0^{\mathcal{O}} + \gamma_1^{\mathcal{O}} \bar{g}^2 + \gamma_2^{\mathcal{O}} \bar{g}^4 + \dots \right\} \quad \bar{g} = \bar{g}_{\overline{\text{MS}}}. \quad (2.67)$$

In the case where the operator \mathcal{O} is the axial vector current defined in eq. (2.50), the corresponding renormalization is fixed by the chiral Ward identities, which imply the independence on a renormalization scale. This simplifies the r.h.s of eq. (2.65), because the second ratio from the left becomes one.

From eqs. (2.58, 2.66, 2.67) it is straightforward to collect the several contributions entering in $\gamma_{\text{match}}^{\mathcal{O}}$, namely

$$\gamma_0^{\mathcal{O}} = \gamma_0^{\mathcal{O},\overline{\text{MS}}}, \quad \gamma_1^{\mathcal{O}} = \gamma_1^{\mathcal{O},\overline{\text{MS}}} + 2b_0 c_1^{\mathcal{O}}(m, m), \quad \dots \quad (2.68)$$

Finally we would like to get rid of the scale dependence of the heavy quark mass. The scale evolution of the latter is given by the renormalization group equation

$$\mu \frac{\partial m}{\partial \mu} = \tau(\bar{g}) m, \quad (2.69)$$

$$\tau(\bar{g}) \stackrel{\bar{g} \rightarrow 0}{\sim} -\bar{g}^2 \{ d_0 + d_1 \bar{g}^2 + d_2 \bar{g}^4 + \dots \}, \quad (2.70)$$

where only the coefficient d_0 is scheme-independent. We thus introduce the RGI and scheme-independent quark mass M , as the asymptotic behavior of any mass $m(\mu)$

$$M = \lim_{\mu \rightarrow \infty} m(\mu) [2b_0 \bar{g}^2(\mu)]^{-d_0/2b_0}. \quad (2.71)$$

Chapter 3

The Schrödinger functional

3.1 Definition

At the classical level the transition from some initial field configuration at time $x_0 = 0$ to a final configuration at $x_0 = T$ is given in terms of only one path, the classical path, which satisfies the principle of least action. In quantum field theory the transition can take place in more than one way, and the total amplitude is the coherent sum of the amplitudes for each way.

Following Feynman, this sum can be written as a path integral, where, in the functional integral formalism, all field configurations are integrated over. The Schrödinger functional (SF) is defined as the integral kernel of the whole transition amplitude.

The following description of the Schrödinger functional in SU(3) gauge theory is carried out with the Euclidean metric following [24] for the gauge part, and [25] for the fermionic part. The transition amplitude that we would like to compute is

$$\mathcal{Z}[\phi_{\text{fin}}, \phi_{\text{in}}] = \langle \phi_{\text{fin}} | e^{-\mathbb{H}T} | \phi_{\text{in}} \rangle, \quad (3.1)$$

where \mathbb{H} is the Hamilton operator. The starting point is now the definition of the quantum mechanical states in the Schrödinger representation.

In order to facilitate the passage to the lattice formulation we start with QCD at a fixed time slice, say $x_0 = 0$, and on a finite spatial volume, a box of size $L \times L \times L$ and periodic boundary conditions. Gauge fields are represented by the vector potentials $A_\mu(\mathbf{x})$, and we work in the temporal gauge, i.e. with $A_0(\mathbf{x}) = 0$. The fields $A_k(\mathbf{x})$ are periodic in space and transform under a gauge transformation according to

$$A_k^\Lambda(\mathbf{x}) = \Lambda(\mathbf{x})A_k(\mathbf{x})\Lambda^{-1}(\mathbf{x}) + \Lambda(\mathbf{x})\partial_k\Lambda^{-1}(\mathbf{x}). \quad (3.2)$$

To preserve the periodicity we admit only periodic gauge functions $\Lambda(\mathbf{x})$

$$A_k(\mathbf{x} + L\hat{k}) = A_k(\mathbf{x}), \quad \Lambda(\mathbf{x} + L\hat{k}) = \Lambda(\mathbf{x}). \quad (3.3)$$

The Schrödinger representation of a quantum mechanical state is the wave functional $\psi[A]$, and a scalar product of two functionals ψ and χ is defined by

$$\langle \psi | \chi \rangle = \int \mathcal{D}[A] \psi[A]^* \chi[A], \quad \mathcal{D}[A] = \prod_{\mathbf{x}, k} dA_k(\mathbf{x}). \quad (3.4)$$

Here, and in the following of this section, color indices have been dropped to lighten the notation. It is understood that $dA_k(\mathbf{x}) = \prod_a dA_k^a(\mathbf{x})$.

In eq. (3.4) only gauge invariant states with $\psi[A^\Lambda] = \psi[A]$ are physical. For any functional $\psi[A]$ the projection onto the physical subspace is achieved by applying the projector \mathbb{P} according to

$$\mathbb{P}\psi[A] = \int \mathcal{D}[\Lambda] \psi[A^\Lambda], \quad \mathcal{D}[\Lambda] = \prod_{\mathbf{x}} d\Lambda(\mathbf{x}), \quad (3.5)$$

where $d\Lambda(\mathbf{x})$ denotes the SU(3) Haar measure.

The Hamilton operator appearing in eq. (3.1) is defined through the curvature tensor (2.5), giving

$$\mathbb{H} = \int_0^L d^3\mathbf{x} \left\{ \frac{g_0^2}{2} \text{tr} \{ F_{0k}(\mathbf{x}) F_{0k}(\mathbf{x}) \} + \frac{1}{4g_0^4} \text{tr} \{ F_{kl}(\mathbf{x}) F_{kl}(\mathbf{x}) \} \right\}. \quad (3.6)$$

Each classical gauge field $C_k(\mathbf{x})$ defines a state $|C\rangle$ and the functional

$$\langle C | \psi \rangle = \psi[C]. \quad (3.7)$$

In general the state $|C\rangle$ is not gauge invariant, but it can be projected onto the corresponding physical subspace through the projector \mathbb{P} .

Given two classical gauge fields C and C' , the first living on the time slice at $x_0 = 0$, the second at $x_0 = T$, we define the Euclidean Schrödinger functional as

$$\mathcal{Z}[C', C] = \langle C' | e^{-\mathbb{H}T} \mathbb{P} | C \rangle. \quad (3.8)$$

Its gauge invariance

$$\mathcal{Z}[C'^\Lambda, C^\Lambda] = \mathcal{Z}[C', C], \quad (3.9)$$

is guaranteed by the integral over Λ in eq. (3.5).

We now have all ingredients to express a matrix element of the time evolution operator $e^{-\mathbb{H}T}$ in terms of the gauge fields $A_\mu(x)$ and the corresponding gauge action in four dimensions, where the time extent is $0 \leq x_0 \leq T$. We impose Dirichlet boundary conditions in time

$$A_k(x) = \begin{cases} C_k^\Lambda(\mathbf{x}) & \text{at } x_0 = 0, \\ C'_k(\mathbf{x}) & \text{at } x_0 = T, \end{cases} \quad (3.10)$$

and we finally write down the functional integral as

$$\mathcal{Z}[C', C] = \int D[\Lambda] \int D[A] e^{-S_{\text{gauge}}[A]}, \quad (3.11)$$

where the gauge action can be obtained from eq. (2.7)

$$S_{\text{gauge}}[A] = -\frac{1}{2g_0^2} \int d^4x \operatorname{tr} \{F_{\mu\nu} F_{\mu\nu}\}, \quad (3.12)$$

and the integration measure is now

$$D[A] = \prod_{x,\mu} dA_\mu(x). \quad (3.13)$$

The integral (3.11) and the boundary conditions (3.10) are invariant under the gauge transformation

$$A_\mu(x) \rightarrow A_\mu^\Omega(x) = \Omega(x) A_\mu(x) \Omega^{-1}(x) + \Omega(x) \partial_\mu \Omega^{-1}(x), \quad (3.14)$$

$$\Lambda(\mathbf{x}) \rightarrow \Lambda^\Omega(\mathbf{x}) = \Omega(x)|_{x_0=0} \Lambda(\mathbf{x}), \quad (3.15)$$

with the necessary condition

$$\Omega(x)|_{x_0=T} = 1. \quad (3.16)$$

For QCD, the inclusion of the quarks as dynamical variables in the path integral can be carried out in a similar way. Nevertheless, imposing Dirichlet boundary conditions on the quark fields requires some attention. This is due to the fact that the Dirac equation is a first order differential equation. In the Schrödinger functional the dynamical degrees of freedom of the quark fields are their components at $0 < x_0 < T$. In order to have a unique solution of the Dirac equation, at the boundaries only half of the Dirac components are defined, and are fixed to be

$$P_+ \psi(x)|_{x_0=0} = \rho(\mathbf{x}), \quad P_- \psi(x)|_{x_0=T} = \rho'(\mathbf{x}), \quad (3.17)$$

$$\bar{\psi}(x) P_- |_{x_0=0} = \bar{\rho}(\mathbf{x}), \quad \bar{\psi}(x) P_+ |_{x_0=T} = \bar{\rho}'(\mathbf{x}), \quad (3.18)$$

where the projectors $P_{\pm} = (1 \pm \gamma_0)/2$ are the same as in Sect. 2.3. It is then evident that

$$P_- \rho(\mathbf{x}) = P_+ \rho'(\mathbf{x}) = \bar{\rho}(\mathbf{x}) P_+ = \bar{\rho}'(\mathbf{x}) P_- = 0. \quad (3.19)$$

In the space direction \hat{k} the quark fields are periodic up to a phase factor θ

$$\psi(x + L\hat{k}) = e^{i\theta} \psi(x), \quad \bar{\psi}(x + L\hat{k}) = \bar{\psi}(x) e^{-i\theta}. \quad (3.20)$$

With these boundaries one finds that the fermionic part of the continuum action (for one flavor) is

$$\begin{aligned} S_{\text{quark}}[A, \bar{\psi}, \psi] &= \int_0^T dx_0 \int_0^L d^3 \mathbf{x} \bar{\psi}(x) \{D_{\mu} \gamma_{\mu} + m\} \psi(x) \\ &\quad - \int_0^L d^3 \mathbf{x} [\bar{\psi}(x) P_- \psi(x)]_{x_0=0} - \int_0^L d^3 \mathbf{x} [\bar{\psi}(x) P_+ \psi(x)]_{x_0=T}. \end{aligned} \quad (3.21)$$

As pointed out in [25], the presence of the boundary terms is due to the requirement for the classical action to be a parity-invariant functional acting on the space of analytical functions, which satisfy the boundary conditions in eqs. (3.17, 3.18). The extension of the pure gauge Schrödinger functional (3.11) to QCD with one quark flavor has the path integral representation

$$\mathcal{Z}[C', \bar{\rho}', \rho', C, \bar{\rho}, \rho] = \int D[\Lambda] D[A] D[\bar{\psi}] D[\psi] e^{-S_{\text{gauge}}[A] - S_{\text{quark}}[A, \bar{\psi}, \psi]}. \quad (3.22)$$

We are left with the discussion of the static quarks. They propagate only forward in time, and they cannot thus cross the spatial borders. However, for later convenience, we formally impose periodic boundary conditions

$$\psi_{\text{h}}(x + L\hat{k}) = \psi_{\text{h}}(x), \quad \bar{\psi}_{\text{h}}(x + L\hat{k}) = \bar{\psi}_{\text{h}}(x). \quad (3.23)$$

Here there is no need to introduce a phase like in eqs. (3.20), because in the considered correlation functions, thanks to the U(1) symmetry under transformations like in (2.41) such a term is irrelevant.

At the time boundaries one has Dirichlet boundary conditions as for QCD, but the heavy quark fields have only two non-vanishing Dirac components, and the projectors are unnecessary

$$\psi_{\text{h}}(x)|_{x_0=0} = \rho_{\text{h}}(\mathbf{x}), \quad \bar{\psi}_{\text{h}}(x)|_{x_0=T} = \bar{\rho}_{\text{h}}(\mathbf{x}). \quad (3.24)$$

In analogy to eq. (3.21), the static quark action reads

$$\begin{aligned} S_{\text{heavy}}[A, \bar{\psi}_{\text{h}}, \psi_{\text{h}}] &= \int_0^T dx_0 \int_0^L d^3 \mathbf{x} \bar{\psi}_{\text{h}}(x) \{D_0 \gamma_0 + \delta m\} \psi_{\text{h}}(x) \\ &\quad - \int_0^L d^3 \mathbf{x} [\bar{\psi}_{\text{h}}(x) \psi_{\text{h}}(x)]_{x_0=T}, \end{aligned} \quad (3.25)$$

and the path integral representation of the Schrödinger functional is

$$\mathcal{Z}[C', \bar{\rho}'_h, C, \rho_h] = \int D[\Lambda] D[A] D[\bar{\psi}_h] D[\psi_h] e^{-S_{\text{gauge}}[A] - S_{\text{heavy}}[A, \bar{\psi}_h, \psi_h]}. \quad (3.26)$$

For completeness we give the heavy antiquark action too

$$S_{\text{heavy}}[A, \bar{\psi}_h, \psi_h] = \int_0^T dx_0 \int_0^L d^3 \mathbf{x} \bar{\psi}_h(x) \{-D_0 \gamma_0 + \delta m\} \psi_h(x) - \int_0^L d^3 \mathbf{x} [\bar{\psi}_h(x) \psi_h(x)]_{x_0=0}, \quad (3.27)$$

with boundary conditions

$$\psi_h(x + L\hat{k}) = \psi_h(x), \quad \bar{\psi}_h(x + L\hat{k}) = \bar{\psi}_h(x), \quad (3.28)$$

$$\psi_h(x)|_{x_0=T} = \rho'_h(\mathbf{x}), \quad \bar{\psi}_h(x)|_{x_0=0} = \bar{\rho}_h(\mathbf{x}). \quad (3.29)$$

3.2 Lattice formulation

To be able to compute interesting QCD and HQET matrix elements through the Schrödinger functional we introduce the lattice regularization. The latter is not unique, and a suitable choice, for our purposes, is explained in this section.

The space-time manifold is discretized in a regular hypercubic lattice. This hypercube preserves the volume $L \times L \times L \times T$ of the continuum, where L and T are now integers multiple of the lattice spacing a . A lattice point x , or site, is identified by the space-time coordinates (x_0, x_1, x_2, x_3) , where

$$x_\mu/a \in \mathbb{Z}^4, \quad 0 \leq x_0 \leq T, \quad 0 \leq x_k < L. \quad (3.30)$$

We define the SU(3) gauge fields through the assignment of a link variable $U_\mu(x) \in \text{SU}(3)$ to each pair of lattice points $(x, x + a\hat{\mu})$. The temporal link variables $U_0(x)$ are defined only for $0 \leq x_0 < T$.

Under a gauge transformation $\Omega(x)$, where $\Omega(x) \in \text{SU}(3)$ and $\Omega(x + L\hat{k}) = \Omega(x)$, the gauge links transform as

$$U_\mu(x) \rightarrow U_\mu^\Omega(x) = \Omega(x) U_\mu(x) \Omega^{-1}(x + a\hat{\mu}). \quad (3.31)$$

To be consistent with the continuum Schrödinger functional, we require the gauge links to be periodic in space

$$U_\mu(x + L\hat{k}) = U_\mu(x), \quad (3.32)$$

and to respect Dirichlet boundary conditions in time

$$U_k(x)|_{x_0=0} = W_k(\mathbf{x}), \quad U_k(x)|_{x_0=T} = W'_k(\mathbf{x}). \quad (3.33)$$

Instead, the temporal gauge links $U_0(x)|_{x_0=0}$ remain unconstrained. The fields W and W' are related to the continuum fields C and C' through

$$W_k(\mathbf{x}) = \mathcal{P} \exp \left\{ a \int_0^1 dt C_k(\mathbf{x} + a\hat{k} - ta\hat{k}) \right\}, \quad (3.34)$$

and analogously for W' and C' . In eq. (3.34) the symbol \mathcal{P} denotes the time-decreasing path ordering. We follow [5] and introduce the gauge action

$$S_G[U] = \frac{1}{g_0^2} \sum_p \omega(p) \text{tr} \{ 1 - U(p) \}, \quad (3.35)$$

where the sum is extended to all oriented plaquettes p , and $U(p)$ is the parallel transporter around p :

$$U(p) = U_\mu(x) U_\nu(x + a\hat{\mu}) U_\mu^{-1}(x + a\hat{\nu}) U_\nu^{-1}(x), \quad \mu \neq \nu. \quad (3.36)$$

In the tree-level improved theory the weight $\omega(p)$ is one except for the spatial plaquettes at the temporal boundaries, where $\omega(p) = 1/2$. It is then straightforward to write down the lattice Schrödinger functional in the pure gauge case

$$\mathcal{Z}[C', C] = \int D[U] e^{-S_G[U]}, \quad D[U] = \prod_{x,\mu} dU_\mu(x). \quad (3.37)$$

We now introduce the QCD Dirac-Wilson action for the quark fields living on the lattice sites x . To be able to write it in an elegant way, we define the discretized forward and backward covariant derivatives

$$\nabla_\mu \psi(x) = \frac{1}{a} [U_\mu(x) \psi(x + a\hat{\mu}) - \psi(x)], \quad (3.38)$$

$$\nabla_\mu^* \bar{\psi}(x) = \frac{1}{a} [\bar{\psi}(x) - U_\mu^{-1}(x - a\hat{\mu}) \bar{\psi}(x - a\hat{\mu})]. \quad (3.39)$$

We extend the fields to all times x_0 by “padding” with zeros, i.e. by setting

$$\psi(x) = \bar{\psi}(x) = 0, \quad \text{for } x_0 < 0 \text{ and } x_0 > T, \quad (3.40)$$

and by supplying the boundary conditions of eqs. (3.17, 3.18) with

$$P_- \psi(x)|_{x_0=0} = 0, \quad P_+ \psi(x)|_{x_0=T} = 0, \quad (3.41)$$

$$\bar{\psi}(x) P_+|_{x_0=0} = 0, \quad \bar{\psi}(x) P_-|_{x_0=T} = 0. \quad (3.42)$$

We can now write the Dirac-Wilson action

$$S_F[U, \bar{\psi}, \psi] = a^4 \sum_x \bar{\psi}(x) (D + m) \psi(x) \quad (3.43)$$

with the Dirac-Wilson operator

$$D = \frac{1}{2} (\gamma_\mu (\nabla_\mu^* + \nabla_\mu) - a \nabla_\mu^* \nabla_\mu) . \quad (3.44)$$

Before dealing with the heavy quark action, we would like to write eq. (3.43) in a different way, which will be useful later on. By using the explicit expression of the Dirac-Wilson operator we get

$$\begin{aligned} S_F &= a^4 \sum_{x,\mu} \bar{\psi}(x) \left\{ \frac{1}{2a} \gamma_\mu \left[U_\mu(x) \psi(x + a\hat{\mu}) - U_\mu^{-1}(x - a\hat{\mu}) \psi(x - a\hat{\mu}) \right] \right. \\ &\quad \left. - \frac{1}{2a} \left[U_\mu(x) \psi(x + a\hat{\mu}) + U_\mu^{-1}(x - a\hat{\mu}) \psi(x - a\hat{\mu}) - \left(2 + \frac{am}{2}\right) \psi(x) \right] \right\} \\ &= a^4 \sum_{x,\mu} \bar{\psi}(x) \left\{ \frac{1}{2a} (\gamma_\mu - 1) U_\mu(x) \psi(x + a\hat{\mu}) \right. \\ &\quad \left. - \frac{1}{2a} (\gamma_\mu + 1) U_\mu^{-1}(x - a\hat{\mu}) \psi(x - a\hat{\mu}) + \left(2 + \frac{am}{2}\right) \psi(x) \right\} . \end{aligned} \quad (3.45)$$

Instead of the bare quark mass m , it is convenient to work with the hopping parameter $\kappa = (8 + 2am)^{-1}$, and, by rescaling the fields $\psi \rightarrow (2\kappa)^{1/2} \psi$ and $\bar{\psi} \rightarrow (2\kappa)^{1/2} \bar{\psi}$, we get the simple expression

$$\begin{aligned} S_F &= a^3 \sum_x \left\{ \bar{\psi}(x) \psi(x) - \kappa \sum_\mu \left[\bar{\psi}(x) (1 - \gamma_\mu) U_\mu(x) \psi(x + a\hat{\mu}) \right. \right. \\ &\quad \left. \left. + \bar{\psi}(x) (1 + \gamma_\mu) U_\mu^{-1}(x - a\hat{\mu}) \psi(x - a\hat{\mu}) \right] \right\} , \end{aligned} \quad (3.46)$$

which is usually written in the compact form

$$S_F = a^3 \sum_{y,x} \bar{\psi}(y) M(y,x) \psi(x) , \quad \text{with} \quad (3.47)$$

$$\begin{aligned} M(y,x) &= \delta_{y,x} - \kappa \sum_\mu \left(\delta_{y,x+a\hat{\mu}} (1 + \gamma_\mu) U_\mu^{-1}(x) \right. \\ &\quad \left. + \delta_{y,x-a\hat{\mu}} (1 - \gamma_\mu) U_\mu(x - a\hat{\mu}) \right) . \end{aligned} \quad (3.48)$$

For static quarks the simplest discretized version of the action in eq. (2.45) has been proposed by Eichten and Hill [26, 27]:

$$S_h[U, \bar{\psi}_h, \psi_h] = \frac{a^4}{1 + a\delta m} \sum_x \bar{\psi}_h(x) (\nabla_0^* + \delta m) \psi_h(x). \quad (3.49)$$

One can also consider a more general action

$$S_h^W[U, \bar{\psi}_h, \psi_h] = \frac{a^4}{1 + a\delta m_W} \sum_x \bar{\psi}_h(x) (D_0^W + \delta m_W) \psi_h(x), \quad (3.50)$$

where

$$D_0^W \psi_h = \frac{1}{a} \left[\psi_h(x) - W_0^\dagger(x - a\hat{0}) \psi_h(x - a\hat{0}) \right], \quad (3.51)$$

and W_μ is a general parallel transporter, differing from U_μ by $O(a^2)$ -terms. Analogously for the heavy antiquarks

$$S_{\bar{h}}^W[U, \bar{\psi}_{\bar{h}}, \psi_{\bar{h}}] = \frac{a^4}{1 + a\delta m_W} \sum_x \bar{\psi}_{\bar{h}}(x) (\bar{D}_0^W + \delta m_W) \psi_{\bar{h}}(x), \quad (3.52)$$

$$\bar{D}_0^W \psi_{\bar{h}} = \frac{1}{a} \left[W_0(x) \psi_{\bar{h}}(x + a\hat{0}) - \psi_{\bar{h}}(x) \right]. \quad (3.53)$$

Under a gauge transformation W_μ transforms as U_μ , and, together with gauge invariance, parity and cubic symmetry, the actions S_h , S_h^W and $S_{\bar{h}}^W$ satisfy the symmetries of the static theory expounded in Sect. 2.4. These alternative discretizations are introduced to reduce, in a Monte Carlo simulation, the noise-to-signal ratio (R_{NS}) of the observables of interest, while remaining with roughly the same discretization errors. This is sufficient to ensure to stay within the same universality class as well as the same $O(a)$ -improvement of the Eichten-Hill action. The authors of [28, 29] have proposed several possible discretizations. Here we present only the so-called HYP actions.

Following [30] the parallel transporter $W_\mu(x)$ is constructed in three concatenated steps. They are

Step 1

$$W_\mu(x) = \mathcal{P}_{\text{SU}(3)} \left[(1 - \alpha_1) U_\mu(x) + \frac{\alpha_1}{6} \sum_{\pm v \neq \mu} \tilde{K}_{v\mu}(x) \right] \quad (3.54)$$

$$\tilde{K}_{v\mu}(x) = \tilde{V}_{v;\mu}(x) \tilde{V}_{\mu;v}(x + a\hat{v}) \tilde{V}_{v;\mu}^\dagger(x + a\hat{\mu}) \quad (3.55)$$

Step 2

$$\tilde{V}_{\nu;\mu}(x) = \mathcal{P}_{\text{SU}(3)} \left[(1 - \alpha_2)U_\mu(x) + \frac{\alpha_2}{4} \sum_{\pm\rho \neq \nu, \mu} \bar{K}_{\rho\nu\mu}(x) \right] \quad (3.56)$$

$$\bar{K}_{\rho\nu\mu}(x) = \bar{V}_{\rho;\nu\mu}(x)\bar{V}_{\mu;\rho\nu}(x + a\hat{\rho})\bar{V}_{\rho;\nu\mu}^\dagger(x + a\hat{\mu}) \quad (3.57)$$

Step 3

$$\bar{V}_{\mu;\nu\rho}(x) = \mathcal{P}_{\text{SU}(3)} \left[(1 - \alpha_3)U_\mu(x) + \frac{\alpha_3}{2} \sum_{\pm\eta \neq \rho, \nu, \mu} K_{\eta\mu}(x) \right] \quad (3.58)$$

$$K_{\eta\mu}(x) = U_\eta(x)U_\mu(x + a\hat{\eta})U_\eta^\dagger(x + a\hat{\mu}) \quad (3.59)$$

Here the greek indices can assume also negative values and $U_{-\mu}(x) = U_\mu^\dagger(x - a\hat{\mu})$. The symbol $\mathcal{P}_{\text{SU}(3)}$ indicates the projection onto SU(3), which is here defined by the rescaling

$$W \rightarrow W / \sqrt{\text{tr}(WW^\dagger)/3}, \quad (3.60)$$

followed by four iterations of

$$W \rightarrow X \left(1 - \frac{i}{3} \text{Im}(\det(X)) \right), \quad \text{where} \quad X = W \left(\frac{3}{2} - \frac{1}{2} W^\dagger W \right). \quad (3.61)$$

The parameters α_1 , α_2 and α_3 can be tuned by requiring an approximate minimization of the R_{NS} of some matrix elements.

3.3 Expectation values and Monte Carlo integration

As it is already clear from eqs. (3.37), the evaluation of the lattice SF requires an integration over an enormous number of variables. If we consider a volume $L^3 \times T$, the number of real parameters to be integrated is approximately

$$[8]_{\text{SU}(3)} \times [4]_{\hat{\mu}} \times [(L/a)^3]_{\text{space}} \times [(T/a)]_{\text{time}}. \quad (3.62)$$

With $L/a = T/a = 10$ we have 320000 real variables. In absence of symmetries and/or approximations capable to drastically reduce the number (3.62), the recourse to statistical methods is necessary.

We start by considering a product \mathcal{O} of fields on the lattice, and we want to evaluate its expectation value $\langle \mathcal{O} \rangle_{\text{QCD}}$ by using the SF scheme in QCD. We thus compute the integral

$$\langle \mathcal{O} \rangle_{\text{QCD}} = \left\{ \frac{1}{\mathcal{Z}} \int \mathbf{D}[U] \mathbf{D}[\bar{\psi}] \mathbf{D}[\psi] \mathcal{O} e^{-S[U, \bar{\psi}, \psi]} \right\}_{\bar{\rho}'=\rho'=\bar{\rho}=\rho=0}, \quad (3.63)$$

where

$$\mathcal{Z} = \int \mathbf{D}[U] \mathbf{D}[\bar{\psi}] \mathbf{D}[\psi] e^{-S[U, \bar{\psi}, \psi]}, \quad S[U, \bar{\psi}, \psi] = S_G[U] + S_F[U, \bar{\psi}, \psi]. \quad (3.64)$$

Apart from the dynamical variables U , $\bar{\psi}$ and ψ integrated over, the product \mathcal{O} may involve the boundary fields

$$\begin{aligned} \zeta(\mathbf{x}) &= \frac{\delta}{\delta \bar{\rho}(\mathbf{x})}, & \bar{\zeta}(\mathbf{x}) &= -\frac{\delta}{\delta \rho(\mathbf{x})}, \\ \zeta'(\mathbf{x}) &= \frac{\delta}{\delta \bar{\rho}'(\mathbf{x})}, & \bar{\zeta}'(\mathbf{x}) &= -\frac{\delta}{\delta \rho'(\mathbf{x})}, \end{aligned} \quad (3.65)$$

having the form of functional derivatives acting on the Boltzmann factor in eq. (3.63).

Since there is (until now) no efficient way of dealing with the Grassmann-valued quark fields in a computer simulation, we exploit the property of the fermionic action S_F to be a bilinear in quark fields, and we analytically integrate out the fermionic variables in eq. (3.63). This defines the new observable

$$[\mathcal{O}]_F[U] \equiv \left\{ \frac{1}{\mathcal{Z}_F} \int \mathbf{D}[\bar{\psi}] \mathbf{D}[\psi] \mathcal{O} e^{-S_F[U, \bar{\psi}, \psi]} \right\}_{\bar{\rho}'=\rho'=\bar{\rho}=\rho=0}, \quad (3.66)$$

depending only on the gauge fields, and

$$\mathcal{Z}_F = \int \mathbf{D}[\bar{\psi}] \mathbf{D}[\psi] e^{-S_F[U, \bar{\psi}, \psi]}. \quad (3.67)$$

We can now rewrite the expectation value (3.63) as

$$\langle \mathcal{O} \rangle_{\text{QCD}} = \frac{\int \mathbf{D}[U] [\mathcal{O}]_F[U] e^{-S_{\text{eff}}[U]}}{\int \mathbf{D}[U] e^{-S_{\text{eff}}[U]}}, \quad (3.68)$$

with the effective action given by

$$S_{\text{eff}}[U] = S_G[U] - \ln(\det(M[U])). \quad (3.69)$$

where M has been defined in eq. (3.48). The computation of (3.68) is considerably simplified by replacing $\det(M[U])$ by 1. This is widely referred to as quenched approximation. In perturbation theory it can be interpreted with the omission of the Feynman diagrams consisting of fermion loops, with an arbitrary number of gluon legs attached to it.

In the case where also static quarks are involved, we calculate in HQET the expectation value of the composite fields \mathcal{O} according to the procedure developed in Sect. 2.5. By using the static action (3.50), we have the path integral expression

$$\langle \mathcal{O} \rangle_{\text{stat}} = \left\{ \frac{1}{\mathcal{Z}} \int \mathcal{D}[U] \mathcal{D}[\bar{\psi}] \mathcal{D}[\psi] \mathcal{D}[\bar{\psi}_h] \mathcal{D}[\psi_h] \mathcal{O} e^{-S[U, \bar{\psi}, \psi, \bar{\psi}_h, \psi_h]} \right\}_{\{\rho\}=0},$$

$$\{\rho\} = \{\bar{\rho}', \rho', \bar{\rho}, \rho, \bar{\rho}_h, \rho_h\}, \quad (3.70)$$

where the action is now

$$S[U, \bar{\psi}, \psi, \bar{\psi}_h, \psi_h] = S_G[U] + S_F[U, \bar{\psi}, \psi] + S_h^W[U, \bar{\psi}_h, \psi_h], \quad (3.71)$$

and the boundary fields

$$\zeta'_h(\mathbf{x}) = \frac{\delta}{\delta \bar{\rho}'_h(\mathbf{x})}, \quad \bar{\zeta}_h(\mathbf{x}) = -\frac{\delta}{\delta \rho_h(\mathbf{x})}, \quad (3.72)$$

may appear besides the ones in eqs. (3.65). Of course an observable \mathcal{O} made of only heavy quark and gauge fields is an interesting case too. The analytical integration of the fermionic observables in eq. (3.70) follows the scheme explained for QCD, without further complications.

For later convenience we define also the boundary fields

$$\zeta_h(\mathbf{x}) = \frac{\delta}{\delta \bar{\rho}_h(\mathbf{x})}, \quad \bar{\zeta}'_h(\mathbf{x}) = -\frac{\delta}{\delta \rho'_h(\mathbf{x})}, \quad (3.73)$$

and through the action

$$S[U, \bar{\psi}, \psi, \bar{\psi}_h, \psi_h, \bar{\psi}_h, \psi_h] = S_G[U] + S_F[U, \bar{\psi}, \psi] + S_h^W[U, \bar{\psi}_h, \psi_h] + S_h^W[U, \bar{\psi}_h, \psi_h], \quad (3.74)$$

the path integral expression

$$\langle \mathcal{O} \rangle_{\text{hh}} = \left\{ \frac{1}{\mathcal{Z}} \int \mathcal{D}[U] \mathcal{D}[\{\psi\}] \mathcal{O} e^{-S[U, \bar{\psi}, \psi, \bar{\psi}_h, \psi_h, \bar{\psi}_h, \psi_h]} \right\}_{\{\rho\}=0},$$

$$\{\rho\} = \{\bar{\rho}', \rho', \bar{\rho}, \rho, \rho'_h, \bar{\rho}_h, \bar{\rho}'_h, \rho_h\}, \quad (3.75)$$

$$\mathcal{D}[\{\psi\}] = \mathcal{D}[\bar{\psi}] \mathcal{D}[\psi] \mathcal{D}[\bar{\psi}_h] \mathcal{D}[\psi_h] \mathcal{D}[\bar{\psi}_h] \mathcal{D}[\psi_h].$$

On a computer, the expectation value $\langle \mathcal{O} \rangle$, in QCD or HQET, is calculated by a Monte Carlo simulation, where an ensemble of N gauge links configurations $U^{(i)}$, with $i = 1, \dots, N$, is generated with probability

$$P^{(i)} \propto \mathcal{D}[U^{(i)}] \exp\{-S_{\text{eff}}[U^{(i)}]\}, \quad (3.76)$$

and $\langle \mathcal{O} \rangle$ is approximated by the average

$$\langle \mathcal{O} \rangle = \bar{\mathcal{O}} \pm \Delta \bar{\mathcal{O}}, \quad (3.77)$$

$$\bar{\mathcal{O}} = \frac{1}{N} \sum_{i=1}^N \mathcal{O}_i = \frac{1}{N} \sum_{i=1}^N [\mathcal{O}]_{\text{F}}[U^{(i)}], \quad \Delta \bar{\mathcal{O}} = \mathcal{O}\left(\frac{1}{\sqrt{N}}\right), \quad (3.78)$$

where $\Delta \bar{\mathcal{O}}$ is the statistical error due to the finiteness of the statistical sample.

The non-perturbative computations reported in this thesis have been performed in the quenched approximation, and we thus have $S_{\text{eff}} = S_{\text{G}}$ in eq. (3.69). Analogously, if the valence sector is just made of a static quark-antiquark pair, in the action (3.74) one can eliminate S_{F} from the very beginning. The ensemble of gauge configurations is generated by means of the so-called local “hybrid over-relaxation” (HOR) algorithm (see e.g. [31]). The basic cycle consists of 1 heathbath (HB) update sweep throughout the whole lattice, followed by N_{OR} over-relaxation (OR) sweeps. The cycle is iterated N_{UP} times, and with the obtained gauge configuration $U^{(i)}$ a computation of $[\mathcal{O}]_{\text{F}}[U^{(i)}]$ is performed. This last step is called measurement (MEAS). The procedure can thus be summarized as

$$\left(\text{HB} \times (\text{OR})^{N_{\text{OR}}} \right)^{N_{\text{UP}}} \times \text{MEAS}, \quad (3.79)$$

and the whole procedure is repeated N times. The algorithm used for the gauge update is local in the sense that one processes one time-slice after the other, and each gauge link $U_{\mu}(x)$ is separately visited and updated. The heathbath algorithm is a modification of Creutz’s algorithm [32] by Fabricius and Haan [33] and independently by Kennedy

and Pendleton [34]. The over-relaxation sweeps are microcanonical and follow [35]. The whole update procedure is executed in embedded $SU(2)$ subgroups according to [36]. Optimized choices of N_{UP} and N_{OR} , for which the statistical errors on our observables are minimized at fixed simulation run time, are $N_{UP} = 5$ and $N_{OR} = L/2a$. The latter is chosen to be a multiple of the correlation length in lattice units in order to minimize the autocorrelation times [37].

The correct estimation of the statistical uncertainty $\Delta\bar{\mathcal{O}}$ plays a fundamental role for the reliability of the results. At this point two issues must be discussed: thermalization and (auto-)correlation. The discussion is presented in App. B.

When considering full QCD, i.e. with an exact treatment of the quark determinant in eq. (3.69), the updating algorithm described above is known to lead to unsatisfactory performances. Other techniques are employed, and for a recent review one can consult [38, 39].

3.4 Improvement

The lattice discretization introduces a cutoff in the Feynman integrals described in the previous section, making them ultraviolet finite. Furthermore such a discretization is particularly suitable to be implemented on a computer. As for other regularization methods, one then proceeds by applying a renormalization program, consisting in defining renormalized Green functions, which approach a finite limit as the cutoff is removed.

The removal of the lattice structure amounts to studying the continuum limit. This is a non-trivial task. Since the bare parameters of the theory depend on the cutoff, they have to be tuned as a function of the lattice spacing with respect to the imposed renormalization conditions. The latter state that some physical quantities, such as the coupling and the particle masses, are to be held fixed as the cutoff is removed. This procedure defines in the parameter space the so-called Line of Constant Physics (LCP).

In the approach to the continuum limit, the presence of effects linear in a usually obliges to vary the size of the lattice spacing over a wide range of physical values before having a reasonable control on the cutoff effects. In addition, the latter can be quite large, compromising the reliability and precision of the continuum extrapolation. It turns out that the effects linear in a can be isolated and cancelled by adding appropriate counterterms vanishing in the continuum. The resulting theory is said to be $O(a)$ -improved.

A successful and interesting way of implementing the improvement has been introduced by Symanzik [40, 41, 42], who provided arguments to cancel the $O(a)$ -effects

in on-shell quantities by adding appropriate counterterms. On-shell quantities are for example particle masses and correlation functions over physical space-time distances. Close to the continuum, the lattice theory can be described by a local effective theory with action [43]

$$S_{\text{eff}} = S_0 + \sum_{k=1}^{\infty} a^k S_k, \quad (3.80)$$

where S_0 is the continuum action, and the consecutive terms are given by

$$S_k = \int d^4x \mathcal{L}_k(x). \quad (3.81)$$

The Lagrangians $\mathcal{L}_k(x)$ gather in a linear combination local and gauge-invariant composite fields respecting the symmetries of the theory, and having mass dimension $4+k$. To give a precise meaning to all terms of the effective action, one can regularize them by using a lattice spacing $a' \ll a$.

Cutoff effects do not stem only from the action. The composite fields, appearing in the observables that we want to compute, are possible sources of discretization errors linear in the lattice spacing. Let us call such a field $\phi(x)$, and examine the connected correlation function

$$G_n(x_1, \dots, x_n) = (Z_\phi)^n \langle \phi(x_1) \dots \phi(x_n) \rangle_{\text{con}}. \quad (3.82)$$

The factor Z_ϕ accounts for the field renormalization and the points x_1, \dots, x_n are kept at non-zero physical distance. The mixing of ϕ with other fields under renormalization is excluded to lighten the discussion. We thus expect that, if the renormalization factor is correctly chosen, the quantity G_n has a well-defined continuum limit.

In the local effective theory an expansion akin to (3.80) can be provided for the renormalized lattice field $Z_\phi \phi(x)$, and reads

$$\phi_{\text{eff}}(x) = \phi_0(x) + \sum_{k=1}^{\infty} a^k \phi_k(x), \quad (3.83)$$

where the fields ϕ_k are linear combinations of composite and local fields with the appropriate dimension and symmetries. Let us now write down the expansion of the correlation function (3.82):

$$\begin{aligned} G_n(x_1, \dots, x_n) &= \langle \phi_0(x_1) \dots \phi_0(x_n) \rangle_{\text{con}} \\ &\quad - a \int d^4y \langle \phi_0(x_1) \dots \phi_0(x_n) \mathcal{L}_1(y) \rangle_{\text{con}} \\ &\quad + a \sum_{k=1}^n \langle \phi_0(x_1) \dots \phi_1(x_k) \dots \phi_0(x_n) \rangle_{\text{con}} + \mathcal{O}(a^2). \end{aligned} \quad (3.84)$$

The reader may notice a strong similarity with the expression (2.55) given for HQET. The expectation values on the r.h.s. are to be taken by using the continuum Lagrangian \mathcal{L}_0 , which is power-counting renormalizable. The integral over y , in the second term of the r.h.s. of eq. (3.84), can produce contact terms leading to divergences and/or to limitations in the use of the field equations. These terms amount to operator insertions, which are constrained by the dimensional analysis and the symmetries of the effective theory, and can be compensated by a redefinition of the field ϕ_1 . As hinted at the beginning of this section, the on-shell $O(a)$ -improvement is achieved by modifying the action and the composite fields through the addition of appropriate counterterms. The latter aim to let \mathcal{L}_1 and ϕ_1 vanish up to term of higher order in a , and have the general form

$$\delta S = a \int d^4x \sum_l c_l \mathcal{O}_l, \quad \delta \phi = a \sum_l c_l^\phi \phi^{(l)}. \quad (3.85)$$

In principle also higher orders of the expansion (3.84) can be improved using the same technique. Nevertheless the number of counterterms to be fine-tuned rapidly increases, and in practice the improvement is usually applied only to the terms linear in the lattice spacing.

We start with the Schrödinger functional formulation of lattice QCD with two mass-degenerate quarks, and the action (3.35) for the gauge fields and the Dirac-Wilson action (3.43) for the fermions. Later on we will discuss the heavy quark case.

We concentrate on the bulk of the lattice, and observe that the Lagrangian \mathcal{L}_1 can be made to vanish by adding to the action a counterterm of the form

$$a^5 \sum_{x_0=a}^{T-a} \sum_{\mathbf{x}} \sum_l c_l \widehat{\mathcal{O}}_l(x), \quad (3.86)$$

where the operators $\widehat{\mathcal{O}}_l$ are a lattice representation of the basis

$$\begin{aligned} \mathcal{O}_1 &= \bar{\Psi} \sigma_{\mu\nu} F_{\mu\nu} \Psi, \\ \mathcal{O}_2 &= m \text{tr} \{ F_{\mu\nu} F_{\mu\nu} \}, \\ \mathcal{O}_3 &= m^2 \bar{\Psi} \Psi. \end{aligned} \quad (3.87)$$

The discretized version $\widehat{F}_{\mu\nu}$ of the curvature tensor (2.5) can be written as

$$\widehat{F}_{\mu\nu}(x) = \frac{1}{8a^2} \{ Q_{\mu\nu}(x) - Q_{\nu\mu}(x) \}, \quad (3.88)$$

with

$$\begin{aligned}
Q_{\mu\nu}(x) = & \left\{ U_\mu(x)U_\nu(x+a\hat{\mu})U_\mu^{-1}(x+a\hat{\nu})U_\nu^{-1}(x) \right. \\
& + U_\nu(x)U_\mu^{-1}(x+a\hat{\nu}-a\hat{\mu})U_\nu^{-1}(x-a\hat{\mu})U_\mu(x-a\hat{\mu}) \\
& + U_\mu^{-1}(x-a\hat{\mu})U_\nu^{-1}(x-a\hat{\mu}-a\hat{\nu})U_\mu(x-a\hat{\mu}-a\hat{\nu})U_\nu(x-a\hat{\nu}) \\
& \left. + U_\nu^{-1}(x-a\hat{\nu})U_\mu(x-a\hat{\nu})U_\nu(x+a\hat{\mu}-a\hat{\nu})U_\mu^{-1}(x) \right\}. \quad (3.89)
\end{aligned}$$

We notice that the operators $\widehat{\mathcal{O}}_2$ and $\widehat{\mathcal{O}}_3$ already appear in the action $S = S_G + S_F$, and they merely lead to a reparametrization of the bare coupling and mass, when the latter get renormalized. We are thus left with the operator $\widehat{\mathcal{O}}_1$, which can be added to the Dirac-Wilson operator

$$D_{\text{impr}} = D + c_{\text{sw}} \frac{ia}{4} \sigma_{\mu\nu} \widehat{F}_{\mu\nu}. \quad (3.90)$$

The coefficient c_{sw} depends on g_0 and must be appropriately tuned. It has been introduced for the first time by Sheikholeslami and Wohlert [44]. Another equivalent way of formulating this improvement is the addition to the action S of the volume term

$$\delta S_V = a^5 \sum_{x_0=a}^{T-a} \sum_{\mathbf{x}} c_{\text{sw}} \bar{\psi} \frac{i}{4} \sigma_{\mu\nu} \widehat{F}_{\mu\nu} \psi. \quad (3.91)$$

Finally we notice that no improvement terms are needed for the gauge action.

So far we have discussed only the bulk of the lattice. We still need to add to the action the improvement terms which account for the effects at the temporal boundaries. The fully improved action can be written in the form

$$S_{\text{impr}}[U, \bar{\psi}, \psi] = S[U, \bar{\psi}, \psi] + \delta S_V[U, \bar{\psi}, \psi] + \delta S_{G,b}[U] + \delta S_{F,b}[U, \bar{\psi}, \psi]. \quad (3.92)$$

The boundary counterterms for the gauge action read [24]:

$$\begin{aligned}
\delta S_{G,b}[U] = & \frac{1}{2g_0^2} (c_s - 1) \sum_{p_s} \text{tr} \{1 - U(p_s)\} \\
& + \frac{1}{g_0^2} (c_t - 1) \sum_{p_t} \text{tr} \{1 - U(p_t)\}. \quad (3.93)
\end{aligned}$$

The sums here are restricted to all oriented plaquettes attached to the temporal boundaries $x_0 = 0$ and $x_0 = T$, being space-like (p_s) or time-like (p_t).

By exploiting the symmetries of the theory, the field equations, and by omitting the terms which can be reabsorbed in the renormalization of the quark masses and of the quark and antiquark fields, a possible choice for $\delta S_{F,b}$ is [43]:

$$\delta S_{F,b}[U, \bar{\psi}, \psi] = a^4 \sum_{\mathbf{x}} \left\{ (\tilde{c}_s - 1) [\hat{\mathcal{O}}_s(\mathbf{x}) + \hat{\mathcal{O}}_s'(\mathbf{x})] + (\tilde{c}_t - 1) [\hat{\mathcal{O}}_t(\mathbf{x}) + \hat{\mathcal{O}}_t'(\mathbf{x})] \right\}, \quad (3.94)$$

where

$$\hat{\mathcal{O}}_s(\mathbf{x}) = \frac{1}{2} \bar{\rho}(\mathbf{x}) \gamma_k (\nabla_k^* + \nabla_k) \rho(\mathbf{x}), \quad (3.95)$$

$$\hat{\mathcal{O}}_s'(\mathbf{x}) = \frac{1}{2} \bar{\rho}'(\mathbf{x}) \gamma_k (\nabla_k^* + \nabla_k) \rho'(\mathbf{x}), \quad (3.96)$$

$$\hat{\mathcal{O}}_t(\mathbf{x}) = \frac{1}{2} \{ \bar{\psi}(y) P_+ \nabla_0^* \psi(y) + \bar{\psi}(y) \overleftarrow{\nabla}_0^* P_- \psi(y) \}_{y=(a,\mathbf{x})}, \quad (3.97)$$

$$\hat{\mathcal{O}}_t'(\mathbf{x}) = \frac{1}{2} \{ \bar{\psi}(y) P_- \nabla_0 \psi(y) + \bar{\psi}(y) \overleftarrow{\nabla}_0 P_+ \psi(y) \}_{y=(T-a,\mathbf{x})}. \quad (3.98)$$

For our choices of the boundary conditions and observables, specified in the following chapters, the terms proportional to c_s and \tilde{c}_s do not contribute. For $N_f = 0$, the coefficient c_{sw} has been non-perturbatively computed in [45], where the parametrization

$$c_{sw}(g_0^2) = \frac{1 - 0.656g_0^2 - 0.152g_0^4 - 0.054g_0^6}{1 - 0.922g_0^2}, \quad (3.99)$$

has been proposed with a precision of 3% in the range $0 \leq g_0 \leq 1$. The coefficients c_t and \tilde{c}_t are only perturbatively known

$$\tilde{c}_t(g_0^2) = 1 - 0.01795(2)g_0^2 + \mathcal{O}(g_0^4), \quad (3.100)$$

$$c_t(g_0^2) = 1 - 0.08900(5)g_0^2 - 0.0294(3)g_0^4 + \mathcal{O}(g_0^6), \quad N_f = 0, \quad (3.101)$$

and have been computed in [46] and [47] respectively.

For the heavy quarks the improvement procedure [48] is much simpler than in the relativistic case. We consider the action (3.71), and besides the improvement terms for S_G and S_F that have just been explained, we examine the possible additional terms

for S_h^W . On the bulk we can write down a possible basis of dimension five operators. Nevertheless only one of them will survive after applying the field equations and the symmetries of the static theory. Their continuum expression reads¹

$$\mathcal{O}_{h,1} = \bar{\Psi}_h \sigma_{0k} F_{0k} \Psi_h, \quad (3.102)$$

$$\mathcal{O}_{h,2} = \bar{\Psi}_h \sigma_{jk} F_{jk} \Psi_h, \quad (3.103)$$

$$\mathcal{O}_{h,3} = \bar{\Psi}_h \{D_0 D_0 + \overleftarrow{D}_0 \overleftarrow{D}_0\} \Psi_h, \quad (3.104)$$

$$\mathcal{O}_{h,4} = m \bar{\Psi}_h \{D_0 - \overleftarrow{D}_0\} \Psi_h, \quad (3.105)$$

$$\mathcal{O}_{h,5} = \bar{\Psi}_h \{D_k D_k + \overleftarrow{D}_k \overleftarrow{D}_k\} \Psi_h, \quad (3.106)$$

$$\mathcal{O}_{h,6} = m \bar{\Psi}_h \{\gamma_k D_k - \overleftarrow{D}_k \gamma_k\} \Psi_h, \quad (3.107)$$

$$\mathcal{O}_{h,7} = m^2 \bar{\Psi}_h \Psi_h, \quad (3.108)$$

where m is the mass of the relativistic quark. The operator $\mathcal{O}_{h,1}$ vanishes because $P_+ \sigma_{0k} P_+ = 0$, while $\mathcal{O}_{h,2}$ is not invariant under the spin rotations (2.40). The operators $\mathcal{O}_{h,3}$ and $\mathcal{O}_{h,4}$ vanish because of the formal equations of motion

$$D_0 \Psi_h(x) = 0, \quad \bar{\Psi}_h(x) \overleftarrow{D}_0 = 0. \quad (3.109)$$

The operators $\mathcal{O}_{h,5}$ and $\mathcal{O}_{h,6}$ break the U(1) symmetry, indeed they are not invariant under the phase transformations (2.41). We are thus left with $\mathcal{O}_{h,7}$. This is just a mass-dependent shift in δm , appearing in eq. (2.45), and will be taken into account when dealing with the renormalization.

In complete analogy to the QCD case, we now analyze the possible boundary counterterms for the heavy quark action. In the continuum, a basis of local operators of dimension 4, which are to be summed over the boundary lattice points at $x_0 = 0$ and $x_0 = T$ and are compatible with the symmetries of the static theory is given by

$$\mathcal{O}_{h,8} = \bar{\Psi}_h D_0 \Psi_h, \quad (3.110)$$

$$\mathcal{O}_{h,9} = \bar{\Psi}_h \overleftarrow{D}_0 \Psi_h, \quad (3.111)$$

$$\mathcal{O}_{h,10} = \bar{\Psi}_h \{\gamma_k D_k - \overleftarrow{D}_k \gamma_k\} \Psi_h, \quad (3.112)$$

$$\widehat{\mathcal{O}}_{h,11} = m \bar{\Psi}_h \Psi_h. \quad (3.113)$$

As $\mathcal{O}_{h,8}$ and $\mathcal{O}_{h,9}$ vanish because of eqs. (3.109), the operator $\mathcal{O}_{h,10}$ is zero because $P_+ \gamma_k P_+ = 0$. It remains only $\mathcal{O}_{h,11}$, which is of the same kind of $\mathcal{O}_{h,7}$, and amounts to a shift in δm .

¹The operator basis in the continuum can be used both for the Eichten-Hill action and a HYP action. They differ by $O(a^2)$ -terms.

We have thus shown that, apart from a redefinition of δm , in the Schrödinger functional static actions of the form (3.50) are already $O(a)$ -improved without additional counterterms.

So far we have not discussed the improvement of the effective fields (3.83). This will be performed for the correlation functions of interest after having appropriately defined them on the lattice.

3.5 Correlation functions

In this section we derive, within the Schrödinger functional scheme, explicit expressions for correlation functions and observables, originated from relativistic quark and static-light bilinear currents. We describe their behavior at large physical time separations by using the transfer matrix formalism [25, 49]. Throughout the first subsection we work it out in the unimproved theory, where the presented relations hold exactly. In the second subsection we determine the $O(a)$ -improvement counterterms for the correlation functions of interest, and in the third subsection we present their renormalized expressions. Since universality implies that the renormalized correlation functions of the improved theory and unimproved theory agree in the continuum limit, and they are multiplicatively renormalized, we expect that the results derived in the first subsection are valid also in the improved theory, provided that the involved physical distances are large compared to the lattice spacing.

3.5.1 Definition

Our starting point is the QCD partition function defined in eqs. (3.64) in the Schrödinger functional scheme. In analogy to the pure gauge case it can be represented as the matrix element of the time evolution from an initial state $|i\rangle$ to a final state $|f\rangle$ through the Euclidean step evolution operator $e^{-\mathbb{H}a}$ applied T/a times, according to the expression

$$\mathcal{Z}[W', \bar{\rho}', \rho', W, \bar{\rho}, \rho] = \langle f | \left(e^{-\mathbb{H}a} \right)^{T/a} \mathbb{P} | i \rangle = \langle f | e^{-\mathbb{H}T} \mathbb{P} | i \rangle. \quad (3.114)$$

The states $|i\rangle$ and $|f\rangle$ live on the Hilbert space at the temporal boundaries, $x_0 = 0$ and $x_0 = T$ respectively, defined by the product space of the pure gauge theory Hilbert space and the fermionic Fock space. The states are given in terms of the boundary fields appearing as arguments of the partition function in eq. (3.114). Gauge invariance is guaranteed by the presence of the projector \mathbb{P} . An equivalent way of writing eq. (3.114)

is by means of the transfer matrix \mathbb{T} between two adjacent time-slices

$$\mathcal{L}[W', \bar{\rho}', \rho', W, \bar{\rho}, \rho] = \langle f | (\mathbb{T})^{T/a} | i \rangle, \quad (3.115)$$

where the projector \mathbb{P} is included in \mathbb{T} . Let us introduce the boundary operators

$$\mathcal{O} = \frac{a^6}{L^3} \sum_{\mathbf{y}, \mathbf{z}} \bar{\zeta}_{q_1}(\mathbf{y}) \gamma_5 \zeta_{q_2}(\mathbf{z}), \quad \mathcal{O}' = \frac{a^6}{L^3} \sum_{\mathbf{y}, \mathbf{z}} \bar{\zeta}'_{q_2}(\mathbf{y}) \gamma_5 \zeta'_{q_1}(\mathbf{z}), \quad (3.116)$$

containing the boundary fields defined in eqs. (3.65). These operators are dimensionless and $\{q_1, q_2\}$ are flavor indices. They define the correlation function

$$f_1 = -\frac{1}{2} \langle \mathcal{O}' \mathcal{O} \rangle, \quad (3.117)$$

whose quantum mechanical representation is

$$f_1 = -\frac{1}{2} \frac{\langle i_\pi | e^{-\mathbb{H}T} \mathbb{P} | i_\pi \rangle}{\langle i_0 | e^{-\mathbb{H}T} \mathbb{P} | i_0 \rangle}. \quad (3.118)$$

Here $|i_\pi\rangle$ indicates a state with the quantum numbers of a pseudoscalar meson with quark content (q_1, \bar{q}_2) and zero momentum, while $|i_0\rangle$ carries the quantum numbers of the vacuum. The latter is obtained by setting to zero the spatial components of the gauge potentials and the fermion fields at the temporal boundaries. Furthermore we associate to the composite operators²

$$A_0(x) = \bar{\Psi}_{q_2}(x) \gamma_0 \gamma_5 \Psi_{q_1}(x), \quad (3.119)$$

$$P(x) = \bar{\Psi}_{q_2}(x) \gamma_5 \Psi_{q_1}(x), \quad (3.120)$$

the correlation functions

$$f_X(x_0) = -\frac{L^3}{2} \langle X(x) \mathcal{O} \rangle = \begin{cases} f_A & \text{if } X(x) = A_0(x) \\ f_P & \text{if } X(x) = P(x) \end{cases}, \quad (3.121)$$

with $a \leq x_0 \leq T - a$ and the quantum mechanical representation

$$f_X(x_0) = -\frac{L^3}{2} \frac{\langle i_0 | e^{-\mathbb{H}(T-x_0)} \mathbb{P} X e^{-\mathbb{H}x_0} \mathbb{P} | i_\pi \rangle}{\langle i_0 | e^{-\mathbb{H}T} \mathbb{P} | i_0 \rangle}. \quad (3.122)$$

The physical interpretation of the correlation functions that we have just defined is

²Of course other bilinears can be formed, but they are not used in this work.

- f_1 is the (normalized) amplitude of a meson state $|i_\pi\rangle$ travelling from the temporal boundary at $x_0 = 0$ to the other boundary at $x_0 = T$ of the four dimensional cylinder.
- f_X is the (normalized) amplitude of a meson state $|i_\pi\rangle$ created at time $x_0 = 0$ and annihilated at time $a \leq x_0 \leq T - a$ by the operator \mathbb{X} ; the latter being the representation of the field X in the Schrödinger picture.

We consider an orthonormal basis $|n, q\rangle$ of gauge invariant eigenstates of the Hamiltonian \mathbb{H} . Their properties explicitly read

$$n = 0, 1, \dots, \quad \mathbb{H}|n, q\rangle = E_n^{(q)}|n, q\rangle, \quad (3.123)$$

$$1 = \sum_{n, q} |n, q\rangle\langle n, q|, \quad \langle n', q'|n, q\rangle = \delta_{n', n} \delta_{q', q},$$

where n is the energy level and q is a shorthand for the full set of internal quantum numbers of the corresponding state. We insert two times the complete set into the numerator of eq. (3.122), and obtain

$$f_X(x_0) = -\frac{L^3}{2} \mathcal{Z}^{-1} \quad (3.124)$$

$$\times \sum_{n, q} \sum_{n', q'} \langle i_0 | e^{-\mathbb{H}(T-x_0)} |n, q\rangle \langle n, q | \mathbb{X} |n', q'\rangle \langle n', q' | e^{-\mathbb{H}x_0} |i_\pi\rangle.$$

Since we are interested in the asymptotic behavior of correlation functions for large values of x_0 and $T - x_0$ and on the ground state, we keep only the $n = 0$ terms, and get

$$f_X(x_0) \approx -\frac{L^3}{2} \mathcal{Z}^{-1} \langle i_0 | e^{-\mathbb{H}(T-x_0)} G_0 \mathbb{X} G_0 e^{-\mathbb{H}x_0} |i_\pi\rangle, \quad (3.125)$$

$$G_0 = |0, 0\rangle\langle 0, 0| + |0, \pi\rangle\langle 0, \pi|. \quad (3.126)$$

By using the properties in eqs. (3.123) we obtain

$$f_X(x_0) \approx -\frac{L^3}{2} \mathcal{Z}^{-1} \langle i_0 | 0, 0\rangle \langle 0, 0 | \mathbb{X} | 0, \pi\rangle \langle 0, \pi | i_\pi\rangle$$

$$\times \exp[-E_0^{(0)}(T - x_0) - E_0^{(\pi)}x_0]. \quad (3.127)$$

The same procedure can be applied to f_1 and \mathcal{Z}

$$f_1 \approx -\frac{1}{2} \mathcal{Z}^{-1} \langle i_\pi | 0, \pi\rangle \langle 0, \pi | i_\pi\rangle e^{-E_0^{(\pi)}T}, \quad (3.128)$$

$$\mathcal{Z} \approx \langle i_0 | 0, 0\rangle \langle 0, 0 | i_0\rangle e^{-E_0^{(0)}T}. \quad (3.129)$$

We can now write down two compact expressions for the correlation functions f_X and f_1 under the form

$$f_X(x_0) \approx -\frac{L^3}{2}\rho \langle 0,0|\mathbb{X}|0,\pi\rangle e^{-m_\pi x_0}, \quad f_1 \approx \frac{1}{2}\rho^2 e^{-m_\pi T}, \quad (3.130)$$

where $\rho = \langle 0,\pi|i_\pi\rangle/\langle 0,0|i_0\rangle$, and $m_\pi = E_0^{(\pi)} - E_0^{(0)}$ is the mass of the ground state meson. We notice that the correlation function f_A is proportional to the matrix element $\langle 0,0|\mathbb{A}_0|0,\pi\rangle$, which is related to the decay constant f_π through

$$Z_A \langle 0,0|\mathbb{A}_0|0,\pi\rangle = f_\pi m_\pi (2m_\pi L^3)^{-1/2}, \quad (3.131)$$

where Z_A is the renormalization constant of the axial current, and the factor

$$(2m_\pi L^3)^{-1/2} \quad (3.132)$$

accounts for the normalization of the one-particle states. There is no unique normalization for the decay constant, and the convention in eq. (3.131) complies with an experimental value of the pion decay constant of 132 MeV. The decay constant f_π can be conveniently extracted from the ratio

$$Z_A f_A(T/2)/\sqrt{f_1} \stackrel{(3.130)}{\approx} -\frac{1}{2} f_\pi \sqrt{m_\pi} L^{3/2}, \quad (3.133)$$

where the ratio ρ , which is a divergent quantity, cancels out. It remains to compute m_π . The latter can be extracted in the pseudoscalar channel from the effective meson mass

$$m_{\text{eff}}(x_0) = \frac{1}{2a} \ln \left(\frac{f_A(x_0 - a)}{f_A(x_0 + a)} \right) \stackrel{(3.130)}{\approx} m_\pi. \quad (3.134)$$

For large values of x_0 and $T - x_0$ the effective meson mass is expected to exhibit a plateau when plotted versus x_0 , where the ground state dominates and no boundary effects are present. Hence we choose as best estimate of m_π the value of m_{eff} at $x_0 = T/2$. While corrections are exponentially suppressed, in the limit of infinite physical time extension the two masses coincide.

The definitions given so far in this subsection can be easily extended to HQET. We introduce the boundary operators

$$\mathcal{O}_{\text{hl}} = \frac{a^6}{L^3} \sum_{\mathbf{y},\mathbf{z}} \bar{\zeta}_{\text{h}}(\mathbf{y}) \gamma_5 \zeta_{\text{l}}(\mathbf{z}), \quad (3.135)$$

$$\mathcal{O}'_{\text{hl}} = \frac{a^6}{L^3} \sum_{\mathbf{y},\mathbf{z}} \bar{\zeta}'_{\text{l}}(\mathbf{y}) \gamma_5 \zeta'_{\text{h}}(\mathbf{z}), \quad (3.136)$$

and the $\mu = 0$ component of the static-light axial vector current³

$$A_0^{\text{stat}}(x) = \bar{\Psi}_1(x) \gamma_0 \gamma_5 \Psi_h(x). \quad (3.137)$$

It is not necessary to define an equivalent of $P(x)$ in the effective theory, because $\bar{\Psi}_1(x) \gamma_0 \gamma_5 \Psi_h(x) = -\bar{\Psi}_1(x) \gamma_5 \Psi_h(x)$, due to $P_+ \Psi_h = \Psi_h$. We can now define the correlation functions

$$f_A^{\text{stat}}(x_0) = -\frac{1}{2} \langle A_0^{\text{stat}}(x) \mathcal{O}_{\text{hl}} \rangle_{\text{stat}}, \quad a \leq x_0 \leq T - a, \quad (3.138)$$

$$f_1^{\text{stat}} = -\frac{1}{2} \langle \mathcal{O}'_{\text{hl}} \mathcal{O}_{\text{hl}} \rangle_{\text{stat}}, \quad (3.139)$$

$$f_1^{\text{hh}}(x_3) = -\frac{a^8}{2L^2} \sum_{x_1, x_2, \mathbf{y}, \mathbf{z}} \langle \bar{\zeta}'_h(\mathbf{x}) \gamma_5 \zeta'_h(\mathbf{0}) \bar{\zeta}_h(\mathbf{y}) \gamma_5 \zeta_h(\mathbf{z}) \rangle_{\text{hh}}. \quad (3.140)$$

It is clear that f_A^{stat} and f_1^{stat} have a physical meaning similar to f_A and f_1 respectively. The meson state is now made of a static quark and a light antiquark. The correlation function f_1^{hh} in turn involves a static quark and a static antiquark in the valence sector. If we carry on the analysis of the correlation functions for large physical x_0 and $T - x_0$, as we have done for the relativistic QCD correlators, we end up with

$$f_A^{\text{stat}}(x_0) \approx -\frac{1}{2} \text{h} \langle 0, 0 | \mathbb{A}_0^{\text{stat}} | 0, \text{B} \rangle e^{-E_{\text{stat}} x_0}, \quad (3.141)$$

$$f_1^{\text{stat}} \approx \frac{1}{2} \text{h}^2 e^{-E_{\text{stat}} T}, \quad (3.142)$$

with $\text{h} = \langle 0, \text{B} | \text{i}_\text{B} \rangle / \langle 0, 0 | \text{i}_0 \rangle$, and the state $|\text{i}_\text{B}\rangle$ has the quantum numbers of a pseudo-scalar static-light meson with zero momentum. Furthermore E_{stat} is the binding energy of the static-light system, and the static-light pseudoscalar decay constant Φ^{stat} can be defined as

$$\Phi^{\text{stat}} \approx -Z_A^{\text{stat}} f_A^{\text{stat}}(T/2) / \sqrt{f_1^{\text{stat}}}. \quad (3.143)$$

One may be tempted to identify Φ^{stat} with the (naïve) static limit of the r.h.s. of eq. (3.133). However, it would be wrong, because one has to take care of the dependence on the renormalization scale introduced by Z_A^{stat} , and of the necessary matching coefficient as discussed in Sect. 2.6. The relation between the two decay constants will be given in the next chapter, after the discussion on the renormalization of the correlation functions in QCD and HQET. As for m_π , the quantity E_{stat} can be extracted from

³This operator has already appeared in eqs. (2.51). Here we reintroduce it in order to preserve the self-consistency of the discussion.

the effective energy

$$E_{\text{eff}}(x_0) = \frac{1}{2a} \ln \left(\frac{f_{\text{A}}^{\text{stat}}(x_0 - a)}{f_{\text{A}}^{\text{stat}}(x_0 + a)} \right) \stackrel{(3.141)}{\approx} E_{\text{stat}}. \quad (3.144)$$

3.5.2 Improvement

In Sect. 3.4 we pointed out that, in order to achieve the $O(a)$ -improvement of the desired correlation functions, the supplement of the action with appropriate counterterms may not be sufficient. One has also to use improved fields. As for the action, an improved field is given in terms of the originally (unimproved) field $\phi(x)$ and an additional counterterm $a\delta\phi(x)$

$$\phi_1(x) = \phi(x) + a\delta\phi(x). \quad (3.145)$$

The counterterm is a linear combination of basis fields with mass dimension $\dim(\phi) + 1$, which have not been included in the lattice action, and have the same lattice symmetries as $\phi(x)$.

We start with A_0 , and, by using the field equations to reduce the number of basis fields, we are left with the continuum basis

$$\mathcal{O}_{\text{A},1} = \bar{\psi}_{\text{q}_2} \gamma_5 \{D_0 + \overleftarrow{D}_0\} \psi_{\text{q}_1}, \quad (3.146)$$

$$\mathcal{O}_{\text{A},2} = m \bar{\psi}_{\text{q}_2} \gamma_5 \gamma_0 \psi_{\text{q}_1}, \quad (3.147)$$

Since the counterterm associated with $\mathcal{O}_{\text{A},2}$ amounts to a renormalization of A_0 , we discuss it in the next subsection. We thus conclude that

$$\delta A_0(x) = c_{\text{A}} \frac{1}{2} (\nabla_0 + \nabla_0^*) P(x). \quad (3.148)$$

In the static approximation the improvement of A_0^{stat} is achieved by starting from the continuum basis

$$\mathcal{O}_{\text{A,h},1} = \bar{\psi}_1 \gamma_5 D_0 \psi_{\text{h}}, \quad (3.149)$$

$$\mathcal{O}_{\text{A,h},2} = \bar{\psi}_1 \overleftarrow{D}_0 \gamma_5 \psi_{\text{h}}, \quad (3.150)$$

$$\mathcal{O}_{\text{A,h},3} = \bar{\psi}_1 \gamma_5 \gamma_j D_j \psi_{\text{h}}, \quad (3.151)$$

$$\mathcal{O}_{\text{A,h},4} = \bar{\psi}_1 \overleftarrow{D}_j \gamma_j \gamma_5 \psi_{\text{h}} \quad (3.152)$$

$$\mathcal{O}_{\text{A,h},5} = m \bar{\psi}_1 \gamma_0 \gamma_5 \psi_{\text{h}}. \quad (3.153)$$

We observe that $\mathcal{O}_{A,h,1}$ vanishes because of the first equation in (3.109), and $\mathcal{O}_{A,h,3}$ breaks the U(1) symmetry of the static approximation, because it is not invariant under the transformations (2.41). One of the remaining three operators can be omitted, because it can be expressed in terms of the other two by means of the light quark equation of motion. We thus neglect $\mathcal{O}_{A,h,2}$ and notice that $\mathcal{O}_{A,h,5}$ is again a term which amounts to a renormalization of A_0^{stat} . It is discussed in the next subsection. The improvement counterterm of the time component of the static-light axial current is thus

$$\delta A_0^{\text{stat}}(x) = c_A^{\text{stat}} \frac{1}{2} \bar{\psi}_1 (\overleftarrow{\nabla}_j + \overleftarrow{\nabla}_j^*) \gamma_j \gamma_5 \psi_h. \quad (3.154)$$

The form of this counterterm is the same for all static actions, which have been considered. However, the improvement coefficient c_A^{stat} depends on the chosen action, and must be determined consequently [29].

The boundary fields appearing in the correlation functions defined in the previous subsection need to be improved too. The counterterms can be reabsorbed in the renormalization of the fields and are discussed in the next subsection.

3.5.3 Renormalization

Since we want to relate the bare quantities computed on the lattice to physical observables, we need to define a renormalization scheme. Furthermore we want to reach the continuum limit, by decreasing a/L and keeping fixed the ratio T/L and the physical length of L , with a rate proportional to a^2 . The bare parameters must thus be scaled to satisfy these requirements, and it is technically advantageous to employ a mass-independent renormalization scheme. In the plane of the bare parameters we define the critical line

$$m_0 = m_c(g_0), \quad (3.155)$$

where the physical quark mass vanishes⁴. It allows to define the subtracted mass

$$m_q = m_0 - m_c. \quad (3.156)$$

We then define a modified bare coupling and bare quark mass

$$\tilde{g}_0^2 = g_0^2 (1 + b_g a m_q), \quad (3.157)$$

$$\tilde{m}_q = m_q (1 + b_m a m_q), \quad (3.158)$$

⁴As it will be clear in the next chapter, the critical line is not unambiguously defined in a regularization without chiral symmetry. It depends on the exact definition of the quark mass.

where the b-coefficients are functions of g_0^2 , and let \tilde{g}_0 and \tilde{m}_q be $O(a)$ -improved. Along the critical line the modified coupling coincides with the ordinary one. It is then natural to define the corresponding renormalized quantities as

$$g_R^2 = \tilde{g}_0^2 Z_g(\tilde{g}_0^2, a\mu), \quad (3.159)$$

$$m_R = \tilde{m}_q Z_m(\tilde{g}_0^2, a\mu). \quad (3.160)$$

Another important point is that, in the scaling of the bare parameters required to reach the continuum limit, the modified coupling is tuned such that it scales independently of the quark mass. Similarly for the modified bare quark mass \tilde{m}_q , which is scaled by a factor dependent on $a\mu$ only.

We extend this procedure to the renormalization of the local field $\phi(x)$. Besides the improvement counterterms considered in the previous subsection, it is natural to include a factor of the form $1 + b(g_0^2)am_q$, thus getting a renormalized field with the expression

$$\phi_R(x) = Z_\phi(\tilde{g}_0^2, a\mu)(1 + b_\phi am_q)\phi_I(x). \quad (3.161)$$

Since the renormalization condition is imposed at zero quark mass, the coefficient b_ϕ does not depend on the details of Z_ϕ .

Let us now apply this scheme to QCD by considering the composite fields (3.119, 3.120). The renormalized and improved axial density and time component of the axial current are given by

$$(P_R)(x) = Z_P(\tilde{g}_0^2, a\mu)(1 + b_P am_q)P(x), \quad (3.162)$$

$$(A_R)_0(x) = Z_A(\tilde{g}_0^2)(1 + b_A am_q)\{A_0(x) + a\delta A_0(x)\}, \quad (3.163)$$

while the renormalized boundary field ζ_R has the form

$$\zeta_R(\mathbf{x}) = Z_\zeta(\tilde{g}_0^2, a\mu)(1 + b_\zeta am_q)\zeta(\mathbf{x}), \quad (3.164)$$

and the other boundary fields are renormalized similarly. The renormalization factor Z_A has no scale dependence. This is a consequence of the fact that the renormalization condition of the axial current can be fixed by imposing a continuum chiral Ward identity, which is locally valid. It is now straightforward to write down the renormalized

correlation functions

$$[f_A(x_0)]_R = Z_A(1 + b_A am_q) Z_\zeta^2 (1 + b_\zeta am_q)^2 f_A^I(x_0), \quad (3.165)$$

$$\text{with } f_A^I(x_0) = f_A(x_0) + c_A \frac{1}{2} a (\partial_0^* + \partial_0) f_P(x_0), \quad (3.166)$$

$$[f_P(x_0)]_R = Z_P(1 + b_P am_q) Z_\zeta^2 (1 + b_\zeta am_q)^2 f_P(x_0), \quad (3.167)$$

$$[f_1]_R = Z_\zeta^4 (1 + b_\zeta am_q)^4 f_1. \quad (3.168)$$

Here we have used the lattice derivatives

$$\partial_\mu f(x) = \frac{1}{a} \{f(x + a\hat{\mu}) - f(x)\}, \quad (3.169)$$

$$\partial_\mu^* f(x) = \frac{1}{a} \{f(x) - f(x - a\hat{\mu})\}. \quad (3.170)$$

In a mass-independent renormalization scheme the renormalized version of the static-light axial density $A_0^{\text{stat}}(x)$ can be written as

$$(A_R^{\text{stat}})_0(x) = Z_A^{\text{stat}}(\tilde{g}_0^2, a\mu) (1 + b_A^{\text{stat}} am_1) (A_0^{\text{stat}}(x) + a\delta A_0^{\text{stat}}(x)). \quad (3.171)$$

As for QCD, the renormalization factor Z_A^{stat} can be written as a function of g_0 instead of \tilde{g}_0 in the quenched approximation. Nevertheless the dependence on the scale μ remains, because in the heavy quark sector of HQET chiral symmetry is not present at all. Furthermore Z_A^{stat} depends on the used action. We can now write down the renormalized and improved correlation functions

$$\begin{aligned} [f_A^{\text{stat}}(x_0)]_R &= (1 + a\delta m)^{-x_0/a} Z_A^{\text{stat}} (1 + b_A^{\text{stat}} am_1) Z_\zeta (1 + b_\zeta am_1) \\ &\quad \times Z_h (1 + b_h am_1) f_A^{\text{stat,I}}(x_0)|_{\delta m=0}, \end{aligned} \quad (3.172)$$

$$\text{with } f_A^{\text{stat,I}}(x_0) = f_A^{\text{stat}}(x_0) - \frac{a}{2} \langle \delta A_0^{\text{stat}}(x) \mathcal{O}_{\text{hl}} \rangle_{\text{stat}}, \quad (3.173)$$

$$\begin{aligned} [f_1^{\text{stat}}]_R &= (1 + a\delta m)^{-T/a} Z_\zeta^2 (1 + b_\zeta am_1)^2 \\ &\quad \times Z_h^2 (1 + b_h am_1)^2 f_1^{\text{stat}}|_{\delta m=0}, \end{aligned} \quad (3.174)$$

$$\left[f_1^{\text{hh}}(x_3) \right]_R = (1 + a\delta m)^{-2T/a} Z_h^4 (1 + b_h am_1)^4 f_1^{\text{hh}}(x_3)|_{\delta m=0}. \quad (3.175)$$

We finally remark that, both in QCD and in HQET, the renormalization factors and the improvement coefficients of the boundary fields do not need to be computed. In the

next chapter we introduce only observables, which can be obtained from functions of the renormalized correlators, where these terms cancel out. The same considerations apply to the factors which are powers of $(1 + a\delta m)$. They will drop out in all computed observables, and we will implicitly set $\delta m = 0$ from now on.

Chapter 4

Combining HQET and relativistic QCD

4.1 The Step Scaling Method

The evaluation of the B_s meson properties represents a challenging problem for lattice QCD. The difficulties arise from the presence of two largely separated energy scales. One of them is the heavy quark mass ($m_b \sim 5$ GeV), while the other one is given by the typical QCD scale Λ_{QCD} , which is of the order of a few hundreds of MeV. The light antiquark mass is of the order of the latter, and, by borrowing the language of HQET, the light antiquark belongs to the light degrees of freedom¹.

An accurate simultaneous treatment of these two scales would require the ability to simulate a very fine lattice to resolve the propagation of the heavy quark, and, at the same time, a large physical volume to correctly accommodate the light degrees of freedom with negligible finite size effects. Such a computation, even in the quenched approximation, is unfeasible with the present computational facilities.

The recourse to an effective theory is a natural approach to the problem. In this context HQET represents a promising way to solve it. Another kind of approach, which keeps the relativistic QCD Lagrangian in the form (3.92), is the Step Scaling Method (SSM) proposed by the authors of [7]. Here we show how to combine the two methods in such a way that we can exploit their respective advantages.

Let us explain the basic ideas of the SSM. We consider an observable $\mathcal{O}(E_l, E_h, L)$ depending on two different scales $E_l \ll E_h$, and computed on a lattice with physical

¹With this choice of valence quarks, the most common in the literature about the subject, the corresponding ground state meson is the $\bar{B}_s^0 = \bar{s}b$. However, thanks to the invariance of the action under charge conjugation, we will keep for the meson the notation B_s throughout the following.

extension L . It is easy to identify E_h with the heavy quark mass, and E_l with the QCD scale mentioned above. Since the light scale is kept fixed in physical units in all simulations, we can simplify the notation, and just write $\mathcal{O}(m_h, L)$. The computation of the observable using the SSM is based on the identity

$$\mathcal{O}(m_h, L_\infty) = \mathcal{O}(m_h, L_0) \frac{\mathcal{O}(m_h, L_1)}{\mathcal{O}(m_h, L_0)} \cdots \frac{\mathcal{O}(m_h, L_N)}{\mathcal{O}(m_h, L_{N-1})} \frac{\mathcal{O}(m_h, L_\infty)}{\mathcal{O}(m_h, L_N)}. \quad (4.1)$$

Here L_0 is a volume small enough to allow to simulate with a lattice cutoff much larger than m_b , where the latter can match its phenomenological value. Clearly the motion of the light antiquark is squeezed in such a box, and the following steps perform the evolution to bigger and bigger volumes until L_∞ is reached. Ideally, the latter is an infinite volume; in practice, it is a box large enough to let consider negligible the finite size effects affecting \mathcal{O} . One in fact reaches the situation where the last ratio

$$\frac{\mathcal{O}(m_h, L_\infty)}{\mathcal{O}(m_h, L_N)} = 1 \pm \delta_\infty, \quad (4.2)$$

is consistent with unity within the numerical precision δ_∞ . In other words, one has reached a physical situation, where a measurement of \mathcal{O} is no more sensitive to changes of the volume. The intermediate correcting factors are the step scaling functions

$$\sigma_{\mathcal{O}}(m_h, L_i) = \frac{\mathcal{O}(m_h, L_i)}{\mathcal{O}(m_h, L_{i-1})}, \quad (4.3)$$

where for the sake of simplicity we choose a fixed ratio $s = L_i/L_{i-1}$ in all steps. The number N and the scale ratio s of the steps are in principle dependent on the considered observable and on the desired level of accuracy. It has been numerically shown [50, 51] that $(N, s) = (2, 2)$ is a suitable choice for the mass and the decay constant of the B_s meson. Indeed, it represents a good compromise between the computational effort and the precision on the physical results.

The main assumption of the method is that the step scaling functions have a mild dependence on the heavy quark mass. A total decoupling would mean that the steps are insensitive to variations of m_h as long as $m_h \gg E_l$:

$$\sigma_{\mathcal{O}}(m_h, L_i) \simeq \sigma_{\mathcal{O}}(L_i). \quad (4.4)$$

To understand it we can get help from HQET. If we imagine a meson made of a light antiquark and a static quark, the latter is just a pointlike source of color. The step scaling function $\sigma_{\mathcal{O}}$ measures the error made by computing \mathcal{O} in a volume L_{i-1} instead of L_i . Indeed this measurement cannot depend on the heavy quark; only the light

degrees of freedom are squeezed. It follows that (4.4) becomes an equation. As the heavy quark mass is made finite, one can expect that a total decoupling never takes place, but the step scaling functions can be expanded as

$$\sigma_{\mathcal{O}}(m_h, L_i) = \sigma_{\mathcal{O}}^{(0)}(L_i) + \frac{\sigma_{\mathcal{O}}^{(1)}(L_i)}{L_i m_h} + \mathcal{O}\left(\frac{1}{(L_i m_h)^2}\right). \quad (4.5)$$

Since we want to keep the discretization errors roughly at the same level in all steps, and each of them is to be extrapolated to the continuum, we must scale the simulated heavy quark masses according to the physical size of the involved volumes. To clarify this point we consider again the starting volume L_0 . Here one can simulate with heavy quark masses around the b-quark mass with an acceptable confidence. If we move to $L_1 = 2L_0$ and want to keep the discretization errors, which are of the order of am_h , of the same magnitude as in L_0 we have to halve the heavy mass. This simply means that we are not simulating a b-quark any more. Nevertheless the SSM predicts that the b-region can be reached through a mild extrapolation lead by the expansion (4.5). As one doubles the volume extension again, the heavy mass is halved once more, and the extrapolation to the b-region becomes more difficult. One can then expect that, as the volume becomes bigger and bigger, while the heavy quark mass smaller and smaller, one arrives to a point where the expansion (4.5) is unreliable.

On the other side, if one computes the coefficients $\sigma_{\mathcal{O}}^{(0)}(L_i)$, for all volumes, by using the static theory developed in HQET, all extrapolations can be turned into interpolations. This implies higher confidence in the approach to the b-quark energy scale as well as increased precision in all steps. Furthermore, one can exploit HQET to directly compute some coefficients $\sigma_{\mathcal{O}}^{(n)}(L_i)$, $n \geq 1$ in order to have a better control on the heavy scale expansion. The combination of the SSM with HQET thus represents a very appealing way to go about studying the heavy-light meson properties [52].

4.2 Simulation parameters

4.2.1 Action

All simulations carried out to get the results of this chapter have been performed within the quenched approximation (cf. Sect. 3.3). The choice of the static action has been restricted to the HYP2 action [29] only, which is a HYP action, as described in Sect. 3.2, with parameters $(\alpha_1, \alpha_2, \alpha_3) = (1.0, 1.0, 0.5)$.

In an early stage of this work, simulations on a small volume ($L = 0.4$ fm) for the static-light pseudoscalar decay constant have shown that other choices of the parameters α_i as well as other discretizations of the static action give results consistent with

HYP2 in the continuum limit, as we expect from universality. However, the precision is sensibly lower, and studies on the subject [29] have shown that this pattern is preserved in bigger volumes too. The simultaneous employment of several actions does not pay off under the point of view of the statistical precision, because whenever all data share the same gauge configurations, they are found to be strongly correlated.

4.2.2 Scale setting

In order to let lattice QCD computations be able to be physically predictive, one has to spend as many experimental input as are the free parameters of the theory. In pure gauge theory the only free parameter is the bare coupling g_0 , and each dimensionful quantity is expressed in units of the lattice spacing. It is therefore of fundamental importance to have an accurate knowledge of the lattice spacing in physical units. The functional dependence of a from g_0 is predicted in the high energy regime by the asymptotic freedom once the scale Λ , appearing in the renormalization group equation of the coupling, is known. As one enters into the low energy regime, a perturbative evaluation of the scale becomes unsatisfactory.

The setting of the scale is thus achieved by using suitable observables, and a widely used one is the hadronic length r_0 [53], whose definition relies on the force $F(r)$ between two static color sources. To be more precise, r_0 is defined as the distance where

$$r^2 F(r)|_{r=r_0} = 1.65. \quad (4.6)$$

The authors of [54, 55] have performed a direct computation of the ratio a/r_0 for several values of the bare coupling, and they have provided a phenomenological representation of $\ln(a/r_0)$ as a polynomial in β . In fact, by choosing the ansatz

$$\ln(a/r_0) = \sum_{n=0}^p a_n (\beta - 6)^n \quad (4.7)$$

they have found that

$$\begin{aligned} \ln(a/r_0) &= -1.6804 - 1.7331(\beta - 6) + 0.7849(\beta - 6)^2 - 0.4428(\beta - 6)^3, \\ &\text{for } 5.7 \leq \beta \leq 6.92, \end{aligned} \quad (4.8)$$

is an excellent approximation of the Monte Carlo results. The accuracy of a/r_0 in eq. (4.8) has been estimated to decrease from about 0.5% at low β to 1% at $\beta = 6.92$.

For values of β greater than 6.92 the validity of parametrization (4.8) cannot be blindly trusted any more. However, the authors of [56] have shown that one can use the non-perturbative results coming from the computation of the Schrödinger functional renormalized coupling [12, 37] and a renormalization group analysis, to obtain

a parametrization of (a/r_0) as a function of the bare coupling for $\beta > 6.92$. The parametrization reads

$$\ln(a/r_0) = -\ln(\lambda_L) - \frac{b_1}{2b_0^2} \ln(b_0 g_0^2) - \frac{1}{2b_0 g_0^2} - I(g_0), \quad (4.9)$$

where

$$I(g_0) = \int_0^{g_0} dx \left[\frac{1}{\beta(x)} + \frac{1}{b_0 x^3} - \frac{b_1}{b_0^2 x} \right], \quad (4.10)$$

$$\beta(x) = -x^3 \{b_0 + b_1 x^2 + b_2 x^4 + b_3 x^6 + \dots\}. \quad (4.11)$$

The function in eq. (4.11) has already appeared in eq. (2.62), and it is reported also here only for reading convenience. Restricting the analysis to the four-loop expression of $\beta(x)$, the coefficients read

$$\begin{aligned} \lambda_L &= 0.0203 & b_0 &= 11/(4\pi)^2, & b_1 &= 102/(4\pi)^4, \\ b_2 &= -0.0015998323314, & b_3 &= -0.0025. \end{aligned}$$

With these values the uncertainty on a/r_0 for $6.92 < \beta < 7.5$ can be estimated to be 2%, worsening to 3% at $\beta = 8.5$. One has to remark that the coefficient b_3 is the result of a fit, and not of a direct computation.

The choice of the value 1.65 in eq. (4.6) is dictated by phenomenological potential models, which predict an approximate value for r_0 of 0.5 fm. The uncertainty on the physical value of r_0 is around 10%, and this is translated in large systematic errors for the quantities converted in physical units through this scale. However, as long as the lattice results are kept in units of r_0 , the precise parametrizations of eq. (4.8) and eq. (4.9) allow to compare determinations of the same physical quantity, obtained from different choices of the lattice setup (action, lattice spacing, volume, ...).

4.2.3 Quark masses

Since quarks are confined inside hadrons, their masses are not physical observables. They are free parameters of the theory, and, as it happens for the gauge coupling, they have to be determined by introducing an experimental input. In addition, there is no universal definition of the quark mass; one is free to use the most suitable definition

for one's purposes. We start by defining the bare current quark mass through the $O(a)$ -improved PCAC relation

$$m_{q_2q_1} = \frac{\tilde{\partial}_0 f_A(x_0) + ac_A \partial_0^* \partial_0 f_P(x_0)}{2f_P(x_0)} \Big|_{x_0=T/2}, \quad \text{with} \quad (4.12)$$

$$\tilde{\partial}_0 = \frac{1}{2}(\partial_0^* + \partial_0). \quad (4.13)$$

Quark masses defined in this way are not affected by the choice of the kinematical parameters (L, T, θ, x_0) up to corrections of $O(a^2)$. This is a consequence of the improvement and of the very derivation of the PCAC relation, relying on the symmetries of the continuum action. The spatial components do not appear on the r.h.s. of eq. (4.12), because they vanish under periodic boundary conditions. The choice $x_0 = T/2$ in eq. (4.12) simply follows from the intention of computing the correlation functions f_A and f_P with the bulk operator inserted as far as possible from the temporal boundaries, and therefore to minimize the cutoff effects.

The coefficient c_A has been computed by the authors of [45], who provided the parametrization

$$c_A(g_0^2) = -0.00756g_0^2 \times \frac{1 - 0.748g_0^2}{1 - 0.977g_0^2}, \quad (4.14)$$

valid in the range of bare couplings $0 \leq g_0 \leq 1$.

In Sect. 3.5.3 we have seen that the Schrödinger functional allows to define a finite volume renormalization scheme, where the correlation functions f_A and f_P are multiplicatively renormalized. We exploit this property to define from eq. (4.12) a renormalized and improved quark mass

$$\bar{m}_{q_2q_1} = \frac{\tilde{\partial}_0 [f_A(x_0)]_R}{[f_P(x_0)]_R} \Big|_{x_0=T/2} \quad (4.15)$$

$$= \frac{Z_A [1 + \frac{1}{2}b_A(am_{q_2} + am_{q_1})]}{Z_P [1 + \frac{1}{2}b_P(am_{q_2} + am_{q_1})]} m_{q_2q_1} \quad (4.16)$$

$$= \frac{Z_A}{Z_P} \left[1 + (b_A - b_P) \frac{am_{q_2} + am_{q_1}}{2} \right] m_{q_2q_1}, \quad (4.17)$$

where each equation is valid up to $O(a^2)$ corrections. At the end of Sect. 2.6 we have introduced the RGI quark mass M , as the asymptotic behavior of any renormalized running mass. This mass has the advantage of being scale and scheme independent,

while $\bar{m}_{q_2q_1}$ misses this property because of the presence of Z_P . However, the two masses can be related by the renormalization group equation

$$M_{q_2q_1} = \bar{m}_{q_2q_1} (2b_0\bar{g}^2)^{-d_0/2b_0} \times \exp \left\{ - \int_0^{\bar{g}} dg \left[\frac{\tau(g)}{\beta(g)} - \frac{d_0}{b_0g} \right] \right\}. \quad (4.18)$$

Actually, there is no unique way of normalizing the mass M . One could multiply the r.h.s. of eq. (4.18) by a factor 2, and obtain a valid mass definition. Here we choose to comply with the conventions of Gasser and Leutwyler [57, 58, 59]. We rewrite eq. (4.18) by showing the explicit dependence on the renormalization scale

$$M_{q_2q_1} = \frac{M_{q_2q_1}}{\bar{m}_{q_2q_1}(\mu)} \frac{Z_A(g_0)}{Z_P(g_0, L)} \left[1 + (b_A - b_P) \frac{am_{q_2} + am_{q_1}}{2} \right] m_{q_2q_1} + \mathcal{O}(a^2),$$

$$\text{with } \mu = 1/L. \quad (4.19)$$

We can now define the total renormalization factor

$$Z_M(g_0) = \frac{M_{q_2q_1}}{\bar{m}_{q_2q_1}(\mu)} \frac{Z_A(g_0)}{Z_P(g_0, L)}, \quad \mu = 1/L, \quad (4.20)$$

such that

$$M_{q_2q_1} = Z_M(g_0) m_{q_2q_1}(g_0) + \mathcal{O}(a^2). \quad (4.21)$$

It relates (up to terms of $\mathcal{O}(a^2)$) the bare current quark mass with the RGI one, and consists of a regularization independent (but scale dependent) part M/\bar{m} , and the ratio Z_A/Z_P , depending on the regularization details.

A single quark mass is obtained by choosing two mass degenerate flavors q_1 and q_2

$$M_q = M_{qq} = Z_M m_{qq} + \mathcal{O}(a^2), \quad (4.22)$$

which we label as diagonal definition. Up to $\mathcal{O}(a^2)$ it can be replaced by the off-diagonal definitions

$$M_{q\{j\}} = 2M_{qj} - M_{qq}. \quad (4.23)$$

The quantities $r_0 M_q$ and $r_0 M_{q\{j\}}$ have the same continuum limit, even if the cutoff effects, still remaining of $\mathcal{O}(a^2)$, may strongly depend on the choice of the j -flavor. It is reasonable to have a light j -flavor, in order to minimize the improvement term proportional to $(b_A - b_P)am_j$.

In addition we consider current quark masses with improved derivatives, by replacing in eq. (4.12),

$$\tilde{\partial}_0 \rightarrow \tilde{\partial}_0 \left(1 - \frac{1}{6} a^2 \partial_0^* \partial_0 \right), \quad \partial_0^* \partial_0 \rightarrow \partial_0^* \partial_0 \left(1 - \frac{1}{12} a^2 \partial_0^* \partial_0 \right). \quad (4.24)$$

| β | [6.0, 6.5] | 6.7370, 6.9630 | 7.1510 | 7.3000, 7.5480 |
|-------------------|------------|----------------|--------|----------------|
| $\Delta(Z_A/Z_P)$ | 1.1% | 1.0% | 0.8% | 0.6% |

Table 4.1: Uncertainties on the regularization dependent part of the total renormalization factor Z_M .

when acting on smooth functions these lattice derivatives have errors of $O(a^4)$ only.

Another way of computing the RGI quark mass starts from the subtracted quark mass m_q defined in eq. (3.156), and is completed by a multiplicative renormalization

$$\hat{M}_q = Z_M(g_0)Z(g_0)[1 + b_m am_q]m_q. \quad (4.25)$$

The renormalization factor Z_M has been computed in [12, 60] for the range of β -values [6.0, 7.6101], and can be parametrized in this range by the expression

$$Z_M(\beta) = 1.755 + 0.188(\beta - 6.0) - 0.024(\beta - 6.0)^2. \quad (4.26)$$

The uncertainty relative to the regularization independent part M/\bar{m} amounts to 0.9% at $\mu = 1/L_0 = 2.5 \text{ fm}^{-1}$, while for the ratio Z_A/Z_P we have estimated the errors $\Delta(Z_A/Z_P)$ reported in Table 4.1. The value of $\Delta(Z_A/Z_P)$ in the range $6.0 \leq \beta \leq 6.5$ has been quoted in [12] to be 1.1%, while the uncertainties for smaller values of the coupling have been estimated from the errors on Z_A and Z_P quoted in [12] and [61] respectively. They are reported in Table 4.1 for the β -values needed in our computations. The factor Z has been defined and computed in [62], where one can read off the parametrization

$$Z(g_0^2) = (1 + 0.090514g_0^2) \times \frac{1 - 0.9678g_0^2 + 0.04284g_0^4 - 0.04373g_0^6}{1 - 0.9678g_0^2}, \quad (4.27)$$

with a relative precision better than 0.04% in the range $0.8881 \leq g_0^2 \leq 1.0$. The authors of [63] have shown that the parametrization (4.27) can be used also for values of g_0^2 smaller than 0.8881, but we did not exploit it in our computations. The reason relies in the improvement coefficient b_m , as it explained in the following discussion.

The quantities $b_A - b_P$ and b_m have been computed in [62], whose authors provided the parametrizations

$$(b_A - b_P)(g_0^2) = -0.00093g_0^2 \times \frac{1 + 23.3060g_0^2 - 27.3712g_0^4}{1 - 0.9833g_0^2}, \quad (4.28)$$

$$b_m(g_0^2) = (-0.5 - 0.09623g_0^2) \times \frac{1 - 0.6905g_0^2 + 0.0584g_0^4}{1 - 0.6905g_0^2}. \quad (4.29)$$

In the range $0.8881 \leq g_0^2 \leq 1.0$ the parametrization (4.28) represents the computed data with an absolute deviation smaller than 0.3%, and the authors of [63] have shown that this can be believed also for smaller values of the gauge coupling, covering the ones needed in our computations. The parametrization (4.29) describes the available non-perturbative data in the range $0.8881 \leq g_0^2 \leq 1.0$ with an absolute deviation smaller than 1.3%, but, as it has been demonstrated in [63], this parametrization cannot be trusted for smaller values of the coupling. For our computations we thus decided to use the mass definition given in eq. (4.25) only for $0.8881 \leq g_0^2 \leq 1.0$.

In terms of the hopping parameter κ introduced in Sect. 3.2, the subtracted bare mass (3.156) reads

$$am_q = \frac{1}{2} \left(\frac{1}{\kappa} - \frac{1}{\kappa_{\text{crit}}} \right). \quad (4.30)$$

For $\kappa = \kappa_{\text{crit}}$ the physical quark mass vanishes, as we require in our renormalization scheme. The value of κ_{crit} is determined, for each choice of the lattice setup, by choosing a set of κ -values κ_i such that, after a short Monte Carlo simulation, part of the corresponding (flavor-degenerate) values of the bare current quark mass (4.12) are positive, and the remaining part is negative or consistent with zero. The data are then represented in a plot am_{ij} vs. $1/2\kappa_i$, and, for the values of am_{ij} which are closest to zero, a linear interpolation is performed. The fitted function $am_{ij} = a_1 + a_2/2\kappa_i$ usually shows $a_2 \approx 1$, and the extracted $-a_2/2a_1$ is our estimate of κ_{crit} . The latter can be used as hopping parameter in a further simulation to check that the computed current mass vanishes within statistical errors. An example is shown in Fig. 4.1. For the simulations with the relativistic QCD action [50, 51], the hopping parameters corresponding to the strange quark have been determined in such a way that, for each choice of the lattice setup, one can arrange three RGI quark masses, according to the definition (4.22), lying around the value

$$M_s = 0.1346(55) \text{ GeV}, \quad (4.31)$$

computed in [64], where the chosen experimental input is the Kaon mass. The dependence of the computed observables on the light quark is very mild, and they are interpolated as linear functions of the simulated light quarks to match eq. (4.31).

The results published in [50, 51] have been used to match the hopping parameters corresponding to the strange quark, by performing a linear fit of the light quark masses $M_i = a + b/\kappa_i$, and extracting the desired κ_s -values as $\kappa_s = b/(M_s - a)$, with M_s quoted in eq. (4.31). These values have been used as input for the simulations with the heavy quark Lagrangian. However, the data appearing in [50, 51], do not cover all lattice setups used in the HQET computations. The missing values of the hopping parameters have then been determined ex novo, by requiring the corresponding RGI quark masses to be consistent with eq. (4.31). A list of all simulation parameters is given in App. C.

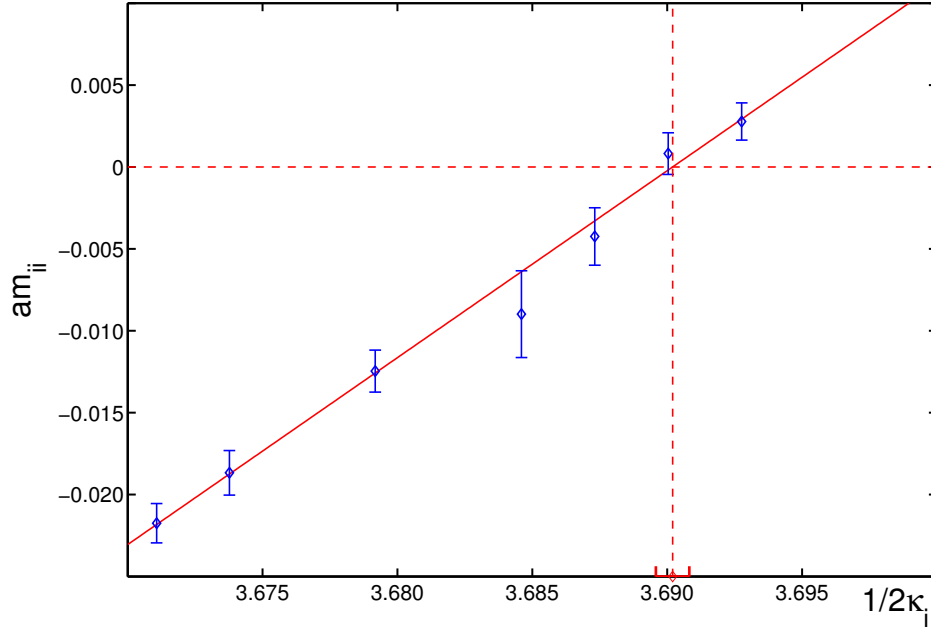


Figure 4.1: Linear interpolation for κ_{crit} . The data refer to a lattice with $\beta = 6.0914$, $L/a = 10$, $T = 2L$ and $\theta = 0.0$. All points are statistically independent.

4.2.4 Improvement coefficients and renormalization factors

All improvement coefficients and renormalization factors needed to determine the simulation parameters have been presented in the previous subsections. However, they are not sufficient to achieve the $O(a)$ -improvement and the renormalization of all computed correlation functions. Here we report the missing ingredients. The improvement coefficient b_A appearing in eq. (3.163) has been computed [46] at 1-loop, and reads

$$b_A(g_0^2) = 1 + 0.15219(5)g_0^2 + O(g_0^4). \quad (4.32)$$

The renormalization factor Z_A has been non-perturbatively computed in [61], where the rational expression

$$Z_A(g_0^2) = \frac{1 - 0.8496g_0^2 + 0.0610g_0^4}{1 - 0.7332g_0^2}, \quad (4.33)$$

has been proposed as good representation of the numerical results in the range of bare couplings $0 \leq g_0 \leq 1$. The uncertainty associated with this parametrization is reported for the couplings of interest in the following table.

| | | | |
|---------------|--------|--------|--------|
| β | 7.1510 | 7.3000 | 7.5480 |
| $\Delta(Z_A)$ | 0.8% | 0.6% | 0.6% |

For HQET the coefficients c_A^{stat} and b_A^{stat} have been computed [29] for the static HYP2 action at 1-loop

$$c_A^{\text{stat}} = 0.220(14)g_0^2 + \mathcal{O}(g_0^4), \quad b_A^{\text{stat}} = 1/2 + 0.259(13)g_0^2 + \mathcal{O}(g_0^4). \quad (4.34)$$

The renormalization factor Z_A^{stat} for the HYP2 action has been computed by the authors of [29], but in a range of couplings, which does not cover all our simulations. Its computation represents part of the work of this thesis.

4.2.5 Quark mass scheme conversion

Once the quark mass has been computed using one of the RGI definitions given in Sect. 4.2.3, it is useful to translate it to the mass in the widely used $\overline{\text{MS}}$ scheme. This is achieved through the equation

$$\frac{M}{\overline{m}(\overline{m})} = (2b_0\overline{g}^2(\overline{m}))^{-d_0/2b_0} \exp \left\{ - \int_0^{\overline{g}(\overline{m})} dg \left[\frac{\tau^{\overline{\text{MS}}}(g)}{\beta^{\overline{\text{MS}}}(g)} - \frac{d_0}{b_0 g} \right] \right\}, \quad (4.35)$$

where $\overline{g} = \overline{g}_{\overline{\text{MS}}}$, $\overline{m} = \overline{m}_{\overline{\text{MS}}}$, and the expression on the r.h.s. can be evaluated with a 4-loop accuracy thanks to the coefficients reported in Table 4.2 and the result $\Lambda_{\overline{\text{MS}}} r_0 = 0.602(48)$ [37, 55].

4.3 Computation of the b-quark mass

4.3.1 General strategy

Our lattice setup is given by the discretized Schrödinger functional, as in Sect. 3.2, with topology $T \times L^3$ and parameters

$$T = 2L, \quad C = C' = 0, \quad \text{and} \quad \theta = 0.0, \quad (4.36)$$

| $\beta^{\overline{\text{MS}}}$ | $\tau^{\overline{\text{MS}}}$ |
|---|-------------------------------------|
| $b_0 = \frac{11}{(4\pi)^2}$ | $d_0 = \frac{8}{(4\pi)^2}$ |
| $b_1 = \frac{102}{(4\pi)^4}$ | $d_1 = \frac{404}{3(4\pi)^4}$ |
| $b_2 = \frac{2857}{2(4\pi)^6}$ | $d_2 = \frac{2498}{(4\pi)^6}$ |
| [65] $b_3 = \frac{29243-5033/18}{(4\pi)^8}$ | $d_3 = \frac{50659}{(4\pi)^8}$ [66] |

Table 4.2: 4-loop β -function and anomalous dimension of the mass in the $\overline{\text{MS}}$ scheme. The references are only for the highest order computations; there one finds also the references for the lower orders too.

for all correlation functions, unless stated otherwise. We first consider the case of a finite volume pseudoscalar meson mass²

$$\mathcal{O}(m_h, L) = M_{\text{PS}}(m_h, L), \quad (4.37)$$

where m_h stands generically for a heavy quark mass, whose precise definition is needed only later. The dependence on the light quark mass, which is fixed in all volumes to the physical strange quark mass as described in Sect. 4.2.3, has been dropped. The meson mass is defined in analogy to the effective mass in eq. (3.134), as

$$M_{\text{PS}}(m_h, L) = \frac{1}{2a} \ln \left[\frac{f_{\text{A}}^{\text{I}}(m_h, L, x_0 - a)}{f_{\text{A}}^{\text{I}}(m_h, L, x_0 + a)} \right]_{x_0=L}. \quad (4.38)$$

The choice of taking f_{A}^{I} around the middle of the temporal lattice is a definition which well suits the Step Scaling Method, and aims also to reduce the cutoff effects in all steps. It is straightforward to conclude that

$$M_{\text{PS}}(m_h, L) \stackrel{m_h \rightarrow m_b}{=} M_{\text{B}_s}(L) \stackrel{L \rightarrow \infty}{=} M_{\text{B}_s}. \quad (4.39)$$

In the expansion (4.5) we simply have $\sigma_{\mathcal{O}}^{(0)} = 1$, and the first non-trivial term $\sigma_{\mathcal{O}}^{(1)}$ is computable in the static approximation of HQET. We further define

$$x(m_h, L) \equiv \frac{1}{LM_{\text{PS}}(m_h, L)} = \frac{1}{Lm_h} + \mathcal{O}\left(\frac{1}{(Lm_h)^2}\right), \quad (4.40)$$

²The mass m_h and the length L are given in physical units through the scale r_0 defined in Sect. 4.2.2. If more rigor is desired, one may identify the observable \mathcal{O} with the dimensionless quantity $LM_{\text{PS}}(Lm_h, L/r_0)$.

as the natural non-perturbative dimensionless mass variable. It is given in terms of physical observables, and there is no uncertainty deriving from a choice of quark mass definition³. The step scaling function for the meson mass assumes then the simple form

$$\sigma_m(x, L_i) \equiv \frac{M_{\text{PS}}(m_h, L_i)}{M_{\text{PS}}(m_h, L_{i-1})} = 1 + \sigma_m^{\text{stat}}(L_i) \cdot x + \mathcal{O}(x^2), \quad (4.41)$$

$$x = x(m_h, L_i),$$

and it is defined for all x, L . Our strategy for its precise numerical evaluation is to compute σ_m^{stat} explicitly in the static approximation, and fix the small remainder by means of relativistic QCD data with (heavy) quarks of masses of the physical charm and higher. In analogy to the mass (4.39) we define

$$\Gamma_{\text{stat}}(L) = \frac{1}{2a} \ln \left[\frac{f_{\text{A}}^{\text{stat}, \text{I}}(L, x_0 - a)}{f_{\text{A}}^{\text{stat}, \text{I}}(L, x_0 + a)} \right]_{x_0=L}, \quad (4.42)$$

whose large volume limit gives

$$\Gamma_{\text{stat}}(L) \stackrel{L \rightarrow \infty}{=} E_{\text{stat}}. \quad (4.43)$$

By considering the case $L_i = 2L_{i-1} = 2L$ we can write a more explicit form for σ_m appearing in eqs. (4.41), that reads

$$\begin{aligned} \frac{M_{\text{PS}}(m_h, 2L)}{M_{\text{PS}}(m_h, L)} &= \frac{m_h + \Gamma_{\text{stat}}^{\text{R}}(2L) + \mathcal{O}(1/Lm_h)}{m_h + \Gamma_{\text{stat}}^{\text{R}}(L) + \mathcal{O}(1/Lm_h)} \\ &= 1 + \frac{\Gamma_{\text{stat}}(2L) - \Gamma_{\text{stat}}(L)}{m_h} + \mathcal{O}(1/L^2 m_h^2) \\ &= 1 + \frac{2L[\Gamma_{\text{stat}}(2L) - \Gamma_{\text{stat}}(L)]}{2Lm_h} + \mathcal{O}(1/L^2 m_h^2) \\ &= 1 + \frac{2L[\Gamma_{\text{stat}}(2L) - \Gamma_{\text{stat}}(L)]}{2LM_{\text{PS}}(m_h, 2L)} + \mathcal{O}(1/L^2 M_{\text{PS}}^2(m_h, 2L)) \\ &= 1 + \sigma_m^{\text{stat}}(2L) \cdot x + \mathcal{O}(x^2), \end{aligned} \quad (4.44)$$

where we can identify the static step scaling function

$$\sigma_m^{\text{stat}}(L_i) = L_i [\Gamma_{\text{stat}}(L_i) - \Gamma_{\text{stat}}(L_{i-1})]. \quad (4.45)$$

³This is certainly true once the continuum limit has been reached.

On the r.h.s. of the first equation in the expansion (4.44), the renormalized static effective mass $\Gamma_{\text{stat}}^{\text{R}}$ appears. It is related to Γ_{stat} , computed at $\delta m = 0$, by

$$\Gamma_{\text{stat}}^{\text{R}} = \Gamma_{\text{stat}} + \frac{1}{a} \ln(1 + a\delta m). \quad (4.46)$$

However, this additive renormalization term cancels out in the following equations, and we do not need to take care of it.

It has been shown in [50], that the choice $L_{\infty} \approx L_2 = 1.6$ fm guarantees to have a box, where lattice computations of $M_{\text{PS}}(m_{\text{h}}, L_{\infty})$ are affected by negligible finite size effects. With the experimental value for the mass of the B_{s} meson, $M_{B_{\text{s}}} = 5.3675(18)$ GeV we fix $x_2 = 1/L_2 M_{B_{\text{s}}}$, and the physical points corresponding to the b-quark are then given by

$$x_2 = 1/L_2 M_{B_{\text{s}}}, \quad x_{i-1} = 2\sigma_{\text{m}}(x_i, L_i) \cdot x_i. \quad (4.47)$$

The numerical results will have to be evaluated at these points. After performing the steps $L_2 \rightarrow L_1 = 0.8$ fm and $L_1 \rightarrow L_0 = 0.4$ fm, we arrive at the small volume⁴ L_0 , which plays a special role. Here we relate the meson mass to the renormalization group invariant quark mass M_{h} defining

$$\rho(x, L_0) = \frac{M_{\text{PS}}(M_{\text{h}}, L_0)}{M_{\text{h}}} = \rho^{(0)}(L_0) + \rho^{(1)}(L_0) \cdot x + \mathcal{O}(x^2). \quad (4.48)$$

We finally gather eqs. (4.47) and eqs. (4.48) to get the connection between the B_{s} meson mass and the RGI b-quark mass M_{b} in the compact form

$$M_{\text{b}} = \frac{M_{B_{\text{s}}}}{\rho(x_0, L_0) \cdot \sigma_{\text{m}}(x_1, L_1) \cdot \sigma_{\text{m}}(x_2, L_2)}. \quad (4.49)$$

4.3.2 The results

The computation of $\sigma_{\text{m}}(x, L_2)$ is performed at finite heavy quark masses around the charm quark mass, on lattices with $\beta = 5.9598, 6.2110, 6.4200$, corresponding to resolutions $L_2/a = 16, 24, 32$ respectively; the continuum limits for the three heaviest quark masses are shown in App. C.

For the static step scaling function we took the results for the bigger volume from [1]. There the spatial extension $L_2 \approx 1.5$ fm, and the ratio T/L , with $T > L$, is not fixed

⁴Thanks to eqs. (4.36) the volume can be identified without ambiguities with the spatial extension. The adjective ‘‘small’’ is here referred to the smallest box where our simulations took place.

to be the same for all values of the bare coupling. However the box is big enough to assume $L_2 \approx L_\infty$ for a B_s meson, and we have

$$\sigma_m^{\text{stat}}(L_2) = 2L_1[E_{\text{stat}} - \Gamma_{\text{stat}}(L_1)]. \quad (4.50)$$

The energy E_{stat} is available from [1] for four values of the coupling, while $\Gamma_{\text{stat}}(L_1)$ is computed with the setup in eqs. (4.36) for the couplings in the third row of the following table.

| | | | | | |
|---|--------|--------|--------|--------|--------|
| β for $\sigma_m(x, L_2)$ | 5.9598 | - | 6.2110 | 6.4200 | - |
| β for E_{stat} | 6.0291 | 6.2885 | 6.4500 | 6.4956 | - |
| β for $\Gamma_{\text{stat}}(L_1)$ | 5.9598 | 6.0914 | 6.2110 | 6.4200 | 6.7370 |

After a quadratic fit of $a\Gamma_{\text{stat}}(L_1)$ vs. β , the computed coefficients are used to interpolate $a\Gamma_{\text{stat}}(L_1)$ at the same values of β used for the computation of E_{stat} . This makes possible to take the continuum limit for the static step scaling function, and get

$$\sigma_m^{\text{stat}}(L_2) = 1.561(53). \quad (4.51)$$

Since the interpolated values of $a\Gamma_{\text{stat}}(L_1)$ are all obtained from the same set of data, it is clear that they are correlated. However, such correlation affects the continuum limit (4.51) by an amount, which is several orders of magnitude smaller than the error quoted in (4.51). The static step scaling function is used to fix (within errors) the first non-trivial term in the expansion (4.41). In practice it consists of a constraint on the slope of the fitting curve. For a quadratic fit, the χ^2 to be minimized has the expression

$$\chi^2 = \sum_i \left(\frac{\sigma_m(x_{(i)}, L_2) - 1 - bx_{(i)} - cx_{(i)}^2}{\Delta\sigma_m(x_{(i)}, L_2)} \right)^2 + \left(\frac{b - \sigma_m^{\text{stat}}(L_2)}{\Delta\sigma_m^{\text{stat}}(L_2)} \right)^2. \quad (4.52)$$

A correct estimate of the uncertainties has to consider the concomitant presence of the errors associated with σ_m and the ones with x . First of all, a fit with only the uncertainties on σ_m is performed, dealing with them as if they were uncorrelated. Then the correlation between the σ_m 's associated with different heavy quark masses is handled by means of the method described in App. E. Finally the errors on x are taken into account according to the procedure described in App. D. However, given the flatness of

the fitting curves, these corrections to the errors are found to be negligible compared to the uncertainty on σ_m itself. For this reason also the correlation between the x 's associated with different heavy quark masses, as well as the correlation between x and σ_m can be neglected. The results of the interpolation are given in Table 4.3.

The step $L_1 \rightarrow L_0 = 0.4$ fm is performed in complete analogy with the previous step. The continuum limit for the static step scaling function

$$\sigma_m^{\text{stat}}(L_1) = 0.233(36), \quad (4.53)$$

is used as constraint on the fitting curves. The results of the interpolations are given in Table 4.3.

On the small volume ($L_0 = 0.4$ fm) only the relativistic QCD data are needed to establish a finite volume relationship between the pseudoscalar meson mass $M_{\text{PS}}(L_0)$ and the RGI quark mass M_{h} , and consequently interpolate the bottom quark mass. First of all a linear fit $\rho(x, L_0)$ vs. x is performed considering only the uncertainties on ρ , without correlation between the data. The latter is taken into account in a successive step through the method described in App. E. Finally, with the computed slope $\rho^{(1)}$, one adds to ρ the uncertainty on x and, for each point, the correlation between the uncertainties on x and ρ according to the procedure of App. D:

$$(\Delta\rho)^2 \rightarrow (\Delta\rho)^2 + (\rho^{(1)}\Delta x)^2 - 2\rho^{(1)}\frac{\partial\rho}{\partial M_{\text{PS}}}\frac{\partial x}{\partial M_{\text{PS}}}(\Delta M_{\text{PS}})^2, \quad (4.54)$$

This last step amounts to a small correction to the errors, justifying the neglect of the correlation between the x 's associated with different heavy quark masses.

The data are shown in Fig. 4.4, where the red point (asterisk) corresponds to the interpolation at the value of x_0 obtained from the step scaling functions with the static constraint. The cyan point (triangle) corresponds to the interpolation at the value of x_0 computed with only the data at finite heavy quark mass.

Using eq. (4.49), the interpolated value

$$\rho(x_0, L_0) = 0.748(11), \quad (4.55)$$

is combined with the above step scaling functions to find the scale and scheme independent number

$$M_{\text{b}} = 6.879(104) \text{ GeV} \Rightarrow \bar{m}_{\text{b},\overline{\text{MS}}}(\bar{m}_{\text{b},\overline{\text{MS}}}) = 4.416(60) \text{ GeV}. \quad (4.56)$$

By performing the whole analysis with only the data at finite heavy quark mass, we get

$$M_{\text{b}}^* = 6.953(108) \text{ GeV} \Rightarrow \bar{m}_{\text{b},\overline{\text{MS}}}^*(\bar{m}_{\text{b},\overline{\text{MS}}}^*) = 4.458(62) \text{ GeV}. \quad (4.57)$$

The conversion of the mass to the $\overline{\text{MS}}$ scheme is performed according to the method outlined in Sect. 4.2.5, and the associated perturbative uncertainty can be safely neglected. Starting from a precisely specified input, in our case the scale r_0 and the experimental K and B_s masses, the result for the b-quark mass is unambiguous in the quenched approximation.

In [67] the b-quark mass has been non-perturbatively determined in HQET, up to and including the $O(1/m_h)$ terms, by starting from r_0 and the experimental values of m_K and of the spin-averaged mass $(M_{B_s} + 3M_{B_s^*})/4$, obtaining $\overline{m}_{b,\overline{\text{MS}}}(\overline{m}_{b,\overline{\text{MS}}}) = 4.347(48)$ GeV. This result can be compared with our determination (4.56) even if the experimental spin-averaged meson mass instead of the pseudoscalar one is used. These different choices affect the value of the b-quark mass by $O(\Lambda_{\text{QCD}}^3/m_b^2)$. The agreement between the two determinations is evident.

Other quenched determinations of $\overline{m}_{b,\overline{\text{MS}}}(\overline{m}_{b,\overline{\text{MS}}})$ are 4.41(5)(10) GeV in HQET [68], extended to smaller values of the lattice spacing in [69] getting consistent results, and 4.34(7) GeV from NRQCD [70]. However, if other inputs are used, one cannot perform a real comparison because r_0 is only approximately known and the quenched approximation is not real QCD. See [71] for a recent review.

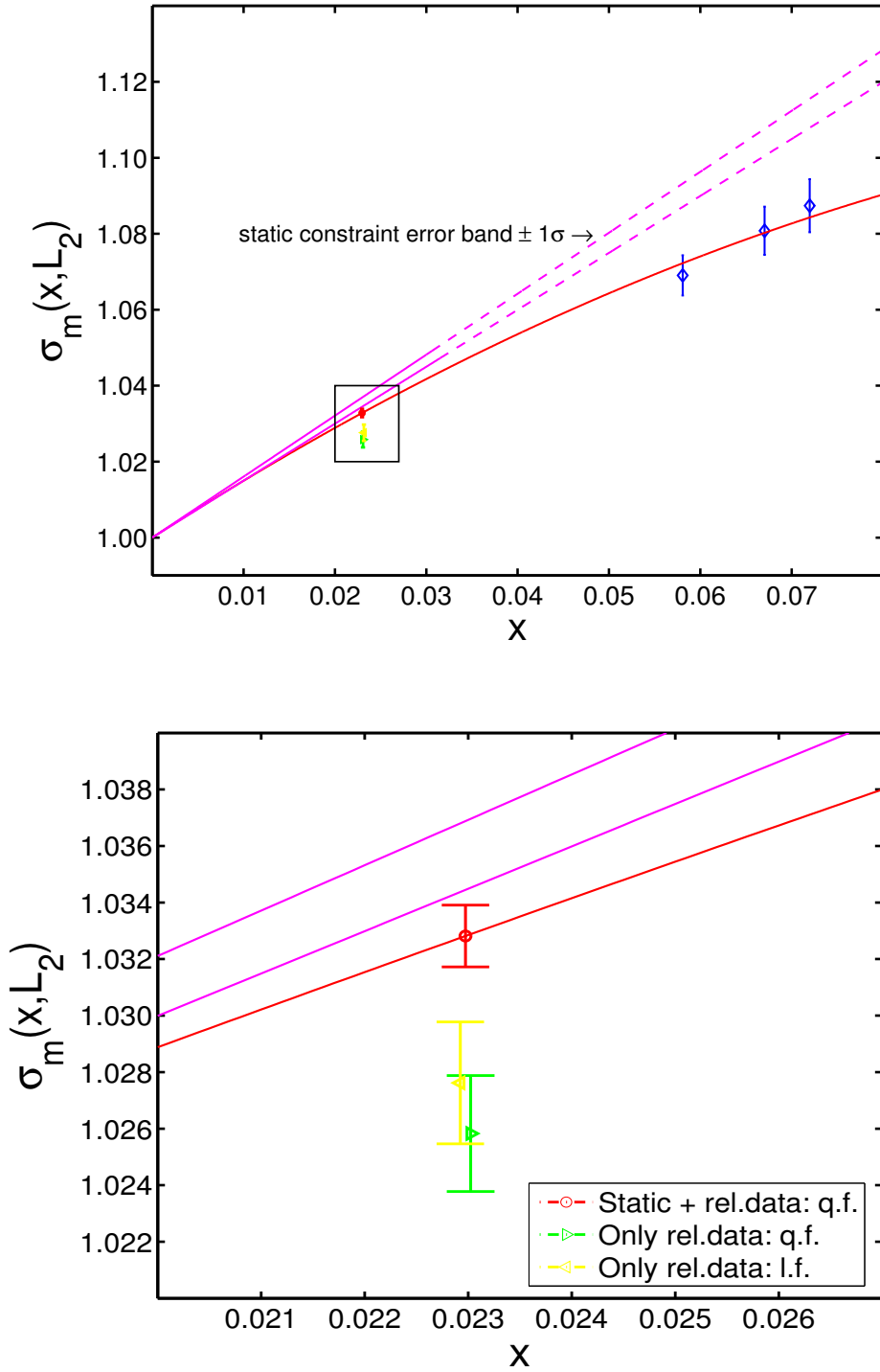


Figure 4.2: Plot of the step scaling function $\sigma_m(x, L_2)$ vs. $x = x(m_h, L_2)$.

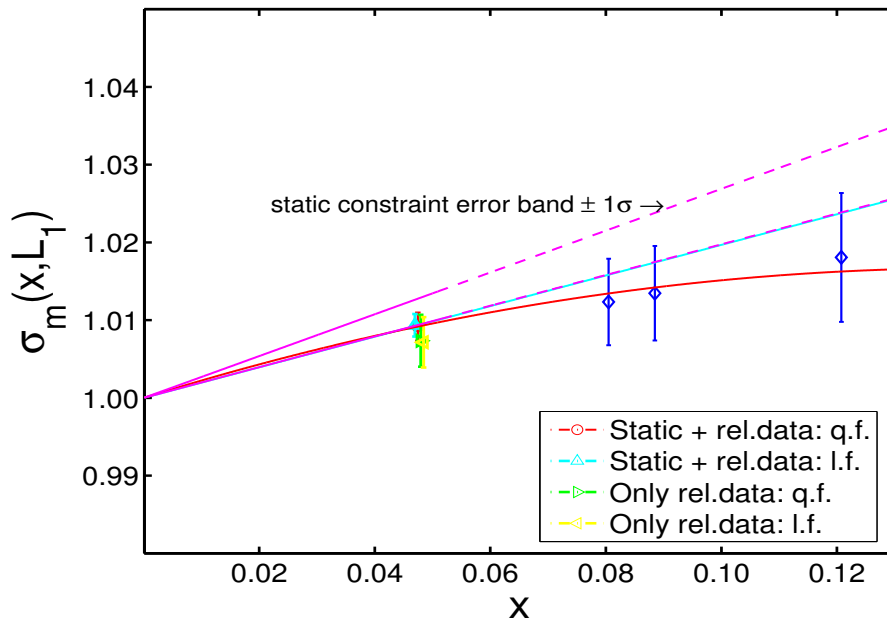


Figure 4.3: Plot of the step scaling function $\sigma_m(x, L_1)$ vs. $x = x(m_h, L_1)$.

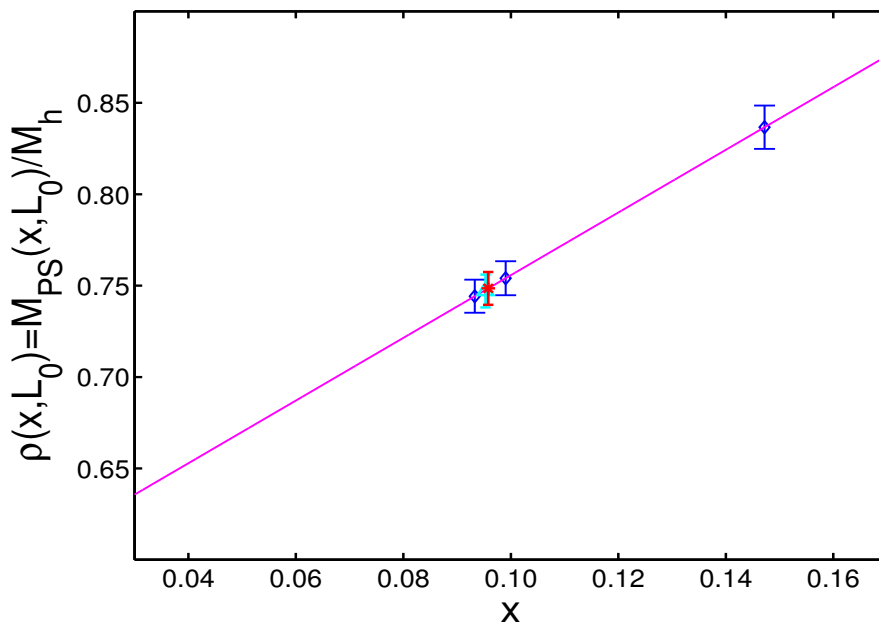


Figure 4.4: Plot of $\rho(x, L_0)$ vs. $x = x(m_h, L_0)$.

4.4 Computation of the meson decay constant

4.4.1 General strategy

With the lattice setup given in eqs. (4.36), we consider the case where our observable is a finite volume meson decay constant times the square root of the corresponding meson mass

$$\mathcal{O}(m_h, L) = f_{\text{PS}}(m_h, L) \sqrt{M_{\text{PS}}(m_h, L)}. \quad (4.58)$$

The decay constant is defined in analogy to (3.133) by

$$f_{\text{PS}}(m_h, L) = \frac{-2}{\sqrt{L^3 M_{\text{PS}}(m_h, L)}} \frac{[f_{\text{A}}(m_h, L, x_0)]_{\text{R}}}{\sqrt{[f_1(m_h, L)]_{\text{R}}}} \Bigg|_{x_0=L}. \quad (4.59)$$

The renormalized and improved correlators $[f_{\text{A}}]_{\text{R}}$ and $[f_1]_{\text{R}}$ are defined in eq. (3.165) and eq. (3.168) respectively. It is worth to notice that in the definition of the decay constant the renormalization factors and the improvement terms of the boundary fields cancel out. In accordance with the large volume behaviour (3.133) we write

$$f_{\text{PS}}(m_h, L) \stackrel{m_h \rightarrow m_b}{\equiv} f_{\text{B}_s}(L) \stackrel{L \rightarrow \infty}{\equiv} f_{\text{B}_s}. \quad (4.60)$$

The step scaling function

$$\sigma_f(x, L_i) \equiv \frac{f_{\text{PS}}(m_h, L_i) \sqrt{M_{\text{PS}}(m_h, L_i)}}{f_{\text{PS}}(m_h, L_{i-1}) \sqrt{M_{\text{PS}}(m_h, L_{i-1})}}, \quad (4.61)$$

with expansion

$$\sigma_f(x, L_i) = \sigma_f^{\text{stat}}(L_i) + \sigma_f^{(1)}(L_i) \cdot x + \mathcal{O}(x^2), \quad (4.62)$$

yields straightforwardly the connection between the finite volume decay constant and the infinite volume one. Since the renormalization factor Z_{A} of the axial current depends only on the bare coupling, it cancels out in the ratio (4.61). The first order term in the expansion (4.62) is computable in the static approximation of HQET. It is convenient to define the renormalized ratio

$$Y_{\text{SF}}(L, \mu) = Z_{\text{A}}^{\text{stat}}(1/\mu) \frac{f_{\text{A}}^{\text{stat,I}}(L, x_0)}{\sqrt{f_1^{\text{stat}}(L)}} \Bigg|_{x_0=L} = Z_{\text{A}}^{\text{stat}}(1/\mu) X_{\text{SF}}(L), \quad (4.63)$$

where $Z_{\text{A}}^{\text{stat}}$ is defined by the “new” renormalization scheme [2]. The latter is based on the condition

$$Z_{\text{A}}^{\text{stat}}(1/\mu) \Xi(L') = \Xi^{(0)}(L'), \quad \text{at vanishing quark mass,} \quad (4.64)$$

with $\mu = 1/L'$, and

$$\Xi(L') = \frac{f_A^{\text{stat,I}}(L', x_0)}{[f_1(L') f_1^{\text{hh}}(L', x_3)]^{1/4}} \Big|_{x_0=x_3=L'/2}, \quad (4.65)$$

where $\Xi^{(0)}(L')$, computed in [2], is the tree-level value of $\Xi(L')$. The lattice setup of the renormalization scheme slightly differs from eqs. (4.36) and reads

$$T' = L', \quad C = C' = 0, \quad \text{and} \quad \theta = 0.5. \quad (4.66)$$

This setup is used exclusively for the computation of Z_A^{stat} . Furthermore, the values of the critical hopping parameter needed to realize, up to $\mathcal{O}(a^2)$, the condition of vanishing quark mass, are computed along the method discussed in Sect. 4.2.3 with the setup in eqs. (4.36).

We now proceed to relate the renormalized matrix element $Y_{\text{SF}}(L, \mu)$ to the renormalization group invariant one defined by

$$Y_{\text{RGI}}(L) = Y_{\text{SF}}(L, \mu) \times [2b_0 \bar{g}^2(\mu)]^{-\gamma_0/2b_0} \exp \left\{ - \int_0^{\bar{g}(\mu)} dg \left[\frac{\gamma(g)}{\beta(g)} - \frac{\gamma_0}{b_0 g} \right] \right\}, \quad (4.67)$$

where the universal leading order coefficients of the β - and γ -functions are given by $b_0 = 11/(4\pi)^2$ and $\gamma_0 = -1/(4\pi)^2$ respectively. The ratio $Y_{\text{RGI}}/Y_{\text{SF}}$ depends only on μ ,

$$I^{\text{stat}}(\mu) = \frac{Y_{\text{RGI}}(L)}{Y_{\text{SF}}(L, \mu)}, \quad (4.68)$$

and it has been non-perturbatively evaluated in [2] for several orders of magnitude in μ , covering all scales involved in our work. The whole procedure can be summarized by introducing the renormalization factor Z_{RGI}

$$Y_{\text{RGI}}(L) = Z_{\text{RGI}} \frac{f_A^{\text{stat,I}}(L, x_0)}{\sqrt{f_1^{\text{stat}}(L)}} \Big|_{x_0=L}, \quad (4.69)$$

$$\text{with} \quad Z_{\text{RGI}} = I^{\text{stat}}(\mu) Z_A^{\text{stat}}(1/\mu), \quad \mu = 1/L'. \quad (4.70)$$

The L -dependence of Y_{RGI} does not originate from the scale introduced by the renormalization factor Z_A^{stat} , but only from the fact that the correlation functions $f_A^{\text{stat,I}}$ and f_1^{stat} have been determined on the volume L . Indeed, the renormalization factor Z_{RGI} depends only on the bare coupling. Furthermore, one is free to set $L' = L$. This choice

will be kept throughout the following. The RGI ratio Y_{RGI} is related to the QCD decay constant f_{PS} via

$$\frac{f_{\text{PS}}(m_h, L) \sqrt{L^3 M_{\text{PS}}(m_h, L)}}{-2C_{\text{PS}}(M_h/\Lambda_{\overline{\text{MS}}})} = Y_{\text{PS}}(x, L) = Y_{\text{RGI}}(L) + \mathcal{O}(x). \quad (4.71)$$

The function $C_{\text{PS}}(M_h/\Lambda_{\overline{\text{MS}}})$, which can be accurately evaluated in perturbation theory, allows to match the HQET matrix element with the QCD one; through the 3-loop anomalous dimension computed in [72], the authors of [73] provided the parametrization

$$C_{\text{PS}}(x) = \begin{cases} t^{\gamma_0^{\text{PS}}/(2b_0)} \{ 1 - 0.065t + 0.048t^2 \} & \text{2-loop } \gamma^{\text{PS}} \\ t^{\gamma_0^{\text{PS}}/(2b_0)} \{ 1 - 0.068t - 0.087t^2 + 0.079t^3 \} & \text{3-loop } \gamma^{\text{PS}} \end{cases} \quad (4.72)$$

where $t = 1/\ln(M_h/\Lambda_{\overline{\text{MS}}})$, the scale $\Lambda_{\overline{\text{MS}}} = 238(19)$ MeV from [12], and the coefficients γ_0^{PS} and b_0 are the same appearing in eq. (4.67). This parametrization guarantees at least 0.2% precision for $t \leq 0.6$. The function C_{PS} is in practice needed only in the small volume. It drops out in the ratio (4.61). The step scaling function for the static decay constant, entering the expansion (4.62), is given by

$$\sigma_{\text{f}}^{\text{stat}}(L_i) = \frac{1}{2^{3/2}} \frac{Y_{\text{RGI}}(L_i)}{Y_{\text{RGI}}(L_{i-1})}. \quad (4.73)$$

In this ratio the renormalization factor Z_{RGI} cancels out. It is needed only in the small volume. We have now all ingredients to combine the static data with the QCD ones, and interpolate at the scale of the b-quark. The final result for f_{B_s} can be expressed in the compact form

$$f_{\text{B}_s} = Y_{\text{PS}}(x_0, L_0) \cdot \sigma_{\text{f}}(x_1, L_1) \cdot \sigma_{\text{f}}(x_2, L_2) \cdot \frac{-2C_{\text{PS}}(M_b/\Lambda_{\overline{\text{MS}}})}{\sqrt{L_0^3 M_{\text{B}_s}}}, \quad (4.74)$$

where the interpolation points x_i are computed through eqs. (4.47), and the b-quark mass through eq. (4.49).

4.4.2 The results

For the computation of $\sigma_{\text{f}}(x, L_2)$ the relativistic data originate from the same gauge configurations used earlier for the pseudoscalar meson mass. In the static case the

decay constant in the bigger volume

$$Y_{\text{RGI}}(L_2) = -4.65(19), \quad (4.75)$$

has been computed and extrapolated to the continuum limit in [1]. The continuum extrapolation of the same quantity in the intermediate volume L_1 gives

$$Y_{\text{RGI}}(L_1) = -1.628(19), \quad (4.76)$$

for which the renormalization factor $Z_{\text{A}}^{\text{stat}}$ has been computed on the volume L_1 . The results are presented in App. C. The regularization independent part of Z_{RGI} can be extracted from the results of [2], and reads⁵

$$I^{\text{stat}}(\mu) = 0.9280(20), \quad \mu = 1/L_1. \quad (4.77)$$

These results allow to compute

$$\sigma_{\text{f}}^{\text{stat}}(L_2) = 1.010(43), \quad (4.78)$$

which is used together with the relativistic data as shown in Fig. 4.5 to get the results in the upper part of Table 4.4. The interpolation procedure as well as the estimate of the uncertainties follow the method employed for the step scaling functions of the meson mass.

Similarly, but by extrapolating the static step scaling function to the continuum limit rather than $Y_{\text{RGI}}(L_1)$ and $Y_{\text{RGI}}(L_0)$ separately, we obtain

$$\sigma_{\text{f}}^{\text{stat}}(L_1) = 0.4337(44), \quad (4.79)$$

which is combined with the relativistic data to give the results in the middle part of Table 4.4. The small volume static result

$$Y_{\text{RGI}}(L_0) = -1.347(13), \quad (4.80)$$

is obtained by exploiting the computations of [2], from which one extracts

$$I^{\text{stat}}(\mu) = 0.8462(62), \quad \mu = 1/L_0. \quad (4.81)$$

Together with the relativistic QCD data we obtain

$$Y_{\text{PS}}(x_0, L_0) = -1.279(17), \quad (4.82)$$

⁵Here the uncertainty does not contain the error coming from $I^{\text{stat}}(\mu = (1.436r_0)^{-1})$, given in [2], because the latter factor cancels out in the step scaling function (4.78). The aforementioned error is included in the factor (4.81) needed in the small volume.

as result of the quadratic fit, performed according to the procedures of App. D and App. E, of the data with the 3-loop expression of C_{PS} shown in Fig. 4.7. For other interpolated numbers we refer to Table 4.4. Also in this case the correction to the uncertainties originating from x has been estimated to be negligible in comparison to the error on Y_{PS} , thus justifying the neglect of the correlation between the several x 's associated with different heavy quark masses. We finally arrive through eq. (4.74) to

$$f_{B_s} = 191(6) \text{ MeV}. \quad (4.83)$$

By performing the whole analysis with only the relativistic QCD data, we obtain

$$f_{B_s}^* = 195(11) \text{ MeV}. \quad (4.84)$$

As last check, the whole analysis is repeated with the 2-loop expression of C_{PS} , giving results which differ from (4.83) and (4.84) by an amount of $O(1 \text{ eV})$.

Our results are consistent with other quenched determinations using the same input parameters. The authors of [74] did a non-perturbative calculation of the decay constant, by combining the results [28] in the static approximation of HQET with computations in relativistic QCD with heavy quark masses around the physical charm and slightly heavier. They obtained $f_{B_s} = 206(10) \text{ MeV}$. An extension [1] of this work produces a more precise and still consistent result. The computations are performed in a large volume and extrapolated to the continuum limit. Another recent non-perturbative determination [75] is obtained by extrapolating to the b-region large volume computations in relativistic QCD. The result is not extrapolated to the continuum, but computed at a fine lattice spacing with $a^{-1} = 4.97 \text{ GeV}$, and reads $f_{B_s} = 206(7)(26) \text{ MeV}$, where the first error is statistical and the second systematic.

As for the b-quark mass, a real comparison with other quenched determinations can be made only if the same input parameters are chosen. For completeness, we cite here the results of a few recent quenched computations

$$f_{B_s}/\text{MeV} = \begin{cases} 220(6) \begin{pmatrix} +23 \\ -28 \end{pmatrix} & [76], \\ 220(2)(15) \begin{pmatrix} +8 \\ -0 \end{pmatrix} & [77], \\ 199(5) \begin{pmatrix} +23 \\ -22 \end{pmatrix} & [78]. \end{cases}$$

For a recent review on the subject we suggest [71].

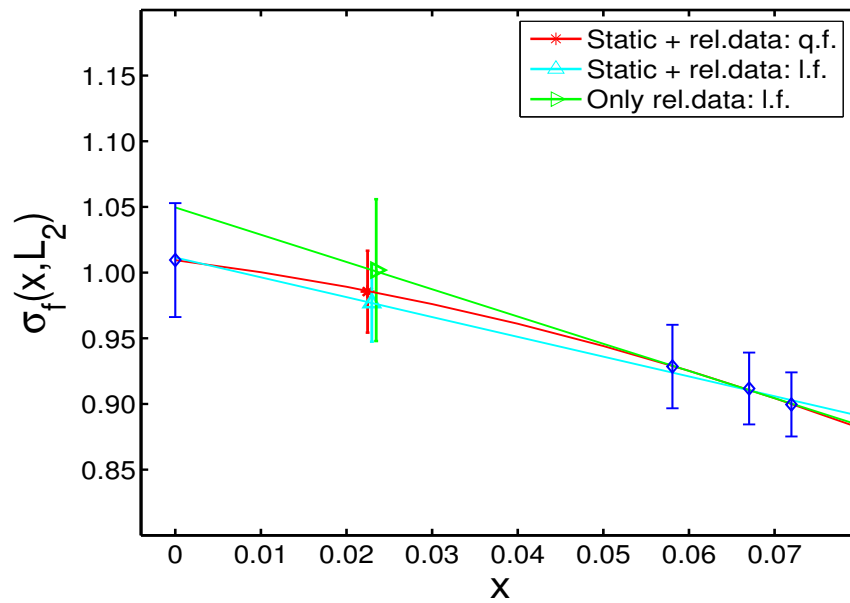


Figure 4.5: Plot of the step scaling function $\sigma_f(x, L_2)$ vs. $x = x(m_h, L_2)$.

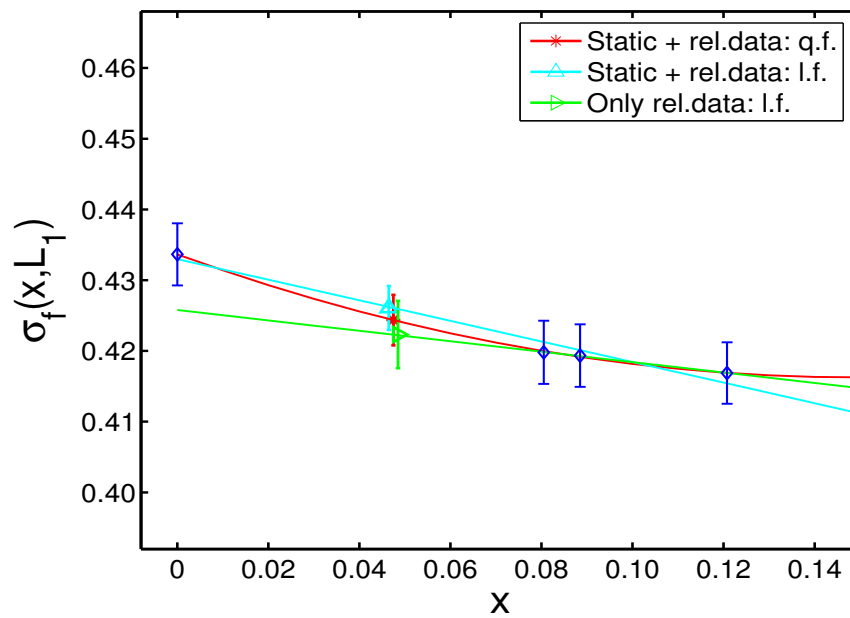


Figure 4.6: Plot of the step scaling function $\sigma_f(x, L_1)$ vs. $x = x(m_h, L_1)$.

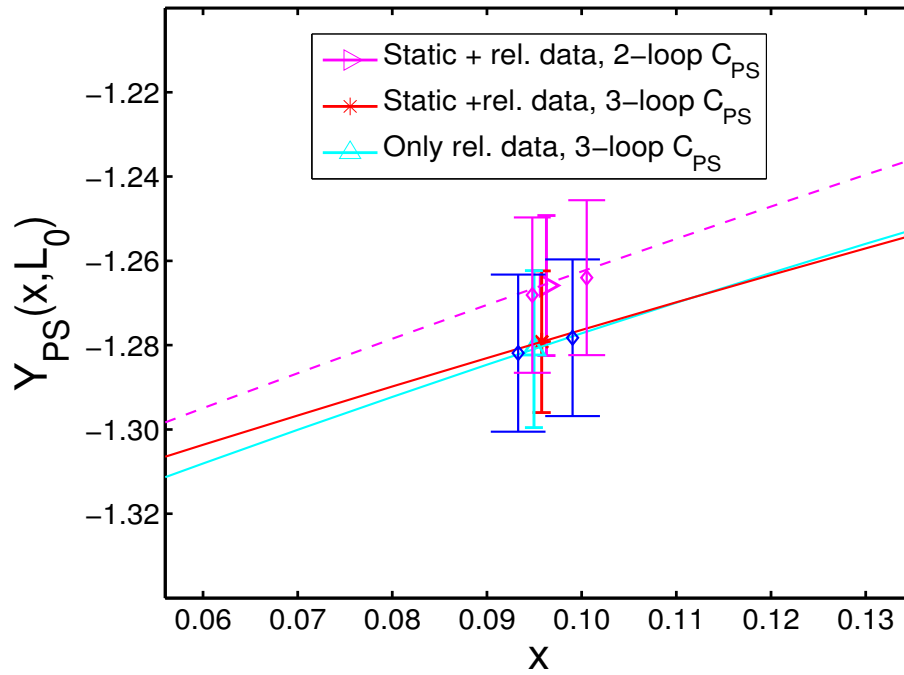
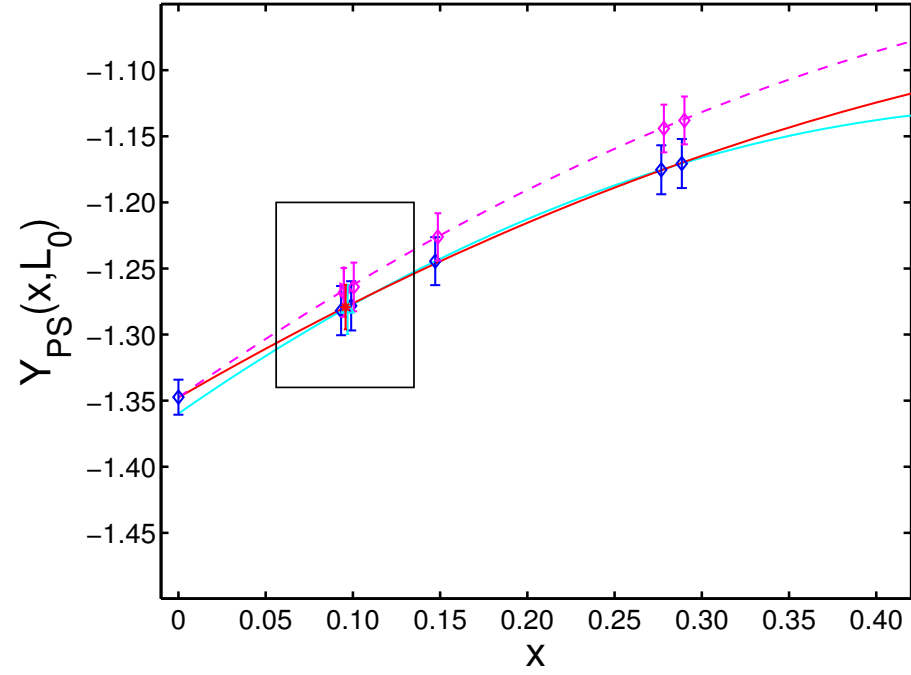


Figure 4.7: Plot of the renormalized pseudoscalar decay constant on the small volume $Y_{PS}(x, L_0)$ vs. $x = x(m_h, L_0)$.

| Constraint on the slope | Fit | $\sigma_m(x_2, L_2)$ |
|-------------------------|-----------|----------------------|
| Yes | quadratic | 1.0330(11) |
| Yes | linear | 1.0319(11) |
| No | quadratic | 1.0258(21) |
| No | linear | 1.0276(22) |

| Constraint on the slope | Fit | $\sigma_m(x_1, L_1)$ |
|-------------------------|-----------|----------------------|
| Yes | quadratic | 1.0092(18) |
| Yes | linear | 1.0093(15) |
| No | quadratic | 1.0074(33) |
| No | linear | 1.0072(32) |

Table 4.3: Results of the interpolation of $\sigma_m(x_2, L_2)$ and $\sigma_m(x_1, L_1)$. For the computation of the masses (4.56) and (4.57) the quadratic fit results have been used.

4.5 Summary

The combination of the Tor Vergata strategy to compute properties of the heavy-light mesons [50, 51] with the expansion of all quantities in HQET [19], changes extrapolations in the former computations into interpolations. The upshot is a very precise and controlled lattice determination, within the quenched approximation, of the b-quark mass and the B_s -meson decay constant. The final result for the former is affected by an uncertainty of 1.5%, mostly due to the mass renormalization factor. The decay constant is computed with a precision slightly worse than 3%, mostly relying on the large volume computations, which have been recently improved in the HQET sector by the authors of [1].

The numerical results of all steps show that the interpolations are very well behaved. The step scaling functions for the pseudoscalar meson mass show small deviations, roughly a few percents, from the static limit, and the HQET constraint on the slope of the fitting curves allows to halve the uncertainty on the interpolated points as well as to have a better control on the fitting parameters. All interpolated points are consistent with the HQET predictions within two standard deviations. However the error associated with the step scaling functions is much smaller than the one stemming

| Inclusion of the static data | Fit | $\sigma_f(x_2, L_2)$ | |
|------------------------------|-----------|----------------------|--------------------|
| Yes | quadratic | 0.985(31) | |
| Yes | linear | 0.977(29) | |
| No | linear | 1.002(54) | |
| Inclusion of the static data | Fit | $\sigma_f(x_1, L_1)$ | |
| Yes | quadratic | 0.4243(36) | |
| Yes | linear | 0.4260(31) | |
| No | linear | 0.4223(48) | |
| Inclusion of the static data | Fit | C_{PS} | $Y_{PS}(x_0, L_0)$ |
| Yes | quadratic | 3-loop | -1.279(17) |
| Yes | quadratic | 2-loop | -1.266(17) |
| No | quadratic | 3-loop | -1.281(19) |

Table 4.4: Results of the computation of $\sigma_f(x_2, L_2)$, $\sigma_f(x_1, L_1)$ and $Y_{PS}(x_0, L_0)$. For the computation of (4.83) and (4.84) the linearly interpolated step scaling functions have been used.

from the small volume interpolation. There only the relativistic QCD data are needed, and their uncertainty is dominated by the total renormalization factor Z_M of the RGI quark mass, whose error amounts to roughly 80% of the final error on the b-quark mass.

The step scaling functions of the pseudoscalar decay constant show an evident flatness, as expected from the Step Scaling Method. In the large volume the presence of the static point plays an important role in the precision and confidence of the interpolation. This is not unexpected. The relativistic QCD data lie in a region where the heavy quark mass is around the physical charm quark mass, and a linear extrapolation to the b-region cannot be considered safe a priori. The pattern is similar in the intermediate volume, where the flatness of the step scaling function is even more evident. In all but one steps the static approximation alone gives very accurate results. The one exception is the decay constant in the small volume, where the $O(1/m_b)$ corrections are around 5%.

The elaborated error analysis, described in Apps. C, D, E and F, ensures that our results do not suffer from any systematic errors apart from the use of the quenched approximation; the uncertainty of the regularization dependent quantities is taken into account before performing the continuum limits. Small systematic errors quoted in [50, 51] stemming from the extrapolations in the inverse of the heavy quark mass have been eliminated.

In order to significantly reduce the error on the b-quark mass the total renormalization factor Z_M has to be computed even more precisely, while for an even more precise determination of decay constant, the major issue is represented by the large volume computations, both in HQET and in QCD.

Concerning dynamical fermion computations, the challenge in this strategy is to simulate in a large volume (such as L_2) with small enough lattice spacings, where quark masses of around m_{charm} and higher can be simulated with confidence.

Chapter 5

Renormalization of the chromo-magnetic operator in HQET

5.1 Spin splitting

In chapter 2 we have discussed how heavy-light quark bound states can be described by an expansion in the inverse of the heavy quark mass according to HQET. There we focused our attention on the phenomenological implications residing in the leading order of the expansion, the static limit. In this chapter we go further on, and inspect the finite heavy quark mass corrections in a systematic way, by considering the mass splitting between vector and pseudoscalar heavy light mesons.

We follow [79] and expand the mass of the ground state pseudoscalar (PS) and vector (V) heavy-light mesons as

$$M_X = m_h + \bar{\Lambda} + \frac{1}{2m_h} \Delta M_X^2 + \mathcal{O}(\Lambda_{\text{QCD}}^3/m_h^2), \quad X = \text{PS, V}, \quad (5.1)$$

where

$$\Delta M_X^2 = -\lambda_1 - d_X \lambda_2, \quad (5.2)$$

with $d_{\text{PS}} = 3$ and $d_{\text{V}} = -1$. The details of the heavy quark mass definition are irrelevant for the present discussion. One may think of a mass renormalized at the scale m_h itself. The parameter λ_1 is associated with the kinetic operator (2.43), and λ_2 with the chromo-magnetic (bare) operator (2.44)

$$\mathcal{O}_{\text{spin}}(x) = \bar{\Psi}_h(x) \frac{1}{2i} F_{kl} \sigma_{kl} \Psi_h(x) = \bar{\Psi}_h(x) \boldsymbol{\sigma} \cdot \boldsymbol{B}(x) \Psi_h(x). \quad (5.3)$$

The latter is responsible for the splitting

$$M_V^2 - M_{PS}^2 = 4\lambda_2 + \mathcal{O}(\Lambda_{\text{QCD}}^3/m_h). \quad (5.4)$$

The parameter λ_2 is a key quantity in HQET. It encodes, at order $1/m_h$, the information on the deviations from the static limit, where $M_V = M_{PS}$, stemming from the spin-dependent interactions inside the heavy-light mesons.

So far we did neither exactly specify how λ_2 is defined and renormalized, nor discuss the matching of the effective theory to QCD. The latter can be worked out by following the procedure discussed in Sect. 2.6; the upshot is

$$M_V^2 - M_{PS}^2 = 4C_{\text{mag}}\lambda_2^{\text{RGI}} + \mathcal{O}(\Lambda_{\text{QCD}}^3/m_h), \quad (5.5)$$

where the matrix element of the effective theory¹

$$\lambda_2^{\text{RGI}} = \frac{1}{3} \frac{\langle \mathbf{B} | \mathcal{O}_{\text{spin}}^{\text{RGI}} | \mathbf{B} \rangle}{\langle \mathbf{B} | \mathbf{B} \rangle}, \quad (5.6)$$

appears. The renormalization group invariant operator $\mathcal{O}_{\text{spin}}^{\text{RGI}}$, is related to the bare local operator (5.3) by a multiplicative, scale and scheme independent renormalization factor $Z_{\text{mag}}^{\text{RGI}}$, which depends only on the bare coupling,

$$\mathcal{O}_{\text{spin}}^{\text{RGI}} = Z_{\text{mag}}^{\text{RGI}}(g_0) \mathcal{O}_{\text{spin}}. \quad (5.7)$$

It follows that the parameter λ_2^{RGI} is independent of any scale and scheme. It is an unambiguous QCD observable, because the l.h.s. of eq. (5.4) can be directly measured by experiments, and the corrections on the r.h.s. vanish in the limit² $m_h \rightarrow \infty$, where also the matching factor C_{mag} is unambiguous and perturbatively computable. The latter originates from the matching between the HQET matrix element and the QCD one.

In order to have a deeper insight into the subject, let us assume that the operator $\mathcal{O}_{\text{spin}}$ has been renormalized

$$\mathcal{O}_{\text{spin}}^{\text{S}}(\mu) = Z_{\text{mag}}^{\text{S}}(\mu) \mathcal{O}_{\text{spin}}, \quad (5.8)$$

in a scheme S, and that the matrix element

$$\lambda_2^{\text{S}}(\mu) = \frac{1}{3} \frac{\langle \mathbf{B} | \mathcal{O}_{\text{spin}}^{\text{S}}(\mu) | \mathbf{B} \rangle}{\langle \mathbf{B} | \mathbf{B} \rangle}, \quad (5.9)$$

¹Here the state $|\mathbf{B}\rangle$ is a shorthand for $|0, \mathbf{B}\rangle$ defined in Sect. 3.5.1.

²Or equivalently $M_X \rightarrow \infty$.

has been computed. The latter is related to the RGI one by

$$\lambda_2^{\text{RGI}}/\lambda_2^{\text{S}}(\mu) = [2b_0\bar{g}_{\text{S}}^2(\mu)]^{-\gamma_0/2b_0} \exp \left\{ - \int_0^{\bar{g}_{\text{S}}(\mu)} dg \left[\frac{\gamma^{\text{S}}(g)}{\beta^{\text{S}}(g)} - \frac{\gamma_0}{b_0 g} \right] \right\}, \quad (5.10)$$

where the anomalous dimension γ^{S} and the β -function in the S scheme with their leading order weak coupling expansion coefficients γ_0 and b_0 appear. The ratio (5.10) then allows to relate the renormalization factors through

$$Z_{\text{mag}}^{\text{RGI}} = Z_{\text{mag}}^{\text{S}}(\mu) \lambda_2^{\text{RGI}}/\lambda_2^{\text{S}}(\mu). \quad (5.11)$$

The matrix element of the bare chromo-magnetic operator can be computed non-perturbatively by lattice HQET simulations [80, 81, 82]. As stated in these references, the major source of uncertainty is the renormalization factor Z_{mag} , which is so far only perturbatively known. Our aim is to compute $Z_{\text{mag}}^{\text{RGI}}$ with high accuracy for values of the bare coupling of interest for phenomenological applications, by starting from a low energy regime (low μ), to arrive to energy scales where the r.h.s. of eq. (5.10) can be safely evaluated in perturbation theory. It is then clear that an accurate knowledge of the perturbative expression of the anomalous dimension plays a fundamental role. This is the subject of the following sections.

5.2 Definition of the renormalization scheme

Our aim is to formulate a renormalization condition for $\mathcal{O}_{\text{spin}}$ in a finite volume, which suits the non-perturbative computation of the associated renormalization factor $Z_{\text{mag}}^{\text{RGI}}$ along the general strategy of [12]. The lattice Schrödinger functional fits well our requirements, and allows accurate non-perturbative computations in the low energy regime as well as the evolution to very high energies. The latter can be achieved through a finite-size scaling technique, which lets reach scales, where perturbation theory can be used to further continue the evolution, and determine the renormalization group invariant renormalization factor with high accuracy. In addition, perturbation theory allows to exactly match renormalization factors computed in different schemes in a very easy way, as explained in the next section.

For the static quarks we consider the Eichten-Hill action (3.49), bearing in mind that one could also employ other actions of the form (3.50) without compromising the validity of the following discussion. In the definition of $\mathcal{O}_{\text{spin}}$, the product $\sigma \cdot B$ between the Pauli matrices σ_k and the magnetic field B_k is a shorthand for

$$\sigma \cdot B \otimes I_2 = \sum_{k,j} \sigma_{kj} \frac{1}{2i} \hat{F}_{kj} = \begin{pmatrix} \sigma_k & 0 \\ 0 & \sigma_k \end{pmatrix} B_k, \quad (5.12)$$

where $\sigma_{kj} = \frac{i}{2}[\gamma_k, \gamma_j]$, and the B -field is related to the lattice version $\widehat{F}_{\mu\nu}$, defined in eq. (3.88), of the gauge field tensor by

$$B_k = i\varepsilon_{qjk}\widehat{F}_{qj}, \quad (5.13)$$

with indices q, j not summed over. For later convenience we report also the relation between the electric field and the tensor $\widehat{F}_{\mu\nu}$:

$$E_k = i\widehat{F}_{0k}. \quad (5.14)$$

The lattice definition of the magnetic field represents a further motivation for the choice of the Schrödinger functional. With any kind of periodic boundary conditions, any correlation function with $\mathcal{O}_{\text{spin}}$ vanishes at tree-level. In order to avoid this, we introduce boundary conditions inducing a non-trivial background field for which $\widehat{F}_{\mu\nu}$ does not vanish at tree-level. This ensures a good signal in the MC simulations at weak coupling and means that a 1-loop computation is sufficient to compute the renormalization factor up to and including $\mathcal{O}(g_0^2)$.

Inspection of the operator $\mathcal{O}_{\text{spin}}$ reveals that it does not contain any light fermion fields. This feature is exploited in the definition of the following correlation functions, where we completely avoid the introduction of light quarks. The upshot is that for $N_f = 0$ we have a pure gauge quantity, without valence quarks. In perturbation theory, the diagrams owing their existence to $N_f \neq 0$ are of order g_0^{2n} , with $n \geq 1$.

Another important observation is that $\mathcal{O}_{\text{spin}}$ does not mix with other operators of the same or lower dimension under renormalization. This has been shown in [9], and can be easily understood by surveying that all but one operators with dimension less or equal to five, and compatible with the symmetries of HQET, trivially transform under spin rotations. The one exception is $\mathcal{O}_{\text{spin}}$.

Our lattice setup is a volume of extension $L_0 \times L_1 \times L_2 \times L_3$, with $L_\mu = L = T$, and Dirichlet boundary conditions inducing an Abelian non-vanishing background field as in [24], with the only difference that here they are imposed in the 3-direction (instead of the temporal one),

$$U_\mu(x)|_{x_3=0} = \exp(aC), \quad U_\mu(x)|_{x_3=L} = \exp(aC'), \quad \mu = 0, 1, 2, \quad (5.15)$$

while periodic boundary conditions are kept with respect to x_0, x_1, x_2 . The temporal coordinate is specified by x_0 with no misunderstandings. It is distinguished from the very beginning in the static action, which describes static quarks propagating only forward in time. The parametrization of the matrices C, C' can be found in App. A. A natural choice for the renormalization condition is then

$$Z_{\text{mag}}^{\text{SF}}(L) \frac{L^2 \langle S_1(x + \frac{L}{2}\hat{0}) \mathcal{O}_{\text{spin}}(x) \rangle}{\langle S_1(x + \frac{L}{2}\hat{0}) S_1(x) \rangle} = \frac{L^2 \langle S_1(x + \frac{L}{2}\hat{0}) \mathcal{O}_{\text{spin}}(x) \rangle}{\langle S_1(x + \frac{L}{2}\hat{0}) S_1(x) \rangle} \Bigg|_{g_0=0}, \quad (5.16)$$

where $x_3 = L/2$. The spin operator

$$S_1(x) = \frac{1}{1+a\delta m} \bar{\psi}_h(x) \sigma_1 U_0^\dagger(x-a\hat{0}) \psi_h(x-a\hat{0}), \quad (5.17)$$

is introduced in order to obtain a non-vanishing trace in spin space. It does not need to be renormalized, because it is the (local) Nöther charge obtained from the invariance of the action under the spin rotations (2.40). There is no special reason for the choice of S_1 instead of S_2 . Instead, if we had chosen B_3 , due to the symmetries of the background field, we would end up with a vanishing numerator at tree-level. If N_f light quarks are present in the action, we intend the condition (5.16) with all of them having vanishing renormalized quark mass. The latter is provided in eq. (4.22). However, in Sect. 5.6 we will see that the details of the quark mass renormalization play no role in our computations. Furthermore the angle θ , appearing in the quark boundary conditions (3.20), is fixed to the value $-\pi/3$. This choice is motivated in Sect. 5.6, and represents a part of the definition of our renormalization scheme for $N_f \neq 0$.

By integrating out the static quark fields we can rewrite eq. (5.16) in a simple form, which suits non-perturbative as well as perturbative computations. An important ingredient is the explicit expression of the static quark propagator [48]:

$$G_h(x,y) = \theta(x_0 - y_0) \delta(\mathbf{x} - \mathbf{y}) (1 + a\delta m)^{-(x_0 - y_0)/a} W^\dagger(y,x) P_+, \quad (5.18)$$

with

$$W(x,x) = 1, \quad (5.19)$$

$$W(x,x+R\hat{\mu}) = U_\mu(x) U_\mu(x+a\hat{\mu}) \dots U_\mu(x+(R-a)\hat{\mu}), \quad R > 0. \quad (5.20)$$

Our lattice δ -functions are

$$\delta(x_\mu) = a^{-1} \delta_{x_\mu,0}, \quad \delta(\mathbf{x}) = \prod_{k=1}^3 \delta(x_k), \quad \delta(x) = \prod_{\mu=0}^3 \delta(x_\mu), \quad (5.21)$$

while for the θ -function we have

$$\begin{cases} \theta(x_\mu) = 1, & \text{for } x_\mu \geq 0, \\ \theta(x_\mu) = 0, & \text{otherwise.} \end{cases} \quad (5.22)$$

It is used in combination with the property of the Pauli matrices

$$\{\sigma_k, \sigma_j\} = 2\delta_{kj}, \quad (5.23)$$

to rewrite the ratio in eq. (5.16) as

$$\frac{\langle S_1(x + \frac{L}{2}\hat{0})\mathcal{O}_{\text{spin}}(x) \rangle}{\langle S_1(x + \frac{L}{2}\hat{0})S_1(x) \rangle} = \frac{\langle \text{Tr}(\mathcal{P}_0(x)B_1(x)P_+) \rangle}{\langle \text{Tr}(\mathcal{P}_0(x)P_+) \rangle}, \quad B_1(x) = i\widehat{F}_{23}(x), \quad (5.24)$$

where the Polyakov loop operator

$$\mathcal{P}_\mu(x) = U_\mu(x)U_\mu(x + a\hat{\mu}) \dots U_\mu(x + (L-a)\hat{\mu}) \quad (5.25)$$

enters. It follows that the renormalization condition (5.16) is expressed in terms of observables where no valence quarks appear. At the denominator we have the (traced) Polyakov loop \mathcal{P}_0 , and at the numerator the (traced) Polyakov loop \mathcal{P}_0 with the insertion of a B field. We stress that the additive renormalization term δm , appearing both in the operator (5.17) and in the propagator (5.18), cancels out in the ratios (5.24), and we do not need to take care of it. In the following, all correlation functions are intended to be computed with $\delta m = 0$. The trace in Dirac space concerns only the matrix P_+ , giving an overall factor 2, which cancels out between numerator and denominator.

We come back to our renormalization condition, and note that it is natural to use the equivalence of all coordinates in Euclidean space to switch to the usual Schrödinger functional boundary conditions [24], and, by using eq. (5.14), get

$$Z_{\text{mag}}^{\text{SF}}(L) \frac{L^2 \langle \text{Tr}(\mathcal{P}_3(x)E_1(x)) \rangle}{\langle \text{Tr}(\mathcal{P}_3(x)) \rangle} = \left. \frac{L^2 \langle \text{Tr}(\mathcal{P}_3(x)E_1(x)) \rangle}{\langle \text{Tr}(\mathcal{P}_3(x)) \rangle} \right|_{g_0=0}, \quad (5.26)$$

where $x_0 = L_0/2$, and $E_1(x) = i\widehat{F}_{01}(x)$. Here it is understood that one has Dirichlet boundary conditions in time. Their exact definition is provided in App. A.

5.3 Connection between different schemes

In the following it is assumed that the theory has been regularized according to the prescriptions of the previous section, with Dirichlet boundary conditions in time. Although some of the following results have very general validity, we further assume to be working at an energy scale where perturbation theory can be applied with confidence.

The scale evolution of the SF renormalized chromo-magnetic operator is ruled by the renormalization group equation

$$\mu \frac{\partial}{\partial \mu} \mathcal{O}_{\text{spin}}^{\text{SF}} = \gamma^{\text{SF}}(\bar{g}_{\text{SF}}) \mathcal{O}_{\text{spin}}^{\text{SF}}, \quad (5.27)$$

where the anomalous dimension γ^{SF} appears. It can be expanded according to

$$\gamma^{\text{SF}}(\bar{g}_{\text{SF}}) = -\bar{g}_{\text{SF}}^2(\gamma_0 + \gamma_1^{\text{SF}}\bar{g}_{\text{SF}}^{-2} + \dots), \quad (5.28)$$

where [8, 9]:

$$\gamma_0 = 3/(8\pi^2), \quad (5.29)$$

is scheme-independent, and the two-loop anomalous dimension γ_1^{SF} can be computed from the one in the $\overline{\text{MS}}$ scheme

$$\gamma_1^{\overline{\text{MS}}} = (\frac{17}{2} - \frac{13}{12}N_f)/(32\pi^4), \quad (5.30)$$

known from [83, 84], by relating the two schemes according to the following method.

In our method an essential ingredient is represented by the lattice minimal subtraction scheme (“lat”). The latter is defined by the requirement that, at each order of perturbation theory, divergences are cancelled by introducing renormalization constants, which are polynomials in $\ln(a\mu)$, without constant parts. At one-loop order, the operator in the minimal subtraction scheme is related to the bare one by

$$\mathcal{O}_{\text{spin}}^{\text{lat}}(\mu) = [1 - g_{\text{lat}}^2\gamma_0 \ln(a\mu)]\mathcal{O}_{\text{spin}}. \quad (5.31)$$

Any two mass independent renormalization schemes “a” and “b” can be related by a finite parameter renormalization of the form [85]:

$$\bar{g}_a = \bar{g}_b \sqrt{\chi_{g,(a,b)}(\bar{g}_b)}, \quad (5.32)$$

$$\mathcal{O}_{\text{spin}}^a = \mathcal{O}_{\text{spin}}^b \cdot \chi_{a,b}(\bar{g}_b), \quad (5.33)$$

where, for simplicity, we assumed that the renormalization scale μ is the same in both schemes. It follows that the operator (5.31) can be related to the ones in the SF and $\overline{\text{MS}}$ schemes by³

$$\mathcal{O}_{\text{spin}}^{\text{SF}}(\mu) = \chi_{\text{SF,lat}}(g_{\text{lat}}(\mu))\mathcal{O}_{\text{spin}}^{\text{lat}}(\mu), \quad (5.34)$$

$$\mathcal{O}_{\text{spin}}^{\overline{\text{MS}}}(\mu) = \chi_{\overline{\text{MS,lat}}}(g_{\text{lat}}(\mu))\mathcal{O}_{\text{spin}}^{\text{lat}}(\mu), \quad (5.35)$$

with the expansion

$$\chi_{a,b}(g) = 1 + \chi_{a,b}^{(1)}g^2 + \dots, \quad (5.36)$$

³A more rigorous notation would require \bar{g}_{lat} instead of g_{lat} . However, we keep the latter to be consistent with the literature on the subject.

which lets us write the one-loop relation between the SF and $\overline{\text{MS}}$ schemes as

$$\chi_{\text{SF},\overline{\text{MS}}}^{(1)} = \chi_{\text{SF},\text{lat}}^{(1)} - \chi_{\overline{\text{MS}},\text{lat}}^{(1)}. \quad (5.37)$$

Thanks to eq. (5.32), we write down the relation between the couplings as

$$\bar{g}_{\text{SF}}^2 = \chi_g \bar{g}_{\overline{\text{MS}}}^2, \quad \chi_g = \chi_{g,(\text{SF},\overline{\text{MS}})} = 1 + \chi_g^{(1)} \bar{g}_{\overline{\text{MS}}}^2 + \dots \quad (5.38)$$

where for the precise definition of the renormalized coupling in the SF scheme we refer to [37]. The scale dependence is usually indicated by $\bar{g}_{\text{SF}}(L)$ and $\bar{g}_{\overline{\text{MS}}}(\mu)$. In eq. (5.38) it is implicitly assumed that $\mu = 1/L$. The renormalization group function β , governing the scale evolution of the coupling, and the anomalous dimension of the chromo-magnetic operator in the SF and $\overline{\text{MS}}$ schemes are related by

$$\beta^{\text{SF}}(\bar{g}_{\text{SF}}) = \left\{ \beta^{\overline{\text{MS}}}(\bar{g}_{\overline{\text{MS}}}) \frac{\partial \bar{g}_{\text{SF}}}{\partial \bar{g}_{\overline{\text{MS}}}} \right\}_{\bar{g}_{\overline{\text{MS}}} = \bar{g}_{\overline{\text{MS}}}(\bar{g}_{\text{SF}})}, \quad (5.39)$$

$$\gamma^{\text{SF}}(\bar{g}_{\text{SF}}) = \left\{ \gamma^{\overline{\text{MS}}}(\bar{g}_{\overline{\text{MS}}}) + \beta^{\overline{\text{MS}}}(\bar{g}_{\overline{\text{MS}}}) \frac{\partial}{\partial \bar{g}_{\overline{\text{MS}}}} \ln \chi_{\text{SF},\overline{\text{MS}}}(\bar{g}_{\overline{\text{MS}}}) \right\}_{\bar{g}_{\overline{\text{MS}}} = \bar{g}_{\overline{\text{MS}}}(\bar{g}_{\text{SF}})}. \quad (5.40)$$

We now work out eq. (5.40) by exploiting the perturbative expansion of the β - and γ -functions, and in particular eq. (2.62),

$$\begin{aligned} \bar{g}_{\text{SF}}^2 \{ \gamma_0 + \gamma_1^{\text{SF}} \bar{g}_{\text{SF}}^2 + \mathcal{O}(\bar{g}_{\text{SF}}^4) \} &= \bar{g}_{\overline{\text{MS}}}^2 \left\{ \gamma_0 + \gamma_1^{\overline{\text{MS}}} \bar{g}_{\overline{\text{MS}}}^2 + \mathcal{O}(\bar{g}_{\overline{\text{MS}}}^4) \right\} \\ &+ \bar{g}_{\overline{\text{MS}}}^3 (b_0 + b_1 \bar{g}_{\overline{\text{MS}}}^2) \frac{\partial}{\partial \bar{g}_{\overline{\text{MS}}}} \ln \left\{ 1 + \chi_{\text{SF},\overline{\text{MS}}}^{(1)} \bar{g}_{\overline{\text{MS}}}^2 + \mathcal{O}(\bar{g}_{\overline{\text{MS}}}^4) \right\} \\ &= \bar{g}_{\overline{\text{MS}}}^2 \left\{ \gamma_0 + \gamma_1^{\overline{\text{MS}}} \bar{g}_{\overline{\text{MS}}}^2 + \mathcal{O}(\bar{g}_{\overline{\text{MS}}}^4) \right\} \\ &+ \bar{g}_{\overline{\text{MS}}}^3 (b_0 + b_1 \bar{g}_{\overline{\text{MS}}}^2) \cdot 2 \frac{\chi_{\text{SF},\overline{\text{MS}}}^{(1)} \bar{g}_{\overline{\text{MS}}} + \mathcal{O}(\bar{g}_{\overline{\text{MS}}}^3)}{1 + \chi_{\text{SF},\overline{\text{MS}}}^{(1)} \bar{g}_{\overline{\text{MS}}}^2 + \mathcal{O}(\bar{g}_{\overline{\text{MS}}}^4)}. \end{aligned}$$

We divide both sides of the equation by \bar{g}_{SF}^2 and, through the Taylor expansion, obtain the relation valid up to $\mathcal{O}(\bar{g}_{\overline{\text{MS}}}^4)$,

$$\begin{aligned} \gamma_0 + \gamma_1^{\text{SF}} \bar{g}_{\text{SF}}^2 &= (\bar{g}_{\overline{\text{MS}}}^2 / \bar{g}_{\text{SF}}^2) \left\{ \gamma_0 + \gamma_1^{\overline{\text{MS}}} \bar{g}_{\overline{\text{MS}}}^2 \right\} + (\bar{g}_{\overline{\text{MS}}}^4 / \bar{g}_{\text{SF}}^2) 2b_0 \chi_{\text{SF},\overline{\text{MS}}}^{(1)} \\ &\stackrel{(5.38)}{=} (1 - \chi_g^{(1)} \bar{g}_{\overline{\text{MS}}}^2) \left\{ \gamma_0 + \gamma_1^{\overline{\text{MS}}} \bar{g}_{\overline{\text{MS}}}^2 \right\} + (\bar{g}_{\overline{\text{MS}}}^4 / \bar{g}_{\text{SF}}^2) 2b_0 \chi_{\text{SF},\overline{\text{MS}}}^{(1)} \\ &= \gamma_0 + \left(\gamma_1^{\overline{\text{MS}}} - \gamma_0 \chi_g^{(1)} \right) \bar{g}_{\overline{\text{MS}}}^2 + (\bar{g}_{\overline{\text{MS}}}^4 / \bar{g}_{\text{SF}}^2) 2b_0 \chi_{\text{SF},\overline{\text{MS}}}^{(1)}. \end{aligned}$$

We subtract γ_0 to both sides of the last equation, and then divide again by \bar{g}_{SF}^2 , getting

$$\gamma_1^{\text{SF}} = \gamma_1^{\overline{\text{MS}}} - \gamma_0 \chi_g^{(1)} + 2b_0 \chi_{\text{SF},\overline{\text{MS}}}^{(1)}, \quad (5.41)$$

where we again used the relation (5.38) between the couplings. Therefore, the two-loop anomalous dimension in the SF scheme can be extracted, through the exact relation (5.41), from the one in the $\overline{\text{MS}}$ scheme, if the one-loop relation between the couplings, i.e. $\chi_g^{(1)}$, and the one-loop relation between the schemes, i.e. $\chi_{\text{SF},\overline{\text{MS}}}^{(1)}$, are known. The former has been computed in [86, 87], and reads

$$\chi_g^{(1)} = -\frac{1}{4\pi}(c_{1,0} + c_{1,1}N_f), \quad c_{1,0} = 1.25563(4), \quad c_{1,1} = 0.039863(2), \quad (5.42)$$

the coefficient $b_0 = (11 - \frac{2}{3}N_f)/(16\pi^2)$ is known from [3, 4], while γ_0 appears in eq. (5.29). Since⁴ Flynn and Hill provided in [88]:

$$\chi_{\overline{\text{MS}},\text{lat}}^{(1)} = 0.3824(3), \quad (5.43)$$

inserting it in eq. (5.37), we recognize that the only missing ingredient is $\chi_{\text{SF},\text{lat}}^{(1)}$. To the computation of the latter we dedicate the rest of the chapter.

5.4 Perturbation theory in the SF scheme

5.4.1 The gauge fixed action

One of the pillars of perturbation theory consists in fixing the gauge. This is necessary, because after having performed the saddle point expansion around the induced background field, the resulting minimal action configuration is found to be unique only up to gauge transformations. Indeed, once that a point on the gauge orbit of the minimal action has been chosen, the perturbative study amounts to parametrize the infinitesimal fluctuations around this minimum. However, not all of them are genuine physical field fluctuations. The gauge fixing procedure separates the latter from the infinitesimal gauge directions.

The following discussion is carried out in pure gauge theory, because the minima of the action are determined by the pure gauge theory alone, and the quark fields only play a secondary role.

⁴We warmly thank Jonathan Flynn for clarifications on this result.

The lattice Schrödinger functional is invariant under all gauge transformations Ω leaving the boundary fields W and W' , defined in eq. (3.34), intact. It has been demonstrated by the authors of [24] that this condition is satisfied only by the gauge functions that are constant and diagonal at the temporal boundaries, i.e.

$$\Omega(x) = \begin{cases} z_m, & \text{at } x_0 = 0, \\ z_{m'}, & \text{at } x_0 = T, \end{cases} \quad (5.44)$$

with $z_m = \exp(2\pi im/3)$, and some integer numbers m and m' . These gauge functions form a group, that we call $\hat{\mathcal{G}}$. Nevertheless, not the whole group is relevant for the gauge fixing. The constant diagonal gauge functions $\Omega(x)$ form a subgroup of $\hat{\mathcal{G}}$, which is isomorphic to the Cartan subgroup C_3 of $SU(3)$, and trivially act on the background field. In addition, there are no further transformations with this property [24]. This group can be left out, and survives as a global symmetry of the theory. The group which needs to be fixed is thus

$$\mathcal{G} = \hat{\mathcal{G}}/C_3, \quad (5.45)$$

and it can be simply identified with the $m' = 0$ component of $\hat{\mathcal{G}}$.

In an arbitrary but small neighborhood of the background field V , the gauge fields U may be parametrized by

$$\begin{aligned} U_\mu(x) &= \exp(g_0 a q_\mu(x)) V_\mu(x) \\ &= \left\{ 1 + g_0 a q_\mu(x) + \frac{1}{2} g_0^2 a^2 q_\mu^2(x) + \mathcal{O}(g_0^3) \right\} V_\mu(x), \end{aligned} \quad (5.46)$$

where the lattice vector fields $q_\mu(x)$ form a linear space, which we name \mathcal{H} , and whose spatial components respect the constraints

$$q_k(0, \mathbf{x}) = q_k(T, \mathbf{x}) = 0, \quad (5.47)$$

while the temporal components are defined for $x_0 \in [0, T)$ and we leave them unconstrained. The condition (5.47) guarantees that U satisfies the boundary conditions (A.13) once V does. The inner product of two vector fields q and r is given by

$$(q, r) = -2a^4 \sum_{x, \mu} \text{tr} \{ q_\mu(x) r_\mu(x) \}. \quad (5.48)$$

The gauge fixing function that we are looking for is a linear mapping from \mathcal{H} to $\mathcal{L}_\mathcal{G}$, where the latter is the Lie algebra of \mathcal{G} , consisting of all fields $\omega(x)$, such that the infinitesimal transformation

$$\Omega(x) = 1 - g_0 \omega(x) + \mathcal{O}(g_0^2) \quad (5.49)$$

belongs to \mathcal{G} . We thus introduce the operator

$$d : \mathcal{L}_g \mapsto \mathcal{H}, \quad (d\omega)_\mu(x) = D_\mu \omega(x), \quad (5.50)$$

where the covariant derivative D_μ and its backward correspondent D_μ^* act according to

$$D_\mu \omega(x) = \frac{1}{a} \left[V_\mu(x) \omega(x + a\hat{\mu}) V_\mu^{-1}(x) - \omega(x) \right], \quad (5.51)$$

$$D_\mu^* \omega(x) = \frac{1}{a} \left[\omega(x) - V_\mu^{-1}(x - a\hat{\mu}) \omega(x - a\hat{\mu}) V_\mu(x - a\hat{\mu}) \right]. \quad (5.52)$$

Analogously, d^* maps any vector field $q \in \mathcal{H}$ onto an element of \mathcal{L}_g such that

$$(d^*q, \omega) = -(q, d\omega). \quad (5.53)$$

According to [89], the desired gauge fixing function has to vanish on the background field and has to be non-vanishing on the gauge modes $d\omega$. These requirements are fulfilled by the function

$$F(U) = d^*q, \quad (5.54)$$

which lets us write the gauge fixing term for the action as

$$S_{\text{gf}}[B, q] = \frac{\lambda_0}{2} (d^*q, d^*q). \quad (5.55)$$

At this point a remark upon the boundary conditions on the fields q is due. A careful analysis of the authors of [24] shows that it is useful to formally extend the time component $q_0(x)$ of the lattice field to all points with $x_0 = -a$ and $x_0 = T$, thus allowing to write on the whole lattice

$$d^*q(x) = D_\mu^* q_\mu(x). \quad (5.56)$$

Besides eqs. (5.47), one has to specify the boundary conditions for the component q_0 . It is worth to express them in momentum space; we exploit the fact that all fields are periodic in space and perform the Fourier transform

$$q_0(\mathbf{p}, x_0) = \sum_{\mathbf{x}} e^{-i\mathbf{p}\cdot\mathbf{x}} q_0(x), \quad (5.57)$$

and decompose it in a basis of the Lie Algebra of SU(3)

$$q_0(\mathbf{p}, x_0) = \tilde{q}_0^a(\mathbf{p}, x_0) I^a. \quad (5.58)$$

The basis I^a used in all our computations can be found in App. A. With our choice of the background field we have a mixture of Dirichlet and Neumann boundary conditions

$$\boxed{\text{lower boundary}} \quad \begin{aligned} \tilde{q}_0^a(\mathbf{p}, -a) &= 0, \text{ if } I^a \in C_3 \text{ and } \mathbf{p} = \mathbf{0}, \\ \partial_0^* \tilde{q}_0^a(\mathbf{p}, x_0)|_{x_0=0} &= 0, \text{ otherwise,} \end{aligned} \quad (5.59)$$

$$\boxed{\text{upper boundary}} \quad \partial_0^* \tilde{q}_0^a(\mathbf{p}, x_0)|_{x_0=T} = 0.$$

The associated Fadeev-Popov ghosts c and \bar{c} can be seen as infinitesimal gauge transformations, except that they obey the Fermi statistics. The corresponding action is given by

$$S_{\text{FP}}[B, q, c, \bar{c}] = -(\bar{c}, d^* \delta_c q), \quad (5.60)$$

with $\delta_c q$ denoting the first order variation of q under the gauge transformation generated by c . We expand it to order g_0^2 , and get

$$\begin{aligned} \delta_c q_\mu &= D_\mu c + g_0 \text{Ad} q_\mu c \\ &+ \left[\frac{1}{2} g_0 a \text{Ad} q_\mu + \frac{1}{12} (g_0 a \text{Ad} q_\mu)^2 + \dots \right] D_\mu c, \end{aligned} \quad (5.61)$$

without summing over μ . The boundary conditions for the ghost fields can be obtained analogously to the gluon fields q . The analysis performed in [90] reveals that, after a Fourier transform as in eq. (5.57) and a group decomposition as in eq. (5.58), one is left

$$\boxed{\text{lower boundary}} \quad \begin{aligned} \partial_0^* \tilde{c}^a(\mathbf{p}, x_0)|_{x_0=0} &= 0, \text{ if } I^a \in C_3 \text{ and } \mathbf{p} = \mathbf{0}, \\ \tilde{c}^a(\mathbf{p}, -a) &= \tilde{c}^a(\mathbf{p}, 0) = 0, \text{ otherwise,} \end{aligned} \quad (5.62)$$

$$\boxed{\text{upper boundary}} \quad \tilde{c}^a(\mathbf{p}, T) = 0,$$

and similarly for \bar{c} .

5.4.2 The total action

After having fixed the gauge, we are ready to write down the gauge fixed functional integral in a form suitable for our perturbative computations. We gather the fully improved action (3.92), the gauge fixing term (5.55) and the Fadeev-Popov action (5.60) into the total action

$$S_{\text{tot}}[b, q, \bar{c}, c, \bar{\psi}, \psi] = S_{\text{impr}}[U, \bar{\psi}, \psi] + S_{\text{gf}}[b, q] + S_{\text{FP}}[b, q, c, \bar{c}], \quad (5.63)$$

where it is understood that U and q are related by eq. (5.46), and the b is defined in eqs. (A.20). We now perform a change of integration variables in the functional integral; we relate the measure $D[U]$ appearing in eqs. (3.37), to the measure

$$D[q] = \prod_{x,\mu,a} d\tilde{q}_\mu^a(x), \quad (5.64)$$

by

$$D[U] = D[q]e^{-S_m[q]} = D[q]\{1 + O(g_0^2)\}. \quad (5.65)$$

The additional contribution to the action stemming from this change of variables is thus of $O(g_0^2)$, and, since in our computations the action is needed only up to $O(g_0)$, we can neglect it from now on. The explicit form of the Schrödinger functional then reads

$$\mathcal{Z} = \int D[q]D[\bar{c}]D[c]D[\bar{\psi}]D[\psi]e^{-S_{\text{tot}}}. \quad (5.66)$$

We consider now an observable \mathcal{O} , consisting of a product of gauge links. An eventual dependence on the quark fields is not discussed here. The situation looks like the one discussed in Sect. 3.3; the difference is that here we want to find out a path integral expression, which suits a perturbative evaluation. We keep the quark determinant resulting from an integration over the quark variables, and write down the expectation value for \mathcal{O} as

$$\langle \mathcal{O} \rangle_G = \frac{1}{\mathcal{Z}} \int D[q]D[\bar{c}]D[c]D[\bar{\psi}]D[\psi] \mathcal{O} e^{-S_{\text{tot}}}. \quad (5.67)$$

We expand \mathcal{O} in a series of g_0 :

$$\langle \mathcal{O} \rangle_G = \mathcal{O}^{(0)} + g_0 \langle \mathcal{O}^{(1)} \rangle_G + g_0^2 \langle \mathcal{O}^{(2)} \rangle_G + O(g_0^3), \quad (5.68)$$

very simple to write down, thanks to eq. (5.46) and the fact that \mathcal{O} is just a product of link variables. It is important to bear in mind that the term $\mathcal{O}^{(n)}$ contains the product of n gluon fields. In turn, the action can be expanded according to

$$S_{\text{tot}} = S_{\text{tot}}^{(0)} + g_0 S_{\text{tot}}^{(1)} + g_0^2 S_{\text{tot}}^{(2)} + O(g_0^3). \quad (5.69)$$

Actually, there should also be a term proportional $S_{\text{tot}}^{(-2)}$ coming from the gluon action. However, such a term depends only on the background field and not on the integration variables appearing in the functional integral, and it drops out in eq. (5.67). It is then straightforward to write down the expansion

$$e^{-S_{\text{tot}}} = \left[1 - g_0 S_{\text{tot}}^{(1)} + g_0^2 \left(\frac{1}{2} (S_{\text{tot}}^{(1)})^2 - S_{\text{tot}}^{(2)} \right) + O(g_0^3) \right] e^{-S_{\text{tot}}^{(0)}}. \quad (5.70)$$

With this expression we can now write the expansion of the expectation value of \mathcal{O} as

$$\langle \mathcal{O} \rangle_G = \mathcal{O}^{(0)} + g_0^2 \left[\langle \mathcal{O}^{(2)} \rangle_0 - \left\langle \mathcal{O}^{(1)} \left[S_{\text{tot}}^{(1)} \right]_F \right\rangle_0 \right] + \mathcal{O}(g_0^4), \quad (5.71)$$

where $\langle \rangle_0$ means that the expectation value is computed using the action $S_{\text{tot}}^{(0)}$ instead of the complete one. Furthermore there are no terms of order g_0 or g_0^3 , because they would involve an integral over an odd number of gluon fields, and vanish. The brackets $[\]_F$ indicate that the quark fields have been integrated out as in Sect. 3.3. Finally we mention that the term containing $S_{\text{tot}}^{(1)}$ appears only because of the presence of a non-vanishing background field.

5.5 Expectation values of Wilson loops at one-loop order

5.5.1 Parametrization of the observable

Our aim is to gather all necessary steps for the computation of the expectation value of an arbitrary Wilson loop at one-loop order in the Schrödinger functional scheme, in a way which suits its numerical implementation. We bear in mind that in the end our observable is a Polyakov loop with, eventually, the insertion of a clover operator. Due to the space-time locality of such an observable, it will be advantageous to compute the gluon loops in x -space, while the tadpole contributions are proportional to the zero-momentum gluon propagator.

To achieve this, we parametrize the loop by a starting point $x^{(\text{start})}$ and an ordered list $\vec{\ell}$ of length ℓ . The entries of the list are directions $\mu_i^{\vec{\ell}}$, $i = 1, \dots, \ell$. These directions take non-zero integer values between -4 and $+4$. An electric plaquette in the (03) plane is thus parametrized by $\vec{\ell} = (3 \ 4 \ -3 \ -4)$. Clearly the loop is closed if and only if each integer appears as many times with the $+$ sign as it does with the $-$ sign, modulo L/a for the spatial directions. The latter is a consequence of the spatial periodic boundary conditions. It means that if we have a lattice setup with $L/a = 4$ and the path is parametrized by $\vec{\ell} = (3 \ 3 \ 3 \ 3)$, the latter specifies a closed loop. We normally drop the $\vec{\ell}$ in $\mu_i^{\vec{\ell}}$ since we will be dealing only with one path at a time.

The sequence of points the loop goes through is obtained as follows:

$$x^{(1)} = x^{(\text{start})}, \quad x^{(i+1)} = x^{(i)} + a\hat{\mu}_i, \quad i = 1, \dots, \ell - 1. \quad (5.72)$$

$\hat{\mu} = \text{sign}(\mu) |\hat{\mu}|$ are unit vectors pointing in the four \pm directions of the lattice. Here and throughout the following, the temporal direction is indicated by $|\mu| = 4$. This

choice is motivated by the necessity of indicating through the index μ the forward and backward direction also in time. For any unspecified notation we refer to App. A.

At tree-level, the expectation value of the Wilson loop is

$$W_\ell[V] = \prod_{i=1}^{\ell} V_{\mu_i}(x^{(i)}). \quad (5.73)$$

In general, for any 4-vector we introduce negative-index components

$$p_{-\mu} = -p_\mu. \quad (5.74)$$

Because of the way the path is parametrized, for any link variable we introduce negative-index components by imposing⁵

$$U_\mu(x) = U_{-\mu}^\dagger(x + a\hat{\mu}), \quad q_\mu^a(x) = -q_{-\mu}^a(x + a\hat{\mu}). \quad (5.75)$$

The Fourier representation is defined for all μ as follows:

$$q_\mu^a(x) = \frac{1}{L^3} \sum_{\mathbf{p}} e^{i\mathbf{p}\cdot\mathbf{x}} e^{i\theta_a(\mathbf{p}, x_0, \mu)} q_\mu^a(\mathbf{p}, x_0). \quad (5.76)$$

where

$$q_\mu^a(\mathbf{p}, x_0) = q_{|\mu|}^a(\mathbf{p}, x_0 - a\delta_{\mu+4,0}), \quad (5.77)$$

and

$$e^{i\theta_a(\mathbf{p}, x_0, \mu)} = \begin{cases} 1 & \text{if } \mu = 4 \\ e^{i(p_k + \phi_a(x_0))/2} & \text{if } \mu = k \\ -e^{i(-p_k + \phi_a(x_0))/2} & \text{if } \mu = -k \\ -1 & \text{if } \mu = -4 \end{cases}$$

$$= \text{sign}(\mu) \left(\delta_{|\mu|,4} + (1 - \delta_{|\mu|,4}) e^{i(p_\mu + \phi_a(x_0))/2} \right). \quad (5.78)$$

With these notations we have

$$\langle q_\mu^a(\mathbf{p}, x_0) q_\nu^b(\mathbf{p}', y_0) \rangle = \delta_{b,\bar{a}} L^3 \delta_{\mathbf{p}+\mathbf{p}', \mathbf{0}} D_{|\mu||\nu|}^a(\mathbf{p}; \tilde{x}_{0,\mu}, \tilde{y}_{0,\nu}), \quad (5.79)$$

where $\tilde{x}_{0,\mu} = x_0 - a\delta_{\mu+4,0}$, and analogously for $\tilde{y}_{0,\nu}$.

⁵Compared to eq. (5.58) the twiddle on the color components of the gluon field is dropped. We keep this notation also for the ghost and quark fields throughout the following. The color index a always appears as an index, unless specified otherwise.

5.5.2 Single gluon radiative corrections

In this subsection we deal with the perturbative corrections associated with the term $\mathcal{O}^{(2)}$ in eq. (5.71). We consider separately two contributions

$$\mathcal{O}^{(2)} = \mathcal{O}^{(2a)} + \mathcal{O}^{(2b)}. \quad (5.80)$$

We observe that our observable is nothing but the product of link variables. To compute $\mathcal{O}^{(2a)}$ we expand each link U according to the parametrization (5.46), and keep, for each link variable, the terms up to order g_0 . The gluon fields q_μ are decomposed as in eq. (5.58) to stress the color structure. We then contract the gluon fields and express the contractions in terms of gluon propagators. Each contraction is multiplied by the trace of the product of two SU(3) matrices I^a and several V matrices. The latter would coincide with the identity matrix if there was no background field. The order of the matrices is determined by the contraction and by the path defining the observable. In this way we obtain

$$\text{tr}\{W_\ell^{(2a)}\} = \sum_{j=1}^{\ell} \sum_{j'=j+1}^{\ell} \text{tr} \left\{ q^{(j)} W_\ell(j \sigma_j | j' \sigma_{j'}) q^{(j')} W_\ell(j' \sigma_{j'} | j \sigma_j) \right\}, \quad (5.81)$$

where we have used the cyclicity of the trace and the shorthand

$$q^{(j)} \equiv q_{\mu_j}(x^{(j)}). \quad (5.82)$$

If we now consider for each gauge link only the terms quadratic in g_0 in the parametrization (5.46), we obtain for $\mathcal{O}^{(2b)}$:

$$\text{tr}\{W_\ell^{(2b)}\} = \frac{1}{2} \sum_{j=1}^{\ell} \text{tr} \left\{ (q_{\mu_j}(x_j))^2 W_\ell[V] \right\}, \quad (5.83)$$

which is 1/2 of the term $j = j'$ on the r.h.s. of eq. (5.81). We also need the notation

$$\sigma_j \equiv \frac{1 - \text{sign}(\mu_j)}{2}, \quad (5.84)$$

and for $n \geq 1$,

$$\bar{n} = 1 + \text{mod}(n - 1, \ell). \quad (5.85)$$

We can now formulate the definition

$$W_\ell(j \sigma_j | j' \sigma_{j'}) = \begin{cases} W_\ell[V], & \text{if } \overline{j + \sigma_j} + \overline{j' + \sigma_{j'}} \text{ and } \sigma_j = 0, \\ W_\ell(\overline{j + \sigma_j} \rightarrow \overline{j' + \sigma_{j'}}), & \text{otherwise,} \end{cases} \quad (5.86)$$

that invokes the parallel transporter along the loop from $x^{(j)}$ to $x^{(j')}$:

$$W_{\bar{\ell}}(j \rightarrow j') = \begin{cases} 1, & \text{if } j = j', \\ \prod_{i=j}^{j'-1} V(x^{(i)}, \mu_i), & \text{if } j < j', \\ \prod_{i=j}^{\ell} V(x^{(i)}, \mu_i) \prod_{i=1}^{j'-1} V(x^{(i)}, \mu_i), & \text{if } j > j'. \end{cases} \quad (5.87)$$

One then finds

$$\begin{aligned} \langle \text{tr} \{ W_{\bar{\ell}}^{(2a)} \} \rangle_0 &= \frac{1}{L^3} \sum_{j=1}^{\ell} \sum_{j'=j+1}^{\ell} \sum_{a=1}^8 \sum_{\mathbf{p}} e^{i\mathbf{p} \cdot (\mathbf{x}^{(j)} - \mathbf{x}^{(j')})} e^{i\theta_a(\mathbf{p}, x_0^{(j)}, \mu_j)} e^{i\theta_{\bar{a}}(-\mathbf{p}, x_0^{(j')}, \mu_{j'})} \\ &\times \text{tr} \{ \Omega_{\bar{\ell}}^a(\mu_j, \mu_{j'}) \} D_{|\mu_j||\mu_{j'}|}^a(\mathbf{p}; x_0^{(j)} - a\delta_{\mu_j+4,0}; x_0^{(j')} - a\delta_{\mu_{j'}+4,0}), \end{aligned} \quad (5.88)$$

$$\Omega_{\bar{\ell}}^a(\mu_j, \mu_{j'}) = I^a W_{\bar{\ell}}(j \sigma_j | j' \sigma_{j'}) I^{\bar{a}} W_{\bar{\ell}}(j' \sigma_{j'} | j \sigma_j). \quad (5.89)$$

We introduce the propagator completely in x -space,

$$\begin{aligned} \Delta_{\mu\nu}^a(\mathbf{x}; x_0, y_0) &\equiv \frac{1}{L^3} \sum_{\mathbf{p}} e^{i\mathbf{p} \cdot \mathbf{x}} e^{i\theta_a(\mathbf{p}, x_0, \mu)} e^{i\theta_{\bar{a}}(-\mathbf{p}, y_0, \nu)} \\ &\times D_{|\mu||\nu|}^a(\mathbf{p}; x_0 - a\delta_{\mu+4}; y_0 - a\delta_{\nu+4}), \end{aligned} \quad (5.90)$$

which lets us now write

$$\begin{aligned} \langle \text{tr} \{ W_{\bar{\ell}}^{(2a)} \} \rangle_0 &= \sum_{j=1}^{\ell} \sum_{j'=j+1}^{\ell} \sum_{a=1}^8 \text{tr} \{ \Omega_{\bar{\ell}}^a(\mu_j, \mu_{j'}) \} \\ &\times \Delta_{\mu_j \mu_{j'}}^a(\mathbf{x}^{(j)} - \mathbf{x}^{(j')}; x_0^{(j)}, x_0^{(j')}), \end{aligned} \quad (5.91)$$

$$\langle \text{tr} \{ W_{\bar{\ell}}^{(2b)} \} \rangle_0 = \frac{1}{2} \sum_{a=1}^8 \text{tr} \{ I^a I^{\bar{a}} W_{\bar{\ell}}[V] \} \sum_{j=1}^{\ell} \Delta_{\mu_j \mu_j}^a(\mathbf{0}; x_0^{(j)}, x_0^{(j)}). \quad (5.92)$$

5.5.3 Tadpole contributions

In this subsection we deal with the one-loop terms stemming from $S_{\text{tot}}^{(1)}$ in eq. (5.71), with the improvement coefficients set to their tree-level values. They are commonly referred to as tadpole contributions, and they owe their existence to the non-vanishing background field. Let us first write $\mathcal{O}^{(1)}$ more explicitly

$$\mathcal{O}^{(1)} = \text{tr} \{ W_{\bar{\ell}}^{(1)} \} = \sum_{j=1}^{\ell} \text{tr} \{ q_{\mu_j}(x^{(j)}) W_{\bar{\ell}}[V] \}. \quad (5.93)$$

The three contributions coming from the order g_0 in the expansion (5.70) of the action are explicitly given in eq. (6.120), eq. (6.123) and eq. (6.127) for the ghost, gluon and quark cases respectively. They enable us to find the formal expression⁶

$$\langle \text{tr} \{ W_{\vec{\ell}}^{(1)} \} S_{\text{tot}}^{(1)} \rangle_0 = - \sum_{a=1}^8 \sum_{\mu=1}^4 \sum_{u_0} \alpha_{\vec{\ell}, \mu}^a(u_0) T_{\mu}^a(u_0), \quad (5.94)$$

with

$$\begin{aligned} \alpha_{\vec{\ell}, \mu}^a(u_0) &= \text{tr} \{ I^{\vec{a}} W_{\vec{\ell}}[V] \} \sum_{j=1}^{\ell} \text{sign}(\mu_j) \left(\delta_{|\mu_j|, 4} + (1 - \delta_{|\mu_j|, 4}) e^{-i\phi_a(x_0^{(j)})/2} \right) \\ &\times D_{\mu|\mu_j|}^a(\mathbf{0}; u_0, x_0^{(j)} - a\delta_{\mu_j+4, 0}), \end{aligned} \quad (5.95)$$

and

$$T_{\mu}^a(u_0) = T_{\mu, \text{gluon}}^a(u_0) + T_{\mu, \text{ghost}}^a(u_0) + N_f T_{\mu, \text{quark}}^a(u_0). \quad (5.96)$$

Since T_{μ}^a vanishes for $\mu = 4$, due to CP-invariance, and for the color indices a different from 3 and 8, due to the structure of the vertices, we can rewrite eq. (5.94) as

$$\langle \text{tr} \{ W_{\vec{\ell}}^{(1)} \} S_{\text{tot}}^{(1)} \rangle_0 = - \sum_{k=1}^3 \sum_{u_0} \left\{ \alpha_{\vec{\ell}, k}^3(u_0) T_k^3(u_0) + \alpha_{\vec{\ell}, k}^8(u_0) T_k^8(u_0) \right\}, \quad (5.97)$$

and exploit the explicit expressions for the tadpoles T_k^a given in Sect. 6.3.

5.5.4 Improvement

In order to be able to reach the continuum limit with a rate proportional to $(a/L)^2$ our observable needs to be improved. Since there are no operators of dimension 6 with the same symmetries of $\mathcal{O}_{\text{spin}}$, non-vanishing at one-loop order, and with no valence quarks, the improvement amounts to compute the additional contributions stemming from the volume and boundary counterterms in the action. From the discussion expounded in Sect. 3.4 we infer that the counterterms proportional to c_s and \tilde{c}_s vanish, because the background field is purely electric and our observable does not involve relativistic fermion fields. The volume term for the quark action has been taken into account since the very beginning, through the term proportional to $c_{\text{sw}}^{(0)}$. The one-loop expression of c_{sw} is not needed. It amounts to a correction of order g_0^4 to our observable. Analogously for \tilde{c}_t . Inspection of eq. (3.94) reveals that the counterterm

⁶Due to the notation employed in this section, the component T_4^a of the tadpole corresponds to T_0^a of Sect. 6.3.

proportional to the one-loop expression of \tilde{c}_t leads to a correction to our observable of order g_0^4 . The only contribution which one needs to take into account comes from the boundary counterterm of the gauge action (3.93) proportional to $c_t^{(1)}$. It is convenient to express the corresponding counterterm in the form

$$\langle \text{tr} \{W_{\vec{\ell}}^{(1)}\} \delta S_{\text{tot,b}}^{(1)} \rangle_0, \quad (5.98)$$

where $\delta S_{\text{tot,b}}^{(1)}$ reads [91]

$$\delta S_{\text{tot,b}}^{(1)} = \frac{2}{\sqrt{3}} c_t^{(1)} \sum_{k=1}^3 [q_k^8(\mathbf{0}, a) - q_k^8(\mathbf{0}, T - a)] [\sin(2\gamma) + \sin(\gamma)], \quad (5.99)$$

and the parameter γ , defined in eq. (A.16), is non-zero only for a non-vanishing background field. The coefficient $c_t^{(1)}$ depends on the flavor number [37, 87]:

$$c_t^{(1)} = -0.08900(5) + 0.0191410(1)N_f. \quad (5.100)$$

The explicit expression of (5.98) can be computed similarly to the tadpoles, and reads

$$\langle \text{tr} \{W_{\vec{\ell}}^{(1)}\} \delta S_{\text{tot,b}}^{(1)} \rangle_0 = \frac{2}{\sqrt{3}} c_t^{(1)} [\sin(2\gamma) + \sin(\gamma)] \text{tr} \{I^8 W_{\vec{\ell}}[V]\} \sum_{k=1}^3 M_{\vec{\ell},k}, \quad (5.101)$$

with

$$M_{\vec{\ell},k} = \sum_{j=1}^{\ell} \text{sign}(\mu_j) \left(\delta_{|\mu_j|,4} + (1 - \delta_{|\mu_j|,4}) e^{-i\phi_8(x_0^{(j)})/2} \right) \times \left(D_{k|\mu_j|}^8(\mathbf{0}, a, x_0^{(j)} - a\delta_{\mu_j+4,0}) - D_{k|\mu_j|}^8(\mathbf{0}, T - a, x_0^{(j)} - a\delta_{\mu_j+4,0}) \right), \quad (5.102)$$

where we exploited the fact that I^8 and the background field are diagonal, and that $I^8 = I^{\bar{8}}$.

5.5.5 Summary

By collecting the results of this section, we obtain that the expectation value of the $O(a)$ -improved Wilson loop at one-loop order is given by

$$\begin{aligned} \langle \text{tr} \{W_{\vec{\ell}}\} \rangle_G = & W_{\vec{\ell}}[V] + g_0^2 \left(\langle \text{tr} \{W_{\vec{\ell}}^{(2a)}\} \rangle_0 + \langle \text{tr} \{W_{\vec{\ell}}^{(2b)}\} \rangle_0 \right. \\ & \left. - \langle \text{tr} \{W_{\vec{\ell}}^{(1)}\} S_{\text{tot}}^{(1)} \rangle_0 - \langle \text{tr} \{W_{\vec{\ell}}^{(1)}\} \delta S_{\text{tot,b}}^{(1)} \rangle_0 \right). \end{aligned} \quad (5.103)$$

The one-loop computation of the Polyakov loop with and without insertion of the clover leaf operator defined in Sect. 5.2 has been performed with the Matlab code `WLINE` described in chapter 6. The tadpole loops do not depend on the observable, and they have been computed and stored on a file. The tadpole contributions $\langle \text{tr} \{W_{\vec{\ell}}^{(1)}\} S_{\text{tot}}^{(1)} \rangle_0$ have then been computed with very little effort. The improvement counterterms are needed only for the Polyakov loop with operator insertion, and their computation is cheap too. The most time consuming computation is the one of the gluon propagator.

In order to give an idea of the computational cost, for $N_f = 2$ and lattice discretization with $L/a = 48$ the computation of all diagrams and improvement counterterms for the Polyakov loop with insertion of the clover leaf operator has been carried out in 2 weeks on a PC, equipped with a single processor Intel Pentium 4 with 2.6 GHz. The scaling can be approximated with a polynomial in L/a , and is asymptotically dominated by the highest power, i.e. $(L/a)^5$.

5.6 Two-loop anomalous dimension and cutoff effects

In perturbation theory the renormalization factor of the chromo-magnetic operator in the Schrödinger functional scheme can be expanded as

$$Z_{\text{mag}}^{\text{SF}}(g_0, L/a) = 1 + Z_{\text{mag}}^{(1)}(L/a)g_0^2 + \mathcal{O}(g_0^2). \quad (5.104)$$

At tree-level it is one, as a consequence of the definition (5.26), while the 1-loop coefficient $Z_{\text{mag}}^{(1)}$ contains a logarithmic divergence. It is hence natural to decompose it in a constant term, a logarithmic divergent term, and other terms vanishing in the continuum limit

$$Z_{\text{mag}}^{(1)}(L/a) = \chi_{\text{SF, lat}}^{(1)} - \gamma_0 \ln(a/L) + \mathcal{O}(a/L). \quad (5.105)$$

These last terms may be written as a linear combination of the form [41]:

$$\sum_{\ell=0}^1 \sum_{n=1}^{\infty} c_{\ell n} \cdot (a/L)^n \ln^{\ell}(a/L).$$

After having implemented the $\mathcal{O}(a)$ -improvement as described in Sect. 5.5.4, the second sum starts from $n = 2$.

In view of a non-perturbative computation of the renormalization factor, we define the step scaling function

$$\Sigma_{\text{mag}}^{\text{SF}}(u, a/L) = \left. \frac{Z_{\text{mag}}^{\text{SF}}(2L)}{Z_{\text{mag}}^{\text{SF}}(L)} \right|_{\bar{g}_{\text{SF}}^2(L)=u}. \quad (5.106)$$

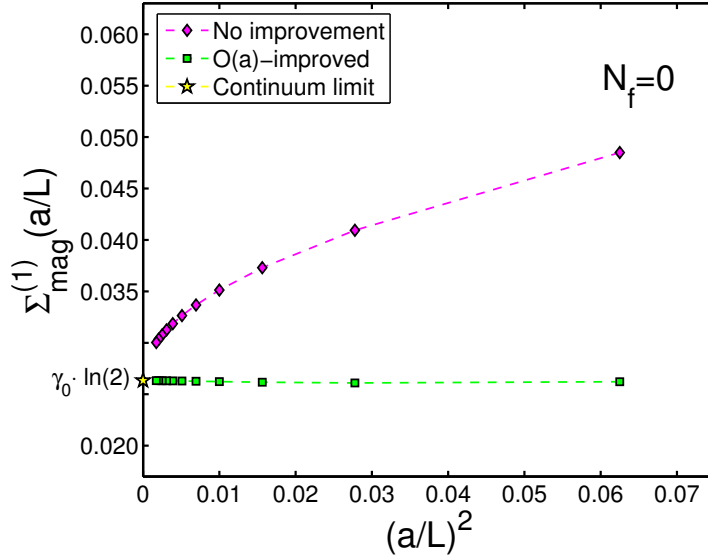


Figure 5.1: One-loop contribution $\Sigma_{\text{mag}}^{(1)}(a/L)$ to the quenched step scaling function of the chromo-magnetic operator.

at vanishing renormalized quark masses. The continuum limit

$$\lim_{a/L \rightarrow 0} \Sigma_{\text{mag}}^{\text{SF}}(u, a/L) = \sigma_{\text{mag}}^{\text{SF}}(u), \quad (5.107)$$

conveys the variation experienced by the renormalized operator $\mathcal{O}_{\text{spin}}^{\text{SF}}(\mu)$ when the scale μ is changed by a factor of two,

$$\mathcal{O}_{\text{spin}}^{\text{SF}}(\mu) = \sigma_{\text{mag}}^{\text{SF}}(\bar{g}_{\text{SF}}^2(L)) \mathcal{O}_{\text{spin}}^{\text{SF}}(2\mu), \quad \mu = 1/L. \quad (5.108)$$

The step scaling function (5.106) may be expanded in perturbation theory

$$\Sigma_{\text{mag}}^{\text{SF}}(u, a/L) = 1 + \Sigma_{\text{mag}}^{(1)}(a/L)u + \mathcal{O}(u^2), \quad (5.109)$$

where the one-loop coefficient is given by

$$\Sigma_{\text{mag}}^{(1)}(a/L) = Z_{\text{mag}}^{(1)}(2L/a) - Z_{\text{mag}}^{(1)}(L/a), \quad (5.110)$$

whose continuum limit is proportional to the one-loop anomalous dimension

$$\lim_{a/L \rightarrow 0} \Sigma_{\text{mag}}^{(1)}(a/L) \stackrel{(5.105)}{=} \gamma_0 \ln(2). \quad (5.111)$$

The deviations of $\Sigma_{\text{mag}}^{\text{SF}}$ from the continuum limit $\sigma_{\text{mag}}^{\text{SF}}$ are referred to as cutoff effects, and they can be expressed in the form

$$\delta(u, a/L) = \frac{\Sigma_{\text{mag}}^{\text{SF}}(u, a/L) - \sigma_{\text{mag}}^{\text{SF}}(u)}{\sigma_{\text{mag}}^{\text{SF}}(u)} = \delta_1(a/L)u + \mathcal{O}(u^2), \quad (5.112)$$

with the one-loop order given by

$$\delta_1(a/L) = \Sigma_{\text{mag}}^{(1)}(a/L) - \gamma_0 \ln(2). \quad (5.113)$$

Here δ_1 can be expanded according to its N_f -dependence,

$$\delta_1(a/L) = \delta_{1,0}(a/L) + N_f \delta_{1,1}(a/L). \quad (5.114)$$

The computation of δ_1 provides important informations upon the cutoff effects affecting the step scaling function. The results are expected to be of guidance also for the non-perturbative simulations, at least in the weak coupling regime. The latter are discussed in the next section.

In Fig. 5.1 the one-loop contribution $\Sigma_{\text{mag}}^{(1)}$ is shown for the quenched case. The lattice discretization ranges from $L/a = 4$ to $L/a = 24$. It means that at the finest lattice we computed $Z_{\text{mag}}^{(1)}(2L/a = 48)$. The green squares and the magenta diamonds show the one-loop contribution to the step scaling function with and without $\mathcal{O}(a)$ -improvement counterterms respectively. The agreement of the continuum limit with the prediction (5.111) is evident, as well as the effect of the $\mathcal{O}(a)$ -improvement.

In Fig. 5.2 the one-loop order and $\mathcal{O}(a)$ -improved term $Z_{\text{mag}}^{(1)}$, after subtracting the logarithmic divergent part, is shown for the quenched case. The lattice discretization ranges from $L/a = 4$ to $L/a = 48$. The extrapolated result represents our estimate of $\chi_{\text{SF, lat}}^{(1)}$ for $N_f = 0$.

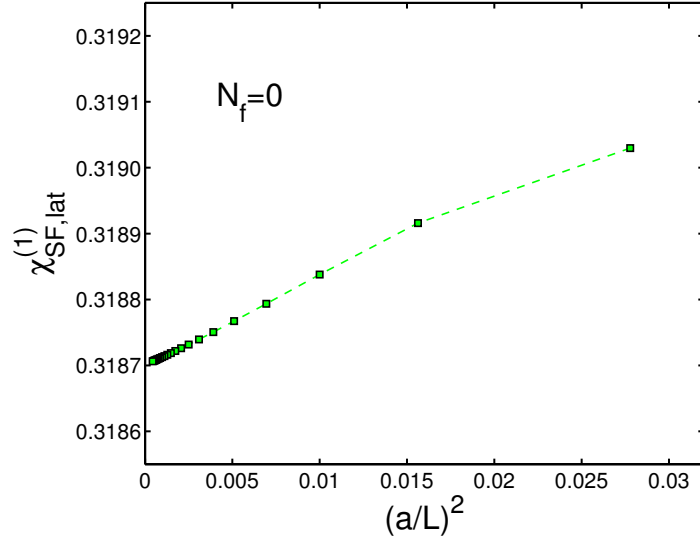


Figure 5.2: One-loop order of Z_{mag} after removing the logarithmic divergent part. The plotted points refer to $L/a \geq 6$.

The computation with $N_f \neq 0$ requires, additionally to the quenched case, the inclusion of the quark tadpole contributions. At this point two remarks are due. The first of them stems from the observation that the action now includes N_f mass degenerate light quarks, and our renormalization condition (5.26) is intended at vanishing quark mass. The latter appears at tree-level in our computation of the quark tadpoles, which already are one-loop contributions. Therefore we can fix the mass to zero at tree-level for all lattice discretizations without compromising the improvement described in Sect. 5.5.4. Other choices may be of interest when the comparison with non-perturbative computations is desired. The second remark concerns the phase factor θ appearing in the quark boundary conditions (3.20). For the computation of the quark tadpoles we take $\theta = -\pi/3$. This choice is motivated by the requirement of having a real renormalization factor $Z_{\text{mag}}^{\text{SF}}$. According to the analysis of [92], the discrete symmetries of the QCD Schrödinger functional, with the boundary conditions specified in App. A, predict that this can be achieved in eq. (5.26) only through the choice $\theta = -\pi/3$.

The one-loop contribution to the step scaling function in the $N_f = 2$ case is shown in Fig. 5.3. Colors and symbols have the same meaning as in the quenched case. The effect of the $O(a)$ -improvement is evident, as well as the fact that, in comparison to the quenched case, the cutoff effects are much bigger. Quantitatively, this can be understood by looking at Table 5.1.

The term $Z_{\text{mag}}^{(1)}$, where the logarithmic divergent part is subtracted, is shown for

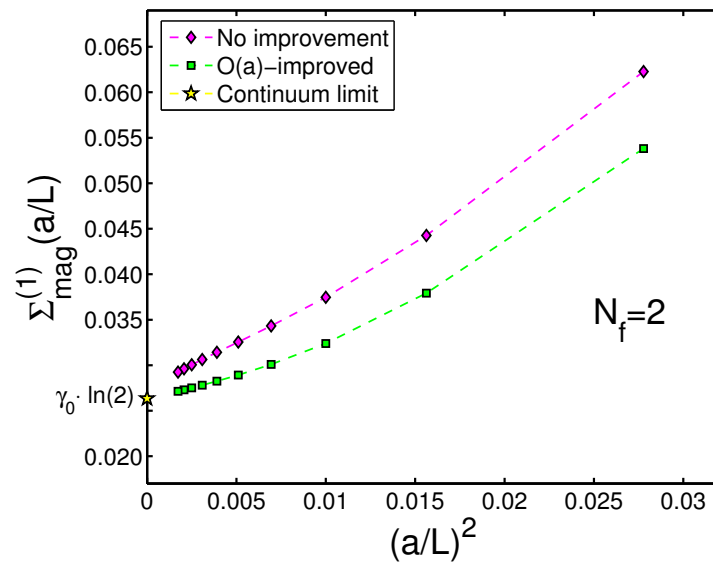


Figure 5.3: One-loop contribution $\Sigma_{\text{mag}}^{(1)}(a/L)$ to the step scaling function of the chromo-magnetic operator in the $N_f = 2$ case.

$N_f = 2$ in Fig. 5.4. There, only the $O(a)$ -improved points are plotted.

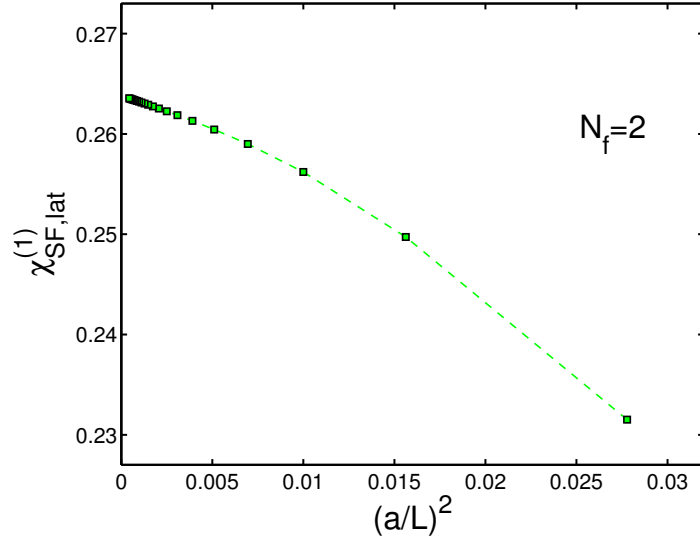


Figure 5.4: One-loop order of Z_{mag} , with $N_f = 2$, after removing the logarithmic divergent part. The plotted points refer to $L/a \geq 6$.

The continuum limits, including the estimate of the uncertainties, are performed according to the method described in [47], with Matlab routines provided by Ulli Wolff. The roundoff errors are modelled by assuming that, in double precision, the rounding amounts to a relative uncertainty of order 10^{-14} for the results at $L/a = 4$. This is compatible with the check on the average plaquette described in Sect. 6.4.1. As in [47], we assume that the errors grow proportionally to $(L/a)^3$, and we treat them as a normally distributed superimposed noise, independent for each lattice discretization. The upshot is that the roundoff errors are negligible compared to the systematic uncertainties. Another source of error has roots in the improvement coefficient c_t , whose one-loop expression is given in eq. (5.100). However, our observables show a very low sensitivity upon variations of c_t within the quoted errors, and the latter can thus be neglected.

The continuum limit for the step scaling functions, both for $N_f = 0$ and for $N_f = 2$, is in agreement with eq. (5.111) within a relative systematic error of $O(10^{-5})$. The continuum limit for the one-loop connection between the SF and the lat schemes gives

$$\chi_{\text{SF,lat}}^{(1)} = 0.3187016(1) - 0.027448(1)N_f. \quad (5.115)$$

| L/a | $\delta_{1,0}(a/L)$ | $\delta_{1,1}(a/L)$ |
|-------|---------------------|---------------------|
| 4 | -0.000116 | 0.036731 |
| 6 | -0.000236 | 0.013742 |
| 8 | -0.000165 | 0.005791 |
| 10 | -0.000106 | 0.003026 |
| 12 | -0.000072 | 0.001876 |
| 14 | -0.000051 | 0.001296 |
| 16 | -0.000038 | 0.000956 |
| 18 | -0.000029 | 0.000738 |
| 20 | -0.000023 | 0.000588 |
| 22 | -0.000019 | 0.000481 |
| 24 | -0.000016 | 0.000400 |

Table 5.1: Lattice spacing effects of Σ_{mag} at one-loop order.

This results can be combined with $\chi_{\overline{\text{MS}},\text{lat}}^{(1)}$, appearing in eq. (5.43), to get

$$\chi_{\overline{\text{SF}},\overline{\text{MS}}}^{(1)} = \chi_{\overline{\text{SF}},\overline{\text{MS}}}^{(1,0)} + \chi_{\overline{\text{SF}},\overline{\text{MS}}}^{(1,1)} N_f, \quad (5.116)$$

$$\chi_{\overline{\text{SF}},\overline{\text{MS}}}^{(1,0)} = -0.0637(3), \quad \chi_{\overline{\text{SF}},\overline{\text{MS}}}^{(1,1)} = -0.027448(1), \quad (5.117)$$

and finally, through eq. (5.41),

$$\gamma_1^{\text{SF}} = -0.00236(4) - 0.003513(2)N_f + 0.000232N_f^2. \quad (5.118)$$

The error is dominated by the uncertainty on $\chi_{\overline{\text{MS}},\text{lat}}^{(1)}$, which mainly affects the pure gauge contribution. Of course also the coefficient in front of the N_f^2 contribution has an error, but it is several orders of magnitude smaller than the others.

5.7 Non-perturbative step scaling functions

In order to perform a non-perturbative study of the cutoff effects affecting $\Sigma_{\text{mag}}^{\text{SF}}$, and compare them with the predictions of perturbation theory, we computed in the quenched approximation two step scaling functions at weak coupling. The simulations

parameters are taken from [12], and refer to the SF renormalized couplings $u = \bar{g}_{\text{SF}}^2 = (0.9944, 1.3293)$.

In order to improve the statistical precision, we fully exploit translational invariance and the equivalence of the three spatial coordinates. In other words, the Polyakov loop is computed in the directions x, y and z , and we average over them. The gauge links building up the Polyakov loop, but not the inserted clover leaf operator, are evaluated by a 10-hit multi-hit procedure, as described in [93]. It means that on the time slice $x_0 = L/2$, each link $U_k(x)$ is replaced by

$$\bar{U}_k(x) = \frac{\int dU_k(x) U_k(x) e^{-S_G[U_k(x)]}}{\int dU_k(x) e^{-S_G[U_k(x)]}}, \quad k = 1, 2, 3, \quad (5.119)$$

where the integration is performed over only one SU(3) matrix and depends on the neighboring links. Each hit consists of one heatbath update according to the algorithm described in Sect. 3.3.

The simulation parameters and the results are reported in Table 5.2; the latter are plotted in Fig. 5.5. The continuum limit extrapolations are performed with the ansatz

$$\Sigma_{\text{mag}}^{\text{SF}}(u, a/L) = \sigma_{\text{mag}}^{\text{SF}}(u) + \rho(u)(a/L)^2, \quad u = \bar{g}_{\text{SF}}^2(L), \quad (5.120)$$

and the results are reported in the following table.

| u | $\sigma_{\text{mag}}^{\text{SF}}(u)$ | $\rho(u)$ |
|--------|--------------------------------------|-----------|
| 0.9944 | 1.025(11) | -0.15(53) |
| 1.3293 | 1.043(12) | -0.66(55) |

As predicted by perturbation theory, in the quenched approximation the cutoff effects in the weak coupling regime are indeed invisible, as long as the statistical precision is around one percent.

The non-perturbative computation of these step scaling functions is part of a work [94, 95], whose main result is the computation of $Z_{\text{mag}}^{\text{RGI}}$ and of the $B_{(s)}^* - B_{(s)}$ mass splitting in the quenched approximation.

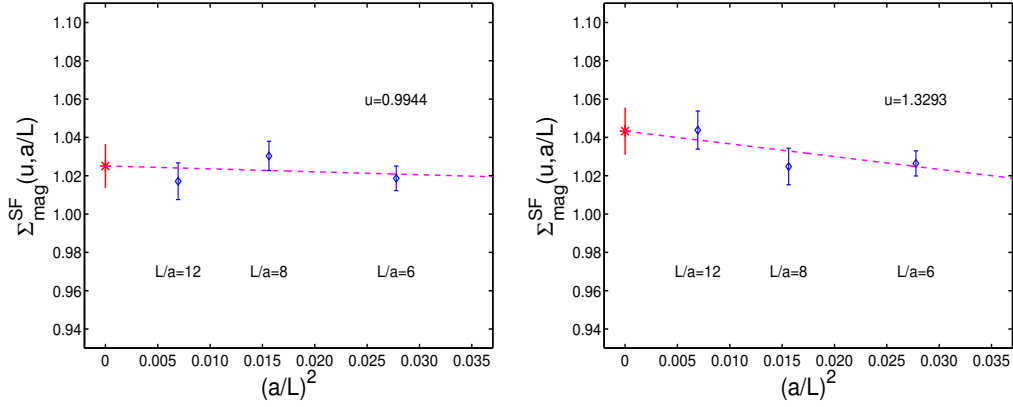


Figure 5.5: Continuum limit extrapolations for the step scaling function $\Sigma_{\text{mag}}^{\text{SF}}$.

| β | L/a | $Z_{\text{mag}}^{\text{SF}}(g_0, L/a)$ | $Z_{\text{mag}}^{\text{SF}}(g_0, 2L/a)$ | $\Sigma_{\text{mag}}^{\text{SF}}(u, a/L)$ |
|--------------|-------|--|---|---|
| $u = 0.9944$ | | | | |
| 10.0500 | 6 | 1.3651(44) | 1.3905(76) | 1.0186(64) |
| 10.3000 | 8 | 1.3514(52) | 1.3924(88) | 1.0303(76) |
| 10.6086 | 12 | 1.3608(53) | 1.384(12) | 1.0171(96) |
| $u = 1.3293$ | | | | |
| 8.6129 | 6 | 1.4727(57) | 1.5116(77) | 1.0264(66) |
| 8.8500 | 8 | 1.4664(71) | 1.503(12) | 1.0248(95) |
| 9.1859 | 12 | 1.4528(65) | 1.517(13) | 1.0438(99) |

Table 5.2: Results for the (quenched) non-perturbative step scaling function $\Sigma_{\text{mag}}^{\text{SF}}$. The simulations have been performed with c_t set to its two-loop value (3.101).

5.8 Summary

The spin splitting in heavy-light quark bound states is a key quantity for testing the validity of the Heavy Quark Effective Theory, both in the bottom channel and the charm one. Lattice computations have started in the quenched approximation, providing, so far, results in disagreement with the experimental predictions. These computations used perturbative estimates for the renormalization factor of the chromo-magnetic operator, introducing a hardly controllable source of uncertainty.

In this chapter a practicable way to non-perturbatively renormalize that operator is introduced. The Schrödinger functional scheme allows to compute the renormalization factor in a low energy regime, where phenomenology directly applies, and to evolve it to high energy scales, where perturbation theory can be safely used to finally compute the renormalization group invariant renormalization factor. There, a one-loop connection between the SF and the widely used $\overline{\text{MS}}$ schemes is performed by exploiting exact relations stemming from the renormalization group equations. For the latter scheme, the two-loop anomalous dimension is known, and the here computed connection enables to get it for the SF scheme too. The computation of the two-loop anomalous dimension represents the main result of the chapter, and constitutes an important ingredient for a precise evaluation of the scale running of the SF renormalization factor.

In the SF scheme a renormalization condition is imposed by introducing correlation functions, which do not involve valence quarks. In the quenched approximation, one then deals with pure gauge quantities, which considerably simplifies the perturbative computations. As light fermions are introduced in the action, their presence emerges only at the n -loop order, with $n \geq 1$.

In order to have a renormalization factor with a non-vanishing tree-level, a background field has been introduced. Unfortunately, this has the disadvantage of making the one-loop perturbative computation much more complicated than in the vanishing background field case. These difficulties have been faced by developing a program which automatically generates and computes the required diagrams, as well as the necessary $\mathcal{O}(a)$ -improvement counterterms, for any closed loop and at the perturbative one-loop level. Among the features of the program, it is worth to mention that, due to the space-time locality of the involved observables, it is advantageous to compute the gluon loops in coordinate space. The ghost, gluon and quark propagators are computed through recursive methods. The details on those, and more, are explained in the next chapter.

The computation of the two-loop anomalous dimension does not represent the only one result of perturbation theory. In view of a non-perturbative computation of the renormalization factor $Z_{\text{mag}}^{\text{SF}}$ for a wide range of renormalization scales, Sect. 5.6 con-

tains an interesting one-loop analysis of the cutoff effects affecting the step scaling functions. The latter measure the variation which the factor $Z_{\text{mag}}^{\text{SF}}$ undergoes, when the renormalization scale is changed by a factor of two. The one-loop predictions are expected to provide a guidance for the non-perturbative computations, at least in the weak coupling regime. This has been confirmed in Sect. 5.7, whose results show that, at least in the quenched case, the cutoff effects are invisible as long as the relative statistical precision is around one percent. For the unquenched case, perturbation theory predicts bigger but still moderate cutoff effects. They may have a strong dependence on the chosen kinematical parameters, and, unfortunately, a non-perturbative check is still missing.

A final remark has roots in the observation that the connection between the Schrödinger functional and the $\overline{\text{MS}}$ schemes is achieved by exploiting as intermediate step the lattice minimal subtraction scheme. The one-loop connection between the latter and the $\overline{\text{MS}}$ scheme is known from the literature with less precision than achieved here for the SF scheme; it dominates the uncertainty on the two-loop SF anomalous dimension. As a valuable check, one may also think of performing a direct two-loop computation in the SF scheme.

Chapter 6

The Matlab code `WLINE`

In this chapter we describe the Matlab code used for our perturbative computations in the Schrödinger functional scheme. We decided to use Matlab in order to combine comfortable programming, simplicity and readability of the code, robustness of the libraries and an acceptable speed for the observables and lattice discretizations of chapter 5.

The first section is devoted to an overview of the structure of the code `WLINE` in its released version 1.0. The latter computes the tree-level and the 1-loop order of the perturbative expansion of any closed Wilson line within the Schrödinger functional scheme on the lattice. The section provides the necessary informations to enable the user to compute the desired Wilson line, by specifying very few input parameters. The generation and the computation of all diagrams, including the $O(a)$ -improvement, are then automatically executed. With “automatic generation” of the diagrams and the improvement counterterms, we intend that all of them are already implemented inside the code. Furthermore, the program has been also conceived as an ensemble of several modules. Each propagator, tadpole, improvement counterterm or diagram is separately accessible.

The second section deals with the free ghost, gluon and quark propagators, and the attention is focused on the techniques used for their numerical computation. The presence of a non-vanishing background field prohibits from obtaining a simple explicit analytical expression for them. A brute force approach would require the inversion of big sparse matrices, and would be computationally more expensive for fine lattices. However, clever recursive methods have been developed by the authors of [47, 90], and they are implemented in our code. To each kind of propagator we dedicate a subsection, which is in turn divided into three parts. The first part contains the basic definitions and the method used for the numerical computation. In the second part we give the

necessary informations which enable to use the implemented subroutines to compute the propagators. The third part is dedicated to the analytical proof of the recursive method used for the computation. The user who just intends to use the program as a black box may skip this part in a first reading. The analytical proofs are partially based on [96]. The computation of the propagators through the recursive method has been successfully checked, up to machine precision, against the aforementioned method, which involves the inversion of big sparse matrices. Further details are given in the corresponding subsections.

The third section is mainly dedicated to the ghost, gluon and quark tadpoles. The latter could be computed through the explicit expressions of the vertices, provided e.g. by [91]. However, the formulae given in [97], which have been analytically proven, are much simpler to implement and have been found to significantly reduce the computational effort. To each kind of tadpole a subsection is dedicated, which is in turn divided into two parts. While the first part contains the basic definitions, the second one provides the necessary informations to use the implemented subroutines. The last subsection is devoted to the $O(a)$ -improvement.

The fourth section provides a short report on two tests of the code. The first test stems from the simple observation, provided by Creutz in [98], that, by approximating the gluon action to be quadratic in the gluon fields, one can derive an exact and analytical expression for the expectation value of the average plaquette just by counting the number of gluonic degrees of freedom. This expression has been successfully checked against our code. The second (successful) test consists in comparing the one-loop results for the average plaquette and the Polyakov loops, as defined in chapter 5, produced by `WLINE`, with the results of the quenched non-perturbative computations, performed at very weak coupling. Finally, we remark that the aforementioned observables have been computed for several values of the gauge fixing parameter λ_0 , appearing in eq. (5.55), always giving results consistent within machine precision. The consistency does not deteriorate when one increases the fineness of the lattice.

The fifth section briefly summarizes the whole chapter, and provides a few observations and an outlook.

We remark that throughout the chapter we work in units of the lattice spacing, and for any unspecified notation we refer to App. A.

6.1 The automated code

The code is available on request or for download from the webpage

<http://www-zeuthen.desy.de/alpha/>

in the directory `Internal/PT software`. After unpacking the file

`WLINE.tar.gz`

the following directories are available:

| | |
|-------------------------------|--|
| <code>WLINE_LAUNCH</code> | Main directory. It contains the files where the input parameters have to be specified, and a short script, which launches the program execution. |
| <code>WLINE_SIMPLE</code> | The pure gauge 1-loop diagrams, not including the tadpoles, are generated and computed. Tree-level computation. |
| <code>TADPOLES_GAUGE</code> | Gluon and ghost tadpoles. |
| <code>TG_CONTRIBUTIONS</code> | The contribution of the gluon and ghost tadpoles to the desired observable. |
| <code>TADPOLE_QUARK</code> | Quark tadpoles. |
| <code>TQ_CONTRIBUTIONS</code> | The contribution of the quark tadpoles to the desired observable. |
| <code>IMPROVEMENT</code> | $O(a)$ -improvement counterterms. |

Inside the main directory `WLINE_LAUNCH` there are six files:

- `topo_parameters.dat`
- `starting_point.dat`
- `wilson_path.dat`
- `wline_automatic.m`
- `check_path.m`
- `generateP.m`

The first of them contains a column vector of length 12, where the lattice topological parameters and other options are specified. An example is the following

```

less topo_parameters.dat

4      %T
4      %L
0.0    %eta
0.0    %nu
1      %if !=0 ==> Activation of the background field
1.0    %lambda_0, gauge fixing parameter
1.0    %1.0=Unix/Linux, 2.0=Windows
1      %Observable: 0, 1 or 2
-1.04719755119660 %theta_angle=-pi./3
1.0    %c_sw_0
0.0    %mass_0
2      %Nf

```

The first two parameters are easy to interpret; they specify the temporal and spatial lattice extensions in units of the lattice spacing. The third and fourth parameters define the non-vanishing background field according to eqs. (A.12). The latter is activated if and only if the fifth parameter is different from zero. The exact value does not matter at all, as long as it does not vanish. If it vanishes, the computation is executed with vanishing background field and boundary fields $C = C' = 0$. The sixth parameter specifies the gauge fixing parameter. The value given in the example, i.e. 1.0, corresponds to the Feynman gauge. It can be used to check that the final result, consisting in the sum of all diagrams, does not depend on the choice of the gauge. This is possible only in the non-vanishing background field case. For vanishing background field only the Feynman gauge is available. If another choice is specified, the execution is interrupted. The value of the seventh parameter has to be chosen according to the kind of operating system. The difference between Unix/Linux and Windows is for the code important only for the way the paths are internally specified. The eighth parameter can be 0, 1 or 2 only. In the first two cases the function `generateP.m` is used for the computation of Polyakov loops. If it is set to 2, it allows for a general Wilson loop. The last four parameters are dedicated to the quark sector. They are of relevance if and only if the last of them, specifying the number of mass degenerate light fermions involved, differs from zero. It can also be a negative integer. The parameter number nine specifies the phase factor θ , appearing in eqs. (3.20). The following parameter specifies the improvement coefficient c_{sw} for the fermionic action as in eq. (3.91). The penultimate parameter corresponds to the mass of all degenerate light fermions.

In all cases, all 12 parameters have to be provided before starting the program. If this condition is not respected, the execution is interrupted.

Let us now have a look to the file `starting_point.dat`. An example is

```
less starting_point.dat
```

```
0 0 0 2
```

It just contains a row vector made of four integers. They specify the Euclidean coordinates, in lattice units, of the Wilson line starting point with order (x, y, z, t) . Similarly for the file `wilson_path.dat`, whose content can read

```
less wilson_path.dat
```

```
3 3 3 3
```

It is an integer row vector as well, specifying the path covered by the Wilson line from the starting point. The given example indicates that the Wilson line is the product of four gauge links pointing in the z -direction. If one wants to insert an electric plaquette, lying on the xt -plane, in the middle of the line, it is sufficient to write the path as

```
3 3 1 4 -1 -4 3 3
```

Translational invariance can be checked by replacing the aforementioned path by

```
3 1 4 -1 -4 3 3 3
```

where, given the default starting point $(0,0,0,2)$, the plaquette has been inserted at the point $(0,0,1,2)$. The file `generateP.m` contains the function

```
function [res] = generateP(option_ins)
```

which is used if and only if the eighth input parameter in `topo_parameters.dat` is 0 or 1. According to the definitions of chapter 5, in the first case the Polyakov loop in the z -direction is chosen as observable, while in the second case the observable is the loop with the insertion of the clover leaf operator. In both cases there is no need to specify the content of `wilson_path.dat`. The latter is produced by the aforementioned function.

Let us suppose that the program user has chosen his Wilson line, and coherently specified the input parameters in the three files, which have just been described. For the computation he can consider the rest of the program as a black box; he is only asked to start Matlab and then from the command shell write:

```
>wline_automatic
```

The user will not interact with the program anymore, no further specifications are needed. The computation of all 1-loop diagrams, including the tadpoles, the tree-level and the $O(a)$ -improvement are then automatically executed, and the final result for the 1-loop expression, normalized by the tree-level, is printed out. The tree-level value is finally accessible by typing

```
>tree_level
```

As anticipated at the beginning of the chapter, the expectation value of each diagram is accessible:

```
>W2a
```

```
>W2b
```

```
>Tad_gauge
```

```
>Tad_quark
```

```
>impr
```

By referring to Sect. 5.5 for the notation, the commands `W2a` and `W2b` produce as output

$$\langle \text{tr} \{ W_{\ell}^{(2a)} \} \rangle_0 \quad \text{and} \quad \langle \text{tr} \{ W_{\ell}^{(2b)} \} \rangle_0$$

respectively, `Tad_gauge` the sum of the tadpole contributions

$$\langle \text{tr} \{ W_{\ell}^{(1)} S_{\text{tot}}^{(1)} \} \rangle_{0,g}$$

restricted to the ghost and gluon cases, `Tad_quark` the quark tadpole contribution

$$\langle \text{tr} \{ W_{\ell}^{(1)} S_{\text{tot}}^{(1)} \} \rangle_{0,q},$$

and `impr` the sum of the $O(a)$ -improvement counterterms

$$\langle \text{tr} \{ W_{\ell}^{(1)} \delta S_{\text{tot,b}}^{(1)} \} \rangle_0.$$

Lower level parts of the computation, e.g. the propagators, can be accessed by following the instructions of the next sections.

The file `check_path.m` contains a function which performs some checks at the very beginning of the computation. In particular, it checks whether the Wilson line is really a closed path, and whether the starting point and the topological parameters have been completely and consistently specified.

6.2 The propagators

6.2.1 The ghost propagator

Definition

Given the expansion of the ghost action

$$S_{\text{gh}} = \sum_{n=0}^{\infty} \frac{1}{n!} g_0^n S_{\text{gh}}^{(n)}, \quad (6.1)$$

we consider the $n = 0$ term, which is quadratic in the ghost fields, and reads

$$S_{\text{gh}}^{(0)} = \frac{1}{L^3} \sum_{\mathbf{p}} \sum_{t,t'} \bar{c}^{\bar{a}}(-\mathbf{p}, t) F^a(\mathbf{p}; t, t') c^a(\mathbf{p}, t'). \quad (6.2)$$

Since in our computations the ghost propagator is present only in connection with the gluon-ghost-ghost vertex, and the latter is non-vanishing only if it involves a neutral gluon and the propagator for charged ghost fields, we need F^a only for a different from 3 and 8, that means

$$F^a(\mathbf{p}; t, t') = \delta_{t,t'} [2 + \mathbf{s}^a(\mathbf{p}, t)^2] - \delta_{t+1,t'} - \delta_{t-1,t'}. \quad (6.3)$$

The free ghost propagator is given by

$$\langle c^a(\mathbf{p}, t) \bar{c}^b(\mathbf{p}', t') \rangle_0 = \delta_{b,\bar{a}} L^3 \delta_{\mathbf{p}+\mathbf{p}', \mathbf{0}} D^a(\mathbf{p}; t, t'), \quad (6.4)$$

where D^a is the inverse of F^a . However, the computation of the propagator through the inversion of the matrix F^a is computationally not very efficient. A better way, which exploits recursive relations, is explained in the following.

We fix the color index a and the momentum \mathbf{p} , and write down the propagator equation in momentum space with a simplified notation as

$$-D(t+1, t') + B(t)D(t, t') - D(t-1, t') = \delta_{t,t'}, \quad (6.5)$$

where

$$D(0, t') = D(T, t') = 0, \quad 1 \leq t' \leq T-1. \quad (6.6)$$

We introduce the forward solution ψ^f , satisfying

$$\psi^f(0) = 0, \quad \psi^f(1) = 1, \quad (6.7)$$

$$\psi^f(t+1) = B(t)\psi^f(t) - \psi^f(t-1), \quad 1 \leq t \leq T-1, \quad (6.8)$$

and the backward solution ψ^b , for which

$$\psi^b(T) = 0, \quad \psi^b(T-1) = 1, \quad (6.9)$$

$$\psi^b(t-1) = B(t)\psi^b(t) - \psi^b(t+1), \quad 1 \leq t \leq T-1. \quad (6.10)$$

Both solutions can be recursively computed and stored. The forward solution allows to compute $W = \psi^f(T)$, which is finally used to compute the solution of eq. (6.5), with boundary conditions given by eqs. (6.6), as

$$D(t, t') = \begin{cases} \frac{1}{W} \psi^f(t) \psi^b(t'), & \text{for } t \leq t', \\ \frac{1}{W} \psi^f(t') \psi^b(t), & \text{for } t \geq t'. \end{cases} \quad (6.11)$$

Implementation

The implementation of the recursive method for the computation of the ghost propagator can be found in the program `WLINE`

as a function in

```
TADPOLES_GAUGE/ghost_p.m
```

Once one is in the directory TADPOLES_GAUGE, it is necessary to load part of the global variables contained in file `topo_parameters.dat`,

```
load_topo_parameters_gtadpole
```

and initialize the remaining global variables through the command

```
initialization
```

The function computing the ghost propagator is

```
function [res] = ghost_p(a_su3,p)
```

The input variable `a_su3` is an integer specifying the color index, while `p` is a 3-dimensional vector specifying the spatial momenta (p_1, p_2, p_3) with $p_k = 2\pi n_k/L$ and $\{n_k \in \mathbb{N}, n_k = 0, 1, \dots, L-1\}$. The result is the ghost propagator (6.11) written in the form of a square matrix with $T+1$ rows.

Proof of the recursive method

First of all we define the function

$$W(t) = \psi^f(t+1)\psi^b(t) - \psi^b(t+1)\psi^f(t), \quad 0 \leq t \leq T-1, \quad (6.12)$$

which we now show to be time-independent. We multiply from the left both sides of eq. (6.8) by $\psi^b(t)$ and both sides of eq. (6.10) by $\psi^f(t)$, and we subtract them

$$\begin{aligned} & \psi^b(t)\psi^f(t+1) - \psi^f(t)\psi^b(t-1) = -\psi^b(t)\psi^f(t-1) + \psi^f(t)\psi^b(t+1) \\ \Rightarrow & \psi^f(t+1)\psi^b(t) - \psi^b(t+1)\psi^f(t) = \psi^f(t)\psi^b(t-1) - \psi^b(t)\psi^f(t-1) \\ \Rightarrow & W(t) = W(t-1), \quad 0 \leq t \leq T-1. \end{aligned} \quad (6.13)$$

It is convenient to compute $W(t)$ at $t=0$ or $t=T$, where it assumes the simple form $W(t) = \psi^b(0) = \psi^f(T) = W$. The correctness of the solution (6.11) can now be checked with a little algebra by verifying that

$$(6.7), (6.9) \Rightarrow (6.6)$$

$$(6.8) \Rightarrow (6.5) \quad \text{for } t < t'$$

$$(6.10) \Rightarrow (6.5) \quad \text{for } t > t'$$

For $t = t'$ we have

$$-D(t+1, t) + B(t)D(t, t) - D(t-1, t) = 1, \quad (6.14)$$

which turns out to be

$$\begin{aligned} & -\frac{1}{W}\psi^f(t)\psi^b(t+1) + \frac{1}{W}B(t)\psi^f(t)\psi^b(t) - \frac{1}{W}\psi^f(t-1)\psi^b(t) = 1 \\ \Rightarrow & -\frac{1}{W}\psi^f(t)\psi^b(t+1) + \frac{1}{W}\psi^b(t)[B(t)\psi^f(t) - \psi^f(t-1)] = 1 \\ \stackrel{(6.8)}{\Rightarrow} & -\frac{1}{W}\psi^f(t)\psi^b(t+1) + \frac{1}{W}\psi^b(t)\psi^f(t+1) = 1 \end{aligned} \quad (6.15)$$

and the last equation can be recognized as an identity through the explicit expression of W given in eq. (6.12).

6.2.2 The gluon propagator

Definition

The quadratic part of the pure gluonic action takes the form

$$S_G^{(0)} = \frac{1}{2L^3} \sum_{\mathbf{p}} \sum_{t, t'=0}^{T-1} \sum_a q_{\mu}^{\bar{a}}(-\mathbf{p}, t) K_{\mu\nu}^a(\mathbf{p}; t, t') q_{\nu}^a(\mathbf{p}, t') \quad (6.16)$$

with

$$\begin{aligned} K_{kl}^a(\mathbf{p}; t, t') &= \delta_{t, t'} [\delta_{kl} s^a(\mathbf{p}, t)^2 - s_k^a(\mathbf{p}, t) s_l^a(\mathbf{p}, t) (1 - \lambda_0)] \\ &\quad + \delta_{kl} [2C_a \delta_{t, t'} - R_a (\delta_{t+1, t'} + \delta_{t-1, t'})], \end{aligned} \quad (6.17)$$

$$\begin{aligned} K_{k0}^a(\mathbf{p}; t, t') &= iR_a [\delta_{t, t'} s_k^a(\mathbf{p}, t+1) - \delta_{t-1, t'} s_k^a(\mathbf{p}, t')] \\ &\quad - i\lambda_0 s_k^a(\mathbf{p}, t) [\delta_{t, t'} - \delta_{t-1, t'}], \end{aligned} \quad (6.18)$$

$$K_{0k}^a(\mathbf{p}; t, t') = -K_{k0}^a(\mathbf{p}; t', t), \quad (6.19)$$

$$\begin{aligned} K_{00}^a(\mathbf{p}; t, t') &= R_a \delta_{t, t'} \mathbf{s}^a(\mathbf{p}, t) \cdot \mathbf{s}^a(\mathbf{p}, t+1) \\ &\quad + \lambda_0 [2\delta_{t, t'} - \delta_{t+1, t'} - \delta_{t-1, t'}] \\ &\quad - \lambda_0 \delta_{t, t'} [\delta_{t, 0} (1 - \chi_a \delta_{\mathbf{p}, \mathbf{0}}) + \delta_{t, T-1}], \end{aligned} \quad (6.20)$$

where $\chi_a = 1$ for $a = 3, 8$ and $\chi_a = 0$ otherwise, and the property

$$K_{\mu\nu}^{\bar{a}}(\mathbf{p}; t, t') = K_{\nu\mu}^a(-\mathbf{p}; t', t) \quad (6.21)$$

holds. The free gluon propagator is given by

$$\langle q_\mu^a(\mathbf{p}, t) q_\nu^b(\mathbf{p}', t') \rangle_0 = \delta_{a,\bar{b}} L^3 \delta_{\mathbf{p}+\mathbf{p}', \mathbf{0}} D_{\mu\nu}^a(\mathbf{p}; t, t'), \quad (6.22)$$

where D^a is the inverse of K^a . A brute force inversion of K^a is not a very efficient way of computing the propagator. A recursive technique can be employed. First of all we write down the difference equation that we want to solve

$$\sum_{t''} \sum_{\mathbf{v}} K_{\mu\nu}^a(\mathbf{p}; t, t'') D_{\nu\sigma}^a(\mathbf{p}; t'', t') = \delta_{t,t'} \delta_{\mu,\sigma}. \quad (6.23)$$

The case $a = 3, 8$ and $\mathbf{p} = \mathbf{0}$ is particularly simple, and the solution is explicitly known

$$D_{\mu\nu}^a(\mathbf{0}; t, t') = \begin{cases} \frac{1}{\lambda_0} (1 + \min(t, t')) & \text{if } \mu = \nu = 0, \\ \frac{1}{R^a} (\min(t, t') - \frac{tt'}{T}) & \text{if } \mu = \nu = k, \\ 0 & \text{if } \mu \neq \nu. \end{cases} \quad (6.24)$$

in all other cases, eq. (6.23) must be numerically solved. We fix the index a and the momentum \mathbf{p} , and decompose the operator K according to

$$K_{\mu\nu}(t, t') = A_{\mu\nu}(t) \delta_{t+1, t'} + B_{\mu\nu}(t) \delta_{t, t'} + A_{\nu\mu}(t-1) \delta_{t-1, t'}. \quad (6.25)$$

With this expression, eq. (6.23) becomes

$$A_{\mu\lambda}(t) D_{\lambda\nu}(t+1, t') + B_{\mu\lambda}(t) D_{\lambda\nu}(t, t') + A_{\mu\lambda}^\dagger(t-1) D_{\lambda\nu}(t-1, t') = \delta_{\mu\nu} \delta_{t, t'},$$

with $0 \leq t \leq T-1$, (6.26)

and A , B and D are, at fixed time, 4×4 matrices. The boundary conditions of the propagator are simply given by

$$\partial_t^* D_{0\nu}(t, t') = D_{k\nu}(t, t') = 0, \quad \text{at } t = 0 \text{ and } t = T. \quad (6.27)$$

We construct two solutions $\psi^f(t)$ and $\psi^b(t)$ of the homogeneous version of eq. (6.26) by a two-step recursion forward and backward in time. The forward solution $\psi^f(t)$ starts from

$$\left. \begin{aligned} \psi_{0\nu}^f(-1) &= \psi_{0\nu}^f(0) = \delta_{0\nu} \\ \psi_{k\nu}^f(0) &= 0 \\ \psi_{k\nu}^f(1) &= \delta_{k\nu} \end{aligned} \right\}, \quad (6.28)$$

while the backward solution $\psi^b(t)$ starts from

$$\left. \begin{aligned} \psi_{0\nu}^b(T) &= \psi_{0\nu}^b(T-1) = \delta_{0\nu} \\ \psi_{k\nu}^b(T) &= 0 \\ \psi_{k\nu}^b(T-1) &= \delta_{k\nu} \end{aligned} \right\}, \quad (6.29)$$

where both ψ^f and ψ^b are, at fixed time, 4×4 matrices. Once one has computed and stored them, the propagator can be expressed in the compact form

$$D_{\mu\nu}(t, t') = \begin{cases} \psi_{\mu\sigma}^f(t) W_{\lambda\sigma}^{-1} \psi_{\mu\lambda}^b(t') & \text{for } t \leq t', \\ \psi_{\mu\sigma}^b(t) W_{\sigma\lambda}^{-1} \psi_{\mu\lambda}^f(t') & \text{for } t \geq t'. \end{cases} \quad (6.30)$$

The Wronskian W is a 4×4 matrix, and can be computed, after that the recursion for ψ^b has been completed, through

$$W_{0\nu} = A_{0\sigma}(0) \psi_{\sigma\nu}^b(1) + (B_{00}(0) + A_{00}^\dagger(-1)) \psi_{0\nu}^b(0), \quad (6.31)$$

$$W_{k\nu} = -A_{jk} \psi_{j\nu}^b(0). \quad (6.32)$$

For the case of vanishing background field with boundary values $C = C' = 0$ the gluon propagator assumes a simple form if the Feynman gauge, i.e. $\lambda_0 = 1$, is chosen [99]. For any momentum \mathbf{p} we define the ‘‘energy’’ ε through

$$\cosh(\varepsilon) = 1 + \frac{1}{2} \hat{\mathbf{p}}^2, \quad \hat{p}_k = 2 \sin(p_k/2). \quad (6.33)$$

For non-zero momenta \mathbf{p} the propagator of the spatial components of the gluon field reads

$$D_{kj}(\mathbf{p}; t, t') = \delta_{kj} \frac{1}{\sinh(\varepsilon) \sinh(\varepsilon T)} \times \begin{cases} \sinh[\varepsilon(T-t)] \sinh(\varepsilon t'), & \text{if } t \geq t', \\ \sinh(\varepsilon t) \sinh[\varepsilon(T-t')], & \text{if } t \leq t', \end{cases} \quad (6.34)$$

while for the time component we have

$$D_{00}(\mathbf{p}; t, t') = \frac{1}{\sinh(\varepsilon) \sinh(\varepsilon T)} \times \begin{cases} \cosh[\varepsilon(T-t) - \frac{1}{2}\varepsilon] \cosh(\varepsilon t' + \frac{1}{2}\varepsilon), & \text{if } t \geq t', \\ \cosh(\varepsilon t + \frac{1}{2}\varepsilon) \cosh[\varepsilon(T-t') - \frac{1}{2}\varepsilon], & \text{if } t \leq t'. \end{cases} \quad (6.35)$$

For $\mathbf{p} = \mathbf{0}$ the propagator coincides with the one given in eq. (6.24) for the non-vanishing background field case; one just has to set $\lambda_0 = 1$ and $R_a = 1$. The mixed components D_{k0} and D_{0k} vanish for all time coordinates and for all momenta \mathbf{p} .

Implementation

The implementation of the recursive method for the computation of the gluon propagator in momentum space can be found in the program **WLINE** as a function in

```
WLINE_SIMPLE/gluon_p.m
```

Once one is in the directory **WLINE_SIMPLE**, it is necessary to load part of the global variables contained in file `topo_parameters.dat`,

```
load_topo_parameters_wsimple
```

and initialize the remaining variables through the command

```
initialization
```

The function computing the gluon propagator is

```
function [res] = gluon_p(a_su3,p,lambda_0)
```

The input variable `a_su3` is an integer specifying the color index, while `p` is a 3-dimensional vector specifying the spatial momenta (p_1, p_2, p_3) with $p_k = 2\pi n_k/L$ and $\{n_k \in \mathbb{N}, n_k = 0, 1, \dots, L-1\}$. The remaining input variable `lambda_0` corresponds to the gauge fixing parameter λ_0 appearing in eq. (5.55). For the non-vanishing background field case, the result is the gluon propagator defined in eq. (6.23), and it is written in the form of an array of dimension $(4, 4, T+1, T+1)$. Through the first two indices one can access the spin structure of the propagator, while the last two indices specify the temporal coordinates. Notice that, due to the way Matlab uses to indicate the elements of an array as well as for convenience of programming, the diagonal component D_{00} corresponds to `res[4, 4, :, :]` in the program. The same holds for the mixed components $D_{0k} \Leftrightarrow \text{res}[4, k, :, :]$, with $k = 1, 2, 3$.

If the background field is deactivated, the gluon propagator is computed only for the boundary values $C = C' = 0$ and in Feynman gauge using a specific function. The latter is internally called by `gluon_p` if it is the case.

The gluon propagator in coordinate space, according to the definition given in eq. (5.90), is computed through the function

```
function [res] = gluon_x(a_su3,i_matrixx,lambda_0)
```

located in the file `WLINE_SIMPLE/gluon_x.m`. The input variables `a_su3` and `lambda_0` have the same meaning as for the propagator in momentum space. The variable `i_matrixx` is a matrix with 7 columns, and a number of rows limited in

principle only by the amount of memory which can be allocated for the propagator and the available computer time. In order to get a deeper insight on it, let us consider the propagator $\Delta_{\mu\nu}^a(\mathbf{x};x_0,y_0)$ in eq. (5.90). After having initialized the necessary global variables as in the case of `gluon_p`, let us suppose that we want to compute $\Delta_{33}^5((0,0,0);2,2)$ in Feynman gauge. This is achieved through the call

```
res = gluon_x(5, [3 3 0 0 0 2 2], 1.0)
```

where `i_matrixx` has only one row. In turn, the function `gluon_x` internally calls `gluon_p` and performs the required Fourier transform.

If we now want to compute $\Delta_{32}^5((0,0,1);2,2)$, inspection of eq. (5.90) reveals that it is not needed to call `gluon_p` again. One could use the results of the previous computation. This suggests to call `gluon_x` at the very beginning in this way

```
res = gluon_x(5, [3 3 0 0 0 2 2; 3 2 0 0 1 2 2], 1.0)
```

It is now straightforward to extend this feature to a path as in Sect. 5.5. The input matrix `i_matrixx` then contains, for fixed color index a , as many rows as the number of coordinate space propagators one wants to compute. It is important to remark that, in compliance with the notation of Sect. 5.5, the temporal direction is denoted by $|\mu| = 4$. The output is given in the form a vector, with as many elements as the rows of `i_matrixx` and the same coordinate ordering. Since the computation of the gluon propagators in momentum space is very expensive, it is clear that this feature allows to save a large amount of computing time in comparison to a naïve implementation.

There is another feature which is worth to mention. The authors of [90] noticed that, since none of the three space directions is distinguished, there is symmetry under permuting them, which corresponds to certain discrete rotations and reflections in spin space. Hence one gains a factor of 6 (asymptotically on large lattices) by computing the gluon propagator in momentum space only for the reduced set of momenta $\mathbf{p}_1 \leq \mathbf{p}_2 \leq \mathbf{p}_3$. Actually, a short computation shows that the number of needed momenta amounts to

$$\frac{L(L+1)(L+2)}{6},$$

to be compared to L^3 of a naïve Fourier transform. The time needed to perform the Fourier transforms is, for the observables in chapter 5, negligible in comparison to the computation of the gluon propagators in momentum space, even for the reduced set of momenta. Hence we found no need of employing a FFT. The function `gluon_x` internally calls another function, called `ppermute` and located in the same directory in the file `ppermute.m`, which calls `gluon_p` only for the reduced set of momenta, and,

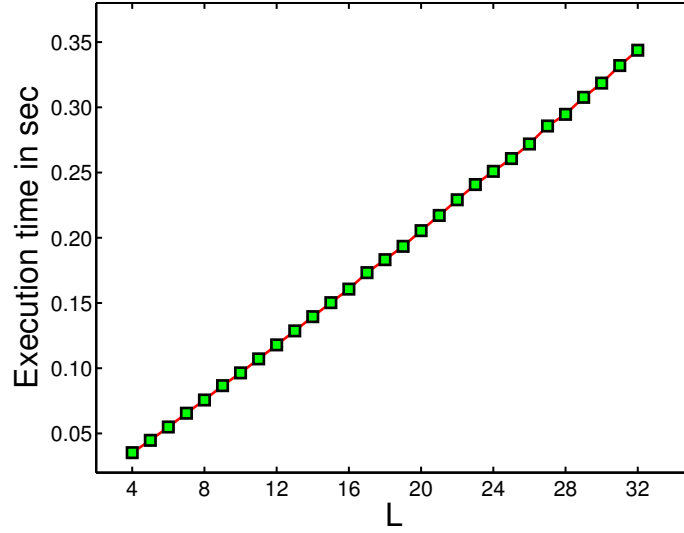


Figure 6.1: Computational cost for the gluon propagator for a fixed momentum. Test performed on a PC with a processor Intel Pentium 4 with 2.6 GHz.

through matrix manipulations optimized for Matlab and of negligible computational cost, produces as output the gluon propagator for all momenta.

Finally, we show in Fig. 6.1 the cost for the computation of the gluon propagator for a fixed momentum and non-trivial color, i.e. $a \neq 3, 8$, in the range $4 \leq L \leq 32$ and for $T = L$. The expected linear scaling is evident. On a computer with processor Intel Pentium 4 with 2.6 GHz, we found

$$\text{cost in seconds} = k_1 + k_2 L, \quad (6.36)$$

with $k_2 \simeq 0.011$.

Proof of the recursive method

So far we listed the basic properties of the recursive method and gave the necessary tools to implement it on a computer. However, we did not demonstrate that (6.30) is the correct and unique solution eq. (6.23). This is the subject of the rest of this subsection.

We start from the forward solution ψ^f and observe that

$$A_{0\lambda} \psi_{\lambda\nu}^f(1) + [B_{00}(0) + A_{00}^\dagger(-1)] \psi_{0\nu}^f(0) = 0, \quad (6.37)$$

which will be our starting point in the implementation of the recursive method. In fact,

together with eqs. (6.28), we notice that

$$v = 0, \quad \psi_{00}^f(1) = -A_{00}^{-1}(0)[B_{00}(0) + A_{00}^\dagger(-1)], \quad (6.38)$$

$$v = j, \quad \psi_{0j}^f(1) = -A_{00}^{-1}(0)A_{0j}(0), \quad (6.39)$$

and we have defined all components of ψ^f for $t = 0, 1$. The matrix A has been checked to be invertible for all times by inspecting its explicit expression. The invertibility holds as long as the gauge fixing parameter $\lambda_0 > 0$ and the constant electric background field does not vanish. Further, we use the following equation

$$A(t)\psi^f(t+1) + B(t)\psi^f(t) + A^\dagger(t-1)\psi^f(t-1) = 0, \quad (6.40)$$

written in a looser notation, to recursively compute $\psi^f(t)$ in the interval $2 \leq t \leq T$. Analogously, we let the backward solution ψ^b satisfy eqs. (6.29) and

$$A(t)\psi^b(t+1) + B(t)\psi^b(t) + A^\dagger(t-1)\psi^b(t-1) = 0. \quad (6.41)$$

The latter is used to compute $\psi^b(t)$ for $0 \leq t \leq T-2a$. We look for a solution of eq. (6.23) having the form

$$D_{\mu\nu}(t, t') = \begin{cases} \psi^f(t)U(t') & \text{for } t \leq t', \\ \psi^b(t)V(t') & \text{for } t \geq t', \end{cases} \quad (6.42)$$

which is compatible with the boundary conditions in eqs. (6.27) and satisfies eq. (6.23) for $t \neq t'$ from the very construction. At $t = t'$ we first require the consistency of the solution (6.42), i.e.

$$\psi^f(t)U(t) = \psi^b(t)V(t), \quad (6.43)$$

and then require to satisfy eq. (6.23); this can be rewritten as

$$A(t)\psi^b(t+1)V(t) + B(t)\psi^f(t)U(t) + A^\dagger(t-1)\psi^f(t)U(t) = 1, \quad (6.44)$$

where we insert eq. (6.40) to be able to get

$$A(t)\psi^b(t+1)V(t) - A(t)\psi^f(t+1)U(t) = 1. \quad (6.45)$$

The latter equation is used together with eq. (6.43) to solve for U and V :

$$(6.43) \Rightarrow V(t) = [\psi^b(t)]^{-1}\psi^f(t)U(t) \quad (6.46)$$

$$(6.45), (6.46) \Rightarrow A(t)\{\psi^b(t+1)[\psi^b(t)]^{-1}\psi^f(t) - \psi^f(t+1)\}U(t) = 1$$

$$\Rightarrow A(t)\{\psi^b(t+1)[\psi^b(t)]^{-1} - \psi^f(t+1)[\psi^f(t)]^{-1}\}\psi^f(t)U(t) = 1$$

and get

$$[U(t)]^{-1} = A(t)\{\psi^b(t+1)[\psi^b(t)]^{-1} - \psi^f(t+1)[\psi^f(t)]^{-1}\}\psi^f(t), \quad (6.47)$$

\Downarrow (6.46)

$$[V(t)]^{-1} = A(t)\{\psi^b(t+1)[\psi^b(t)]^{-1} - \psi^f(t+1)[\psi^f(t)]^{-1}\}\psi^b(t). \quad (6.48)$$

With these two expressions we have determined the solution in the interval $1 \leq t' \leq T-1$. For $t' = 0$ we proceed as follows. With

$$D(t, 0) = \psi^b(t)V(0), \quad 0 \leq t \leq T, \quad (6.49)$$

and the boundary condition $D_{kv}(0, 0) = 0$ we get

$$\psi_{kv}^b(0)V_{\lambda v}(0) = 0, \quad (6.50)$$

and consider eq. (6.26) for $t = 0$, which is for $\mu = 0$

$$A_{0\lambda}(0)\psi_{\lambda\sigma}^b(1)V_{\sigma v}(0) + [B_{00}(0) + A_{00}^\dagger(-1)]\psi_{0\sigma}^b(0)V_{\sigma v}(0) = \delta_{0v}. \quad (6.51)$$

Finally we can gather eq. (6.50) and eq. (6.51) onto a the compact

$$NV = R, \quad R_{kv} = 0, \quad R_{0v} = \delta_{0v}. \quad (6.52)$$

$$N_{kv} = \psi_{kv}^b(0), \quad N_{0v} = A_{0\lambda}(0)\psi_{\lambda v}^b(1) + [B_{00}(0) + A_{00}^\dagger(-1)]\psi_{0v}^b(0). \quad (6.53)$$

The final step is the construction of the Wronskian matrix. We multiply eq. (6.40) by $[\psi^b(t)]^\dagger$ from the left, and the hermitian conjugate of both sides of eq. (6.41) by $\psi^f(t)$ from the right. The subtraction of the l.h.s. of the two resulting equations gives

$$\begin{aligned} & [\psi^b(t)]^\dagger A(t)\psi^f(t+1) - [\psi^b(t+1)]^\dagger A^\dagger(t)\psi^f(t) \\ &= [\psi^b(t-1)]^\dagger A(t-1)\psi^f(t) - [\psi^b(t)]^\dagger A^\dagger(t-1)\psi^f(t-1), \end{aligned} \quad (6.54)$$

valid in the interval $1 \leq t \leq T-1$. We define the 4×4 matrix

$$W_{21}(t) = -[\psi^b(t)]^\dagger A(t)\psi^f(t+1) + [\psi^b(t+1)]^\dagger A^\dagger(t)\psi^f(t), \quad (6.55)$$

in the interval $0 \leq t \leq T-1$, and observe that, thanks to eq. (6.54), W_{21} is time-independent

$$W_{21}(t) = W_{21}(t-1), \quad 1 \leq t \leq T-1. \quad (6.56)$$

We repeat the procedure and multiply both sides of eq. (6.40) by $[\psi^f(t)]^\dagger$ and then subtract their hermitian conjugates. The result

$$\begin{aligned} & [\psi^f(t)]^\dagger A(t) \psi^f(t+1) - [\psi^f(t+1)]^\dagger A^\dagger(t) \psi^f(t) \\ &= [\psi^f(t-1)]^\dagger A(t-1) \psi^f(t) - [\psi^f(t)]^\dagger A^\dagger(t-1) \psi^f(t-1), \end{aligned} \quad (6.57)$$

valid in the interval $1 \leq t \leq T-1$, implies that the 4×4 matrix

$$W_{11}(t) = [\psi^f(t)]^\dagger A(t) \psi^f(t+1) - [\psi^f(t+1)]^\dagger A^\dagger(t) \psi^f(t), \quad (6.58)$$

is time-independent. The same procedure but by starting with eq. (6.41) instead of eq. (6.40) let us conclude that the matrix

$$W_{22}(t) = [\psi^b(t)]^\dagger A(t) \psi^b(t+1) - [\psi^b(t+1)]^\dagger A^\dagger(t) \psi^b(t), \quad (6.59)$$

is time independent too. The matrix W_{ij} , with $W_{12} = W_{21}^\dagger$, is the Wronskian matrix and it is time-independent. Inspection of the explicit expression of W_{11} at $t=0$ and of W_{22} at $t=T-1$ reveals that

$$W_{11} = W_{22} = 0. \quad (6.60)$$

To evaluate W_{21} we can set $t=0$ in eq. (6.55) and get

$$W_{21} = -[\psi^b(0)]^\dagger A(0) \psi^f(1) + [\psi^b(1)]^\dagger A^\dagger(0) \psi^f(0). \quad (6.61)$$

Now we go back to eq. (6.47)

$$\begin{aligned} & [\psi^b(t)]^\dagger [U(t)]^{-1} = [\psi^b(t)]^\dagger A(t) \psi^b(t+1) [\psi^b(t)]^{-1} \psi^f(t) - [\psi^b(t)]^\dagger A(t) \psi^f(t+1) \\ & \stackrel{(6.59), (6.60)}{=} [\psi^b(t+1)]^\dagger A^\dagger(t) \psi^f(t) - [\psi^b(t)]^\dagger A(t) \psi^f(t+1) \\ & \stackrel{(6.55)}{=} W_{21} \end{aligned} \quad (6.62)$$

We consider now eq. (6.48), and proceed in the same way

$$\begin{aligned} & [\psi^f(t)]^\dagger [V(t)]^{-1} = [\psi^f(t)]^\dagger A(t) \psi^b(t+1) \\ & \quad - [\psi^f(t)]^\dagger A(t) \psi^f(t+1) [\psi^f(t)]^{-1} \psi^b(t) \\ & \stackrel{(6.58), (6.60)}{=} [\psi^f(t)]^\dagger A(t) \psi^b(t+1) - [\psi^f(t+1)]^\dagger A^\dagger(t) \psi^b(t) \\ & \stackrel{(6.55)}{=} W_{21}^\dagger = W_{12} \end{aligned} \quad (6.63)$$

This allows us to write the solution (6.42) as

$$D_{\mu\nu}(t, t') = \begin{cases} \psi^f(t) W_{21}^{-1} [\psi^b(t')]^\dagger & \text{for } t \leq t', \\ \psi^b(t) [W_{21}^\dagger]^{-1} [\psi^f(t')]^\dagger & \text{for } t \geq t', \end{cases} \quad (6.64)$$

holding for $t = t'$ too. Now we work out W_{12} in detail

$$W_{12} = [\psi^f(0)]^\dagger A(0) \psi^b(1) - [\psi^f(1)]^\dagger A^\dagger(0) \psi^b(0), \quad (6.65)$$

and have a look at

$$[W_{12}]_{0\nu} = \psi_{\sigma 0}^f(0) A_{\sigma\lambda}(0) \psi_{\lambda\nu}^b(1) - \psi_{\sigma 0}^f(1) A_{\lambda\sigma}(0) \psi_{\lambda\nu}^b(0) \quad (6.66)$$

$$\stackrel{(6.28)}{=} A_{0\lambda}(0) \psi_{\lambda\nu}^b(1) - \psi_{00}^f(1) A_{\lambda 0}(0) \psi_{\lambda\nu}^b(0). \quad (6.67)$$

From eq. (6.37) we have that

$$A_{00}(0) \psi_{00}^f(1) + A_{0k}(0) \psi_{k0}^f(1) + [B_{00}(0) + A_{00}^\dagger(-1)] \psi_{00}^f(0) = 0, \quad (6.68)$$

$$(6.28) \Rightarrow A_{00}(0) \psi_{00}^f(1) = -[B_{00}(0) + A_{00}^\dagger(-1)], \quad (6.69)$$

and consequently

$$[W_{12}]_{0\nu} = A_{0\lambda}(0) \psi_{\lambda\nu}^b(1) + \frac{B_{00}(0) + A_{00}^\dagger(-1)}{A_{00}(0)} A_{\lambda 0}(0) \psi_{\lambda\nu}^b(0). \quad (6.70)$$

Since $A_{k0}(0) = 0$ we have

$$[W_{12}]_{0\nu} = A_{0\lambda}(0) \psi_{\lambda\nu}^b(1) + [B_{00}(0) + A_{00}^\dagger(-1)] \psi_{0\nu}^b(0). \quad (6.71)$$

The last step consists in considering

$$[W_{12}]_{k\nu} = \psi_{\sigma k}^f(0) A_{\sigma\lambda}(0) \psi_{\lambda\nu}^b(1) - \psi_{\sigma k}^f(1) A_{\lambda\sigma}(0) \psi_{\lambda\nu}^b(0). \quad (6.72)$$

The boundary conditions on ψ^f let us write that

$$\psi_{\sigma k}^f(1) A_{\lambda\sigma}(0) \psi_{\lambda\nu}^b(0) = A_{\lambda k}(0) \psi_{\lambda\nu}^b(0) + \psi_{0k}^f(1) A_{\lambda 0}(0) \psi_{\lambda\nu}^b(0), \quad (6.73)$$

and from eq. (6.37) we have that

$$A_{00}(0) \psi_{0k}^f(1) + A_{0j}(0) \psi_{jk}(a) + [B_{00}(0) + A_{00}^\dagger(-1)] \psi_{0k}^f(0) = 0, \quad (6.74)$$

which can be simplified by using again the boundary conditions on ψ^f :

$$A_{00}(0)\psi_{0k}^f(1) + A_{0k}(0) = 0 \Rightarrow \psi_{0k}^f(1) = -\frac{A_{0k}(0)}{A_{00}(0)}. \quad (6.75)$$

This lets us write

$$[W_{12}]_{k\nu} = -A_{\lambda k}(0)\psi_{\lambda\nu}^b(0) + \frac{A_{0k}(0)}{A_{00}(0)}A_{\lambda 0}(0)\psi_{\lambda\nu}^b(0) \\ \stackrel{A_{k0}(0)=0}{=} -A_{\lambda k}(0)\psi_{\lambda\nu}^b(0) + A_{0k}(0)\psi_{0\nu}^b(0) \quad (6.76)$$

$$= -A_{jk}(0)\psi_{j\nu}^b(0). \quad (6.77)$$

If we now rename the matrix W_{12} simply W , we demonstrated that (6.30) is solution of eq. (6.23).

6.2.3 The quark propagator

Definition

We introduce the Fourier transformed quark fields according to

$$\bar{\psi}(\mathbf{x}, t) = \frac{1}{L^3} \sum_{\mathbf{p}} e^{i\mathbf{p}\mathbf{x}} \bar{\psi}(\mathbf{p}, t), \quad (6.78)$$

$$\psi(\mathbf{x}, t) = \frac{1}{L^3} \sum_{\mathbf{p}} e^{i\mathbf{p}\mathbf{x}} \psi(\mathbf{p}, t), \quad (6.79)$$

whose representation in momentum space is used to express the free part of the quark action as

$$S_F^{(0)} = \frac{1}{L^3} \sum_{\mathbf{p}} \sum_{t, t'} \bar{\psi}(-\mathbf{p}, t) \tilde{D}(\mathbf{p}; t, t') \psi(\mathbf{p}, t'), \quad (6.80)$$

where \tilde{D} is the improved Dirac-Wilson operator, including the mass term, at lowest order in g_0 . It is diagonal in momentum and color space for the background field under consideration. It can be written as

$$\tilde{D}(\mathbf{p}; t, t') = -P_- \delta_{t+1, t'} + B(\mathbf{p}^+, t) \delta_{t, t'} - P_+ \delta_{t-1, t'}, \quad (6.81)$$

where the matrices P_{\pm} are defined in App. A, $p_k^+ = p_k + \theta/L$, and the matrix B reads

$$B(\mathbf{p}, t) = 4 + m_0 - \sum_k \left[\frac{1}{2} (1 + \gamma_k) e^{-ip_k V^\dagger(t)} + \frac{1}{2} (1 - \gamma_k) e^{ip_k V(t)} \right] + iH\gamma_0 \sum_k \gamma_k. \quad (6.82)$$

The matrix H is proportional to the tree-level value of c_{sw} , and is diagonal in color space with the elements

$$H_{\alpha\alpha} = -\frac{1}{2} c_{sw}^{(0)} \sin \mathcal{E}_\alpha. \quad (6.83)$$

The propagator S is the inverse of the Dirac-Wilson operator,

$$\sum_{t''} \tilde{D}(\mathbf{p}; t, t'') S(\mathbf{p}; t'', t') = \delta_{t, t'}, \quad 0 < t, t' < T, \quad (6.84)$$

and is pseudo-hermitian,

$$\gamma_5 S(\mathbf{p}; t, t') \gamma_5 = S(\mathbf{p}; t', t)^\dagger, \quad (6.85)$$

as well as the operator \tilde{D} . The boundary conditions are given by

$$P_+ S(\mathbf{p}; t, t')|_{t=0} = P_- S(\mathbf{p}; t, t')|_{t=T} = 0, \quad (6.86)$$

$$S(\mathbf{p}; t, t') P_-|_{t'=0} = S(\mathbf{p}; t, t') P_+|_{t'=T} = 0. \quad (6.87)$$

The computation of S by a brute force inversion of \tilde{D} can become computationally very expensive for fine lattices. We prefer to proceed in analogy to the ghost and gluon cases, by fixing the momentum \mathbf{p} , and by constructing the solutions of the homogeneous equation by forward and backward recursion. We call these solutions ψ^f and ψ^b respectively; they are 4×2 matrices, and satisfy

$$\sum_{t'} \tilde{D}(t, t') \psi^f(t') = 0, \quad P_+ \psi^f(0) = \psi_+^f(0) = 0, \quad (6.88)$$

$$\sum_{t'} \tilde{D}(t, t') \psi^b(t') = 0, \quad P_- \psi^b(T) = \psi_-^b(T) = 0. \quad (6.89)$$

The recursion is simpler than in the gluon case, because here one has to solve a first order difference equation. To see this, we define

$$F^{f/b}(t) = P_- \psi^{f/b}(t) + P_+ \psi^{f/b}(t-1), \quad (6.90)$$

which enables us to write the homogeneous equation as

$$[B(t)P_+ - P_-]F^{f/b}(t+1) + [B(t)P_- - P_+]F^{f/b}(t) = 0. \quad (6.91)$$

Once the forward and backward solutions have been computed, the quark propagator can be constructed through

$$S(t, t') = \begin{cases} \psi^f(t) \mathcal{V} [\psi^b(t')]^\dagger \gamma_5 & \text{for } t < t', \\ \psi^b(t) \mathcal{V}^\dagger [\psi^f(t')]^\dagger \gamma_5 & \text{for } t > t', \\ \psi_-^f(t) \mathcal{V} [\psi^b(t)]^\dagger \gamma_5 \\ + \psi_+^b(t) \mathcal{V}^\dagger [\psi^f(t)]^\dagger \gamma_5 & \text{for } t = t'. \end{cases} \quad (6.92)$$

The 2×2 matrix \mathcal{V} can be computed from

$$[\mathcal{V}^\dagger]^{-1} = [\psi_-^f(1)]^\dagger \gamma_5 \psi_+^b(0). \quad (6.93)$$

Implementation

The implementation of the recursive method for the computation of the quark propagator can be found in the program `WLINE` as a function in

`TADPOLE_QUARK/quark_p.m`

Once one is in the directory `TADPOLES_GAUGE`, it is necessary to load part of the global variables contained in file `topo_parameters.dat`,

```
load_topo_parameters_qtadpole
```

and initialize the remaining global variables through the command

```
initialization
```

The function computing the quark propagator is

```
function [res] = quark_p(p, theta_angle, csw_0, mass_0)
```

The variable `p` is a 3-dimensional vector specifying the spatial momenta (p_1, p_2, p_3) with $p_k = 2\pi n_k/L$ and $\{n_k \in \mathbb{N}, n_k = 0, 1, \dots, L-1\}$, `theta_angle` specifies the phase appearing in eqs. (3.20), `csw_0` is the tree-level value of c_{sw} entering in the improvement counterterm to the fermion action defined in eq. (3.91), and `mass_0` is the quark mass according to eq. (6.82). The output is the propagator (6.92) in the form of an array of dimension $(3, T+1, T+1, 4, 4)$. Through the first index one accesses the color structure. The propagator is diagonal in color space, and that index selects the diagonal elements. The second and third indices refer to the temporal coordinates t and t' , while the last two indices specify the Dirac structure.

Proof of the recursive method

We now show that (6.92) is the solution of the difference equation (6.84). We proceed in analogy to the gluon case, and, first of all, look for a solution of the form

$$S(t, t') = \begin{cases} \psi^f(t) N^f(t') \gamma_5 & \text{for } t < t', \\ \psi^b(t) N^b(t') \gamma_5 & \text{for } t > t', \end{cases} \quad (6.94)$$

To determine N^f and N^b we exploit the pseudo-hermicity of the propagator given in eq. (6.85), to get

$$N^f(t') = \mathcal{V}[\psi^b(t')]^\dagger, \quad N^b(t') = \mathcal{V}^\dagger[\psi^f(t')]^\dagger. \quad (6.95)$$

We now inspect eq. (6.84) for $t' = t + 1$,

$$P_- S(t + 1, t + 1) = -P_+ S(t - 1, t + 1) + B(t) S(t, t + 1). \quad (6.96)$$

The identity

$$B(t) S(t, t + 1) = B(t) (P_+ + P_-) \psi^f(t) \mathcal{V}[\psi^b(t + 1)]^\dagger \gamma_5, \quad (6.97)$$

together with the forward version of eq. (6.91) in the form

$$B(t) (P_+ + P_-) \psi^f(t) = P_- \psi^f(t + 1) + P_+ \psi^f(t - 1), \quad (6.98)$$

let us rewrite eq. (6.96) as

$$P_- S(t + 1, t + 1) = P_- \psi^f(t + 1) \mathcal{V}[\psi^b(t + 1)]^\dagger \gamma_5, \quad (6.99)$$

Analogously, we inspect eq. (6.84) for $t' = t - 1$,

$$P_+ S(t - 1, t - 1) = -P_- S(t + 1, t - 1) + B(t) S(t, t - 1). \quad (6.100)$$

The identity

$$B(t) S(t, t - 1) = B(t) (P_+ + P_-) \psi^b(t) \mathcal{V}^\dagger[\psi^f(t - 1)]^\dagger \gamma_5, \quad (6.101)$$

and the backward version of eq. (6.91) in the form

$$B(t) (P_+ - P_-) \psi^b(t) = P_- \psi^b(t + 1) + P_+ \psi^b(t - 1), \quad (6.102)$$

let us rewrite eq. (6.100) as

$$P_+ S(t-1, t-1) = P_+ \psi^b(t-1) \mathcal{V}^\dagger [\psi^f(t-1)]^\dagger \gamma_5. \quad (6.103)$$

It is now clear that eqs. (6.99, 6.103) prove the correctness of the solution (6.92) for $t = t'$. It remains now to determine the explicit expression of \mathcal{V} . First of all we notice that the pseudo-hermicity of the propagator implies the following useful relations

$$\psi_-^f(t) \mathcal{V} [\psi_-^b(t)]^\dagger \gamma_5 = \psi_-^b(t) \mathcal{V}^\dagger [\psi_-^f(t)]^\dagger \gamma_5, \quad (6.104)$$

$$\psi_+^f(t) \mathcal{V} [\psi_+^b(t)]^\dagger \gamma_5 = \psi_+^b(t) \mathcal{V}^\dagger [\psi_+^f(t)]^\dagger \gamma_5, \quad (6.105)$$

and we then proceed by checking that the equation

$$\begin{aligned} 1 = & -\psi_+^f(t-1) \mathcal{V} [\psi_-^b(t)]^\dagger \gamma_5 + \psi_+^b(t-1) \mathcal{V}^\dagger [\psi_-^f(t)]^\dagger \gamma_5 \\ & + \psi_-^f(t+1) \mathcal{V} [\psi_+^b(t)]^\dagger \gamma_5 - \psi_-^b(t+1) \mathcal{V}^\dagger [\psi_+^f(t)]^\dagger \gamma_5 \end{aligned} \quad (6.106)$$

holds for $a \leq t < T$. We write down eq. (6.84) for $t = t'$,

$$\begin{aligned} 1 = & -\psi_-^b(t+1) \mathcal{V}^\dagger [\psi^f(t)]^\dagger \gamma_5 - \psi_+^f(t-1) \mathcal{V} [\psi^b(t)]^\dagger \gamma_5 \\ & + B(t) \left\{ \psi_-^f(t) \mathcal{V} [\psi^b(t)]^\dagger \gamma_5 + \psi_+^b(t) \mathcal{V}^\dagger [\psi^f(t)]^\dagger \gamma_5 \right\}, \end{aligned} \quad (6.107)$$

and multiply it by P_- from the right

$$\begin{aligned} P_- = & -\psi_-^b(t+1) \mathcal{V}^\dagger [\psi^f(t)_+]^\dagger \gamma_5 - \psi_+^f(t-1) \mathcal{V} [\psi^b(t)_+]^\dagger \gamma_5 \\ & + B(t) \left\{ \psi_-^f(t) \mathcal{V} [\psi^b(t)_+]^\dagger \gamma_5 + \psi_+^b(t) \mathcal{V}^\dagger [\psi^f(t)_+]^\dagger \gamma_5 \right\}. \end{aligned}$$

Then we observe that

$$\begin{aligned} & B(t) \left\{ \psi_-^f(t) \mathcal{V} [\psi_+^b(t)]^\dagger \gamma_5 + \psi_+^b(t) \mathcal{V}^\dagger [\psi_+^f(t)]^\dagger \gamma_5 \right\} \\ & \stackrel{(6.105)}{=} B(t) \left\{ \psi_-^f(t) \mathcal{V} [\psi_+^b(t)]^\dagger \gamma_5 + \psi_+^f(t) \mathcal{V} [\psi_+^b(t)]^\dagger \gamma_5 \right\} \\ & = B(t) (P_- + P_+) \psi^f(t) \mathcal{V} [\psi_+^b(t)]^\dagger \gamma_5 \\ & \stackrel{(6.98)}{=} \left\{ \psi_-^f(t+1) + \psi_+^f(t-1) \right\} \mathcal{V} [\psi_+^b(t)]^\dagger \gamma_5, \end{aligned}$$

which yields

$$P_- = -\psi_-^b(t+1)\mathcal{V}^\dagger[\psi_+^f(t)]^\dagger\gamma_5 + \psi_-^f(t+1)\mathcal{V}[\psi_+^b(t)]^\dagger\gamma_5. \quad (6.108)$$

By multiplying eq. (6.107) by P_+ from the right and proceeding analogously, we get

$$P_+ = -\psi_+^f(t-1)\mathcal{V}[\psi_-^b(t)]^\dagger\gamma_5 + \psi_+^b(t-1)\mathcal{V}^\dagger[\psi_-^f(t)]^\dagger\gamma_5. \quad (6.109)$$

It is now very easy to see that eqs. (6.108, 6.109) imply eq. (6.107). The next step consists in showing that

$$[\psi^f(t-1)]^\dagger\gamma_5\psi_-^f(t) - [\psi^f(t)]^\dagger\gamma_5\psi_+^f(t-1) = 0, \quad (6.110)$$

holds for $1 \leq t \leq T$. First of all, we demonstrate that the l.h.s. is time-independent. We notice that

$$B(t) = \gamma_5[B(t)]^\dagger\gamma_5, \quad (6.111)$$

and write the forward homogeneous equation in two equivalent forms

$$B(t)\psi^f(t) = \psi_-^f(t+1) + \psi_+^f(t-1), \quad (6.112)$$

$$[\psi^f(t)]^\dagger[B(t)]^\dagger = [\psi_-^f(t+1)]^\dagger + [\psi_+^f(t-1)]^\dagger. \quad (6.113)$$

We multiply the first equation by $[\psi^f(t)]^\dagger\gamma_5$ from the right

$$\begin{aligned} [\psi^f(t)]^\dagger\gamma_5 B(t)\psi^f(t) &= \underbrace{[\psi^f(t)]^\dagger\gamma_5\psi_-^f(t+1)}_{\oplus} + \underbrace{[\psi^f(t)]^\dagger\gamma_5\psi_+^f(t-1)}_{\ominus} \\ &\stackrel{(6.111)}{=} [\psi^f(t)]^\dagger[B(t)]^\dagger\gamma_5\psi^f(t) \\ &\stackrel{(6.113)}{=} \underbrace{[\psi_-^f(t+1)]^\dagger\gamma_5\psi^f(t)}_{\odot} + \underbrace{[\psi_+^f(t-1)]^\dagger\gamma_5\psi^f(t)}_{\otimes}, \end{aligned}$$

and by noticing that $[\psi_\pm^f]^\dagger\gamma_5\psi^f = [\psi^f]^\dagger\gamma_5\psi_\mp^f$, we have that the equation $\otimes - \ominus = \oplus - \odot$ reads

$$\begin{aligned} [\psi^f(t-1)]^\dagger\gamma_5\psi_-^f(t) - [\psi^f(t)]^\dagger\gamma_5\psi_+^f(t-1) \\ = [\psi^f(t)]^\dagger\gamma_5\psi_-^f(t+1) - [\psi^f(t+1)]^\dagger\gamma_5\psi_+^f(t), \end{aligned} \quad (6.114)$$

which proves that the l.h.s. of eq. (6.110) is time-independent. Furthermore we observe that, due to the boundary condition $\psi_+^f(0) = 0$, it vanishes at $t = 1$. The time-independence implies that eq. (6.110) is valid in the whole interval $1 \leq t \leq T$.

We multiply eq. (6.106) by P_+ from the left and by $\psi^f(t-1)$ from the right

$$\begin{aligned}
P_+ \psi^f(t-1) &= -\psi_+^f(t-1) \mathcal{V} [\psi_-^b(t)]^\dagger \gamma_5 \psi^f(t-1) \\
&\quad + \psi_+^b(t-1) \mathcal{V}^\dagger [\psi_-^f(t)]^\dagger \gamma_5 \psi^f(t-1) \\
&\stackrel{(6.110)}{=} -\psi_+^f(t-1) \mathcal{V} [\psi_-^b(t)]^\dagger \gamma_5 \psi^f(t-1) \\
&\quad + \psi_+^b(t-1) \mathcal{V}^\dagger [\psi_+^f(t-1)]^\dagger \gamma_5 \psi^f(t) \\
&\stackrel{(6.105)}{=} -\psi_+^f(t-1) \mathcal{V} [\psi_-^b(t)]^\dagger \gamma_5 \psi^f(t-1) \\
&\quad + \psi_+^f(t-1) \mathcal{V} [\psi_+^b(t-1)]^\dagger \gamma_5 \psi^f(t) \\
&= \psi_+^f(t-1) \mathcal{V} \left\{ [\psi_+^b(t-1)]^\dagger \gamma_5 \psi^f(t) - [\psi_-^b(t)]^\dagger \gamma_5 \psi^f(t-1) \right\},
\end{aligned}$$

and conclude that

$$\mathcal{V}^{-1} = [\psi_+^b(t-1)]^\dagger \gamma_5 \psi^f(t) - [\psi_-^b(t)]^\dagger \gamma_5 \psi^f(t-1), \quad (6.115)$$

or equivalently

$$[\mathcal{V}^\dagger]^{-1} = [\psi^f(t)]^\dagger \gamma_5 \psi_+^b(t-1) - [\psi^f(t-1)]^\dagger \gamma_5 \psi_-^b(t). \quad (6.116)$$

Finally we show that the r.h.s. of the above equation is time-independent. To achieve that, we multiply eq. (6.102) by $[\psi^f(t)]^\dagger \gamma_5$ from the left

$$[\psi^f(t)]^\dagger \gamma_5 B(t) \psi^b(t) \stackrel{(6.102)}{=} [\psi^f(t)]^\dagger \gamma_5 \psi_-^b(t+1) + [\psi^f(t)]^\dagger \gamma_5 \psi_+^b(t-1), \quad (6.117)$$

and eq. (6.113) by $\gamma_5 \psi^b(t)$ from the right

$$[\psi^f(t)]^\dagger [B(t)]^\dagger \gamma_5 \psi^b(t) = [\psi^f(t)]^\dagger \gamma_5 B(t) \psi^b(t) \quad (6.118)$$

$$\stackrel{(6.98)}{=} [\psi_-^f(t+1)]^\dagger \gamma_5 \psi^b(t) + [\psi_+^f(t-1)]^\dagger \gamma_5 \psi^b(t),$$

and subtract them. It follows that

$$\begin{aligned}
&[\psi^f(t)]^\dagger \gamma_5 \psi_-^b(t+1) + [\psi^f(t)]^\dagger \gamma_5 \psi_+^b(t-1) \\
&= [\psi_-^f(t+1)]^\dagger \gamma_5 \psi^b(t) + [\psi_+^f(t-1)]^\dagger \gamma_5 \psi^b(t) \\
&= [\psi^f(t+1)]^\dagger \gamma_5 \psi_+^b(t) + [\psi^f(t-1)]^\dagger \gamma_5 \psi_-^b(t),
\end{aligned}$$

which can be rewritten as

$$\begin{aligned} & [\psi^f(t)]^\dagger \gamma_5 \psi_+^b(t-1) - [\psi^f(t-1)]^\dagger \gamma_5 \psi_-^b(t) \\ &= [\psi^f(t+1)]^\dagger \gamma_5 \psi_+^b(t) - [\psi^f(t)]^\dagger \gamma_5 \psi_-^b(t+1), \end{aligned} \quad (6.119)$$

and shows the time independence of the r.h.s. of eq. (6.116). The latter, due to the boundary conditions, becomes particularly simple for $t = 1$, that is the expression in eq. (6.93).

6.3 Tadpoles and improvement

In this subsection we provide the definitions relative to the tadpoles as well as their implementation in `WLINE`. It is important to stress that if one wants to compute several observables, it is not necessary to compute the tadpoles for each of them. The tadpole loops $T_{k,\text{ghost}}^a(u_0)$, $T_{k,\text{gluon}}^a(u_0)$ and $T_{k,\text{quark}}^a(u_0)$ do not depend on the observable, but only on the kinematics. They can thus be computed and stored. Then, for each observable, the tadpole contributions can be calculated according to the formulae given in Sect. 5.5.3. This latter computation is much cheaper than the tadpole loops.

The last subsection is devoted to the $O(a)$ -improvement counterterms. Under the point of view of the theory, there is nothing to add to Sect. 5.5.4, and we describe only the Matlab implementation.

6.3.1 Ghost tadpole

Definition

The $O(g_0)$ -term of the perturbative expansion of the ghost action is given by

$$\begin{aligned} S_{\text{gh}}^{(1)} &= \frac{1}{L^6} \sum_{\mathbf{p}, \mathbf{p}', \mathbf{q}} \delta_{\mathbf{p}}(\mathbf{p} + \mathbf{p}' + \mathbf{q}) \sum_{s_0, t_0, u_0} \sum_{\mu} \\ &\sum_{a, b, c} \bar{c}^a(-\mathbf{p}', s_0) F_{\mu}^{abc}(\mathbf{p}', \mathbf{p}, \mathbf{q}; s_0, t_0, u_0) c^b(-\mathbf{p}, t_0) q_{\mu}^c(-\mathbf{q}, u_0). \end{aligned} \quad (6.120)$$

where $\delta_{\mathbf{p}}$ indicates the periodic delta function, i.e. the delta function modulo 2π , and F is the gluon-ghost-ghost vertex, whose explicit expression is readable e.g. in [91]. It enters in the ghost tadpole, formally given by

$$T_{\mu, \text{ghost}}^a(u_0) = \frac{1}{L^3} \sum_{\mathbf{q}} \sum_{s_0, t_0} \sum_c F_{\mu}^{\bar{c}ca}(\mathbf{q}, -\mathbf{q}, \mathbf{0}; s_0, t_0, u_0) D^c(\mathbf{q}; t_0, s_0), \quad (6.121)$$

which is non-vanishing only for $\mu \neq 0$ and $a = 3, 8$. The non-vanishing components can be computed through [97]:

$$T_{k,\text{ghost}}^a(u_0) = \frac{1}{L^3} \sum_{\mathbf{q}} \sum_c c_{\bar{c}ca} \sin[q_k + \phi_c(u_0)] D^c(\mathbf{q}; u_0, u_0). \quad (6.122)$$

Implementation

The implementation of the ghost tadpole according to eq. (6.122) can be found in the program `WLINE` as a function in

```
TADPOLES_GAUGE/ghost_tadpole.m
```

Once one is in the directory `TADPOLES_GAUGE`, it is necessary to load the global variables,

```
T L eta nu
```

contained in file `topo_parameters.dat`, through the command

```
load_topo_parameters_gtadpole
```

and initialize the remaining global variables through

```
initialization
```

The function computing the ghost tadpole is

```
function [res] = ghost_tadpole()
```

The output has dimension

```
size(res) = 2 3 T+1
```

The first index refers to the color; if it is 1, it corresponds to the color $a = 3$, if 2 to $a = 8$. The second index refers to k , and the last one to the temporal coordinate u_0 .

6.3.2 Gluon tadpole

Definition

At order g_0 the gluon action can be expressed in the compact form

$$\begin{aligned}
 S_G^{(1)} &= \frac{1}{6L^6} \sum_{\mathbf{q}_1, \mathbf{q}_2, \mathbf{q}_3} \delta_{\mathbf{P}}(\mathbf{q}_1 + \mathbf{q}_2 + \mathbf{q}_3) \\
 &\times \sum_{\mu_1, \mu_2, \mu_3} \sum_{t_1, t_2, t_3} \sum_{a_1, a_2, a_3} V_{\mu_1 \mu_2 \mu_3}^{a_1 a_2 a_3}(\mathbf{q}_1, \mathbf{q}_2, \mathbf{q}_3; t_1, t_2, t_3) \prod_j q_{\mu_j}^{a_j}(-\mathbf{q}_j, t_j),
 \end{aligned} \tag{6.123}$$

where V is the triple gluon vertex. The latter has a quite involved expression, and is readable e.g. in [91]. It is needed to compute the gluon tadpole, which reads

$$T_{\mu, \text{gluon}}^a(u_0) = -\frac{1}{2L^3} \sum_{\mathbf{q}} \sum_{\nu, \rho} \sum_{s_0, t_0} \sum_c V_{\nu \rho \mu}^{\bar{c} c a}(\mathbf{q}, -\mathbf{q}, \mathbf{0}; s_0, t_0, u_0) D_{\rho \nu}^c(\mathbf{q}; t_0, s_0). \tag{6.124}$$

As mentioned at the beginning of this chapter, the tadpole is non-vanishing only for $\mu \neq 0$ and $a = 3, 8$. It assumes the expression [97]:

$$\begin{aligned}
T_{k,\text{gluon}}^a(u_0) = & -\frac{1}{2L^3} \sum_{\mathbf{q}} \sum_c \left\{ \right. \\
& -c_{ac\bar{c}} c_k^c(\mathbf{q}, u_0) \sum_j \left(D_{jj}^c(\mathbf{q}; u_0, u_0) s_k^c(\mathbf{q}, u_0) - D_{jk}^c(\mathbf{q}; u_0, u_0) s_j^c(\mathbf{q}, u_0) \right) \\
& -\frac{1}{2} f_{ac}^+ \left(D_{kk}^c(\mathbf{q}; u_0 - 1, u_0 - 1) - D_{kk}^c(\mathbf{q}; u_0 + 1, u_0 + 1) \right) \\
& -e_{ac}^+ \left(D_{kk}^c(\mathbf{q}; u_0, u_0 + 1) - D_{kk}^c(\mathbf{q}; u_0, u_0 - 1) \right) \\
& -ie_{ac}^+ \left[-D_{0k}^c(\mathbf{q}; u_0, u_0) s_k^c(\mathbf{q}, u_0 + 1) - D_{0k}^c(\mathbf{q}; u_0 - 1, u_0) s_k^c(\mathbf{q}, u_0 - 1) \right. \\
& \left. + \left(D_{0k}^c(\mathbf{q}; u_0 - 1, u_0 - 1) + D_{0k}^c(\mathbf{q}; u_0, u_0 + 1) \right) s_k^c(\mathbf{q}, u_0) \right] \\
& -ie_{ac}^- \left(D_{0k}^c(\mathbf{q}; u_0 - 1, u_0 - 1) - D_{0k}^c(\mathbf{q}; u_0, u_0 + 1) \right) c_k^c(\mathbf{q}, u_0) \\
& -\frac{1}{2} f_{ac}^+ \left(D_{00}^c(\mathbf{q}; u_0 - 1, u_0 - 1) s_k^c(\mathbf{q}, u_0 - 1) \right)^2 \\
& -D_{00}^c(\mathbf{q}; u_0, u_0) s_k^c(\mathbf{q}, u_0 + 1)^2 \\
& -\frac{1}{2} f_{ac}^- \left(D_{00}^c(\mathbf{q}; u_0 - 1, u_0 - 1) s_k^c(\mathbf{q}, u_0 - 1) c_k^c(\mathbf{q}, u_0 - 1) \right. \\
& \left. + D_{00}^c(u_0, u_0) s_k^c(\mathbf{q}, u_0 + 1) c_k^c(\mathbf{q}, u_0 + 1) \right) \left. \right\}, \tag{6.125}
\end{aligned}$$

where it is understood that at the temporal boundaries

$$D(\mathbf{p}; t_0, v_0) = 0, \quad \text{if } t_0 \text{ or } v_0 = -1, T + 1. \tag{6.126}$$

Implementation

The implementation of the gluon tadpole according to eq. (6.125) can be found in the program `WLINE` as a function in

TADPOLES_GAUGE/gluon_tadpole.m

Once one is in the directory TADPOLES_GAUGE, it is necessary to load the global variables,

```
T L eta nu lambda_0
```

contained in file topo_parameters.dat, through the command

```
load_topo_parameters_gtadpole
```

and initialize the remaining global variables through

```
initialization
```

The function computing the ghost tadpole is

```
function [res] = gluon_tadpole()
```

The output has dimension

```
size(res) = 2 3 T+1
```

The first index refers to the color; if it is 1, it corresponds to the color $a = 3$, if 2 to $a = 8$. The second index refers to k , and the last one to the temporal coordinate u_0 .

6.3.3 Quark tadpole

Definition

We proceed in analogy with the ghost and gluon cases, and study the term of the perturbative expansion of the quark action appearing at order g_0 . The Wilson part takes the form

$$S_{F,Wilson}^{(1)} = \frac{1}{L^6} \sum_{\mathbf{p}, \mathbf{p}', \mathbf{q}} \delta_{\mathbf{p}(\mathbf{p} + \mathbf{p}' + \mathbf{q})} \sum_{\mu} \sum_{x_0, y_0, z_0} \bar{\Psi}(-\mathbf{p}', x_0) V_{\mu}^a(\mathbf{s}; x_0, y_0, z_0) \Psi(-\mathbf{p}, y_0) q_{\mu}^a(-\mathbf{q}, z_0), \quad (6.127)$$

with $\mathbf{s} = (\mathbf{p}' - \mathbf{p})/2$. It comes together with the Sheikholeslami-Wohlert part

$$\delta S_V^{(n)} = \frac{c_{sw}^{(0)}}{L^6} \sum_{\mathbf{p}, \mathbf{p}', \mathbf{q}} \delta_{\mathbf{p}(\mathbf{p} + \mathbf{p}' + \mathbf{q})} \sum_{x_0, z_0} \sum_{\mu} \sum_a \bar{\Psi}(-\mathbf{p}', x_0) S_{\mu}^a(\mathbf{q}; x_0, z_0) \Psi(-\mathbf{p}, x_0) q_{\mu}^a(-\mathbf{q}, z_0). \quad (6.128)$$

It follows that the complete gluon-quark-quark vertex is given by

$$V_\mu^a(\mathbf{p}', \mathbf{p}, \mathbf{q}; s_0, t_0, u_0) = V_\mu^a(\mathbf{s}; s_0, t_0, u_0) + c_{\text{sw}}^{(0)} S_\mu^a(\mathbf{q}; s_0, u_0) \delta_{s_0, t_0}, \quad (6.129)$$

entering in the quark tadpole as

$$T_{\mu, \text{quark}}^a(u_0) = \frac{1}{L^3} \sum_{\mathbf{q}} \sum_{s_0, t_0} \text{Tr} \left\{ V_\mu^a(\mathbf{q}, -\mathbf{q}, \mathbf{0}; s_0, t_0, u_0) S(\mathbf{q}; t_0, s_0) \right\}. \quad (6.130)$$

The latter is non-vanishing only for $\mu \neq 0$ and $a = 3, 8$; the explicit expression reads

$$\begin{aligned} T_{k, \text{quark}}^a(u_0) = & \quad (6.131) \\ & - \frac{1}{L^3} \sum_{\mathbf{q}} \text{Tr} I^a \left\{ \left(i \sin[\alpha_k(\mathbf{q}, u_0)] - \gamma_k \cos[\alpha_k(\mathbf{q}, u_0)] \right) S(\mathbf{q}; u_0, u_0) \right. \\ & \left. + \frac{i}{4} c_{\text{sw}}^{(0)} \cos(\mathcal{E}) \sigma_{0k} \left(S(\mathbf{q}; u_0 + 1, u_0 + 1) - S(\mathbf{q}; u_0 - 1, u_0 - 1) \right) \right\}. \end{aligned}$$

Implementation

The implementation of the quark tadpole according to eq. (6.131) can be found in the program `WLINE` as a function in

`TADPOLE_QUARK/quark_tadpole.m`

Once one is in the directory `TADPOLE_QUARK`, it is necessary to load the global variables,

```
T L eta nu theta_angle csw_0 mass_0
```

contained in file `topo_parameters.dat`, through the command

```
load_topo_parameters_qtadpole
```

and initialize the remaining global variables through

```
initialization
```

The function computing the quark tadpole is

```
function [res] = quark_tadpole()
```

The output has dimension

```
size(res) = 2 3 T+1
```

The first index refers to the color; if it is 1, it corresponds to the color $a = 3$, if 2 to $a = 8$. The second index refers to k , and the last one to the temporal coordinate u_0 .

6.3.4 Improvement

Implementation

The implementation of the $O(a)$ -improvement counterterms according to eq. (5.101) can be found in the program `WLINE` as a function in

```
IMPROVEMENT/wline_impr.m
```

Once one is in the directory `IMPROVEMENT`, it is necessary to load the global variables,

```
T L eta nu back_switch lambda_0 Nf
```

contained in file `topo_parameters.dat`, through the command

```
load_topo_parameters_impr
```

and initialize the remaining global variables through

```
initialization
```

The function computing the improvement counterterm is

```
function [res] = wline_impr(starting_point,wilson_path)
```

which needs the starting point and the path describing the Wilson loop as is explained in Sect. 6.1. The output is a complex number, and precisely the expectation value in eq. (5.101).

6.4 Tests of the code

6.4.1 The average plaquette

We consider the unimproved gauge action

$$S_G[U] = \frac{\beta}{3} \sum_p \text{Re tr} \{1 - U(p)\}, \quad (6.132)$$

where the sum is over all unoriented plaquettes, and rewrite the parametrization (5.46) of the gauge links in the form

$$U_\mu(x) = \{1 + \sigma_\mu(x) + O(\sigma^2)\} V_\mu(x), \quad \sigma = O(\beta^{-1/2}), \quad (6.133)$$

where the fields σ_μ are nothing but a rescaling of the gluon fields q_μ . In the following we assume that the gauge has been fixed. Although the details of the gauge fixing are not relevant for the present discussion, one may assume that we have followed the procedure described in Sect. 5.4.1. In the weak coupling regime we expand the action in powers of $1/\beta$, and write the partition function in the simplified form

$$\mathcal{Z} = K \int \mathbf{D}[\sigma] \exp \left\{ -\frac{1}{2} \beta \sigma D^{-1} \sigma + \text{higher orders} \right\}. \quad (6.134)$$

Here K is an overall constant factor and D is the gluon propagator defined in eq. (6.23). Since the integral in eq. (6.134) is Gaussian, its value is a determinant

$$\mathcal{Z} = K' |D/\beta|^{1/2} (1 + \mathcal{O}(\beta^{-1})). \quad (6.135)$$

The matrix D has the dimensionality of the parameter space after gauge fixing. In other words, it is a square matrix with N_g rows, where N_g is the number of physical gluonic degrees of freedom. Removing a factor of β from each row of the matrix, we find

$$\mathcal{Z} = K' |D|^{1/2} \beta^{-N_g/2} (1 + \mathcal{O}(\beta^{-1})). \quad (6.136)$$

We now exploit this result to obtain the following 1-loop prediction for the average plaquette

$$\begin{aligned} \frac{1}{3N_p} \left\langle \sum_p \text{Re tr} \{1 - U(p)\} \right\rangle &= -\frac{1}{N_p} \frac{\partial}{\partial \beta} \ln \mathcal{Z} \\ &= -\frac{1}{N_p} \frac{-\frac{N_g}{2} \beta^{-1} (1 + \mathcal{O}(\beta^{-1})) + \mathcal{O}(\beta^{-2})}{1 + \mathcal{O}(\beta^{-1})} \\ &= \frac{N_g}{2N_p \beta} + \mathcal{O}(\beta^{-2}), \end{aligned} \quad (6.137)$$

where we have summed only over the $N_p = 3L^3(2T - 1)$ dynamical plaquettes, and we have kept the factor $1/3$ in order to normalize the trace of the unity matrix. The number of degrees of freedom is given by

$$N_g = 8[L^3(4T - 3) - L^3(T - 1)] - \nu. \quad (6.138)$$

The factor 8 in front stems from the fact that the Lie algebra $su(3)$ of $SU(3)$ is a real vector space of dimension 8. The first factor in square brackets counts the lattice variables $q_\mu(x)$, and the second factor subtracts the gauge fixed ones. The volume term ν is given by

$$\nu = \begin{cases} 8, & \text{for irreducible background field,} \\ 2, & \text{for non-vanishing Abelian background field.} \end{cases} \quad (6.139)$$

For irreducible background field we intend e.g. a setup as in chapter 4, with boundary values $C = C' = 0$. The value $\nu = 8$ stems from the zero momentum q_0 gluons at the temporal boundary $x_0 = 0$. We have eight of them, because $\dim(\mathfrak{su}(3)) = 8$. They obey Dirichlet boundary conditions, and are associated with spatially constant diagonal modes. The latter are not fixed by the gauge fixing procedure, as pointed out in Sect. 5.4.1, and do not belong to the degrees of freedom. They just survive as a global symmetry of the theory. For the non-vanishing background field case the situation is analogous, with the only difference that at the lower temporal boundary we have a mixture of Dirichlet and Neumann boundary conditions. Inspection of eqs. (5.59) reveals that only the two gluons obeying Dirichlet boundary conditions are associated with spatially constant diagonal modes; this implies $\nu = 2$.

In order to test the code, we have reproduced, for various choices of L and T up to 32, the result (6.137), for both vanishing and non-vanishing background field, with a numerical precision up to 12 digits.

6.4.2 Comparison with Monte Carlo results

The perturbative results for the plaquette and the Polyakov loops with and without insertion of the electric operator have been checked against the corresponding non-perturbative (quenched) computations. The latter have been performed at small bare couplings, $0.015 \leq g_0^2 \leq 0.06$, setting the improvement coefficient c_t to its tree-level value. In all cases $L = T = 4$. The 1-loop contribution for the observable \mathcal{O} is extracted from the non-perturbative result $\langle \mathcal{O} \rangle$ according to

$$\langle \mathcal{O}^{(1)} \rangle = \lim_{g_0^2 \rightarrow 0} (\langle \mathcal{O}(g_0^2) \rangle - 1) / g_0^2, \quad (6.140)$$

where the observable is normalized by its tree-level value. The plot on the left of Fig. 6.2 shows the case where the observable is the average plaquette. The upper and lower plots on the right show the simple Polyakov loop and the Polyakov loop with insertion of the clover leaf operator respectively. The extrapolation is achieved through a simple linear fit. The agreement is found within the statistical uncertainty.

6.5 Summary

The program `WLINE` has been conceived as a double-purpose project. The first purpose is to provide a program able to compute the expectation value, at one-loop order of perturbation theory, of any QCD Wilson line in the Schrödinger functional scheme with

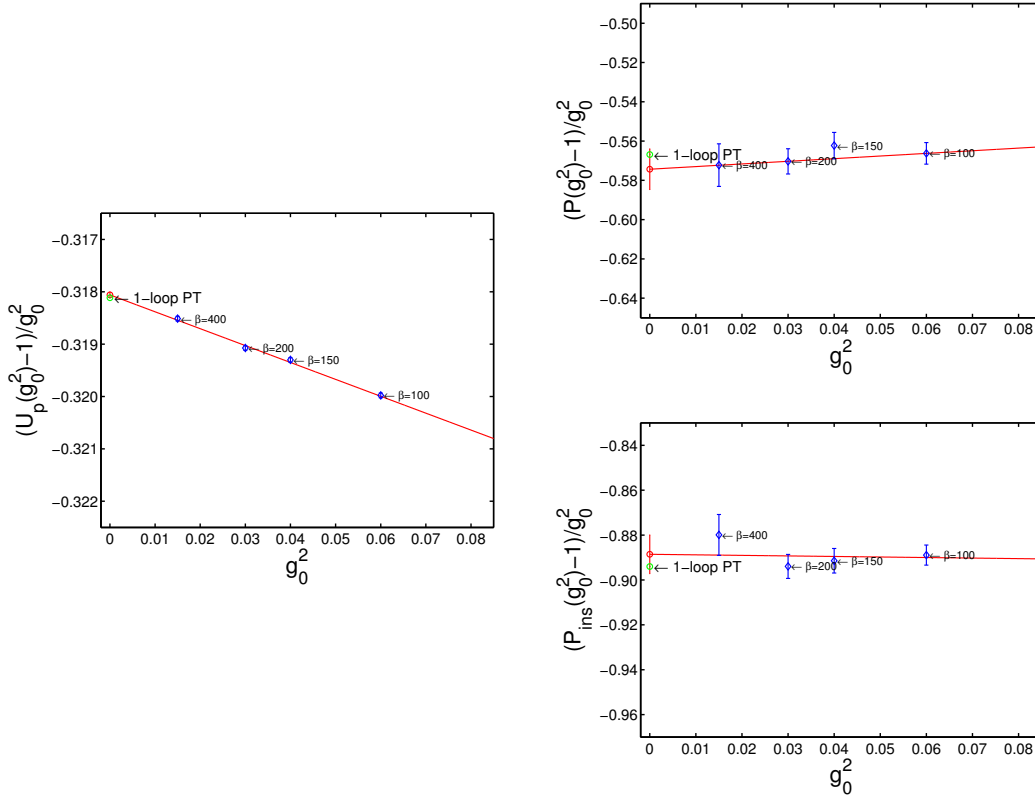


Figure 6.2: Comparison of the perturbative results with the non-perturbative ($N_f = 0$) ones.

vanishing or non-vanishing background field, by generating and computing all needed diagrams and the improvement counterterms. The user is asked to specify only the path describing the Wilson line and a few kinematical parameters. The rest of the program can be seen as a black box, and the execution does not require any further effort from the user's side. The second purpose is to provide a structure with several modules. Each module has its own task, and can easily be accessed and used outside the program. Each function computing the propagators, the tadpoles or the improvement counterterms shares with the rest of program only the necessary kinematical variables.

The presence of a non-vanishing background field precludes from finding a simple analytical expression for the ghost, gluon and quark propagators. By starting from the very definition of the latter, one is found to invert big sparse matrices. As a consequence, the computational cost increases very rapidly with the fineness of the lattice. A much more viable way is provided in Sect. 6.2, where recursive methods are introduced. They allow to considerably reduce the computational cost, which is found to

linearly scale with the lattice extension. For each propagator, a detailed proof of the recursive method is provided.

The non-vanishing background field is also the cause of the presence of the tadpole diagrams. Although they could be computed from the complete expression of the vertices, the formulae provided by Peter Weisz allow to significantly reduce the programming as well as the computational efforts. The tadpole loops are observable independent. They can be separately computed and stored once the kinematics is defined. Of course, their contribution to the one-loop expansion of the desired observable depends on the observable itself, but this last calculation is computationally not very time consuming if the loops are already stored.

The improvement is restricted to the computation of the terms stemming from the one-loop expansion of the boundary counterterms of the gauge action, and in particular to the time-like plaquettes. They owe their existence to the presence of a non-vanishing background field, and are not computationally demanding, even in the $N_f \neq 0$ case.

Among all tests performed to check the correctness of the code, it is worth mentioning the computation of the average plaquette. It is a simple test comparing the result of the program with the predictions of the theory, in which only the counting of the gluonic degrees of freedom enters. This kind of test can be straightforwardly extended to other actions and choices of boundary conditions.

The program `WLINE` is available in its released version 1.0. Plans for a version 1.1 are already established. Apart from a few small improvements, mainly addressed to speed up the computation, the main purpose is to remove the restriction of an observable consisting of a closed loop of gauge links, and admit a more general class of observables, including, among others, two separated Wilson loops. In a next future, a version 2.0, allowing for smeared gauge links, is expected to enhance the support given by perturbation theory to non-perturbative HQET computations.

Chapter 7

Conclusions

The subject of the first part of this work is the combination of the Tor Vergata Step Scaling Method, involving the relativistic QCD Lagrangian, and HQET. The final result is a very precise and controlled lattice determination, in the continuum limit, of the b-quark mass and B_s -meson decay constant. The former is affected by an uncertainty of 1.5%, while the decay constant is extracted with a precision slightly worse than 3%. The meticulous error analysis attending the simulations ensures that these results do not suffer from any systematic errors, apart from the use of the quenched approximation. Neither extrapolations in the heavy quark mass, nor other approximations on the kinematics of the quark-antiquark pair are introduced.

The results of this study are not restricted only to these two numbers. The interplay of relativistic QCD and HQET shows that the static limit alone provides high precision results, which lie very close to the interpolated final numbers, with only one exception. The latter is the decay constant in the small volume, where the finite quark mass corrections amount to roughly 5%. On the other side, the Step Scaling Method is shown to be a successful and powerful tool to investigate two-scale problems. However, without the support of the effective theory the extrapolation to the b-region is difficult to control, especially when the simulated quark masses are much lighter than the extrapolated one.

The second part of this thesis deals with the renormalization of the chromo-magnetic operator, appearing at order $1/m$ in the HQET Lagrangian. It is the leading order operator, in the effective theory, responsible for the spin splitting in heavy-light quark bound states. A precise computation of its renormalization group invariant expression, along the guidelines of the ALPHA collaboration, requires in turn an accurate knowledge of the scale running of the renormalization factor in the Schrödinger functional scheme. The main result for this purpose is the two-loop anomalous dimension

of the operator, as well as a both perturbative and non-perturbative (in the quenched approximation) study of the cutoff effects affecting the renormalization factor and the corresponding step scaling functions. The latter measure the variation which the former undergoes, when the renormalization scale is changed by a factor of two.

The anomalous dimension is computed by starting from the known two-loop expression in the $\overline{\text{MS}}$ scheme as well as the one-loop connection between the latter and an intermediate scheme, the lattice minimal subtraction one. By computing the one-loop connection between the latter and the Schrödinger functional, one ends up with the two-loop SF anomalous dimension.

Perturbation theory, at one-loop order, and the non-perturbative simulations, without sea quarks, agree with the fact that the cutoff effects associated with the step scaling functions are invisible as long as the relative statistical precision is around one percent. In presence of sea quarks, perturbation theory predicts bigger but still moderate deviations from the continuum limit. Unfortunately, a non-perturbative confirmation is still missing.

The perturbative computations in the Schrödinger functional scheme are complicated by the presence of a non-vanishing background field. With respect to the vanishing case, it introduces new diagrams and forbids to have a simple analytical expression for the propagators. Furthermore, it requires the addition of the $O(a)$ -improvement counterterms in order to reach the continuum limit with a rate proportional to $(a/L)^2$. The problem is faced by carrying out the perturbative expansion in position space. This yields a considerable speed-up in comparison with a momentum space computation. This is part of the background of the Matlab code `WLINE`, which joins the requirements of a robust, efficient and reasonably fast program, with a very user-friendly interface.

In an ideal to-do list, we would write the following points:

- *Reduction of the uncertainty associated with the renormalization factor of the quark mass.*
- *Improvement of the precision of the large volume computations both in HQET and in relativistic QCD.*
- *Computation of $Z_{\text{mag}}^{\text{RGI}}$ via matching between HQET and QCD. At first in the quenched approximation.*
- *Dynamical fermions.*
- *Development of the code `WLINE`.*

The first point has roots in the observation that the uncertainty on the final result for the b-quark mass is dominated by the one on the total renormalization factor Z_M of the RGI quark mass.

The second point originates from the importance that large volume computations already in the static approximation have in a precise determination of the bottom-light decay constant. The use of actions with smeared gauge links as well as refined fitting techniques [1] are helpful, but, so far, not sufficient to overcome the problem of the degradation of the signal-to-noise ratio in the heavy-light and heavy-heavy correlators. Especially in view of the inclusion of sea quarks, the most promising way is probably represented by the all-to-all propagators [100].

About the third point it is worth mentioning an alternative approach for the renormalization of the chromo-magnetic operator. It can be achieved by following the procedure [19, 67], consisting in a non-perturbative matching between HQET and QCD, where, unlike in chapter 5, valence light quarks appear.

The fourth point certainly represents the next future. For the combination of HQET and relativistic QCD the challenge is to perform simulations in a large volume ($\gtrsim 1.5$ fm) with a lattice resolution, where quarks like the charm and heavier can be handled with confidence. For the renormalization of the chromo-magnetic operator the two-loop anomalous dimension is now known also for non-vanishing N_f . However, the renormalization procedure depicted in chapter 5 has shown in [94], for $N_f = 0$, to require a large amount of gauge configurations to achieve a good statistical precision. This is of course an unpleasant situation in presence of dynamical fermions, for which the production of statistically uncorrelated gauge samples is computationally very expensive. The method mentioned in the third point may provide a more viable approach.

The code `WLINE` has been successfully applied for the computations reported in chapter 5. Its double-purpose structure will be helpful in the future for testing other perturbative and non-perturbative codes, as well as to perturbatively compute other observables and study their cutoff effects.

Bibliography

- [1] Michele Della Morte et al. Heavy-strange meson decay constants in the continuum limit of quenched QCD. 2007. arXiv:0710.2201 [hep-lat].
- [2] Jochen Heitger, Martin Kurth, and Rainer Sommer. Non-perturbative renormalization of the static axial current in quenched QCD. *Nucl. Phys.*, B669:173–206, 2003.
- [3] H. David Politzer. Reliable perturbative results for strong interactions? *Phys. Rev. Lett.*, 30:1346–1349, 1973.
- [4] D. J. Gross and Frank Wilczek. Ultraviolet behavior of non-abelian gauge theories. *Phys. Rev. Lett.*, 30:1343–1346, 1973.
- [5] Kenneth G. Wilson. Confinement of quarks. *Phys. Rev.*, D10:2445–2459, 1974.
- [6] E. Eichten. Heavy quarks on the lattice. *Nucl. Phys. Proc. Suppl.*, 4:170, 1988.
- [7] Marco Guagnelli, Filippo Palombi, Roberto Petronzio, and Nazario Tantalo. $f(B)$ and two scales problems in lattice QCD. *Phys. Lett.*, B546:237–246, 2002.
- [8] Estia Eichten and Brian Hill. Static effective field theory: $1/m$ corrections. *Phys. Lett.*, B243:427–431, 1990.
- [9] Adam F. Falk, Benjamin Grinstein, and Michael E. Luke. Leading mass corrections to the heavy quark effective theory. *Nucl. Phys.*, B357:185–207, 1991.
- [10] Martin Lüscher, Peter Weisz, and Ulli Wolff. A numerical method to compute the running coupling in asymptotically free theories. *Nucl. Phys.*, B359:221–243, 1991.
- [11] Achim Bode et al. First results on the running coupling in QCD with two massless flavors. *Phys. Lett.*, B515:49–56, 2001.

- [12] Stefano Capitani, Martin Lüscher, Rainer Sommer, and Hartmut Wittig. Non-perturbative quark mass renormalization in quenched lattice QCD. *Nucl. Phys.*, B544:669, 1999.
- [13] Nathan Isgur and Mark B. Wise. Weak decays of heavy mesons in the static quark approximation. *Phys. Lett.*, B232:113, 1989.
- [14] J. G. Korner and George Thompson. The heavy mass limit in field theory and the heavy quark effective theory. *Phys. Lett.*, B264:185–192, 1991.
- [15] Rainer Sommer. Non-perturbative QCD: Renormalization, $O(a)$ -improvement and matching to heavy quark effective theory, 2006. hep-lat/0611020.
- [16] Howard Georgi. An effective field theory for heavy quarks at low-energies. *Phys. Lett.*, B240:447–450, 1990.
- [17] Nathan Isgur and Mark B. Wise. Weak transition form-factors between heavy mesons. *Phys. Lett.*, B237:527, 1990.
- [18] Martin Kurth and Rainer Sommer. Renormalization and $O(a)$ -improvement of the static axial current. *Nucl. Phys.*, B597:488–518, 2001.
- [19] Jochen Heitger and Rainer Sommer. Non-perturbative heavy quark effective theory. *JHEP*, 02:022, 2004.
- [20] John C. Collins. *Renormalization. An introduction to renormalization, the renormalization group, and the operator product expansion.* Cambridge, UK: Univ. Pr., 1984.
- [21] L. Maiani, G. Martinelli, and C. T. Sachrajda. Nonperturbative subtractions in the heavy quark effective field theory. *Nucl. Phys.*, B368:281–292, 1992.
- [22] G. 't Hooft. Dimensional regularization and the renormalization group. *Nucl. Phys.*, B61:455–468, 1973.
- [23] William A. Bardeen, A. J. Buras, D. W. Duke, and T. Muta. Deep inelastic scattering beyond the leading order in asymptotically free gauge theories. *Phys. Rev.*, D18:3998, 1978.
- [24] Martin Lüscher, Rajamani Narayanan, Peter Weisz, and Ulli Wolff. The Schrödinger functional: A renormalizable probe for nonabelian gauge theories. *Nucl. Phys.*, B384:168–228, 1992.

- [25] Stefan Sint. On the Schrödinger functional in QCD. *Nucl. Phys.*, B421:135–158, 1994.
- [26] Estia Eichten and Brian Hill. An effective field theory for the calculation of matrix elements involving heavy quarks. *Phys. Lett.*, B234:511, 1990.
- [27] Estia Eichten and Brian Hill. Renormalization of heavy-light bilinears and $f(B)$ for Wilson fermions. *Phys. Lett.*, B240:193, 1990.
- [28] Michele Della Morte et al. Lattice HQET with exponentially improved statistical precision. *Phys. Lett.*, B581:93–98, 2004.
- [29] Michele Della Morte, Andrea Shindler, and Rainer Sommer. On lattice actions for static quarks. *JHEP*, 08:051, 2005.
- [30] Anna Hasenfratz and Francesco Knechtli. Flavor symmetry and the static potential with hypercubic blocking. *Phys. Rev.*, D64:034504, 2001.
- [31] G. M. de Divitiis, R. Frezzotti, M. Guagnelli, and R. Petronzio. Nonperturbative determination of the running coupling constant in quenched SU(2). *Nucl. Phys.*, B433:390–402, 1995.
- [32] M. Creutz. Monte carlo study of quantized SU(2) gauge theory. *Phys. Rev.*, D21:2308, 1980.
- [33] K. Fabricius and O. Haan. Heat bath method for the twisted Eguchi-Kawai model. *Phys. Lett.*, B143:459, 1984.
- [34] A. D. Kennedy and B. J. Pendleton. Improved heat bath method for Monte Carlo calculations in lattice gauge theories. *Phys. Lett.*, B156:393–399, 1985.
- [35] Michael Creutz. Overrelaxation and Monte Carlo simulation. *Phys. Rev.*, D36:515, 1987.
- [36] N. Cabibbo and E. Marinari. A new method for updating SU(N) matrices in computer simulations of gauge theories. *Phys. Lett.*, B119:387–390, 1982.
- [37] Martin Lüscher, Rainer Sommer, Peter Weisz, and Ulli Wolff. A precise determination of the running coupling in the SU(3) Yang-Mills theory. *Nucl. Phys.*, B413:481–502, 1994.
- [38] A. D. Kennedy. Algorithms for dynamical fermions, 2006. hep-lat/0607038.

- [39] Leonardo Giusti. Light dynamical fermions on the lattice: Toward the chiral regime of QCD. *PoS.*, LAT2006, 2007.
- [40] K. Symanzik, 1982. Some topics in quantum field theory, in Mathematical problems in theoretical physics, eds. R. Schrader et al., Lecture Notes in Physics. Vol. 153 (Springer, New York, 1982).
- [41] K. Symanzik. Continuum limit and improved action in lattice theories. 1. Principles and ϕ^4 theory. *Nucl. Phys.*, B226:187, 1983.
- [42] K. Symanzik. Continuum limit and improved action in lattice theories. 2. $O(N)$ nonlinear sigma model in perturbation theory. *Nucl. Phys.*, B226:205, 1983.
- [43] Martin Lüscher, Stefan Sint, Rainer Sommer, and Peter Weisz. Chiral symmetry and $O(a)$ improvement in lattice QCD. *Nucl. Phys.*, B478:365–400, 1996.
- [44] B. Sheikholeslami and R. Wohlert. Improved continuum limit lattice action for QCD with Wilson fermions. *Nucl. Phys.*, B259:572, 1985.
- [45] Martin Lüscher, Stefan Sint, Rainer Sommer, Peter Weisz, and Ulli Wolff. Non-perturbative $O(a)$ improvement of lattice QCD. *Nucl. Phys.*, B491:323–343, 1997.
- [46] Stefan Sint and Peter Weisz. Further results on $O(a)$ improved lattice QCD to one loop order of perturbation theory. *Nucl. Phys.*, B502:251, 1997.
- [47] Achim Bode, Peter Weisz, and Ulli Wolff. Two loop computation of the Schrödinger functional in lattice QCD. *Nucl. Phys.*, B576:517–539, 2000.
- [48] Martin Kurth and Rainer Sommer. Renormalization and $O(a)$ -improvement of the static axial current. *Nucl. Phys.*, B597:488–518, 2001.
- [49] Marco Guagnelli, Jochen Heitger, Rainer Sommer, and Hartmut Wittig. Hadron masses and matrix elements from the QCD Schrödinger functional. *Nucl. Phys.*, B560:465, 1999.
- [50] Giulia Maria de Divitiis, Marco Guagnelli, Roberto Petronzio, Nazario Tantalo, and Filippo Palombi. Heavy quark masses in the continuum limit of lattice QCD. *Nucl. Phys.*, B675:309–332, 2003.
- [51] G. M. de Divitiis, M. Guagnelli, F. Palombi, R. Petronzio, and N. Tantalo. Heavy-light decay constants in the continuum limit of lattice QCD. *Nucl. Phys.*, B672:372–386, 2003.

- [52] Damiano Guazzini, Rainer Sommer, and Nazario Tantalo. Precision for B-meson matrix elements. 2007. arXiv:0710.2229 [hep-lat].
- [53] R. Sommer. A new way to set the energy scale in lattice gauge theories and its applications to the static force and α_s in SU(2) Yang-Mills theory. *Nucl. Phys.*, B411:839, 1994.
- [54] Marco Guagnelli, Rainer Sommer, and Hartmut Wittig. Precision computation of a low-energy reference scale in quenched lattice QCD. *Nucl. Phys.*, B535:389, 1998.
- [55] Silvia Necco and Rainer Sommer. The $N(f) = 0$ heavy quark potential from short to intermediate distances. *Nucl. Phys.*, B622:328–346, 2002.
- [56] Marco Guagnelli, Roberto Petronzio, and Nazario Tantalo. The lattice scale at large beta in quenched QCD. *Phys. Lett.*, B548:58–62, 2002.
- [57] J. Gasser and H. Leutwyler. Quark masses. *Phys. Rept.*, 87:77–169, 1982.
- [58] J. Gasser and H. Leutwyler. Chiral perturbation theory to one loop. *Ann. Phys.*, 158:142, 1984.
- [59] J. Gasser and H. Leutwyler. Chiral perturbation theory: Expansions in the mass of the strange quark. *Nucl. Phys.*, B250:465, 1985.
- [60] Damiano Guazzini, Rainer Sommer, and Nazario Tantalo. $m(b)$ and $f(B/s)$ from a combination of HQET and QCD. *PoS*, LAT2006:084, 2006.
- [61] Martin Lüscher, Stefan Sint, Rainer Sommer, and Hartmut Wittig. Nonperturbative determination of the axial current normalization constant in $O(a)$ improved lattice QCD. *Nucl. Phys.*, B491:344–364, 1997.
- [62] Marco Guagnelli et al. Non-perturbative results for the coefficients b_m and $b_A - b_P$ in $O(a)$ improved lattice QCD. *Nucl. Phys.*, B595:44–62, 2001.
- [63] Jochen Heitger and Jan Wennekers. Effective heavy-light meson energies in small-volume quenched QCD. *JHEP*, 02:064, 2004.
- [64] Joyce Garden, Jochen Heitger, Rainer Sommer, and Hartmut Wittig. Precision computation of the strange quark’s mass in quenched QCD. *Nucl. Phys.*, B571:237–256, 2000.

- [65] T. van Ritbergen, J. A. M. Vermaseren, and S. A. Larin. The four loop beta function in quantum chromodynamics. *Phys. Lett.*, B400:379–384, 1997.
- [66] J. A. M. Vermaseren, S. A. Larin, and T. van Ritbergen. The four loop quark mass anomalous dimension and the invariant quark mass. *Phys. Lett.*, B405:327–333, 1997.
- [67] Michele Della Morte, Nicolas Garron, Mauro Papinutto, and Rainer Sommer. Heavy quark effective theory computation of the mass of the bottom quark. *JHEP*, 01:007, 2007.
- [68] G. Martinelli and C. T. Sachrajda. Computation of the b-quark mass with perturbative matching at the next-to-next-to-leading order. *Nucl. Phys.*, B559:429, 1999.
- [69] V. Gimenez, L. Giusti, G. Martinelli, and F. Rapuano. NNLO unquenched calculation of the b quark mass. *JHEP*, 03:018, 2000.
- [70] S. Collins. The mass of the b quark from lattice NRQCD. *Wien 2000, Quark confinement and the hadron spectrum*, pages 325–327, 2000. hep-lat/0009040.
- [71] Tetsuya Onogi. Heavy flavor physics from lattice QCD. *PoS*, LAT2006:017, 2006.
- [72] K. G. Chetyrkin and A. G. Grozin. Three-loop anomalous dimension of the heavy-light quark current in HQET. *Nucl. Phys.*, B666:289–302, 2003.
- [73] Jochen Heitger, Andreas Jüttner, Rainer Sommer, and Jan Wennekers. Non-perturbative tests of heavy quark effective theory. *JHEP*, 11:048, 2004.
- [74] J. Rolf et al. Towards a precision computation of $f(B/s)$ in quenched QCD. *Nucl. Phys. Proc. Suppl.*, 129:322–324, 2004.
- [75] A. Ali Khan et al. Decay constants of charm and beauty pseudoscalar heavy-light mesons on fine lattices, 2007. hep-lat/0701015.
- [76] K. C. Bowler et al. Decay constants of B and D mesons from non-perturbatively improved lattice QCD. *Nucl. Phys.*, B619:507–537, 2001.
- [77] A. Ali Khan et al. Decay constants of B and D mesons from improved relativistic lattice QCD with two flavours of sea quarks. *Phys. Rev.*, D64:034505, 2001.

- [78] C. Bernard et al. Lattice calculation of heavy-light decay constants with two flavors of dynamical quarks. *Phys. Rev.*, D66:094501, 2002.
- [79] Matthias Neubert. Heavy quark symmetry. *Phys. Rept.*, 245:259–396, 1994.
- [80] M. Bochicchio, G. Martinelli, C. R. Allton, Christopher T. Sachrajda, and D. B. Carpenter. Heavy quark spectroscopy on the lattice. *Nucl. Phys.*, B372:403–420, 1992.
- [81] V. Gimenez, G. Martinelli, and Christopher T. Sachrajda. A high-statistics lattice calculation of $\lambda(1)$ and $\lambda(2)$ in the B-meson. *Nucl. Phys.*, B486:227–244, 1997.
- [82] S. Aoki et al. Heavy quark expansion parameters from lattice NRQCD. *Phys. Rev.*, D69:094512, 2004.
- [83] G. Amoros, M. Beneke, and M. Neubert. Two-loop anomalous dimension of the chromo-magnetic moment of a heavy quark. *Phys. Lett.*, B401:81–90, 1997.
- [84] A. Czarnecki and A. G. Grozin. HQET chromomagnetic interaction at two loops. *Phys. Lett.*, B405:142–149, 1997.
- [85] Stefan Sint and Peter Weisz. The running quark mass in the SF scheme and its two loop anomalous dimension. *Nucl. Phys.*, B545:529, 1999.
- [86] M. Lüscher and P. Weisz. $O(a)$ improvement of the axial current in lattice QCD to one loop order of perturbation theory. *Nucl. Phys.*, B479:429–260, 1996.
- [87] Stefan Sint and Rainer Sommer. The running coupling from the QCD Schrödinger functional: A one loop analysis. *Nucl. Phys.*, B465:71–98, 1996.
- [88] Jonathan M. Flynn and Brian Russell Hill. B - B* splitting: A test of heavy quark methods. *Phys. Lett.*, B264:173–177, 1991.
- [89] M. Lüscher. Selected topics in lattice field theory, 1988. Lectures given at Summer School 'Fields, Strings and Critical Phenomena', Les Houches, France, Jun 28 - Aug 5, 1988.
- [90] Rajamani Narayanan and Ulli Wolff. Two loop computation of a running coupling in lattice Yang-Mills theory. *Nucl. Phys.*, B444:425–446, 1995.

- [91] Stefan Kurth. *The renormalised quark mass in the Schrödinger functional of lattice QCD: A one-loop calculation with a non-vanishing background field*. PhD thesis, Humboldt U., Berlin, 2002. hep-lat/0211011.
- [92] M. Della Morte, R. Hoffmann, and F. Knechtli. Discrete symmetries of lattice QCD. *Internal notes of the ALPHA collaboration*, 2005.
- [93] G. Parisi, R. Petronzio, and F. Rapuano. A measurement of the string tension near the continuum limit. *Phys. Lett.*, 128B:418, 1983.
- [94] Damiano Guazzini, Harvey B. Meyer, and Rainer Sommer. Non-perturbative renormalization of the chromo-magnetic operator in heavy quark effective theory and the $B^* - B$ mass splitting. *JHEP*, 10:081, 2007.
- [95] A. G. Grozin et al. The B-meson mass splitting from non-perturbative quenched lattice QCD. *PoS, LAT2007:100*, 2007.
- [96] R. Narayanan and U. Wolff, 1992. Unpublished notes.
- [97] Peter Weisz. Computation of the improvement coefficient $c(\text{sw})$ to 1-loop. *Internal notes of the ALPHA collaboration*, 1996.
- [98] M. Creutz. *Quarks, gluons and lattices*. Cambridge, Uk: Univ. Pr. 169 P. (Cambridge Monographs On Mathematical Physics), 1984.
- [99] Martin Lüscher. Improved axial current at one-loop order of perturbation theory. *Internal notes of the ALPHA collaboration*, 1996.
- [100] Justin Foley et al. Practical all-to-all propagators for lattice QCD. *Comput. Phys. Commun.*, 172:145–162, 2005.
- [101] Ulli Wolff. Monte Carlo errors with less errors. *Comput. Phys. Commun.*, 156: 143–153, 2004.
- [102] William H. Press, Brian P. Flannery, Saul A. Teukolsky, and William T. Vetterling. *Numerical Recipes in C : The Art of Scientific Computing*. Cambridge University Press, October 1992. ISBN 0521431085. URL <http://www.amazon.co.uk/exec/obidos/ASIN/0521431085/citeulike-21>.

Appendix A

Notations and conventions

A.1 The Dirac matrices

We employ the hermitian euclidean Dirac matrices γ_μ with

$$\gamma_0 = \begin{pmatrix} 1 & 0 \\ 0 & -1 \end{pmatrix}, \quad \gamma_k = \begin{pmatrix} 0 & -i\sigma_k \\ i\sigma_k & 0 \end{pmatrix}, \quad k = 1, 2, 3, \quad (\text{A.1})$$

where the Pauli matrices

$$\sigma_1 = \begin{pmatrix} 0 & 1 \\ 1 & 0 \end{pmatrix}, \quad \sigma_2 = \begin{pmatrix} 0 & -i \\ i & 0 \end{pmatrix}, \quad \sigma_3 = \begin{pmatrix} 1 & 0 \\ 0 & -1 \end{pmatrix}, \quad (\text{A.2})$$

appear. In this representation $\gamma_5 = \gamma_0\gamma_1\gamma_2\gamma_3$ is not diagonal

$$\gamma_5 = \begin{pmatrix} 0 & -1 \\ -1 & 0 \end{pmatrix}, \quad (\text{A.3})$$

The anticommutation relations are given by

$$\{\gamma_\mu, \gamma_\nu\} = 2\delta_{\mu\nu}, \quad \{\gamma_5, \gamma_\nu\} = 0. \quad (\text{A.4})$$

Finally the projectors

$$P_+ = \frac{1}{2}(1 + \gamma_0) = \begin{pmatrix} 1 & 0 \\ 0 & 0 \end{pmatrix}, \quad P_- = \frac{1}{2}(1 - \gamma_0) = \begin{pmatrix} 0 & 0 \\ 0 & 1 \end{pmatrix}, \quad (\text{A.5})$$

are used.

A.2 The basis of the Lie algebra

The Lie algebra $su(3)$ of $SU(3)$ can be identified with the space of complex 3×3 matrices constructed as in [97] from the modified Gell-Mann matrices

$$\begin{aligned}
 \tilde{\lambda}_1 &= \begin{pmatrix} 0 & 1 & 0 \\ 1 & 0 & 0 \\ 0 & 0 & 0 \end{pmatrix}, & \tilde{\lambda}_2 &= \begin{pmatrix} 0 & -i & 0 \\ i & 0 & 0 \\ 0 & 0 & 0 \end{pmatrix}, \\
 \tilde{\lambda}_4 &= \begin{pmatrix} 0 & 0 & 1 \\ 0 & 0 & 0 \\ 1 & 0 & 0 \end{pmatrix}, & \tilde{\lambda}_5 &= \begin{pmatrix} 0 & 0 & -i \\ 0 & 0 & 0 \\ i & 0 & 0 \end{pmatrix}, \\
 \tilde{\lambda}_6 &= \begin{pmatrix} 0 & 0 & 0 \\ 0 & 0 & 1 \\ 0 & 1 & 0 \end{pmatrix}, & \tilde{\lambda}_7 &= \begin{pmatrix} 0 & 0 & 0 \\ 0 & 0 & -i \\ 0 & i & 0 \end{pmatrix}, \\
 \tilde{\lambda}_3 &= \begin{pmatrix} 0 & 0 & 0 \\ 0 & 1 & 0 \\ 0 & 0 & -1 \end{pmatrix}, & \tilde{\lambda}_8 &= \frac{1}{\sqrt{3}} \begin{pmatrix} 2 & 0 & 0 \\ 0 & -1 & 0 \\ 0 & 0 & -1 \end{pmatrix}.
 \end{aligned} \tag{A.6}$$

For $a = 1, \dots, 8$ we define

$$T_a = \frac{1}{2i} \tilde{\lambda}_a, \tag{A.7}$$

and finally the basis

$$\begin{aligned}
 I^1 &= \frac{1}{\sqrt{2}}(T_1 + iT_2), & I^2 &= \frac{1}{\sqrt{2}}(T_1 - iT_2), \\
 I^4 &= \frac{1}{\sqrt{2}}(T_4 + iT_5), & I^5 &= \frac{1}{\sqrt{2}}(T_4 - iT_5), \\
 I^6 &= \frac{1}{\sqrt{2}}(T_6 + iT_7), & I^7 &= \frac{1}{\sqrt{2}}(T_6 - iT_7), \\
 I^3 &= T_3, & I^8 &= T_8,
 \end{aligned} \tag{A.8}$$

where only the last two matrices are diagonal. With this choice

$$[I^a]^\dagger = I^{\bar{a}}, \quad \text{tr}\{I^a I^b\} = -\frac{1}{2} \delta_{b\bar{a}} \tag{A.9}$$

where

$$\bar{1} = 2, \quad \bar{4} = 5, \quad \bar{6} = 7, \tag{A.10}$$

and vice versa. For the diagonal matrices $\bar{3} = 3$ and $\bar{8} = 8$.

A.3 The non-vanishing background field

We work in units of the lattice spacing and remark that the non-vanishing background field, appearing in chapters 5 and 6, is induced by the spatially constant Abelian boundary fields [24]:

$$C = \frac{i}{L} \text{diag}(\phi_1, \phi_2, \phi_3), \quad C' = \frac{i}{L} \text{diag}(\phi'_1, \phi'_2, \phi'_3), \quad (\text{A.11})$$

where the angles ϕ_m and ϕ'_m are given in terms of the parameters η and ν

$$\begin{aligned} \phi_1 &= \eta - \frac{\pi}{3}, & \phi'_1 &= -\eta - \pi, \\ \phi_2 &= \eta(-\frac{1}{2} + \nu), & \phi'_2 &= \eta(\frac{1}{2} + \nu) + \frac{\pi}{3}, \\ \phi_3 &= -\eta(\frac{1}{2} + \nu) + \frac{\pi}{3} & \phi'_3 &= \eta(\frac{1}{2} - \nu) + \frac{2\pi}{3}. \end{aligned} \quad (\text{A.12})$$

The ‘‘point A’’ is defined as in [37] by the choice $\eta = \nu = 0$. The renormalization condition in eq. (5.26) is given with Dirichlet boundary conditions in time, i.e.

$$U_k(x)|_{x_0=0} = \exp(C), \quad U_k(x)|_{x_0=T} = \exp(C'), \quad k = 1, 2, 3, \quad (\text{A.13})$$

and $U_0(x)|_{x_0=0}$ unconstrained. The background field represents a constant electric field

$$\mathcal{E} = -i[C' - C]/T, \quad (\text{A.14})$$

which can be rewritten in terms of the matrix I^8 , appearing in eqs. (A.6), as

$$\mathcal{E} = -\gamma \begin{pmatrix} 2 & 0 & 0 \\ 0 & -1 & 0 \\ 0 & 0 & -1 \end{pmatrix}, \quad (\text{A.15})$$

with

$$\gamma = \frac{1}{LT} \left(\eta + \frac{\pi}{3} \right). \quad (\text{A.16})$$

The configuration V of least action appearing in the parametrization (5.46) is

$$V_0(x) = 1, \quad V_k(x) = V(x_0), \quad (\text{A.17})$$

with

$$V(x_0) = \exp\{i[\mathcal{E}x_0 - iC]\}. \quad (\text{A.18})$$

| a | C_a | R_a | $\phi_a(x_0)$ |
|-----|--|--|--|
| 1 | $\frac{1}{2}(\cos 2\gamma + \cos \gamma)$ | $\cos \frac{\gamma}{2}$ | $-3\gamma x_0 + \frac{1}{L}(\eta[\frac{3}{2} - \nu] - \frac{\pi}{3})$ |
| 3 | $\cos \gamma$ | $\cos \gamma$ | 0 |
| 4 | $\frac{1}{2}(\cos 2\gamma + \cos \gamma)$ | $\cos \frac{\gamma}{2}$ | $-3\gamma x_0 + \frac{1}{L}(\eta[\frac{3}{2} + \nu] - \frac{2\pi}{3})$ |
| 6 | $\cos \gamma$ | $\cos \gamma$ | $\frac{1}{L}(2\eta\nu + \frac{\pi}{3})$ |
| 8 | $\frac{1}{3}(2\cos 2\gamma + \cos \gamma)$ | $\frac{1}{3}(2\cos 2\gamma + \cos \gamma)$ | 0 |

Table A.1: C_a , R_a and ϕ_a for the gauge group SU(3). The other coefficients are $C_2 = C_1$, $C_5 = C_4$, $C_7 = C_6$, $R_2 = R_1$, $R_5 = R_4$, $R_7 = R_6$, $\phi_2 = -\phi_1$, $\phi_5 = -\phi_4$ and $\phi_7 = -\phi_6$.

An equivalent parametrization of V used in chapters 5 and 6 is

$$V_\mu(x) = \exp\{ib_\mu(x)\}, \quad (\text{A.19})$$

with

$$b_0(x) = 0, \quad \text{and} \quad b_k(x) = b_k(x_0) = \mathcal{E}x_0 - iC. \quad (\text{A.20})$$

Other functions appearing in chapter 6 are given in Table A.1, and

$$s_k^a(\mathbf{p}, x_0) = 2 \sin \left[\frac{1}{2} \left(p_k + \phi_a(x_0) \right) \right], \quad (\text{A.21})$$

$$c_k^a(\mathbf{p}, x_0) = 2 \cos \left[\frac{1}{2} \left(p_k + \phi_a(x_0) \right) \right], \quad (\text{A.22})$$

$$c_{abc} = -2i \operatorname{tr} \left\{ I^a [I^b, I^c] \right\}, \quad (\text{A.23})$$

$$e_{abc} = -2i \operatorname{tr} \left\{ e^{i\mathcal{E}} I^a I^b I^c - e^{-i\mathcal{E}} I^a I^c I^b \right\}, \quad (\text{A.24})$$

$$\alpha_k(\mathbf{p}, x_0) = b_k(x_0) + p_k^+. \quad (\text{A.25})$$

The following formulae are used to compute the tadpoles and are valid only for a neutral label ($\Leftrightarrow a = 3, 8$)

$$f_{ac}^+ = \frac{i}{2} \left(e_{ac\bar{c}} + e_{a\bar{c}c} \right), \quad (\text{A.26})$$

$$f_{ac}^- = \frac{1}{2} \left(e_{ac\bar{c}} - e_{a\bar{c}c} \right), \quad (\text{A.27})$$

$$e_{ac}^+ = \frac{i}{2} \left(e_{ac\bar{c}} e^{-\frac{i}{2}\check{\phi}_c} + e_{a\bar{c}c} e^{\frac{i}{2}\check{\phi}_c} \right), \quad (\text{A.28})$$

$$e_{ac}^- = \frac{1}{2} \left(e_{ac\bar{c}} e^{-\frac{i}{2}\check{\phi}_c} - e_{a\bar{c}c} e^{\frac{i}{2}\check{\phi}_c} \right), \quad (\text{A.29})$$

where $\check{\phi}_c = \partial_0 \phi_c(x_0)$ which is independent of x_0 .

Appendix B

Statistical uncertainties in Monte Carlo simulations

B.1 Thermalization

The initial configuration of gauge fields can be arbitrarily chosen, but the average $\overline{\mathcal{O}}$ over many configurations cannot sensibly depend on the initial one. For this reason one starts from a fixed configuration, e.g. where $U_\mu(x) = 1_{3 \times 3}$ for all dynamical links (eventually with some random noise), and the updating algorithm proceeds as discussed above. The number N_{UP} of updates must be chosen to be large enough to let the system “forget” the initial configuration. At the end of the computation, one calculates several averages $\overline{\mathcal{O}}$ by discarding the first N_{disc} configurations, and checks that, as a function of N_{disc} , the fluctuations on these averages are much smaller (order of magnitudes) than the statistical error $\overline{\mathcal{O}}$. The latter depends of course on N_{disc} , but the dependence is negligible as long as $N_{\text{disc}} \ll N$. If the check is successful, one can assume that the thermal equilibrium has been reached, and the analysis is performed only on the last $N - N_{\text{disc}}$ measurements.

B.2 Autocorrelation and errors estimate

In this section we explain how the statistical errors in our Monte Carlo simulations have been estimated. The whole section is far from being original, and it is mainly based on [101].

The first subsection is devoted to a short explanation of the Γ -method, which has been used for the error analysis of our HQET data. The second subsection reports the

key formulae of the jackknife error analysis, which has been used by the Tor Vergata group for the analysis of the relativistic QCD data. In Ref. [101] it is shown that the first method leads to more reliable and robust error estimate. On the other side, the jackknife allows to compute the correlation between derived observable in a simple way.

B.2.1 The Gamma method

We assume that the thermal equilibrium has been reached, and to have a number of primary observables labelled by a Greek index with exact statistical mean values A_α . Our derived observable is a function of these,

$$\mathcal{O} \equiv f(A_1, A_2, \dots) \equiv f(A_\alpha). \quad (\text{B.1})$$

The Monte Carlo estimates of the primary observables are labelled by $a_\alpha^{i,r}$, where $i = 1, \dots, N_r$ counts the measurements for each replicum, and $r = 1, \dots, R$ the number of statistically independent replica. From them one can compute the autocorrelation function $\Gamma_{\alpha\beta}$, defined by

$$\langle (a_\alpha^{i,r} - A_\alpha)(a_\beta^{j,s} - A_\beta) \rangle = \delta_{r,s} \Gamma_{\alpha\beta}(j-i), \quad \Gamma_{\alpha\beta}(n) = \Gamma_{\beta\alpha}(-n). \quad (\text{B.2})$$

Here and in the following of this section the averages $\langle \cdot \rangle$ refer to an ensemble of identical numerical experiments with independent random numbers and initial states. By means of the per replicum means

$$\bar{a}_\alpha^r = \frac{1}{N_r} \sum_{i=1}^{N_r} a_\alpha^{i,r}, \quad (\text{B.3})$$

we define the natural estimator of the primary quantities A_α as

$$\bar{a}_\alpha = \frac{1}{N} \sum_{r=1}^R N_r \bar{a}_\alpha^r, \quad N = \sum_{r=1}^R N_r. \quad (\text{B.4})$$

The covariance matrix assumes the simple form

$$\text{Cov}(\bar{a}_\alpha, \bar{a}_\beta) = \frac{1}{N} C_{\alpha\beta} \times \{1 + \mathcal{O}(R\tau/N)\}, \quad (\text{B.5})$$

where

$$C_{\alpha\beta} = \sum_{t=-\infty}^{\infty} \Gamma_{\alpha\beta}(t), \quad (\text{B.6})$$

and the finite scale τ characterizes the asymptotic exponential decay of $\Gamma_{\alpha\beta}$

$$\Gamma_{\alpha\beta}(t) \stackrel{|t| \rightarrow \infty}{\sim} e^{-|t|/\tau}. \quad (\text{B.7})$$

To determine \mathcal{O} we consider the estimator

$$\bar{\mathcal{O}} = f(\bar{a}_\alpha), \quad (\text{B.8})$$

and the derivatives $f_\alpha = \partial f / \partial A_\alpha$, taken at the exact values A_1, A_2, \dots . One can then write the variance of \mathcal{O} through the expression

$$\sigma_{\mathcal{O}}^2 = \frac{2\tau_{\text{int},\mathcal{O}}}{N} v_{\mathcal{O}}. \quad (\text{B.9})$$

Here $v_{\mathcal{O}}$ is the naïve, i.e. disregarding autocorrelations, variance

$$v_{\mathcal{O}} = \sum_{\alpha\beta} f_\alpha f_\beta \Gamma_{\alpha\beta}(0), \quad (\text{B.10})$$

and the integrated autocorrelation time for \mathcal{O} reads

$$\tau_{\text{int},\mathcal{O}} = \frac{1}{2v_{\mathcal{O}}} \sum_{t=-\infty}^{\infty} \sum_{\alpha\beta} f_\alpha f_\beta \Gamma_{\alpha\beta}(t). \quad (\text{B.11})$$

Our best estimate for \mathcal{O} is given by eq. (B.8), and, in absence of autocorrelations, we would have $\Gamma_{\alpha\beta}(t) \propto \delta_{t,0}$, which implies $\tau_{\text{int},\mathcal{O}} = 0.5$. The integrated autocorrelation time thus represents an estimate of the efficiency of the algorithm in use for the determination of \mathcal{O} .

The next step consists in the computation of the gradient f_α and of $\Gamma_{\alpha\beta}$. For the former we define the estimator \bar{f}_α , where the derivative is evaluated at arguments $\bar{a}_1, \bar{a}_2, \dots$, while for the autocorrelation function we have

$$\bar{\Gamma}_{\alpha\beta}(t) = \frac{1}{N - Rt} \sum_{r=1}^R \left[\sum_{i=1}^{N_r-t} (a_\alpha^{i,r} - \bar{a}_\alpha)(a_\beta^{i+t,r} - \bar{a}_\beta) \right], \quad (\text{B.12})$$

from which one computes the projected autocorrelation function

$$\bar{\Gamma}_{\mathcal{O}}(t) = \sum_{\alpha\beta} \bar{f}_\alpha \bar{f}_\beta \bar{\Gamma}_{\alpha\beta}(t). \quad (\text{B.13})$$

The latter is finally used to compute

$$\bar{v}_\varrho = \bar{\Gamma}_\varrho(0), \quad \text{and} \quad (\text{B.14})$$

$$\bar{\sigma}_\varrho^2 = \frac{1}{N} \left[\bar{\Gamma}_\varrho(0) + 2 \sum_{t=1}^W \bar{\Gamma}_\varrho(t) \right], \quad (\text{B.15})$$

where the last equation defines our best estimate of the variance. There we have introduced the summation window W , in order to get a good estimator of the autocorrelation time. This cut-off is necessary because the signal for $\Gamma_\varrho(t)/\Gamma_\varrho(0)$ is overwhelmed by the noise for $|t| \gg \tau$. At the same time, the summation should not be truncated too early, because it would compromise the accuracy of $\bar{\sigma}_\varrho^2$.

A Matlab routine, called `UWerr.m`, that implements the whole method, including an automatic windowing procedure, the necessary plots and much more, is documented and offered by Ulli Wolff for download from the webpage:

`www-com.physik.hu-berlin.de/ALPHAsoft`.

B.2.2 Jackknife

We borrow the notation of the previous subsection, and give the basic formulae for error estimation by jackknife. We assume data a_α^i where possible replica are sewed to one history

$$a_\alpha^{j+\sum_{k=1}^{r-1} N_k} = a_\alpha^{j,r}, \quad (\text{B.16})$$

of length $N = BN_B$ which we divide into N_B sections of B consecutive measurements each. Through the average

$$\bar{a}_\alpha = \frac{1}{N} \sum_{i=1}^N a_\alpha^i, \quad (\text{B.17})$$

we take as best estimate for ϱ

$$\bar{\varrho} = f(\bar{a}_\alpha), \quad (\text{B.18})$$

where it is understood that $\bar{\varrho} = \bar{\bar{\varrho}}$, the latter appearing in eq. (B.8). We further proceed by forming the blocked measurements

$$b_\alpha^k = \frac{1}{B} \sum_{i=1}^B a_\alpha^{(k-1)B+i}, \quad k = 1, \dots, N_B, \quad (\text{B.19})$$

and the jackknife bins

$$c_\alpha^k = \frac{1}{N-B} \left(\sum_{i=1}^N a_\alpha^i - B b_\alpha^k \right). \quad (\text{B.20})$$

The resulting jackknife error estimator is given by

$$\bar{\sigma}_{\mathcal{O},\text{Jack}}^2 = \frac{N_B - 1}{N_B} \sum_{k=1}^{N_B} (f(c_\alpha^k) - \bar{\mathcal{O}})^2. \quad (\text{B.21})$$

Finally we consider the case where we want to compute another observable \mathcal{Q} , sharing with \mathcal{O} the same gauge configurations, and eventually expressed as function of primary observables, whose a group may be in common with \mathcal{O} . We thus have $\mathcal{O} \equiv f(A_\alpha)$ and $\mathcal{Q} \equiv g(A_\alpha)$, and the correlation between the two observables can be easily computed by jackknife

$$\text{Cov}(\mathcal{O}, \mathcal{Q})_{\text{Jack}} = \frac{N_B - 1}{N_B} \sum_{k=1}^{N_B} (f(c_\alpha^k) - \bar{\mathcal{O}})(g(c_\alpha^k) - \bar{\mathcal{Q}}). \quad (\text{B.22})$$

By performing the whole analysis with different choices of the bin length B , one can check the stability of the estimated correlation.

Appendix C

Simulation results

This appendix is devoted to collect the results of the simulations performed to apply the Step Scaling Method. More emphasis and details are given for the static simulations, which have been performed after the relativistic QCD results were published [50, 51]. They have been reanalyzed, taking into account the correlation between observables computed on the same gauge configurations. The statistical uncertainties on the regularization dependent part of the renormalization constants and the lattice spacing are included before performing the continuum limit extrapolations; they do not appear as a separate uncertainty.

C.1 Static data

The parameters for the HQET simulations exploited in the Step Scaling Method are reported in Table C.1. The method employed to compute them is explained in Sect. 4.2. The first column of the table indicates on which volume the parameters are determined. For the volumes indicated by L_0^* the values of κ_s are obtained through an interpolation of the data in [50]. The errors on the last column for the RGI strange quark mass include the uncertainties on k_c and on the PCAC mass (4.17). An additional error is added in quadrature to take into account the uncertainty on the regularization dependent part of the renormalization constants of the RGI quark mass and on r_0/a according to Sect. 4.2.

In the following tables and figures the observables at non-vanishing lattice spacing borrow the continuum notation. The uncertainty stemming from the perturbative determination of c_A^{stat} and b_A^{stat} is negligible compared to the statistical errors on all observables.

| Volume | L/a | β | κ_{crit} | κ_s | M_s (GeV) |
|---------|-------|---------|------------------------|------------|-------------|
| L_0 | 6 | 6.2110 | 0.135625(15) | 0.134766 | 0.1381(20) |
| L_0 | 8 | 6.4200 | 0.135616(13) | 0.135015 | 0.1365(20) |
| L_0^* | 12 | 6.7370 | 0.135235(5) | 0.134801 | 0.1367(20) |
| L_0^* | 16 | 6.9630 | 0.134832(4) | 0.134526 | 0.1343(21) |
| L_0^* | 24 | 7.3000 | 0.134235(3) | 0.134041 | 0.1396(18) |
| L_1 | 8 | 5.9598 | 0.134700(18) | 0.133274 | 0.1373(16) |
| L_1 | 10 | 6.0914 | 0.135494(23) | 0.134476 | 0.1362(15) |
| L_1 | 12 | 6.2110 | 0.135772(8) | 0.134908 | 0.1352(15) |
| L_1 | 16 | 6.4200 | 0.135687(8) | 0.135087 | 0.1322(15) |
| L_1 | 24 | 6.7370 | 0.135221(7) | 0.134832 | 0.1340(17) |

Table C.1: Collection of all simulation parameters for the HQET part of the Step Scaling Method.

| Observable | C.L. | c_A^{stat} | b_A^{stat} |
|-------------------------------|------------|---------------------|---------------------|
| $\sigma_m^{\text{stat}}(L_2)$ | 1.561(53) | 1-loop | - |
| $\sigma_m^{\text{stat}}(L_1)$ | 0.233(36) | 1-loop | - |
| | 0.240(36) | tree-level | - |
| $Y_{\text{SF}}(L_2, \mu)$ | 5.06(21) | 1-loop | 1-loop |
| $Y_{\text{SF}}(L_1, 1/L_1)$ | -1.754(21) | 1-loop | 1-loop |
| | -1.752(21) | 1-loop | tree-level |
| | -1.749(20) | tree-level | 1-loop |
| | -1.746(20) | tree-level | tree-level |
| $\sigma_f^{\text{stat}}(L_1)$ | 0.4337(44) | 1-loop | - |
| | 0.4339(44) | tree-level | - |
| $Y_{\text{SF}}(L_0, 1/L_0)$ | -1.592(11) | 1-loop | 1-loop |
| | -1.591(10) | 1-loop | tree-level |
| | -1.590(10) | tree-level | 1-loop |
| | -1.589(10) | tree-level | tree-level |

Table C.2: Collection of all continuum limit extrapolations for the HQET part of the Step Scaling Method. The result $Y_{\text{SF}}(L_2, \mu)$ is taken from [1], and is intended to be multiplied by $I^{\text{stat}}(\mu = (1.436r_0)^{-1}) = 0.9191(83)$ computed in [2] to get eq. (4.75).

| c_A^{stat} | β | L_1/a | κ_s | $a\Gamma_{\text{stat}}(L_1)$ | | |
|----------------------|---------|---------|--------------------|---|------------------------------|------------------------------|
| 1-loop tree-level | 5.9598 | 8 | 0.133274 | 0.31830(84) 0.31823(85) | | |
| 1-loop tree-level | 6.0914 | 10 | 0.134476 | 0.28053(63) 0.28051(63) | | |
| 1-loop tree-level | 6.2110 | 12 | 0.134908 | 0.25328(58) 0.25326(59) | | |
| 1-loop tree-level | 6.4200 | 16 | 0.135087 | 0.21140(74) 0.21139(75) | | |
| 1-loop tree-level | 6.7370 | 24 | 0.134832 | 0.1722(16) 0.1722(16) | | |
| c_A^{stat} | β | L_2/a | aE_{stat} | Interpolated results for $a\Gamma_{\text{stat}}(L_1)$ | | |
| 1-loop tree-level | 6.0219 | 16 | 0.4053(49) | 0.30003(51) 0.29998(51) | | |
| 1-loop tree-level | 6.2885 | 24 | 0.3011(33) | 0.23602(47) 0.23601(47) | | |
| 1-loop tree-level | 6.4500 | 32 | 0.2564(9) | 0.20671(57) 0.20671(57) | | |
| 1-loop tree-level | 6.4956 | 32 | 0.2461(14) | 0.19972(63) 0.19973(63) | | |
| c_A^{stat} | β | L_1/a | L_0/a | κ_s | $a\Gamma_{\text{stat}}(L_1)$ | $a\Gamma_{\text{stat}}(L_0)$ |
| 1-loop tree-level | 6.2110 | 12 | 6 | 0.134766 | 0.2558(18) 0.2558(18) | 0.22717(91) 0.22587(91) |
| 1-loop tree-level | 6.4200 | 16 | 8 | 0.135015 | 0.2154(11) 0.2154(11) | 0.19575(92) 0.19497(93) |
| 1-loop tree-level | 6.7370 | 24 | 12 | 0.134801 | 0.1663(17) 0.1662(17) | 0.15608(83) 0.15564(85) |
| 1-loop tree-level | 6.9630 | 32 | 16 | 0.134526 | 0.1426(14) 0.1427(14) | 0.13545(66) 0.13524(65) |

Table C.3: Collection of results at finite lattice spacing, for the computation of the static step scaling functions of the meson mass.

| c_A^{stat} | β | L_1/a | κ_s | $X_{\text{SF}}(L_1)$ | | |
|----------------------|---------|---------|------------------------|----------------------------|--------------------------|----------------------------|
| 1-loop tree-level | 6.2110 | 12 | 0.134766 | -2.221(13) -2.102(12) | | |
| 1-loop tree-level | 6.4200 | 16 | 0.135015 | -2.266(13) -2.159(12) | | |
| 1-loop tree-level | 6.7370 | 24 | 0.134801 | -2.279(28) -2.192(27) | | |
| 1-loop tree-level | 6.9630 | 32 | 0.134526 | -2.344(35) -2.266(34) | | |
| c_A^{stat} | β | L_1/a | κ_{crit} | $\Xi^{-1}(L_1)$ | $\Xi(L_1)^{(0)}$ | |
| 1-loop tree-level | 6.2110 | 12 | 0.135625 | -0.4934(24) -0.5164(25) | -1.6019540566018 | |
| 1-loop tree-level | 6.4200 | 16 | 0.135616 | -0.4787(28) -0.4987(29) | -1.6027594410020 | |
| 1-loop tree-level | 6.7370 | 24 | 0.135235 | -0.4772(33) -0.4939(34) | -1.6033361949926 | |
| 1-loop tree-level | 6.9630 | 32 | 0.134832 | -0.4712(30) -0.4860(31) | -1.6035384024722 | |
| c_A^{stat} | β | L_1/a | L_0/a | κ_s | $X_{\text{SF}}(L_1)$ | $X_{\text{SF}}(L_0)$ |
| 1-loop tree-level | 6.2110 | 12 | 6 | 0.134766 | -2.221(13) -2.102(12) | -1.8054(34) -1.7170(32) |
| 1-loop tree-level | 6.4200 | 16 | 8 | 0.135015 | -2.266(13) -2.159(12) | -1.8372(46) -1.7540(44) |
| 1-loop tree-level | 6.7370 | 24 | 12 | 0.134801 | -2.279(28) -2.192(27) | -1.8806(63) -1.8122(60) |
| 1-loop tree-level | 6.9630 | 32 | 16 | 0.134526 | -2.344(35) -2.266(34) | -1.8986(65) -1.8370(63) |

Table C.4: Collection of results at finite lattice spacing for the static pseudoscalar decay constant. All numbers are obtained with the 1-loop expression of b_A^{stat} .

| c_A^{stat} | β | L_0/a | κ_s | $X_{\text{SF}}(L_0)$ | |
|----------------------|---------|---------|------------|----------------------|-------------|
| 1-loop tree-level | 6.4200 | 8 | 0.135015 | -1.8372(46) | -1.7540(44) |
| 1-loop tree-level | 6.7370 | 12 | 0.134801 | -1.8806(63) | -1.8122(60) |
| 1-loop tree-level | 6.9630 | 16 | 0.134526 | -1.8986(65) | -1.8370(63) |
| 1-loop tree-level | 7.3000 | 24 | 0.134041 | -1.9182(102) | -1.8660(99) |

| c_A^{stat} | β | L_0/a | κ_{crit} | $\Xi^{-1}(L_0)$ | $\Xi^{(0)}(L_0)$ | |
|----------------------|---------|---------|------------------------|-----------------|------------------|------------------|
| 1-loop tree-level | 6.4200 | 8 | 0.135616 | -0.5467(13) | -0.5686(13) | -1.5996643156321 |
| 1-loop tree-level | 6.7370 | 12 | 0.135235 | -0.53272(64) | -0.55109(66) | -1.6019540566018 |
| 1-loop tree-level | 6.9630 | 16 | 0.134832 | -0.5246(13) | -0.5407(14) | -1.6027594410020 |
| 1-loop tree-level | 7.3000 | 24 | 0.134235 | -0.5182(13) | -0.5319(13) | -1.6033361949926 |

Table C.4: (continued)

An accurate data analysis reveals that the quantities

$$\sigma_f^{\text{stat}}(L_2), \quad \sigma_f^{\text{stat}}(L_1) \quad \text{and} \quad Y_{\text{SF}}(L_0, 1/L_0) \quad (\text{C.1})$$

are slightly correlated, because they share the same data for $X_{\text{SF}}(L_1)$ and $X_{\text{SF}}(L_0)$. However, the error on the final result for the decay constant is dominated by the uncertainty stemming from the large volume simulations. Furthermore we observe that, if we approximate f_{B_s} , computed through eq. (4.74), to simply have a linear dependence on the static decay constant, the relations

$$f_{B_s} \propto Y_{\text{SF}}(L_0, 1/L_0) \cdot \sigma_f^{\text{stat}}(L_1) \cdot \sigma_f^{\text{stat}}(L_2) \quad (\text{C.2})$$

$$\propto X_{\text{SF}}(L_0) \cdot \frac{X_{\text{SF}}(L_1)}{X_{\text{SF}}(L_0)} \cdot \frac{1}{X_{\text{SF}}(L_1)}, \quad (\text{C.3})$$

show that this correlation is expected to further reduce the uncertainty quoted in (4.83). We neglect it, because it is small in comparison with the large volume uncertainties.

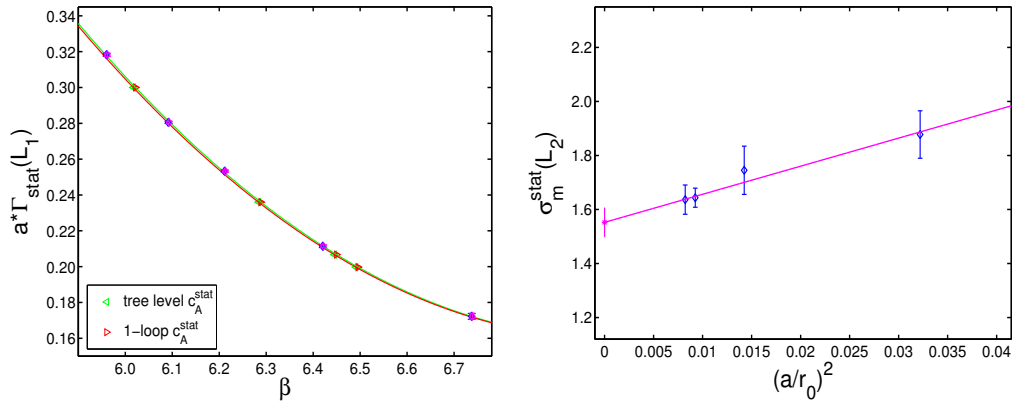


Figure C.1: On the left: β -dependence of $a\Gamma_{\text{stat}}(L_1)$. The red curve shows the quadratic fit of the data with c_A^{stat} at 1-loop (blue points), while the green one fits the data with c_A^{stat} at tree-level (magenta points). The two curves almost overlap. On the right: continuum extrapolation to get $\sigma_m^{\text{stat}}(L_2)$.

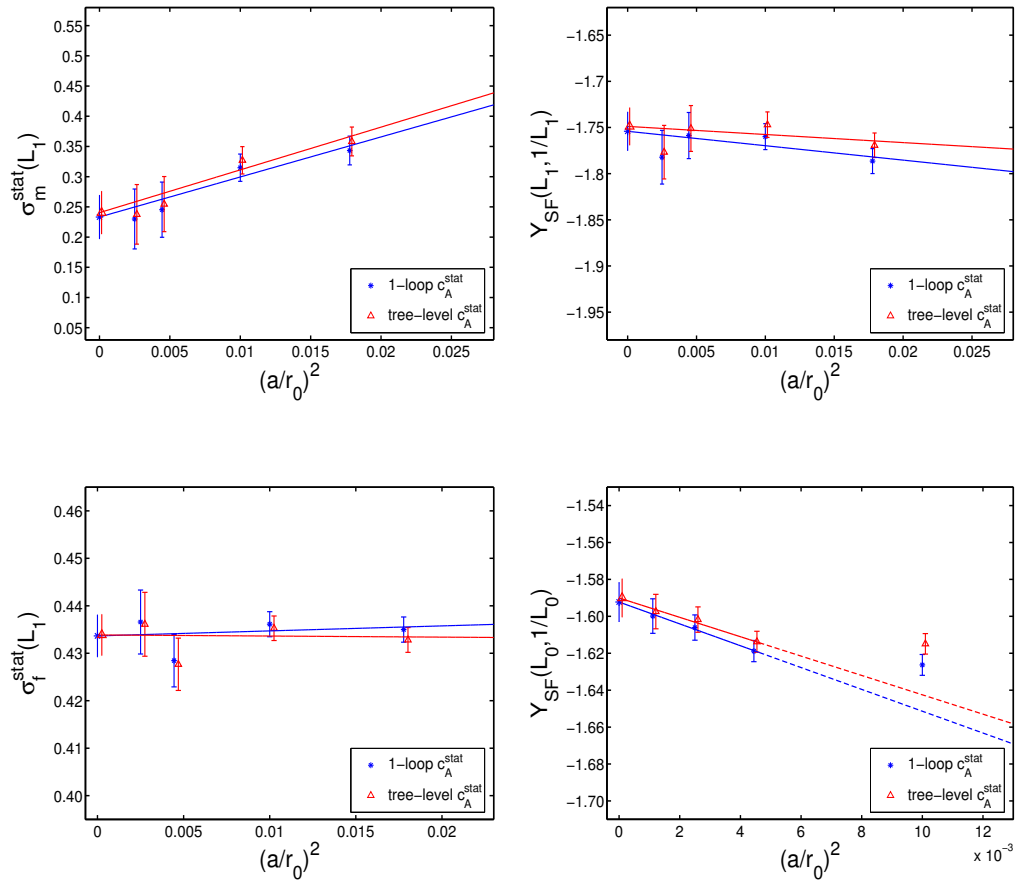


Figure C.2: Various HQET continuum limit extrapolations for the Step Scaling Method.

C.2 Relativistic QCD data

The data at finite heavy quark mass have been produced by the Tor Vergata group, and published in [50, 51]. In these references one can find all simulation parameters, which have been determined with the method explained in Sect. 4.2. In this section we report the new data analysis, collecting the results of the continuum limit extrapolations.

The latter are performed according to the method outlined in Sect. E.1. Here, the way followed to define the Line of Constant Physics (cf. Sect. 3.4) has to be clarified. Let us assume that we are at fixed finite volume L and lattice spacing, and consider an observable \mathcal{O} . The quark mass definition is firstly only one, say eq. (4.22). The observable is computed for several quark-antiquark couples. Therefore, there exist a bijective correspondence between the computed observable \mathcal{O} and the couples (LM_{q_2}, LM_{q_1}) . Since we are interested in the heavy-strange meson properties, the observable is interpolated in such a way that one of the two quark masses matches the physical strange quark mass; then the remaining quark mass is matched to a set of some conveniently chosen values of LM_h . This two-step interpolation procedure is repeated for all discretizations belonging to the volume L . We are now able to perform the continuum limit extrapolations of the observable \mathcal{O} , where the couples (LM_s, LM_h) are kept fixed in all discretizations. By repeating the whole procedure for several quark mass definitions, whose details are given in Sect. 4.2.3, we have the setup described in Sect. E.1. Therefore, at fixed lattice spacing one has several determinations of \mathcal{O} , differing by being associated with different quark mass definitions. These determinations share the same gauge configurations, and are statistically correlated. Each of these definitions follows a different Line of Constant Physics, but universality imposes that they are indistinguishable in the continuum limit. Furthermore, one can infer from the $O(a)$ -improvement, that, at non-vanishing but small lattice spacing, these definitions differ by $O(a^2)$ -terms.

Table C.5 summarizes all continuum limit results, and the extrapolations are shown in Fig. C.3. The plot on the lower right corner shows the continuum limit (cyan point) for $L_0 M_{\text{PS}}(L_0)$, performed according to the averaging method of Sect. E.1. On the lower left corner each definition is separately fitted. The cyan point of the r.h.s. plot is pasted here to show the very good agreement between each single definition and the averaged one.

In all continuum limit extrapolations the uncertainty on the improvement coefficients c_A and b_A is found to be negligible.

| $L_2 M_h$ | $L_2 M_{\text{PS}}(L_2)$ | $\sigma_m(L_2)$ | $\sigma_f(L_2)$ |
|-----------|--------------------------|-----------------|--|
| 16.2 | 17.221(44) | 1.0690(53) | 0.929(32) |
| 12.6 | 14.918(43) | 1.0808(63) | 0.912(27) |
| 10.9 | 13.894(43) | 1.0874(70) | 0.900(24) |
| $L_1 M_h$ | $L_1 M_{\text{PS}}(L_1)$ | $\sigma_m(L_1)$ | $\sigma_f(L_1)$ |
| 14.4 | 12.438(52) | 1.0123(56) | 0.4198(45) |
| 12.7 | 11.319(52) | 1.0135(61) | 0.4193(45) |
| 8.11 | 8.307(52) | 1.0181(83) | 0.4169(43) |
| $L_0 M_h$ | $L_0 M_{\text{PS}}(L_0)$ | $\rho(L_0)$ | $f_{\text{PS}}(L_0) \sqrt{L_0^3 M_{\text{PS}}(L_0)}$ |
| 14.4 | 10.719(47) | 0.7442(88) | 3.120(45) |
| 13.4 | 10.097(47) | 0.7541(90) | 3.097(45) |
| 8.11 | 6.793(46) | 0.8367(108) | 2.911(43) |
| 3.45 | 3.613(44) | - | 2.534(40) |
| 3.24 | 3.466(44) | - | 2.505(40) |

Table C.5: Continuum limit results for the relativistic QCD data used in the Step Scaling Method.

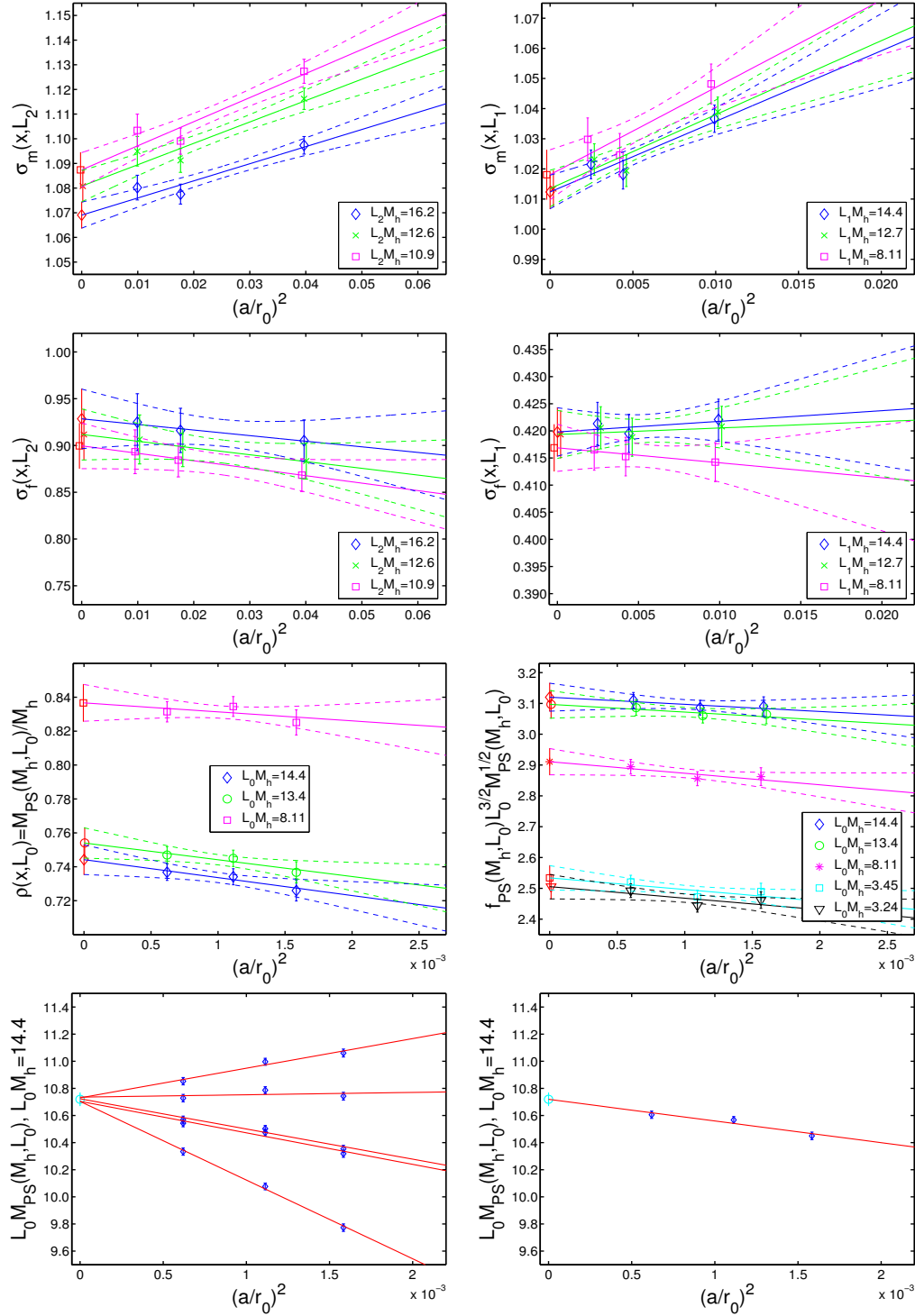


Figure C.3: Continuum limit extrapolations for the relativistic QCD data used in the Step Scaling Method.

Appendix D

Correlated errors in both coordinates

This appendix contains a short digression about error analysis. A few formulae are derived to deal with the case of a two dimensional fit with correlated variables on the y - and x -axes.

Let us consider the case where we want to fit a certain quantity y vs. x , and the uncertainties Δy and Δx , respectively on y and x , are correlated. To simplify the problem let us assume that the fit is of the kind $y = a + bx$, but the following considerations hold more generally. Having the set of data $\{y_i, x_i, i = 1, \dots, N\}$ with correlated errors $\{\Delta y_i, \Delta x_i, i = 1, \dots, N\}$, following [102], it is straightforward to write down the appropriate χ^2 for this case,

$$\chi^2(a, b) = \sum_{i=1}^N \frac{(y_i - a - bx_i)^2}{\sigma_i^2}. \quad (\text{D.1})$$

The variance appearing in the denominator of eq. (D.1) can be understood both as the variance in the direction of the smallest χ^2 between each data point and the line with slope b , as well as the variance of the linear combination $z_i = y_i - a - bx_i$ of the variables y_i and x_i ,

$$\begin{aligned} \sigma_i^2 = \text{Var}(z_i) &= \left(\frac{\partial z_i}{\partial y_i}\right)^2 \text{Var}(y_i) + \left(\frac{\partial z_i}{\partial x_i}\right)^2 \text{Var}(x_i) \\ &+ 2 \frac{\partial z_i}{\partial y_i} \frac{\partial z_i}{\partial x_i} \text{Cov}(y_i; x_i) \end{aligned} \quad (\text{D.2})$$

$$= \text{Var}(y_i) + b^2 \text{Var}(x_i) - 2b \text{Cov}(y_i; x_i). \quad (\text{D.3})$$

The expressions (D.2) and (D.3) can be generalized to the case of y_i depending on the set of variables $\{\omega_{i,k}, k = 1, \dots, N\}$, and x_i depending on $\{\omega_{i,l}, l = N + 1, \dots, M\}$, with the ω 's correlated with each other. In that case $z_i = z_i(\omega_{i,s})$ with $s = 1, \dots, M$ and one can write a compact expression for $\text{Var}(z_i)$, which reads

$$\text{Var}(z_i) = \sum_{s,s'=1}^M \frac{\partial z_i}{\partial \omega_{i,s}} \text{Cov}(\omega_{i,s}; \omega_{i,s'}) \frac{\partial z_i}{\partial \omega_{i,s'}}. \quad (\text{D.4})$$

Let us take as example a linear fit of $y(\omega_1, \omega_2)$ vs. $x(\omega_2, \omega_3)$, with the couples $\{\omega_1, \omega_2\}$ and $\{\omega_2, \omega_3\}$ statistically uncorrelated. It is clear that the uncertainty on the y_i 's is correlated with the one on the x_i 's, because they all depend on ω_2 . In this case eq. (D.4) reduces to

$$\begin{aligned} \text{Var}(z_i) = & \left(\frac{\partial y_i}{\partial \omega_{i,1}} \Delta \omega_{i,1} \right)^2 + \left(\frac{\partial y_i}{\partial \omega_{i,2}} \Delta \omega_{i,2} \right)^2 + b^2 \left(\frac{\partial x_i}{\partial \omega_{i,2}} \Delta \omega_{i,2} \right)^2 \\ & + b^2 \left(\frac{\partial x_i}{\partial \omega_{i,3}} \Delta \omega_{i,3} \right)^2 - 2b \frac{\partial y_i}{\partial \omega_{i,2}} \frac{\partial x_i}{\partial \omega_{i,2}} (\Delta \omega_{i,2})^2. \end{aligned} \quad (\text{D.5})$$

Coming back to the general case (D.4), we want to minimize eq. (D.1) with respect to a and b . Unfortunately, the occurrence of b in the denominator of eq. (D.1) makes the resulting equation for the slope $\partial \chi^2 / \partial b = 0$ nonlinear. In most cases it is sufficient to approximate the slope b by performing the fit without the uncertainties coming from the x_i 's, then one computes the σ_i 's according to (D.4) and repeats the fit. The procedure has to be iterated with the new b until successive estimates of b agree within the desired tolerance.

Appendix E

Fit of the correlated relativistic QCD data

This appendix is devoted to the explanation of the method used to take into account the correlations between the relativistic QCD data. The latter are characterized by a non-vanishing correlation between the observables belonging to the same lattice spacing, but differing by being associated with different definitions of the quark mass. In addition, observables computed on the same lattice but for different masses share the same set of gauge configurations, and are indeed correlated.

E.1 Performing the continuum limits

Let us consider an observable $\mathcal{O}(m_h)$ depending on the heavy quark mass m_h . In our case the light quark is matched to be the strange one in all cases, and the corresponding dependence is omitted in the following to simplify the notation. The same holds for the volume dependence; it plays no role for the present discussion.

To compute the continuum limit of the quantity $\mathcal{O}(m_k)$, with fixed m_k , the setup of the data can be summarized by introducing the notation

$$x_i = \left(\frac{a}{L}\right)_i^2, \quad (\text{E.1})$$

$$y_{ij}(m_k) = \mathcal{O}\left(\left(\frac{a}{L}\right)_i^2, \text{mass def} = j, \text{heavy mass} = m_k\right). \quad (\text{E.2})$$

The x_i variable refers to the different discretizations, while $y_{ij}(m_k)$ refers to the observable \mathcal{O} with discretization i , quark mass definition j and heavy quark mass m_k . The

several $y_{ij}(m_k)$'s with the same i are correlated, because they are obtained from the same set of gauge configurations.

One possibility to perform the continuum limit is the following procedure. First of all, at fixed lattice spacing, the observables are averaged over the different mass definitions according to

$$\bar{y}_i(m_k) = \sum_j y_{ij}(m_k)/N, \quad N_i = \sum_j 1 = N, \quad \forall i, \quad (\text{E.3})$$

$$\text{remarking that } \frac{\partial \bar{y}_i(m_k)}{\partial y_{ij}(m_k)} = 1/N, \quad \forall j, \quad (\text{E.4})$$

$$(\Delta \bar{y}_i(m_k))^2 = \frac{1}{N^2} \sum_{l,m} \text{Cov}(y_{il}(m_k), y_{im}(m_k)), \quad (\text{E.5})$$

taking into account the correlations as shown in eq. (E.5). Remembering that the averaged quantities $\bar{y}_i(m_k)$ at different lattice spacing i are statistically uncorrelated, we can perform the continuum limit in the usual way, i.e. by minimizing the χ^2 :

$$\chi^2 = \sum_i \left(\frac{\bar{y}_i(m_k) - a_0 - a_1 x_i}{\Delta \bar{y}_i(m_k)} \right)^2. \quad (\text{E.6})$$

The result of the continuum limit is finally $a_0 = \bar{y}(m_k)$. For reasons which will be clear in the following section, it is useful to compute and store

$$\frac{\partial \bar{y}(m_k)}{\partial \bar{y}_l(m_k)} = \frac{1}{\Delta_T \cdot (\Delta \bar{y}_l(m_k))^2} (T_{xx} - x_l T_x), \quad (\text{E.7})$$

where

$$\Delta_T = T T_{xx} - T_x^2, \quad T = \sum_i \frac{1}{(\Delta \bar{y}_i(m_k))^2} \quad (\text{E.8})$$

$$T_{xx} = \sum_i \frac{x_i^2}{(\Delta \bar{y}_i(m_k))^2}, \quad T_x = \sum_i \frac{x_i}{(\Delta \bar{y}_i(m_k))^2}. \quad (\text{E.9})$$

E.2 Fitting the mass dependence

The procedure described in the previous section is repeated for several heavy quark masses, and it allows to arrange the data for a fit $\bar{y}(m)$ vs. $z = 1/(Lm)$ with L fixed.

Eventually the points z_k can be chosen to be $1/(LM(m_k))$, where $M(m_k)$ is the meson mass associated with m_k . The choice of the definition of z_k is irrelevant for the present discussion, because here we consider as source of uncertainty only the statistical error on $\bar{y}(m_k)$, while the one associated with z_k and other systematics are neglected.

The first step for the fit $\bar{y}(m)$ vs. $z = 1/(Lm)$ can be performed by dealing with the $\bar{y}(m_k)$'s as independent quantities. The merit function χ^2

$$\chi^2 = \sum_k \left(\frac{\bar{y}(m_k) - f(z_k, c)}{\Delta \bar{y}(m_k)} \right)^2, \quad (\text{E.10})$$

is minimized with respect to the parameters c . Taking as example the case of a linear fit $f(z, \{c\}) = c_0 + c_1 z$. The parameters $\{c\}$ are given by

$$c_0 = \frac{S_{xx}S_y - S_x S_{xy}}{\Delta}, \quad c_1 = \frac{SS_{xy} - S_x S_y}{\Delta}, \quad (\text{E.11})$$

where

$$S = \sum_k \frac{1}{(\Delta \bar{y}(m_k))^2}, \quad S_x = \sum_k \frac{z_k}{(\Delta \bar{y}(m_k))^2}, \quad S_y = \sum_k \frac{\bar{y}(m_k)}{(\Delta \bar{y}(m_k))^2}$$

$$S_{xx} = \sum_k \frac{z_k^2}{(\Delta \bar{y}(m_k))^2}, \quad S_{xy} = \sum_k \frac{z_k \bar{y}(m_k)}{(\Delta \bar{y}(m_k))^2}, \quad \Delta = SS_{xx} - S_x^2.$$

The estimate of the uncertainty on the parameters $\{c\}$ and their correlation takes into account the correlation between the data as follows

$$(\Delta c_0)^2 = \sum_{k,k'} \frac{\partial c_0}{\partial \bar{y}(m_k)} \text{Cov}(\bar{y}(m_k), \bar{y}(m_{k'})) \frac{\partial c_0}{\partial \bar{y}(m_{k'})}, \quad (\text{E.12})$$

$$(\Delta c_1)^2 = \sum_{k,k'} \frac{\partial c_1}{\partial \bar{y}(m_k)} \text{Cov}(\bar{y}(m_k), \bar{y}(m_{k'})) \frac{\partial c_1}{\partial \bar{y}(m_{k'})}, \quad (\text{E.13})$$

$$\text{Cov}(c_0, c_1) = \sum_{k,k'} \frac{\partial c_0}{\partial \bar{y}(m_k)} \text{Cov}(\bar{y}(m_k), \bar{y}(m_{k'})) \frac{\partial c_1}{\partial \bar{y}(m_{k'})}, \quad (\text{E.14})$$

where one uses

$$\frac{\partial c_0}{\partial \bar{y}(m_k)} = \frac{1}{\Delta \cdot (\Delta \bar{y}(m_k))^2} (S_{xx} - z_k S_x), \quad (\text{E.15})$$

$$\frac{\partial c_1}{\partial \bar{y}(m_k)} = \frac{1}{\Delta \cdot (\Delta \bar{y}(m_k))^2} (z_k S - S_x), \quad (\text{E.16})$$

$$\text{Cov}(\bar{y}(m_k), \bar{y}(m_{k'})) = \sum_{l,m} \frac{\partial \bar{y}(m_k)}{\partial \bar{y}_l(m_k)} \text{Cov}(\bar{y}_l(m_k), \bar{y}_m(m_{k'})) \frac{\partial \bar{y}(m_{k'})}{\partial \bar{y}_m(m_{k'})}. \quad (\text{E.17})$$

The sums in eq. (E.17) can be simplified, because $\text{Cov}(\bar{y}_l(m_k), \bar{y}_m(m_{k'})) = 0$ for $l \neq m$. Thus

$$\text{Cov}(\bar{y}(m_k), \bar{y}(m_{k'})) = \sum_l \frac{\partial \bar{y}(m_k)}{\partial \bar{y}_l(m_k)} \text{Cov}(\bar{y}_l(m_k), \bar{y}_l(m_{k'})) \frac{\partial \bar{y}(m_{k'})}{\partial \bar{y}_l(m_{k'})}. \quad (\text{E.18})$$

The term $\partial \bar{y}(m_k) / \partial \bar{y}_l(m_k)$ is taken from eq. (E.7), while for the covariance matrix we write

$$\text{Cov}(\bar{y}_l(m_k), \bar{y}_l(m_{k'})) = \sum_{s,t} \frac{\partial \bar{y}_l(m_k)}{\partial y_{ls}(m_k)} \text{Cov}(y_{ls}(m_k), y_{lt}(m_{k'})) \frac{\partial \bar{y}_l(m_{k'})}{\partial y_{lt}(m_{k'})}, \quad (\text{E.19})$$

where $\partial \bar{y}_l(m_k) / \partial y_{ls}(m_k)$ is taken from (E.4), and the covariance matrix of the r.h.s. is directly computed by jackknife (cf. eq. (B.22)). This procedure can be straightforwardly generalized to the other fitting functions $f(z, \{c\})$. For more complicated fitting functions the procedure may become quite knotty. In that case, it may be convenient to numerically approximate the partial derivatives of the coefficients $\{c\}$ with respect to $\bar{y}(m_k)$.

The importance of the correlation between the data can be better understood by looking at Fig. E.1. The blue data points (diamonds) and the interpolated green and cyan points (asterisks) are the same appearing in Fig. 4.5. For the plot on the left only the data at finite heavy quark mass have been considered in the fits. The magenta area (the bigger one) covers one standard deviation for the fitting line if the correlation between the data associated with different heavy quark masses is not included, while the green area is computed taking the correlation into account. Similarly for the plot on the right. Here the static data point is included. The cyan area (the bigger one) has been computed considering the correlation, while the magenta one ignores it.

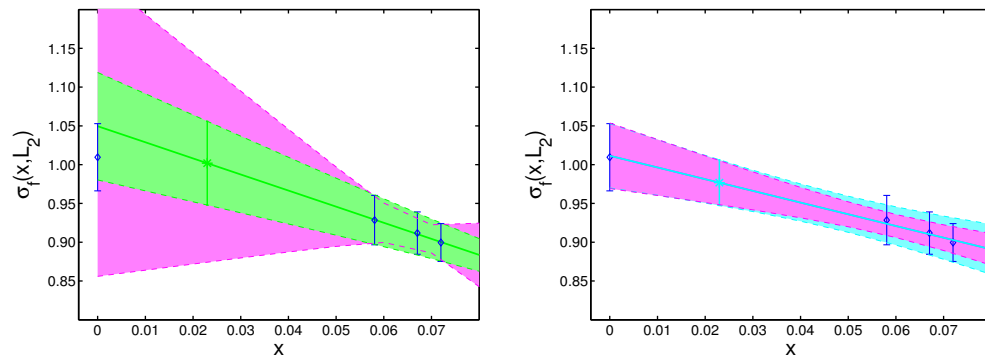


Figure E.1: Importance of data correlation for the step scaling function $\sigma_f(L_2)$.

Appendix F

Estimate of the uncertainty related to the scale setting

In this appendix we explain how the statistical uncertainty on r_0/a propagates into the quantities of interest in the work combining HQET and relativistic QCD in the Step Scaling Method.

The quantity r_0/a has been computed in [54, 55, 56] for the range of couplings covering all our SSM simulations with a statistical accuracy between 0.5% and 2.0%. Here we show that for our observables and our precision this uncertainty is negligible. The analysis is carried out for the static observables, but it remains valid for the corresponding observables at finite heavy quark mass too, because the uncertainty on r_0/a can be seen as an uncertainty on the volume, and the light degrees of freedom, which are dealt with by HQET and QCD in the same way, are much more sensitive than the heavy quark to volume changes. Bearing in mind that in our computations the light quark is fixed to be the strange one, we consider an observable $\mathcal{O}(L/a, r_0/a)$ and observe that the uncertainty $\Delta(r_0/a)$ propagates as

$$\Delta(\mathcal{O}(r_0/a, L/a)) = \frac{\partial \mathcal{O}(r_0/a, L/a)}{\partial (r_0/a)} \Delta(r_0/a). \quad (\text{F.1})$$

The arguments of \mathcal{O} differs from the ones appearing in the fourth chapter. There the propagation of the uncertainty on r_0/a is not discussed, and the explicit dependence on it is omitted to lighten the notation. The statistical error on r_0/a can be seen as an uncertainty on the volume, thus suggesting the following strategy for the computation of (F.1). One approximates the derivative in eq. (F.1) by computing the observable \mathcal{O} with simulation parameters $(\beta, L/a, \kappa_s, \kappa_{\text{crit}})$, and then repeats the computation with parameters $(\beta, L'/a, k_s, k_c)$. The change $L/a \rightarrow L'/a$ at fixed β clearly plays the role of

varying the volume in physical units. In order to optimally approximate the derivative in eq. (F.1), the values of L/a and L'/a should be as near as possible. The values of the hopping parameters can be left identical for the two computations, because they are protected by changes of the volume by the axial Ward identity.

F.1 Static decay constant

We borrow the notation from the fourth chapter, and consider the quantities

$$Y_{\text{RGI}}(L/r_0) = I^{\text{stat}}(r_0/L) \cdot \lim_{a/L \rightarrow 0} \frac{\Xi^{(0)}(L/a)}{\Xi(r_0/a, L/a)} X_{\text{SF}}(r_0/a, L/a), \quad (\text{F.2})$$

$$= I^{\text{stat}}(r_0/L) \cdot \lim_{a/L \rightarrow 0} Y_{\text{SF}}(r_0/a, L/a). \quad (\text{F.3})$$

at fixed L/r_0 . The aforementioned strategy is applied to Y_{SF} on the small volume with $L/r_0 = 0.8$, giving the results in the following table for

$$(\beta, \kappa_s, \kappa_{\text{crit}}) = (6.4200, 0.135015, 0.135616).$$

| L/a | $X_{\text{SF}}(r_0/a, L/a)$ | $[\Xi(r_0/a, L/a)]^{-1}$ | $\Xi^{(0)}(L/a)$ | $Y_{\text{SF}}(r_0/a, L/a)$ |
|-------|-----------------------------|--------------------------|------------------|-----------------------------|
| 8 | -1.8372(46) | -0.54673(130) | -1.5996643156321 | -1.6068(55) |
| 10 | -1.9048(37) | -0.52842(37) | -1.6011462370857 | -1.6116(33) |

where the values of $\Xi^{(0)}$ are taken from [2]. By observing that the ratio

$$Y_{\text{SF}}(r_0/a, L/a = 8) / Y_{\text{SF}}(r_0/a, L/a = 10) = 1.003(4),$$

one concludes that even increasing the volume by 25%, no appreciable change is observed in Y_{SF} , and the uncertainty on r_0/a can thus be considered negligible. The factor I^{stat} is already extrapolated to the continuum, and this discussion does not affect it. It is finally straightforward to extend the validity of this result to the step scaling functions of the decay constant, i.e. $Y_{\text{RGI}}(2L/r_0) / (2^{3/2} Y_{\text{RGI}}(L/r_0))$.

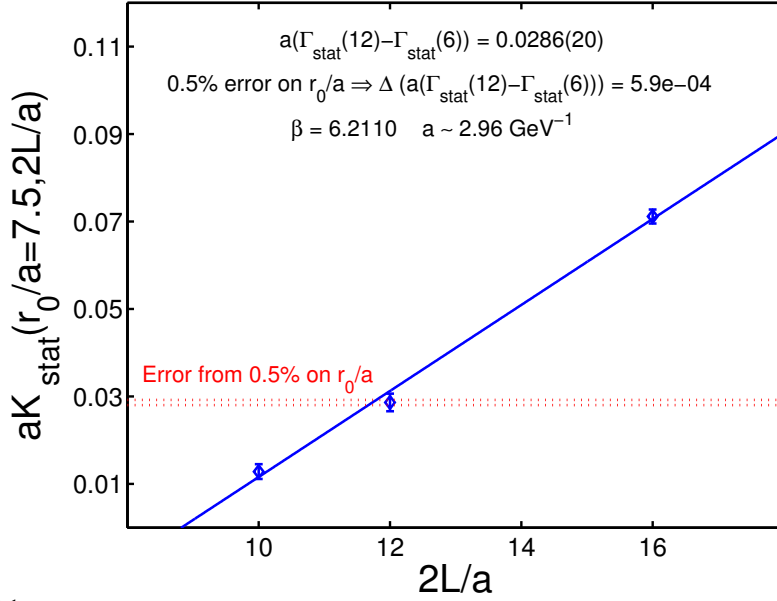


Figure F.1: Estimate on the propagation of the uncertainty on r_0/a for the static meson step scaling function.

F.2 Static meson step scaling function

With the notation borrowed from the fourth chapter

$$\Gamma_{\text{stat}}(r_0/a, L/a) = \frac{1}{2a} \ln \left[\frac{f_{\text{A}}^{\text{stat,I}}(r_0/a, L/a, x_0 - a)}{f_{\text{A}}^{\text{stat,I}}(r_0/a, L/a, x_0 + a)} \right]_{x_0=L}, \quad (\text{F.4})$$

$$\Sigma_{\text{m,stat}}(r_0/a, 2L/a) = 2L[\Gamma_{\text{stat}}(r_0/a, 2L/a) - \Gamma_{\text{stat}}(r_0/a, L/a)], \quad (\text{F.5})$$

we write the propagation of the uncertainty on r_0/a as

$$\frac{\Delta \Sigma_{\text{m,stat}}(r_0/a, 2L/a)}{\Delta(r_0/a)} = \frac{2L}{a} \cdot \frac{\partial(aK_{\text{stat}}(r_0/a, 2L/a))}{\partial(r_0/a)}, \quad (\text{F.6})$$

$$K_{\text{stat}}(r_0/a, 2L/a) = \Gamma_{\text{stat}}(r_0/a, 2L/a) - \Gamma_{\text{stat}}(r_0/a, L/a). \quad (\text{F.7})$$

On a volume with $L/r_0 = 0.8$ and with simulation parameters

$$(\beta, \kappa_s) = (6.2110, 0.134766),$$

we follow the strategy used for the static decay constant, and get the results in Table F.1.

These results are graphically represented in Fig. F.1. From the slope of the linear fitting curve we estimate that, for the point with $L/a = 6$, the uncertainty introduced by r_0/a is more than three times smaller than the statistical error from the Monte Carlo simulation, and it can thus be neglected. The Monte Carlo uncertainties computed here are of the same order (in physical units) of the ones appearing in Table C.3. It justifies the validity of our estimate for all computed data.

| $L/a :$ | 5 | 6 | 8 |
|-----------------------------------|------------|------------|------------|
| $aK_{\text{stat}}(r_0/a, 2L/a) :$ | 0.0128(17) | 0.0286(20) | 0.0711(16) |

Table F.1: Results of the test for aK_{stat} .

Appendix G

Perturbation theory results

In this appendix we report the details on the results relative to the perturbative computations described in chapter 5. All numbers are given with 15 decimal digits, although the last two or three of them may be insignificant. The expectation values of the one-loop diagrams are normalized by the corresponding tree-level values. We indicate with the shorthand \mathcal{P}_3 the Polyakov loop (5.25) in the z -direction, and with $\mathcal{P}_{3,\text{ins}}$ the loop with the insertion of the clover leaf operator. We use lattice units throughout the appendix.

G.1 Tree-level

With the boundary condition defined in App. A, the tree-level of the Polyakov loop with and without insertion of the clover leaf operator is given by

$$L^2 \langle \text{tr}(\mathcal{P}_3(x)E_1(x)) \rangle_{g_0=0} = L^2 \sum_{m=1}^3 \exp \left\{ \frac{i}{L} [x_0 \phi'_m + (L-x_0) \phi_m] \right\} \\ \times \sin \left\{ \frac{1}{L^2} (\phi'_m - \phi_m) \right\}, \quad (\text{G.1})$$

$$\langle \text{tr}(\mathcal{P}_3(x)) \rangle_{g_0=0} = \sum_{m=1}^3 \exp \left\{ \frac{i}{L} [x_0 \phi'_m + (L-x_0) \phi_m] \right\}. \quad (\text{G.2})$$

With the choice of the angles ϕ' and ϕ defining the “point A” and $x_0 = L/2$, we get

$$Z^{(0)} = L^2 \frac{\langle \text{tr}(\mathcal{P}_3(x)E_1(x)) \rangle}{\langle \text{tr}(\mathcal{P}_3(x)) \rangle} \Big|_{g_0=0} = \frac{\pi}{6} \cdot \frac{1 + \sqrt{3}}{2 - \sqrt{3}} + \mathcal{O}((1/L)^4). \quad (\text{G.3})$$

The raw data are presented in Table G.1.

| L | $Z^{(0)}$ |
|-----|-------------------|
| 4 | 5.328760954837700 |
| 6 | 5.336729884747326 |
| 8 | 5.338071744079632 |
| 10 | 5.338438481936987 |
| 12 | 5.338570217499896 |
| 14 | 5.338626689965802 |
| 16 | 5.338654098887551 |
| 18 | 5.338668685775827 |
| 20 | 5.338677021409115 |
| 22 | 5.338682062421030 |
| 24 | 5.338685255099240 |
| 26 | 5.338687356279386 |
| 28 | 5.338688784675057 |
| 30 | 5.338689783019587 |
| 32 | 5.338690497745269 |
| 34 | 5.338691020276737 |
| 36 | 5.338691409429812 |
| 38 | 5.338691704052065 |
| 40 | 5.338691930408358 |
| 42 | 5.338692106630467 |
| 44 | 5.338692245472193 |
| 46 | 5.338692356057547 |
| 48 | 5.338692445014839 |

Table G.1: Raw data for $Z^{(0)}$ defined in eq. (G.3).

G.2 One-loop

| Observable \mathcal{P}_3 | | | |
|----------------------------|---|---|---|
| L | $\langle \text{tr} \{W_{\ell}^{(2a)}\} \rangle_0$ | $\langle \text{tr} \{W_{\ell}^{(2b)}\} \rangle_0$ | $\langle \text{tr} \{W_{\ell}^{(1)} S_{\text{tot}}^{(1)}\} \rangle_{0,g}$ |
| 4 | -0.205624873077021 | -0.413925832829039 | -0.052711610791353 |
| 6 | -0.335983123704290 | -0.619721517834779 | -0.047296572492624 |
| 8 | -0.466256052696041 | -0.826190695109537 | -0.045862904701804 |
| 10 | -0.596569618044621 | -1.032755647453710 | -0.045306225863750 |
| 12 | -0.726911000985525 | -1.239339863635439 | -0.045026523495318 |
| 14 | -0.857269180261336 | -1.445927930087319 | -0.044864334845029 |
| 16 | -0.987637860416361 | -1.652515987946074 | -0.044761438013021 |
| 18 | -1.118013423667861 | -1.859103059892027 | -0.044691916905935 |
| 20 | -1.248393696882175 | -2.065688990758283 | -0.044642684612822 |
| 22 | -1.378777313656793 | -2.272273864188386 | -0.044606518969622 |
| 24 | -1.509163378918473 | -2.478857821155862 | -0.044579158321204 |
| 26 | -1.639551285119290 | -2.685441002278846 | -0.044557951823340 |
| 28 | -1.769940607019591 | -2.892023531121173 | -0.044541178560616 |
| 30 | -1.900331038967060 | -3.098605511382531 | -0.044527680992760 |
| 32 | -2.030722356124227 | -3.305187028572897 | -0.044516656863397 |
| 34 | -2.161114389713687 | -3.511768152828316 | -0.044507535716189 |
| 36 | -2.291507010754891 | -3.718348941705426 | -0.044499902806717 |
| 38 | -2.421900119103333 | -3.924929442602486 | -0.044493450675978 |
| 40 | -2.552293635894514 | -4.131509694747048 | -0.044487947452020 |
| 42 | -2.682687498227030 | -4.338089730788150 | -0.044483215574556 |
| 44 | -2.813081655352524 | -4.544669578061099 | -0.044479117195471 |
| 46 | -2.943476065899737 | -4.751249259588366 | -0.044475543966035 |
| 48 | -3.073870695820916 | -4.957828794872859 | -0.044472409769887 |

Table G.2: Expectation values for the one-loop diagrams of \mathcal{P}_3 . The tadpole contributions in the fourth column are restricted to the ghost and gluon cases.

| Observable $\mathcal{P}_{3,\text{ins}}$ | | | |
|---|---|---|--|
| L | $\langle \text{tr} \{W_{\bar{\ell}}^{(2a)}\} \rangle_0$ | $\langle \text{tr} \{W_{\bar{\ell}}^{(2b)}\} \rangle_0$ | $\langle \text{tr} \{W_{\bar{\ell}}^{(1)} S_{\text{tot}}^{(1)}\} \rangle_{0,\text{g}}$ |
| 4 | -0.168913284554384 | -0.828842066442129 | -0.103736065134993 |
| 6 | -0.328214103185254 | -1.033387450326697 | -0.095754952883402 |
| 8 | -0.473097009376418 | -1.239118347533455 | -0.089957016052714 |
| 10 | -0.613350760169861 | -1.445417860912832 | -0.086224254118902 |
| 12 | -0.751325152405088 | -1.651913219737156 | -0.083638868463676 |
| 14 | -0.887922338616729 | -1.858481585753028 | -0.081746166996522 |
| 16 | -1.023587362197832 | -2.065078524083960 | -0.080302220743496 |
| 18 | -1.158574780275292 | -2.271686295222065 | -0.079165010168635 |
| 20 | -1.293045010271327 | -2.478297336786256 | -0.078246482909905 |
| 22 | -1.427106264182078 | -2.684908327463667 | -0.077489242249884 |
| 24 | -1.560835300983253 | -2.891517830373068 | -0.076854314324669 |
| 26 | -1.694288710683514 | -3.098125281857394 | -0.076314322909446 |
| 28 | -1.827509507624724 | -3.304730531080386 | -0.075849482178954 |
| 30 | -1.960531207496043 | -3.511333621025847 | -0.075445140515130 |
| 32 | -2.093380466272667 | -3.717934681183583 | -0.075090218683396 |
| 34 | -2.226078853805829 | -3.924533874158024 | -0.074776184725976 |
| 36 | -2.358644083951775 | -4.131131369165570 | -0.074496362329055 |
| 38 | -2.491090890892763 | -4.337727329248135 | -0.074245452725766 |
| 40 | -2.623431667925845 | -4.544321905574580 | -0.074019197063928 |
| 42 | -2.755676942497500 | -4.750915235397367 | -0.073814133373627 |
| 44 | -2.887835735723776 | -4.957507441885920 | -0.073627418607532 |
| 46 | -3.019915838719822 | -5.164098634849609 | -0.073456696294221 |
| 48 | -3.151924027957572 | -5.370688911857737 | -0.073299996770239 |

Table G.3: Expectation values for the one-loop diagrams of $\mathcal{P}_{3,\text{ins}}$. The tadpole contributions in the fourth column are restricted to the ghost and gluon cases.

| | Observable \mathcal{P}_3 | Observable $\mathcal{P}_{3,\text{ins}}$ |
|---|---|---|
| L | $\langle \text{tr} \{ W_{\bar{\ell}}^{(1)} S_{\text{tot}}^{(1)} \} \rangle_{0,q}$ | $\langle \text{tr} \{ W_{\bar{\ell}}^{(1)} S_{\text{tot}}^{(1)} \} \rangle_{0,q}$ |
| 4 | 0.102777840715519 | 0.040970131432917 |
| 6 | 0.067072789721730 | 0.029695487491120 |
| 8 | 0.054503845697270 | 0.024694965023325 |
| 10 | 0.049999831469804 | 0.022511928275922 |
| 12 | 0.048081890180969 | 0.021373558175997 |
| 14 | 0.047098380274648 | 0.020672378807829 |
| 16 | 0.046518689745521 | 0.020190464451924 |
| 18 | 0.046143744791383 | 0.019835881834839 |
| 20 | 0.045885452353958 | 0.019562935855346 |
| 22 | 0.045699248493680 | 0.019345912965656 |
| 24 | 0.045560279263445 | 0.019169041088309 |
| 26 | 0.045453664962997 | 0.019022036326953 |
| 28 | 0.045370006920341 | 0.018897879688656 |
| 30 | 0.045303112072779 | 0.018791605608642 |
| 32 | 0.045248756321208 | 0.018699597263028 |
| 34 | 0.045203974156447 | 0.018619155375739 |
| 36 | 0.045166631835496 | 0.018548223386947 |
| 38 | 0.045135161130017 | 0.018485206249965 |
| 40 | 0.045108387852467 | 0.018428847480900 |
| 42 | 0.045085418331307 | 0.018378143643499 |
| 44 | 0.045065562413796 | 0.018332283573234 |
| 46 | 0.045048280116459 | 0.018290604352713 |
| 48 | 0.045033143949942 | 0.018252558876089 |
| $N_f = 2, \quad \theta = -\pi/3, \quad m_0 = 0$ | | |

Table G.4: Expectation values for the one-loop quark tadpole contributions.

| Observable $\mathcal{P}_{3,\text{ins}}$ | | |
|---|---|---|
| L | $\langle \text{tr} \{ W_{\vec{\ell}}^{(1)} \delta S_{\text{tot,b}}^{(1)} \} \rangle_0$ $N_f = 0$ | $\langle \text{tr} \{ W_{\vec{\ell}}^{(1)} \delta S_{\text{tot,b}}^{(1)} \} \rangle_0$ $N_f = 2$ |
| 4 | 0.044525081527306 | 0.012686646544393 |
| 6 | 0.029669953296613 | 0.008453936467964 |
| 8 | 0.022250779285418 | 0.006339972043808 |
| 10 | 0.017800255298336 | 0.005071872742815 |
| 12 | 0.014833435923651 | 0.004226529231324 |
| 14 | 0.012714333177513 | 0.003622727809534 |
| 16 | 0.011125024343901 | 0.003169881936371 |
| 18 | 0.009888902397903 | 0.002817670515825 |
| 20 | 0.008900007976896 | 0.002535902272878 |
| 22 | 0.008090914043919 | 0.002305365047637 |
| 24 | 0.007416669872386 | 0.002113250913414 |
| 26 | 0.006846155994550 | 0.001950692919840 |
| 28 | 0.006357144340312 | 0.001811357565460 |
| 30 | 0.005933334383781 | 0.001690600299307 |
| 32 | 0.005562500760730 | 0.001584937716757 |
| 34 | 0.005235294679453 | 0.001491706042430 |
| 36 | 0.004944444866595 | 0.001408833453618 |
| 38 | 0.004684210848468 | 0.001334684302318 |
| 40 | 0.004450000249276 | 0.001267950071027 |
| 42 | 0.004238095433409 | 0.001207571484223 |
| 44 | 0.004045454700235 | 0.001152681862284 |
| 46 | 0.003869565341325 | 0.001102565252704 |
| 48 | 0.003708333433511 | 0.001056625028544 |

Table G.5: $O(a)$ -improvement counterterms for $\mathcal{P}_{3,\text{ins}}$ at one-loop order. The simple Polyakov loop \mathcal{P}_3 does not require any counterterm.

Acknowledgements

Here I would like to thank all persons whose contribution has been indispensable for a successful completion of this thesis.

- I would like to thank Rainer Sommer for proposing me the subject of this thesis, and for supporting me all the while with inestimable suggestions and encouragements. His help has been for me invaluable.
- Many thanks to Ulli Wolff for fruitful discussions, especially on perturbation theory and its implementation.
- I thank Nazario Tantalo for providing the relativistic QCD data and for useful discussions about the combination of them with HQET.
- I am grateful to Michele Della Morte, Nicolas Garron, Jochen Heitger, Björn Leder and Harvey Meyer for an enjoyable and fruitful collaboration.
- Thanks to Hubert Simma for introducing me to the TAO programming language. I thank DESY for allocating computer time on the APEmille computers at DESY Zeuthen and the APE group for its help, in particular Dirk Pleiter for the prompt assistance.
- I thank all collaborators of DESY Zeuthen and the Humboldt University in Berlin with whom I spent the three years of my PhD studies.
- Special thanks to Griseldis. She is part of my life.
- Finally I would like to thank my family, which I have always felt near me.

Lebenslauf

Name: Damiano Guazzini

07.1999 Abitur am “Liceo Scientifico Statale B. Touschek”
in Grottaferrata, Rom (Italien)

10.1999–12.2003 Studium an der “Università di Roma II Tor Vergata”
in der Fachrichtung Physik

01.2004–03.2004 Wissenschaftlicher Mitarbeiter an
der “Università di Roma II Tor Vergata”

seit 04.2004 Wissenschaftlicher Mitarbeiter beim
Deutschen Elektronen-Synchrotron DESY Zeuthen

Selbständigkeitserklärung

Hiermit erkläre ich, die vorliegende Arbeit selbständig ohne fremde Hilfe verfaßt und nur die angegebene Literatur und Hilfsmittel verwendet zu haben.

Damiano Guazzini
29. März 2007